Biosurfactant Mediated Nano-Heterostructures of 2D Layered MoS_2 for Azo Dyes Degradation and Antibiotic Drug Sensing

Thesis Submitted for the Award of the Degree of

DOCTOR OF PHILOSOPHY

in

Biotechnology

By

Mandeep Kaur

Registration Number: 11919656

Supervised By

Dr. Vineet Kumar (21644)

Professor,

Department of Biotechnology,

School of Bioengineering & Biosciences

LOVELY PROFESSIONAL UNIVERSITY
PUNJAB
2025

DECLARATION

I, hereby declared that the presented work in the thesis entitled "Biosurfactant mediated nano-heterostructures of 2D layered MoS_2 for azo dyes degradation and antibiotic drug sensing" in fulfilment of degree of **Doctor of Philosophy (Ph. D.)** is outcome of research work carried out by me under the supervision of Dr. Vineet Kumar working as Professor, in the Bioengineering & Biosciences of Lovely Professional University, Punjab, India. In keeping with general practice of reporting scientific observations, due acknowledgements have been made whenever work described here has been based on findings of other investigator. This work has not been submitted in part or full to any other University or Institute for the award of any degree.

Mandeep Kaur

(Signature of Scholar)

Name of the scholar: Mandeep Kaur

Registration No.:11919656

Department/school: Biotechnology/Bioengineering & Biosciences

University: Lovely Professional University, Punjab, India

CERTIFICATE

This is to certify that the work reported in the Ph. D. thesis entitled "*Biosurfactant mediated nano-heterostructures of 2D layered MoS_2 for azo dyes degradation and antibiotic drug sensing*" submitted in fulfillment of the requirement for the award of degree of **Doctor of Philosophy (Ph.D.)** in the Biotechnology, School of Bioengineering & Biosciences is a research work carried out by Mandeep Kaur, 11919656 is bonafide record of her original work carried out under my supervision and that no part of thesis has been submitted for any other degree, diploma or equivalent course.

(Signature of Supervisor

Name of supervisor: Dr.Vineet Kumar

Designation: Professor

Department/school: Biotechnology/Bioengineering & Biosciences

University: Lovely Professional University, Punjab, India

Abstract

Introduction

A variety of factors, including sewage discharge, industrial waste, residues of fertilizers, and pesticides that seep into the ground water or run off into water streams from agricultural lands, contribute to water contamination. Water pollution may have disastrous impacts, including the extinction of aquatic life, harm to human health, and destruction of agricultural crops and overall ecosystems. Water contamination by dyes seriously affects the environment, and all life forms including humanhealth worldwide. Nanomaterials are better alternate to traditional waste treatment and detection apparoches. However, nanomaterials prepared using chemical approach may lead to environmental contamination. The applicability of greener nanomaterials in environmental remediation has unveiled their tremendous properties and potentiality to eradicate the pollutants from nature in ecofriendly manner.

Material & methods

The current work reports the biosurfactant–mediated greener synthesis of MoS_2 nano-heterostructures and their utilization for the solar light–assisted degradation of methylene blue (MB), commercial blue (CB) and industrial sample (IS). The MoS_2 nano-heterostructures were obtained by functionalization of MoS_2 nano-structures with carbon quantum dots derived from citric acid. The synthesized product was characterized by UV-Visible spectroscopy, High resolution transmission electron microscope, X-ray diffraction, and Fourier transform infrared spectroscopy. The surface morphology of nano-heterostructures was examined using High Resolution Transmission Electron Microscope (HR-TEM). X-ray diffraction (XRD) was perfomed to check the crystallinity and crystallite particle size of the obtained product. The functional groups involved in the nanoscaling of the pristine MoS_2 were determined using Fourier transform infrared spectroscopy (FTIR). The mechanism behind the photcatalysis of MB was studied using the free radical trap experiment and the reusability test was done to check the multiple use of the material for the same application.The nanosensing of the functionalized MoS_2@GQDs obtained from the gum Arabic and sodium alginate has been evaluated using cyclic voltammetry (CV) and differential pulse voltammetric analysis (DPV). Additionally, the antioxidative potential of

the synthesized nano-structures and nano-heterostructures was analysed using DPPH scavenging assay.The antimicrobial effect of the nanomaterials was tested against the *E. coli* MTCC 495 and *S.aureus* MTCC 7443 using well-diffusion technique. The effect of MoS_2 nanostructures and nano-heterostructures treated MB, CB and IS test samples on the growth of *L. delbrueckii* MTCC 10307 (Lactic acid bacterium) was studied using streak agar plate method.

Results & Discussion

MoS_2 nano-heterostructures prepared using gum arabic, sodium alginate and stem extract of *Tinospora cordifolia* biosurfactants possessed photocatalytic activity against MB, CB, and IS. The photocatalytic property of the MoS_2 nano-heterostructures was influenced by various parameters like irradiation time, photocatalyst dose, and pH. After studying all these crucial factors, the final experiment was performed for the photocatalytic degradation of MB, CB, and IS at optimal reaction conditions. Overall, the MoS_2 nano-heterostructures have shown photodegradation efficiency in the range of 80-99%. The synergistic contribution of hydroxyl and superoxide ions in the photodegradation of MB has been demonstrated by free radical trapping experiment. These nanomaterials have shown potent electrochemical sensing of Ciprofloxacin (antibiotic) with improved efficiency when compared to the bare electrode. Furthermore, the nano-heterostructures have shown antioxidative as well as antimicrobial properties. At highest concentration (1000µg/mL), 82.93±0.43%, 84.93±0.55%, 93.53±1.18 and 100% of free radical scavenging activity was exhibited by GA-MoS_2 NPs, GA-MoS_2@GQDs, *TcSE*-MoS_2 and *TcSE*-MoS_2@GQDs, respectively. The SA-MoS_2 NS and SA- MoS_2@GQDs have shown 88.46±3.42% and 100% activity at maximum concentration of 1000 µg/mL and 600µg/mL, respectively. In the well diffusion method, GA-MoS_2 NPs, GA-MoS_2@GQDs, SA-MoS_2 NS, SA-MoS_2@GQDs, *TcSE*-MoS_2 NS and *TcSE*-MoS_2@GQDs,exhibited a zone of diameter of 14±2.5, 20±1.3, 17.3±2.1, 25±0.8, 35±1.9, and 42±2.9 mm against *E.coli* and 21±1.8, 24.5±1.7, 24.3, 27.4, 24.9±1.1, and 27.4±1.8 mm against *S.aureus*, respectively. The agar plates with untreated MB dye solution showed a few colonies whereas the agar plates containing MoS_2 nanoheterostructures–treated dye solution had a better growth.

Conclusion

From the studies, it has been concluded that the Gum Arabic, sodium alginate, and *Tinospora cordifolia* stem extract can be used as exfoliators to obtain MoS_2 nano-structures by using ultra sonication and microwave treatment. The imbedding of obtained nanostructures with the quantum dots derived from citric acid, led to fabrication of MoS_2 nano-heterostructures. Furthermore, the photocatalytic activity of the obtained nano-heterostructures have been successfully degraded the MB, CB, IS in the presence of direct sunlight. The nano-heterostrctures are useful for the electrochemical sensing of ciprofloxacin. The antioxidant and antimicrobial activities possed by nano-heterostrctures will be useful for various biological applications.

Keywords: MoS_2 nano-hetrostructures; Biosurfactants; Water pollution; MoS_2@GQDs, Photocatalysis; Methylene Blue; Nanosensing; Ciprofloxacin.

Graphical abstract

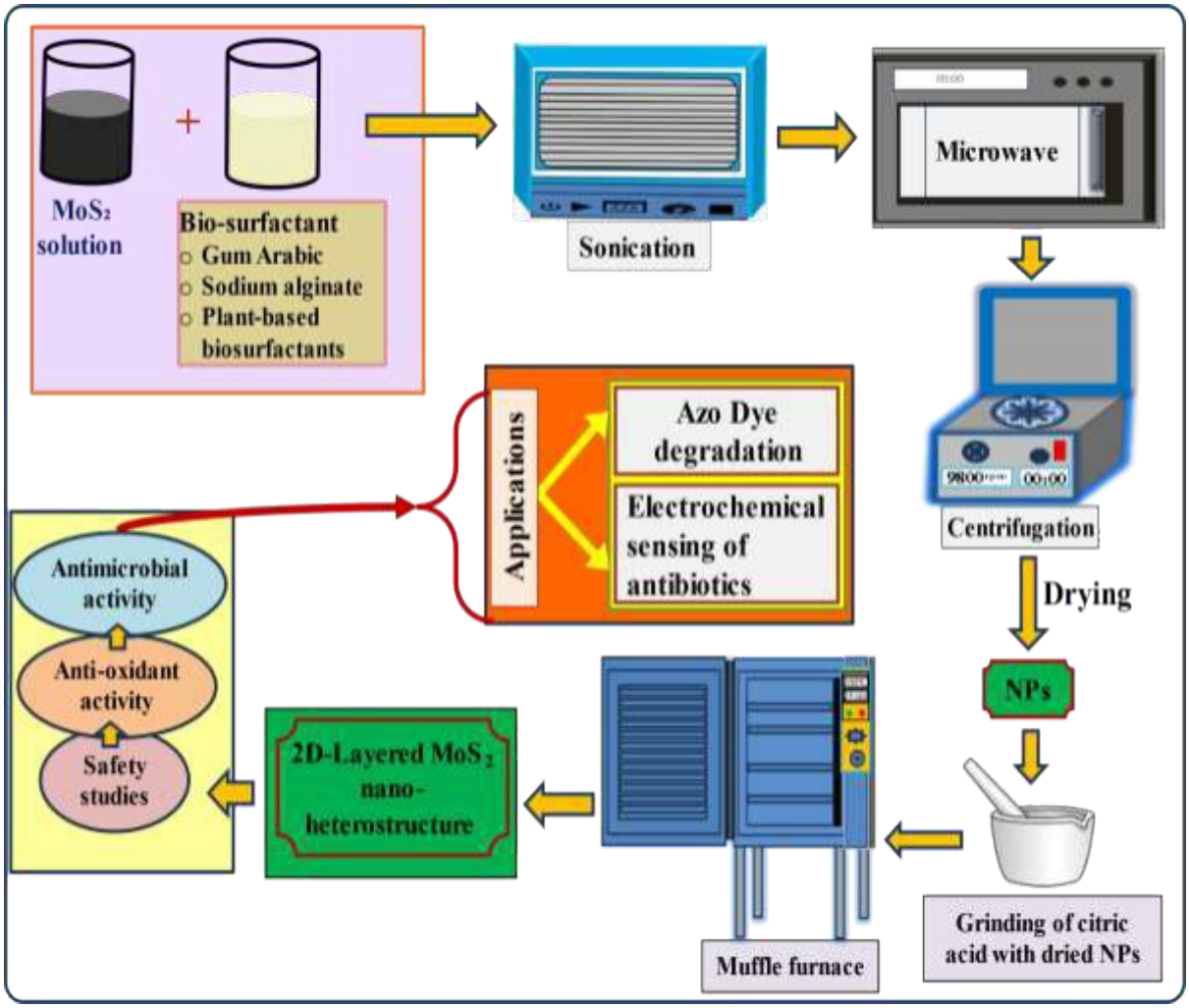

Figure legend: Schematic representation of biosurfactant mediated synthesis of 2D layered MoS_2 nano- heterostructures for dyes degradation and antibiotic drug sensing.

Acknowledgement

Firstly, I am profoundly grateful to the **Waheguru** for bestowing upon me the power and vision to effectively complete my work.

I wish to express my sincere gratitude to my supervisor, **Dr. Vineet Kumar**, Professor, Department of Biotechnology at Lovely Professional University, for his direction, perseverance, commitment, and unwavering support during this research endeavour. With the virtue of his lead, I am able to overcome the hurdles and successfully submitting my Ph.D. thesis.

I would also like to use this opportunity to thanks the entire faculty members of the School of Bioscience and Bioengineering most especially our very active head of school in person of **Dr. Neeta Raj Sharma**, Dean & Professor, Department of Biotechnology at Lovely Professional University who always try her best to see that we have all the necessary material, teaching and Laboratory support throughout these years of research. I am deeply grateful to **Dr. Kulvinder Singh** (Assistant Professor, Dept. of Chemistry, DAV college, Chandigarh) for his assistance and guidance in my Ph.D. work.

I am thankful to **Ms. Prabhjot Kaur**, Lab Technician, for her assistance and the support she provided during my experimental work. I am grateful to Mr. Rajesh for his assistance whenever I required support.

I am thankful to my parents (Mr. Gurmail Singh & Mrs. Sita Rani) and my family members for the immense love and support. With their help I am able to maintain my personal and professional front. My nephews Yuvraj and Gurnoor's loving embrace has been a comfort on my difficult path.

It would not have been possible to get my Ph.D. without the encouragement of my friends **(Neha Rana)** and lab-mates. They have been there for me through thick and thin, sharing in both my triumphs and my lows. Being in the company of these wonderful people is a blessing. I had a wonderful time on my journey and made many beautiful memories with them.

Contents

List of Tables

List of Figures

	microwave and sonication steps. Low peak intensity designates low exfoliation potential if microwave and sonication are done in reverse order. (b) Effect of sonication on gum Arabic at different time interval. This was a experiment to check if sonication of gum Arabic can have false peaks in the UV-vis absorption region of MoS_2 NPs. (c) Effect of pH on the UV-vis absorption of gum Arabic. No change in absorption wavelength indicates exfoliation can be carried out at any pH, (d) Bare exfoliation experiment in the absence of gum Arabic. Bulk MoS_2 was subjected to sonication followed by microwave treatment. Low peak intensity and lack of MoS_2 NPs characteristic peak show no significant exfoliation in the absence of gum Arabic	
5.3.	Characterization of as GA synthesized MoS_2 NPs. (a) UV–vis spectrum of MoS_2 NPs. (b) FT-IR spectrum of NPs to examine the functional group present (black-gum arabic; red MoS_2 NPs). (c) X-ray diffraction pattern of GA-MoS_2 NPs. (d) HR-TEM image of the NPs (inset SAED pattern).	55
5.4.	Different criteria affecting the synthesis of MoS_2 NS using sodium alginate as exfoliating agent at different physiochemical parameters. (a) Sodium alginate (b) Bulk MoS_2, (c) Sonication time. Increase in sonication time up to 4 h led to increase in peak intensity (d) Effect of pH on the synthesis of MoS_2 NS using sodium alginate as exfoliating agent.	58
5.5.	Visible observation of green color reflecting synthesis of MoS_2 NS showing successful exfoliation using sodium alginate.	60
5.6.	Characterization of as synthesized SA-MoS_2 NS. (a) UV–vis spectrum of MoS_2 NS. (b) FT-IR spectrum of NS to examine the functional group present (black-sodium alginate; red MoS_2 NS). (c) X-ray diffraction pattern of MoS_2 NS. (d) HR-TEM image of the NS.	60
5.7.	Optimization of parameters for the TcSE mediated MoS_2 nanostructure's synthesis: (a) Sonication time (b) Microwave time (c) Precursor concentration (d) pH.	62

Chapter 1:

Introduction

In the recent years, environmental issues become one of the major concerns throughout the world (Wang et al., 2019). Several researchers around the globe are working on various environmental problems (Ahmad et al., 2022a; Akhtar et al., 2021a; Choudhury et al., 2021; Khan et al., 2022). In this context, water pollution is the most important issue as around 80% of the waste from different sources is discharged in the water system (Akhtar et al., 2021b). Wastewater treatment is a highly recommended method according to industrial regulations to protect the environment from pollution. However, the textile and pharmaceutical sectors contribute significantly to water pollution, which poses a huge concern due to its harmful impact on biodiversity. Few rivers receive wastewater that contains dyes upto fifty percent of total pollutants generally contributed by the production (Verma et al., 2021). In the textile and printing industries, azo dyes provide vivid colours, superior colour durability, and four times brightness compared to the nearest alternatives, making them extremely useful to the sectors. The textile industry uses 60% of the azo dyes produced each year, a total of to 7×10^5 tonnes (Bafana et al., 2011; Sarker et al., 2019; Khalid et al., 2014). Within the textile sector, certain azo dyes have been discovered to decompose producing hazardous aromatic amines mainly benzidine, which have the potential to induce cancer and other health complications. Hence, these dyes are well known for their mutagenic, carcinogenic, teratogenic, genotoxic, cytotoxic, and allergenic effects on human health summarised in table 1 (Gao et al., 2019; Chung et al., 2016). Consequently, several nations have implemented prohibitions or limitations on the utilisation of specific azo dyes in the textile industry (Chequer et al., 2013).

According to the European Environment Agency (ETC-CE Report 2023/5), there is an instant need of effluent treatment due to enhancing global textile fibre production (109 million tonnes in 2020) and estimated to projected to 145 million tonnes by 2030.Even now, textile industry is one of top three industries, contributing highest in water pollution. Along with, $1/5^{th}$ part of overall water pollution occurs due to dyeing and finishing processing of textile industry. Hence, it is a need of time to tackle

wastewater generated from the textile industry in a cost effective, green, and eco-friendly manner.

On the other hand, the occurrence of antibiotic compounds that are readily accessible in the water system has led to shaping microbial evolution. Antimicrobial resistance (AMR) in waterborne pathogens mainly caused by altering the composition of bacterial communities, affects their ecological functions, and increasing the development and persistence of drug resistance (Kulik et al., 2023). The impact of azo dyes and antibiotic contamination on human health and the economy is profound along with a serious threat to aquatic life and water supplies (Manzoor et al., 2020). Due to a lack of efficient water filtration methods, various countries are struggling to remediate the textile industrial effluent.

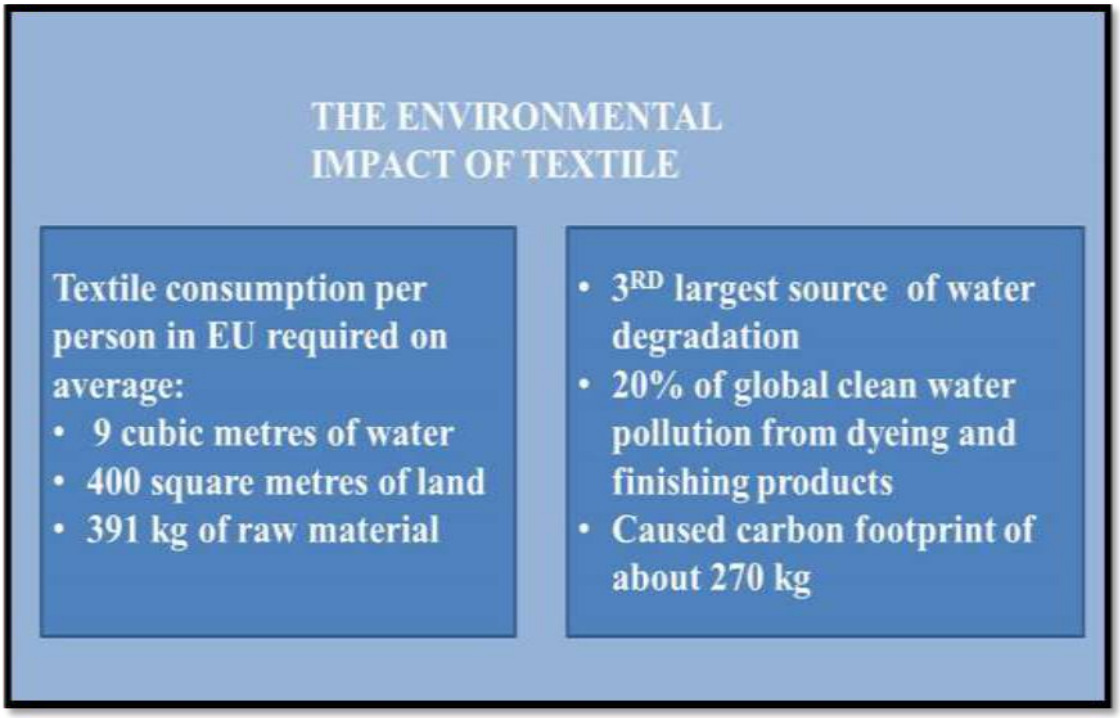

Figure 1.1. Environmental impact of textile industry according to European Environment Agency report.

There are several methodologies developed until now for efficient wastewater treatment involve physicochemical processes such as adsorption, reverse osmosis,

filtration, irradiation, oxidation, precipitation, coagulation, and Fenton processes (Obotey et al., 2020; Rashid et al., 2021; Domingues et al., 2021; Nguyen et al., 2020; Ashar et al., 2020; Crini et al., 2018). However, due to several limitations such as excessive energy consumption, generation of hazardous sludge, and being less ecologically sustainable and cost-effective (Choudhari et al., 2022), there has been a need to develop an efficient methodology with less time consuming, more economical, more efficiency that requires less energy, etc. (Thakur et al., 2020). In the last decade, researchers have developed a process that uses advanced oxidation process (AOP) for wastewater treatment (Mandal et al., 2010). This method results into complete mineralization of the organic compounds that not completely mineralized by the biological entities (Rani et al., 2020).

Photocatalysts based on nanotechnology provide an efficient, eco-friendly, and cost-effective way to remove stubborn contaminants from water matrices, which greatly aids in protecting the environment from harmful waste (Parida et al., 2023; Sivaraman et al., 2022). Molybdenum disulphide (MoS_2) is the most stable semiconductor among dichalcogenides. This is because of its low band-gap energy, extensive surface area, a powerful ability to absorb substances, a multitude of exposed edges, a low barrier to charge transfer, and a high level of chemical tolerance (Su et al., 2017; Samy et al., 2021). Recently, MoS_2 and their heterostructures have been utilized for the organic dye degradation in water system (Li et al., 2018). Although MoS_2 nano-structures show excellent visible light absorption efficiency with an excellent 1.8 eV band gap, the utilization of pristine MoS_2 is less due its fast electron hole recombination rate (Yuan et al., 2021). The sole reason behind it is the feeble van der Waal force between the stacked layers of Mo-S-Mo, which leads to re-aggregation and the subsequent collapse of the active and responsive sites on its surface. To overcome the recombination rate, modifications have been done in the pristine structure of MoS_2 nano-structures that include doping, functionalization, defect generation, and forming heterostructures in order to make it an efficient light-driven photocatalyst and effective electrocatalyst for detecting different analytes with improved sensitivity and specificity (Sivaranjani et al., 2022; Thomas et al., 2021).

Various bottom-up approaches have earlier been documented for the preparation of MoS_2 nano-structures and its heterostructures for the pollutant removal applications (Luo et al., 2018; Mulu et al., 2021; Sadhanala et al., 2018; Tien et al., 2022; Ullah et al., 2021). However, use of toxic chemicals and drastic reaction conditions for the synthesis and modifcation of nanostructured MoS_2 is a major drawback. To avoid the negative outcomes of chemical and physical routes of nano-synthesis, green nanotechnology is most promising method.

Bio-surfactant has been widely used for the exfoliation for different 2D-layered materials; however, only a study documented bio-surfactant mediated exfoliation of MoS_2 (Garg et al., 2020; Li et al., 2019a; Peng et al., 2020). The biosurfactant acts as a binder to provide interconnecting link to the precursor molecules. Liquid-phase exfoliation (LPE) is the prevailing and practical technique for separating nanosheets from bulk 2D materials by introducing biosurfactant between the layers and reducing the connection between them. Various notable techniques have been devised, including as sonication, shear force, ion intercalation, electrochemical exfoliation, and ion exchange. Sonication-assisted exfoliation is a highly prevalent and extensively developed method for exfoliating a wide range of two-dimensional materials (2DMs)(Wu et al., 2018).

In the present work, different biosurfactants (Gum arabic, sodium alginate, plant material) have been used to fabricate MoS_2 nano-structures using liquid phase exfoliation using ultrasonic treatment followed by microwave to control the size that influences the electron hole recombination rate. The synthesized MoS_2 nano-structures were functionalized with quantum dots to prepare MoS_2 nano-heterostructures. The obtained MoS_2 nanoheterostructures were used as photocatalyst and electrocatalyst for methylene blue (MB) degradation and electrochemical sensing of antibiotics. The electrochemical characterization and electrocatalytic response towards antibiotics were measured by cyclic voltammetry (CV) and differential pulse voltammetry (DPV) techniques.

Chapter 2:

Review of literature

.1. Biosurfactants

A new area of study in nanotechnology is the synthesis of nanomaterials using biosurfactants; this method is known as "green chemistry" or "green synthesis" and it is characterized by its lack of toxicity, low environmental impact, high stability at extreme physical factors and increased energy efficiency owing to the use of renewable resources. For their environmentally beneficial properties, biosurfactants are actually referred to as "green molecules" (Vecino et al., 2020).

Biosurfactants are amphipathic biomolecules that exhibit surface activity and are produced by several biological sources, including fungi, yeast, plants, and bacteria. The hydrophilic (water loving) component is derived from carbohydrates, peptides, amino acids, carboxylic acid (COOH), and alcohol (OH). The hydrophobic (water repelling) components may consist of fatty acids, specifically long-chain fatty acids, as well as hydroxyl or alkyl hydroxyl fatty acids (Płaza et al., 2014; Kaur, et al., 2022).

In biotechnological processes, microorganisms (such as bacteria, yeast, and fungi) generate surface-active chemicals called biosurfactants (BS), often made up of carbohydrates, lipids, and proteins (Gómez-Graña et al., 2017). They can operate as capping, stabilizing, and dispersing agents, as well as coating and reducing agents. The biosurfactant adheres to the metallic NPs' surface, enhancing its stability and preventing the nanoparticles (NPs) from clumping together. They serve as a template for NPs, enhancing their structural, functional, and physicochemical properties (Kiran et al., 2011). Hence, biosurfactants have recently been utilised in the production of NPs consisting of various metals and metal oxides (Table 2.1.). These biosurfactants possess distinctive characteristics i.e. it can decrease the level of activity on different surfaces, possess emulsifying characteristics, and function as a capping, reducing, and stabilising agent. Consequently, they show great potential in the environmentally friendly synthesis of NPs (Rane et al., 2021).

1. Reduce agglomeration by maintaining an unobstructed surface that allows for both steric and electrostatic stability.

2. Enhance the NPs growth by making diffusion barrier.
3. Enable homogeneous distribution of NPs in the liquid media.
4. As an exfoliator and stabilizing agent don't hinder the basic properties of the pristine material.

2.2. Exfoliation of MoS_2 using biosurfactants

Exfoliating MoS_2 in water is difficult due to its hydrophobic nature. A potential approach to tackle this problem is to employ surfactants, which enable the exfoliated sheets to stay suspended (Liu et al., 2015). Currently, only a limited number of block copolymers, charged macromolecular compounds, and tiny organic salts have been employed to maintain the stability of exfoliated MoS_2 in an aqueous environment. Table 2.1 presents several nanomaterials synthesised using biosurfactants as reducing and capping agents.

Table 2.1. Biosurfactant mediated synthesis of different nanomaterials

Biosurfactant	**NPs**	**Shape/Size (nm)**	**Reference**
Rhamnolipid	CuO	Spherical/0.25nm	Athira et al., 2021
Averrhoa carambola leaf extract	AgNPs-RGO nanocomposite	Cubic/90-120nm	Devi et al., 2021
Furostanol Saponin (FS)	Iron oxide	Cubic spinal/12nm	Sunder et al., 2020
Rhamnolipid	Zinc oxide	Polycrystalline/40-50 nm	Malakar et al., 2021
Gelatin	CuO	Rod	Ahmad et al.,

		shaped/30 ± 2 nm	2020
Glycolipid mannosyl-erythritol lipid (MEL)	Gold	Spherical	Bakur et al., 2019
Rhamnolipid	Gold	Spherical/53nm	Bayee et al., 2020
Sophorolipid	Gold	Spherically clumped/40 ± 10 nm	Shikha et al., 2020
Lipopeptide from *Bacillus subtilis* ANR 88	Gold	Hexagonal/40-60nm	Rane et al., 2017
	Silver	Spherical/4-18nm	
Extracellular polymeric substance(Alcaligene sp)	Iron oxide	Spherical/160-180nm	Sharma et al., 2021
Acacia concinna extract	Iron oxide	Amorphous/ 19 nm	Arde et al., 2020
Rhaminolipid	Silver	spherical/ 38-53 nm	Bilai et al., 2022
Rhaminolipid	Silver	Spherical/ 1 to 3 nm	Shepida et al., 2021
Mannosylerythritol lipid (MELs)	Silver	Spherical	Ga'al et al., 2021
Paenibacillus polymyxa strain Sx3	Zinc oxide	Cubic/62.8nm	Ogunyemi et al., 2020
	Mangnese oxide	Sheet-like/18.8nm	
	Magnesium oxide	Spherical/10.9 nm	

2.3. Two dimensional (2D) materials

Based on dimensionality, 2D materials have at least one nano-dimension along with two macroscopic dimensions**.** 2D materials are defined as layered solids having strong in-plane bonds and weak inter-planar interactions, usually caused by van der Waals forces. Furthermore, new synthetic methods allow for the reduction of thicknesses to a few nanometers, or even to monoatomic dimensions in certain instances. Through this transformation, most captivating characteristics such as the emergence of photoluminescence, electrical conductivity, and other adjustable properties can be attained which are not present in their bulk structures. Additionally, they possess extraordinary electrical, optical, and mechanical properties due to distinctive capability to trap electrons within their extremely thin layer. The strong in-plane covalent bonding provides opportunities for the creation of multiple heterojunctions and heterostructures (Novoselov et al., 2005; Neto et al., 2011).

Due to their unique features, 2D nano-structures represent a frontier in materials chemistry. 2D nanomaterials, free of metals are particularly attractive since they are more affordable and less harmful than many inorganic structures. Some metal-free 2D semiconductors have made breakthroughs into the field of organic synthesis owing to their exceptional electrical properties. Here, they can serve as high-performance photocatalysts, promoting the environmentally friendly synthesis of valuable organic compounds (Wang et al., 2023).

Photocatalysis is one of the many promising uses of these materials; it conforms to many of the tenets of the "green chemistry" contemporary ideology, the central goal of which is to incorporate sustainability principles into chemical production. 2D geometry enhances the separation and migration of charge carriers, which are necessary for efficient photocatalysis, as well as increases the density of surface-active sites. Furthermore, it is possible to make familiar modifications to the chemical and morphological structures, allowing for the adjustment of the defect density (Zhang et al., 2020). Alongwith, quantum confinement causes the band gap to increase, resulting in an upward shift of the conduction band (CB). This leads to an increase in both the potential energy of the electrons created by light and their

capacity to undergo reduction reactions (She et al., 2016). The photocatalytic activity of the 2D semiconductors is mainly influenced by many factors (Raza et al., 2021);

1. Optimal band gap: To achieve maximum solar absorption, the difference in energy levels between the bands should exceed the energy required for free water splitting, The variation in energy between the bands must be greater than the energy needed for water splitting to occur easily (1.23 eV), and should be less than approximately 3 eV (Tan et al., 2014).

2. Water insoluble: The 2D semiconductor exhibit water insolubility when dissolved in an aqueous (aqs) solution (Singh et al., 2015).

3. Reaction temperature: Raising the reaction temperature often enhances the efficiency of the photocatalytic process. Nevertheless, maintaining a reaction temperature higher than 80°C prevents the recombination of the charge carriers, resulting in a decrease in the adsorption of organic contaminants on the surface of the 2D semiconductor (Kumar et al., 2017).

4. Low excitonic recombination rate: The recombination of the electron-hole pairs generated by the photoexcitation process results in the dissipation of excess energy in the form of either heat or light (Ikram et al., 2020).

5. Low excitonic binding energy: A reduced binding energy of excitons results in the conversion of splitting excitons into unbound charge carriers (Ikram et al., 2021).

6. Lower reverse reaction rate: The kinetics of reactions can facilitate a swift progression of the forward process with reduced reverse reaction rate to complete energy efficient reaction (Kumar et al., 2017).

7. Ability to utilize visible light: A semiconductor must capture a significant portion of the visible spectrum, as it represents more than 40% of solar energy, in contrast to ultraviolet radiation, which reflects less than 5% (Kumar et al., 2017).

8. Passivation of edges: 2D semiconductor edges exhibit passivity to remove ions from solution (Kumar et al., 2017).

9. Suspension stable in water: The 2D content must exhibit a high degree of dispersion in an aqueous solution and demonstrate resistance to clumping together to

effectively utilise its huge surface area and facilitate quick diffusion excitation (Kumar et al., 2017).

2.4. Dichalcogenides

In recent years, there has been significant interest in 2D transition metal dichalcogenides (TMDs). In TMDs, metal atoms (M) are arranged in hexagonal layers within two layers of chalcogen atoms (X) in a stoichiometric relationship abbreviated as MX2 (Xia et al., 2018). The sheets are joined together through covalent bonding, while the neighbouring sheets are held together by van der Waals forces, culminating in the formation of a three-dimensional crystalline structure.

2.4.1. Molybdenum disulphide (MoS_2)

From a list of various 2D materials, MoS_2 has become prime choice for catalytic and electrocatalytic applications by virtue of its distinctive lamellar structure, exceptional electrical carrier mobility, elevated chemical activity, favourable optical response, and extensive specific surface area (Guo et al., 2018).In addition to possessing graphene-like characteristics such as high carrier concentration, mobility, and a strong two-dimensional structure, MoS_2 has an advantage over graphene because it has inherent band gaps, which measure 1.3 eV for bulk MoS_2 and 1.8 eV for a single layer(Verble et al., 1970). MoS_2 nano-structures have become increasingly popular due to their non-toxic nature, excellent light absorption capabilities, significant photocatalytic activity, superior resistance to photo corrosion, and cost-effectiveness (Tavker et al., 2020)

The MoS_2 structure consists of monolayers of Mo atoms that are firmly bonded between two S atoms in an S-Mo-S arrangement, like graphene. The thickness of each monolayer is 6.5 Å. The covalent bond between the interlayer Mo-S atoms, which is 2.42 Å long, is primarily covalent. The multilayered molybdenum disulfide is made up of several single layers of molybdenum disulfide, with no more than five levels being common. On the other hand, the sandwich layers have weak bonding and consist of van der Waals (vdW) forces. This allows the crystal to easily break along its surface layer direction (He et al., 2016; Wang et al., 2018; Luo et al., 2020). MoS_2

exhibits a greater current switching ratio and electron mobility. Additionally, the UV absorption spectra of MoS_2 display two distinct absorption peaks (Tuteja et al., 2017).

The significance of few-layer MoS_2 nanosheets (NS) lies in their anisotropic feature and the presence of unsaturated d-orbitals, which make them suitable for a wide range of applications in catalysts (photocatlyst/electrocatalyst), semimetals, semiconductors, ferro-magnets, and even superconductors (energy productions) (Jawaid et al., 2016).The property of thickness dependence and significant spin-orbit coupling is advantageous for several applications in nano-electronics, sensings of gases, biological sensing, and spintronics.

2.4.2. Growth methods of 2D metal dichalcogenides

In nanotechnology, two principle approaches have been applied for the nanoscaling of the bulk materials i.e. top-down and bottom-up methods. The top-down approach is further sub categorized into mechanical exfoliation (Li et al., 2014), liquid phase exfoliation (Yu et al., 2018), intercalation and exfoliation (Ambrosi et al., 2015) and thinning (Cai et al., 2018). Similarly, bottom-up techniques are reportedly further categorised into vapor deposition (Jeon et al., 2017) and solution-based synthesis (Chai et al., 2018).

2.4.2.1. Micromechanical exfoliation

To accomplish exfoliation, the micromechanical exfoliation method relies on the adhesive force of adhesive tape to counteract the weaker van der Waals force between molybdenum disulfide molecular layers.

Positives

MoS_2 NS, obtained through micromechanical exfoliation, possess a pristine, pure, and high-quality structure (Pena-Alvarez et al., 2015).

Negatives

The nanosheets formed through micromechanical exfoliation exhibit low yields and pose challenges for large-scale preparation (Li et al., 2014).

2.4.2.2. Ion intercalation method

The fundamental concept involves incorporating a lithium-ion intercalant, such as butyl lithium (n-C_4H_9Li), into the molybdenum disulfide powder to create an intercalation molecule called $LixMoS_2$ (where x is equal to or greater than 1). Intercalation compounds react with protonic solvents to generate a significant quantity of hydrogen. This hydrogen causes the interlayer spacing of MoS_2 to expand, leading to the creation of lamellar MoS_2 (Liu et al., 2020; Matte et al., 2010).

Positives

This method exhibits a significant productivity and is also compatible with various other stratified compound systems.

Negatives

This method of preparation necessitates a higher temperature of 373 K and a longer duration of 3 days. Additionally, it lacks the ability to regulate the extent of lithium insertion, which may result in incomplete detachment of the sheet layer or the formation of Li_2S, leading to potential harm to the lamellae (Zeng et al., 2011).

2.4.2.3. Chemical vapour deposition.

Chemical vapour deposition (CVD) is a stable and effective method for producing superior MoS_2 layers. This approach provides numerous benefits compared to conventional exfoliation techniques, such as the ability to easily adjust the size and reproduce the results consistently (Karamat et al., 2020). This process involves the reaction of a gaseous or vaporous substance at either a gas phase or a gas-solid interface, resulting in the formation of a solid precipitate.

Positives

CVD enables the formation of MoS_2 across large areas with good quality, excellent compactness, no residual stress, error-free surface, and optimal crystallisation and purity, rendering it well-suited for industrial applications. The approach exhibits greater scalability and reproducibility in comparison to conventional exfoliation techniques.

Negatives

This process requires high temperature for the reaction and use of hazardous chemicals for the reaction. This technique is time consuming and need specialized handling (Seravalli et al., 2021). The reactant and the resulting gas in this process have the potential to ignite, explode, or be toxic. Consequently, it is necessary to implement environmental safeguards and, at times, corrosion prevention measures.

2.4.2.4. Hydrothermal method

The hydrothermal method is a highly efficient process for exfoliating and synthesizing nanosheets of MoS_2 with adjustable characteristics. The fundamental principle entails the dissolution of precursors in water at elevated temperature and pressure, facilitating a specific formation and expansion of MoS_2 phases (Duraisamy et al., 2021).

Positives

The hydrothermal approach has the benefits of straightforward operation and the ability to generate particles with diverse morphologies and sizes. Its primary application is in the manufacture of MoS_2 with varying shape and structure such as nanosheets, nanorods, and microflowers (Lang et al., 2023).

Negatives

The experimental results are significantly influenced by the reaction temperature and reaction duration, making it challenging to directly create single-layer MoS_2 (Liu et al., 2020).

2.4.2.5. Liquid phase exfoliation

There are various strategies to exfoliate MoS_2 due to its exceptional photoelectric characteristics and prospective applications in the biological arena. Currently, the primary methods used to create single-layer MoS_2 are physical and chemical techniques. Mechanical stripping and laser refining are physical procedures that employ micromechanical forces to separate the atomic layers of MoS_2. Nevertheless, these techniques are both time-consuming and require a significant amount of manual labour, making them unsuitable for large-scale production that demands exceptional quality (Zhang et al., 2018). The chemical technique employed is liquid phase exfoliation, which relies on the introduction of molecules from a solution, such as

lithium ion (Li^+), sodium ion (Na^+), bovine serum albumin (BSA), and polyvinylpyrrolidone (PVP), between the atomic layers of MoS_2. The subsequent separation is achieved using chemical forces or ultrasonic treatment (Varrla et al., 2015; Zhang et al., 2018).

Advantages include, liquid-phase ultrasonic exfoliation is unaffected by the presence of water and air, making it well-suited for large-scale manufacturing. Additionally, the resulting sheets may be easily assembled into films. This method also possesses the advantageous quality of being universally applicable and straightforward to use. There are environmental and financial benefits to exfoliating MoS_2 in aqueous media rather than organic solvents. Disadvantage of this approach is that controlling the degree of exfoliation is a challenging task.

2.4.2.5.1. Ultra-Sonication

The sonochemical method is known for its fast chemical reactions because of the unique reaction effect of the ultra sound irradiation, this method has a rapid reaction rate, controllable reaction conditions and the ability to form NPs with uniform shapes, narrow size distributions and high purity (Esmaeili-Zare et al., 2012).

A sonication equipment generates ultrasound waves that can travel through any material, including solids, liquids, and gases. MoS_2, a two-dimensional layered material, possesses excellent elastic characteristics. Consequently, the ultrasonic waves will compress and rarefy, causing the molecules in the medium to be affected. This motion will then be transferred to nearby molecules, resulting in an energetic behaviour within the solution containing bulk MoS_2 (Jiang et al., 2015). Sonication ultimately affects the average intermolecular distance, causing it to either decrease or increase. When the average distance between molecules exceeds the critical molecular distance, a significant negative pressure is generated in the liquid. This process causes the molecular connections to disintegrate, resulting in the formation of empty spaces and cavities, which are filled with vapours and form micro bubbles. To generate cavitation bubbles, the negative pressure must surpass the inherent cohesive forces within the solution. The process of cavitation bubble formation advances to growth and finally bursts abruptly and forcefully, resulting in the generation of high-pressure jets that strip away the layers (Mason et al., 2002; Niu et al., 2016).It involves using

ultrasound to help the solvent interact with the exfoliated bulk materials in a way that minimises the surface energy of 2D nanomaterials. This allows the nanomaterials to be dissolved stably in the solvent without agglomeration or flocculation, thereby overcoming the van der Waals force between the layers. The use of sonication to assist in the exfoliation of layered solids is now universally recognised as the most effective method for producing high concentrations of single or few layered nanosheets in dispersion. Sonication induces shear forces by the implosion of cavitation bubbles, which can detach the layers. Various exfoliation techniques are enumerated in Table 2.2 to illustrate the effective synthesis of MoS_2 nanomaterials.

Table 2.2. Different exfoliation techniques for synthesis of MoS_2 nanosheet

Method	**Exfoliator**	**Treatment**	**Advantages**	**Drawbacks**	**Reference**
Ion intercalation	n-BuLi	Ultra-sonication	Singnificant dimension, high production and exceptional ability to disperse	Lower rate of reaction, prolonged reaction time, and stringent reaction criteria Insufficient output, limited dimensions, and demanding operational conditions The operation costs of the device are high, and there is a risk of damaging the original semiconductor	Fan et al., 2015
	Lithium				Yuwen et al., 2016
	Sodium naphthalenide				Luxa et al., 2016
	Sodium dodecyl benzene sulfonate (SDBS)				Guan et al., 2015
	Sodium alginate (SA)				Xuan et al., 2017

				properties of the materials.	
BSA-induced	BSA	Sonication	Exfoliator as well as stabilizer, improves biocompatibility, better yield, good dispersion in water, thinner nanosheets, Excellent stability, minimal toxicity, and a high ratio of surface area to mass.	Denaturation of protein molecule at extreme physical conditions	Coleman et al., 2011; Smith et al., 2011; Guan et al., 2018; Deng et al., 2016; Liu et al., 2016; Guan et al., 2015
PVP-mediated exfoliation	PVP (ethanol solution)	Ultrasonication	aggregation resistance, even dispersion after freeze-drying,	Solvent incompatibility	Liu et al., 2012
	PVP aqueous solution	Grinding +sonication			Daniloska et al., 2014
	PVP	ultrasonication-milling	synergistic effect showed highest		Dong et al.,

			exfoliation with better yield		2016
	PVP		high yield, good biocompatibility, low cytotoxicity and small size.		Yu et al., 2016; Yu et al., 2018
	PVP	pulsed laser ablation	-		Han et al., 2018
Chemical	SDBS	solvent-surfactant assisted sonication	stable dispersions	-	Rani et al., 2021
	NMP (N-methylpyrrolidone), cyclohexane, n-hexane and ACN (acetonitrile)	abrasive-assisted ultrasonic exfoliation	thinner nanosheets	-	Nguyen et al., 2015; Xu et al., 2014; Vasi et al., 2024
	DMF as solvent	CO_2-assisted ultrasound exfoliation	Transverse size obtained was 0.5~2μm	-	Mukherjee et al., 2015
	IPA/water as solvent	LPE	Thickness :3-5nm	Better lateral size with fine sheets	Akeredolu et al.,2024
Surfactant	SDS, SDBS, SHS	LPE	Less than 10nm	Stabilized enhanced yield	Pozzati et al.,2024
Green synthesis	Hemicellulose	LPE	8-9 layers	Ecofriendly, simple, and mass production	Aksorngul et al.,2024

2.5. Synthesis of MoS_2 nano-heterostructures

MoS_2 carries some drawbacks which limits its practical application i.e. low absorption coefficient and high rate of recombination by electron-hole pair (Melnikova-Kominkova et al., 2019; Munoz et al., 2022).These drawback can be overcome by mainly two ways one is to decrease the size of MoS_2 nanostructure second is to make the hybrid with other conducting/semiconducting nanomaterials (Cui et al., 2017; Fioravanti et al., 2023).There are several reports present in the literature where MoS_2 is decorated with other semiconducting materials that not only improves the recombination rate but also enhance the charge flow to the pollutants and indirectly improves the efficacy of photocatalysis(Ghasemipour et al., 2020; Zhang et al., 2016). Various researchers have synthesized several MoS_2 based nanocomposites (doping, heterostructures etc.) that effectively degrade the different dyes and other environmental pollutants by utilizing visible part of the sunlight. Sehrawat et al. have fabricated Cu_2O decorated MoS_2 nanostructure using precipitation method for the treatment of indigo carmine dye photocatalytically (Sehrawat et al., 2022). Li et al. have synthesized CuS/ MoS_2 nanocomposite for the efficient treatment of MB and RhB dye piezocatalytically (Li et al., 2022).Furthermore, a one step hydrothermal technique was used to synthesize molybdenum disulfide/tin oxide (MoS_2/SnO_2) composite as successful photocatalyst for photoreduction of hexavalent chromium and photodecomposition of MB (Szkoda et al., 2022).The hydrothermal technique is considered to be promising for the synthesis of novel nanoheterostructures.Relatedly, MoS_2@coniferous ZnO have been synthesized using hydrothermal technique which acted as efficient photocatalyst for the degradation of MB and RhB along with 5 times reusability of hybrid(Kao et al., 2023).Rahaman et al. have decorated the MoS_2 nanoflowers with Co_3O_4 NP hydrothermally to effectively degrade the MB(Rahaman et al., 2023).Moreover, a ternary Z-Scheme $LaFeO_3/MoS_2$/graphene nanocomposite photocatalyst (facile two-step hydrothermal approach) have been shown high efficiency and stable performance toward the photodegradation of MB (Huang et al., 2023). Similarly, Tahir et al., have fabricated a ternary hybrid (Silver tungstate/ MoS_2 /graphene) for the photocatalytic degradation of methyl orange (MO) using direct

sunlight (Tahir et al., 2023). Recently, Rajan et al, have incorporated the perylene NPs on MoS_2 for effective photocatalytic performance against MB, RhB and crystal violet (CV) dyes under sunlight (Rajan et al., 2023).

From a list of hybrid materials, graphene is good template which comprises sp^2 arrangement consists of carbon atoms organised in a hexagonal lattice resembling a honeycomb structure.It serves as an excellent charge carrier semiconductor. In addition, when the size of graphene is restricted to quantum regime, it acts as an electron conducting surface and channel which increases the oxidation process manifolds in photocatalysis. The fabrication of co-catalyst i.e. graphene quantum dots (GQDs) with MoS_2 will provide positive synergistic effect to enhance the photocatalytic degradation of dyes by producing stronger interface effect and retarding the formation of an electron-hole pair through recombination (Cui et al., 2017). Due to enhanced interfacial charge transfer, the photo-generated electrons could be easily transferred onto graphene which lead to effective separation of photo-generated electrons and holes, and thus improves the photocatalytic performance (Zhang et al., 2016).In this heterostructure nanocomposite (MoS_2@GQDs), more reactive sites and photogenerated holes are being provided to participate in photocatalysis.

2.6. Environmental pollution due to azo dye

2.6.1. Azo dyes

Azo dyes are a type of synthetic organic dyes that are identified by the presence of one or more azo groups (-N=N-) linking aromatic rings. These links might be broken enzymatically to produce aromatic amines. Their structure can be shown as Ar-N=N-Ar', with Ar and Ar' representing aromatic groups (Ajmal et al., 2014).

Azo dyes are commonly employed for the purpose of imparting colour to several materials, including textiles, paper, food products, beauty products, pharmaceuticals, and various other applications (Eltaboni et al., 2022).

1. Amphoteric nature: A variety of functional groups, including carboxyl, hydroxyl, amino, and sulfonyl, are responsible for their amphoteric characteristics. Both hydrophilic and hydrophobic azo dyes have the potential to be degraded or reduced extracellularly and intracellularly by bacteria, respectively (Zafar et al., 2022).

2. Water soluble: Azo dyes are water soluble because their structural backbone contains a variety of polar functional moieties (Bafana et al., 2011).

2.6.2. Synthesis

The main reaction mechanism behind synthesizing azo dye is two step methodology; Diazotization reaction followed by coupling reaction. The initial stage involves the diazotization process, in which a primary aromatic amine, such as 4-aminophenol, is transformed into a diazonium salt through the reaction with sodium nitrite ($NaNO_2$) in the presence of hydrochloric acid (HCl) at low temperatures ranging from 0 to 5 degrees Celsius. An unstable diazonium ion intermediate is formed. Next, in the coupling reaction, the diazonium salt has a reaction with an aromatic chemical that possesses a surplus of electrons, typically a phenol or an aromatic amine. This reaction commonly takes place at either the para or ortho position with respect to the activating group on the aromatic ring, resulting in the creation of the azo bond (-N=N) (Gürses et al., 2016).

2.6.3. Useful caharacteristics

Azo dyes are widely used because of their chemical adaptability, generates various vivid colors. They also do not smell bad, light and moisture resistant, inexpensive, easily available, reliable, and constant and persistant (Mahmoodi et al., 2016; Barciela et al., 2023).

2.6.4. Toxicity

The toxic effect of azo has been summerized in the following table 2.3.:

1. Mutagenic: Azo dyes are known for their mutagenic property. These dyes act as mutagen and cause various genetic and chromosomal abrreations (Hashemi et al., 2022).

2. Azo dyes exhibit low susceptibility to oxidation in the presence of oxygen at biological treatment facilities (Rathi et al., 2022).

3. Formation of some toxic products occurs on degradation of azo dyes. These toxic byproducts attacks on the microbiota present on the skin and intestine, leading to conversion into carcinogenic metabolites (Gottlieb et al., 2003; Feng et al., 2012).

Table 2.3. Harmful effects of azo dyes on humans

Azo dye	**Application**	**Harmful effect**	**Reference**
Congo red	Pharmaceutical	bladder cancer	Feng et al., 2012
Acid orange 6		Mutagen,	
Tartrazine	Pharmaceutica & Cosmetics	Mutagenic, cytotoxic, genotoxic	Floriano et al., 2018
Sunset yellow (FD&C 6)	food and drug colorants	Genotoxic and cytotoxic	Khayyat et al., 2018; Qu et al., 2017
Amaranth	Food	Genotoxic, allergic, asthama causing	Uysal et al., 2017
Allura Red	Food	Allergic, chromosome damage	Rajan et al., 2017
Disperse Blue 373, CI Disperse Violet 93	Textile	Mutagenic and carcinogenic	de Lima et al., 2007
Congo red	Paper and textile	mutagenic, teratogenic, and carcinogenic	Siddiqui et al., 2023

Eriochrome Black-T (EBT)	Textile	Toxic and carcinogen	Khalid et al., 2018
MO	Textile and paper	Toxic, carcinogenic, mutagenic	Iwuozor, et al., 2021
Methyl Red	Textile, food	Mutagenic dye	Saha et al., 2022
Sudan 1	Food, cosmetic	Carcinogenic, mutagen	Stiborová et al, 2002
CV	Textile, printing	Genotoxic, cytotoxic, corneal and conjunctiva irritation, skin & respiratory problems	Mani et al., 2016
MB	Textile, printing	Fatal serotonin toxicity, central nervous system (CNS) toxicity, carcinogenic,respiratory disorders,teratogenic,mutagenic	Oladoye et al., 2022; Majeed et al., 2024; Vo et al., 2024

2.7. Methylene blue

2.7.1. Chemical structure:

Methylene blue (MB) is an aromatic heterocyclic dye having molecular weight of 319.85g mol^{-1}. It was first synthesised by Heinrich Caro in 1800 (Pomicpic et al., 2020). MB is a cationic and primary thiazine dye belonging to the class of polymethine dyes. It contains an amino autochrome unit and is a positively charged molecule (Allen et al., 2005; Anushree & Philip 2019). According to IUPAC, chemical name of methylene blue is (3,7-bis(dimethylamino) phenothiazine chloride tetra methylthionine chloride), featuring a colour index of 52015.The chemical formula of methylene blue is $C_{16}H_{18}N_3ClS$ and its maximum absorbance is at 663-

665nm. Methylene blue is a basic dye and a redox indicator, however it is not a pH indicator. It is extensively utilised in the textile industry as well as biological applications.

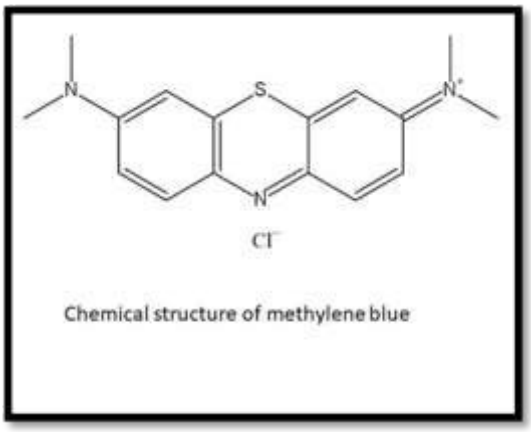

Figure 2.1. Chemical structure of Methylene blue

2.7.2. Properties

MB have properties of solid powder form in dark green colour without any odour at room temperature and exhibit deep blue colour when mixed with water. MB is having two states: oxidized and reducing. In the oxidizing stage, it imparts deep blue colour due to its chromophore group as well as an auxochrome group. Its chromophore group consists of a conjugated system between nitrogen and sulphur on the core aromatic heterocycle. On the other hand, its auxochrome group is made up of nitrogen-containing groups that have lone pair electrons on the benzene ring (Yang et al., 2017; Khan et al., 2022).

After the use of MB, the released effluent containing the dye in environment causes the toxicity due to its recalcitrant nature. It readily dissolves in water, contaminating aquatic ecosystems, which subsequently affects other environmental systems utilised by many organisms, resulting in habitat disruption.

2.7.3. Uses

MB has been referred to as a "photosensitizer," which implies that it could absorb light and transmit that energy to another substance (Kirk-Othomer encyclopedia, 1981). MB is used for various therapeutic procedures and diagnostics. It was used as antimalaria agent in late 19^{th} and early 20^{th} centuary (Lu et al., 2018). It is used as

photodyanamic inactivating agent of RNA viruses like hepatitis B, hepatitis C and HIV in plasma and help in treating cancer. It is a leading compound for development of chlorpromazine, a tricyclic antidepressant and helps in detecting various difficult neuroendocrine tumours like insulinoma. The textile industry is the one that uses MB the most frequently because of its ability to adhere tightly to fibre interstitial gaps, making it a preferred fabric colorant. Also, in several other fields MB is used as photosensitizer as redox indicator and trace analysis of anionic surfactants, as dye sensitized material in solar cells, microbial fuel cells and sensors also.

2.7.4. Toxicity of Methylene Blue

MB is a cancer causing (carcinogenic) and non-biodegradable dye (pollutant) which causes distress to life forms (Patel et al., 2024). It causes severe effect on human health by mental disorder, abdominal distress like diarrhoea, stomach pain, vomiting, nausea, gastritis etc, and skin and eye problems too. A direct disposal of these dyes in the waterstreams without any treatment rise the chemical oxygen demand (COD) concentrations leading increased toxicity in water systems (Mohammed et al., 2014; Rahmiana et al., 2022). MB has high molar absorption coefficient ~8.4×10^4 L mol^{-1} cm^{-1} at 664 nm due to which it hinders the sunlight transmittance and lowers the solubitility of oxygen in water. Low availability of oxygen and light affects the photosynthetic efficiency of aquatic life and produce negative impact on diversity and aesthetics of the biological community (Zhou et al., 2019; Lawagon et al., 2019; Ahmed et al., 2018; Kosswattaaracchchi & Cook et al., 2018).

2.8. Photocatalysis

Photocatalysis is a versatile technology that efficiently produces reactive oxygen species (ROS) when exposed to light.

The dye can be degraded by various ways:

1. Breaking of azo double bond;
2. Sequential demethylation and hydration of MB structure
3. Detachment of sulfonated group from the ring
4. Cleavage of C-N bond in dimethylamino group and between the aromatic ring and azo bond.

5. Involvement of radicals.

A researcher explained the process of photocatalytic degradation of methyl orange using titanium oxide nanoparticles, which resulted in demethylation, breaking of the C-N bond between the aromatic ring and azo bond, and cleavage of the -N=N- bond (El Mragui et al., 2021). The photocatalyst and sunlight are essential for the efficient degradation of the dye. The sunlight triggers the excitation process of the semiconductor by generating electron-hole pairs on the catalyst surface. The azo bonds may undergo oxidation by positive (holes or hydroxyl radicals), or reduction by electrons in the conduction band. Similarly, the CaO molecules have undergone excitation in the presence of sunlight, resulting in the transfer of an electron to the conduction band. This is followed by the reduction of molecular oxygen and the creation of the superoxide radical. The superoxide radicals produce hydroxyl radicals through the reaction with hydrogen peroxide or organic peroxide. These hydroxyl radicals (·OH) function as powerful oxidising agents, leading to the degradation of dye (Madhusudhana et al., 2012). In a separate investigation, the dye molecule functions as a photosensitizer upon being struck by a photon. The resulting photogenerated charged species then interact with absorbed O_2 and H_2O molecules, leading to the formation of ·OH as well as superoxide radicals ($\cdot O_2$).

The radicals undergo a chemical reaction with the dye molecules, causing their degradation (Borthakur et al., 2017). In addition, the CN-TiO_2/$ZnFe_2O_4$ nanocomposite effectively decomposed the direct red 16 dye that was present in the water or wastewater. The small energy difference between the valence band and conduction band in $ZnFe_2O_4$ allows electrons to be excited from the valence band to the conduction band, resulting in the formation of holes on the catalyst's surface. When the electrons in the conduction band (CB) of $ZnFe_2O_4$ are exposed to light, they can move to the conduction band of TiO_2. In this new location, they can react with dissolved oxygen (O_2) to produce reactive oxygen species ($O_2^{\bullet-}$, H_2O_2•, and •OH) (Zangeneh et al., 2020). In a similar manner, the NGO/ZnO nanocomposite underwent a three-step process to degrade the rhodamine B dye: 1) N-deethylation, 2) cleavage

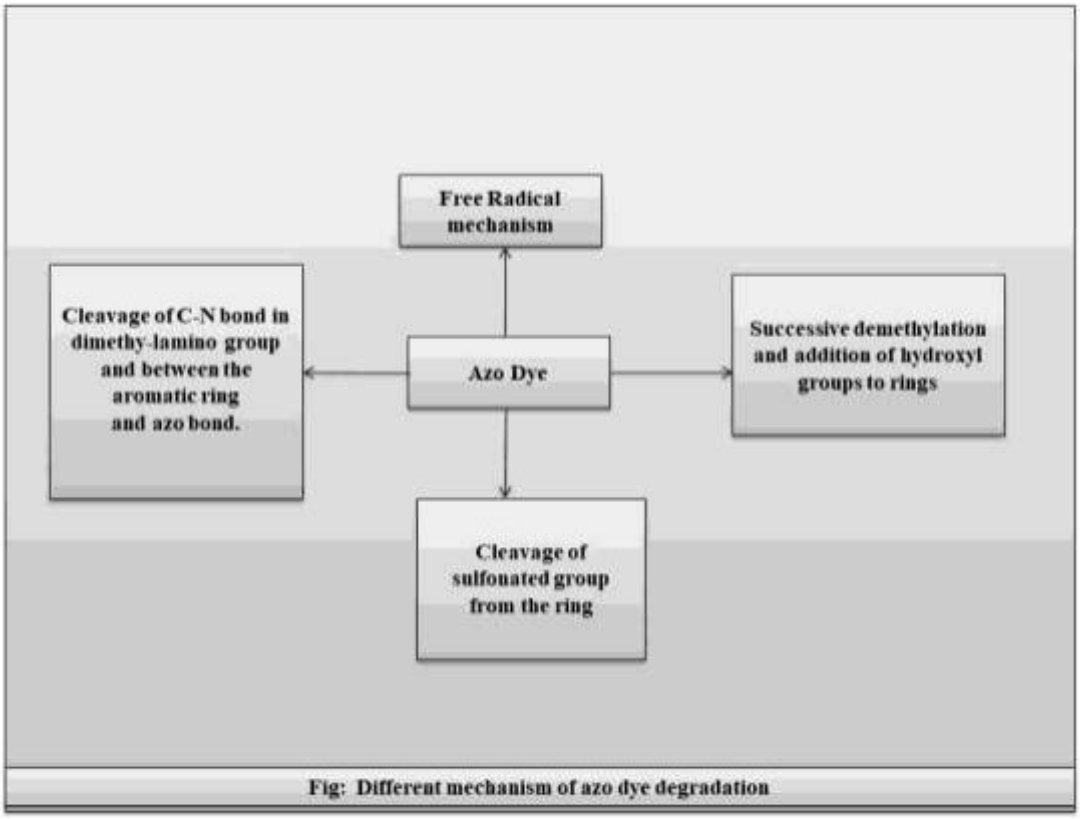

Figure 2.2. Different mechanisms of azo dye degardation

of the chromophore, and 3) mineralization of the dye. When a photon interacts with a nanocomposite, the electrons in the valence band become energised and go to the conduction band, acquiring energy that is equivalent to or more than the band gap energy. The positive hole reacts with water, generating hydroxyl radicals that swiftly attack dye molecules both on the surface and in solution. This process mineralizes the dyes, converting them into water, carbon dioxide, nitrate, and NH_4^+ (Mathew et al., 2020).

2.8.1. Mechanism of photocatalysis

The process of dye degradation utilising MoS_2 nano-structures can be elucidated by two primary pathways: the conventional mechanism and the Z-scheme mechanism.

2.8.1.1. Conventional method:

In the presence of UV or solar radiation, when the photon energy is more than the band gap of semiconductor, then the electrons are excited from valence band to

conduction band. This led to the formation of holes (positively charged) and free electrons (negatively charged) in the valence and conduction band, respectively.

Unlike other approaches, inhere because of oxidation and reduction of pollutants by electron and holes, the contaminants are converted into relatively non-toxic products such as, carbon dioxide and water (Ayodhya et al., 2018; Lee et al., 2017; Shubha et al., 2022).

2.8.1.2. Z-scheme mechanism

The Z-scheme mechanism entails an electron transfer process that occurs in a zig-zag pattern. Under the influence of light irradiation, electrons transition from the valence band to the conduction band and subsequently relocate to the valence band of the closest atom. This mechanism has been suggested for binary systems such as MoS_2 /g-C_3N_4 and ternary systems such as MoS_2 /CdS/TiO_2 (Jaleel et al., 2022).

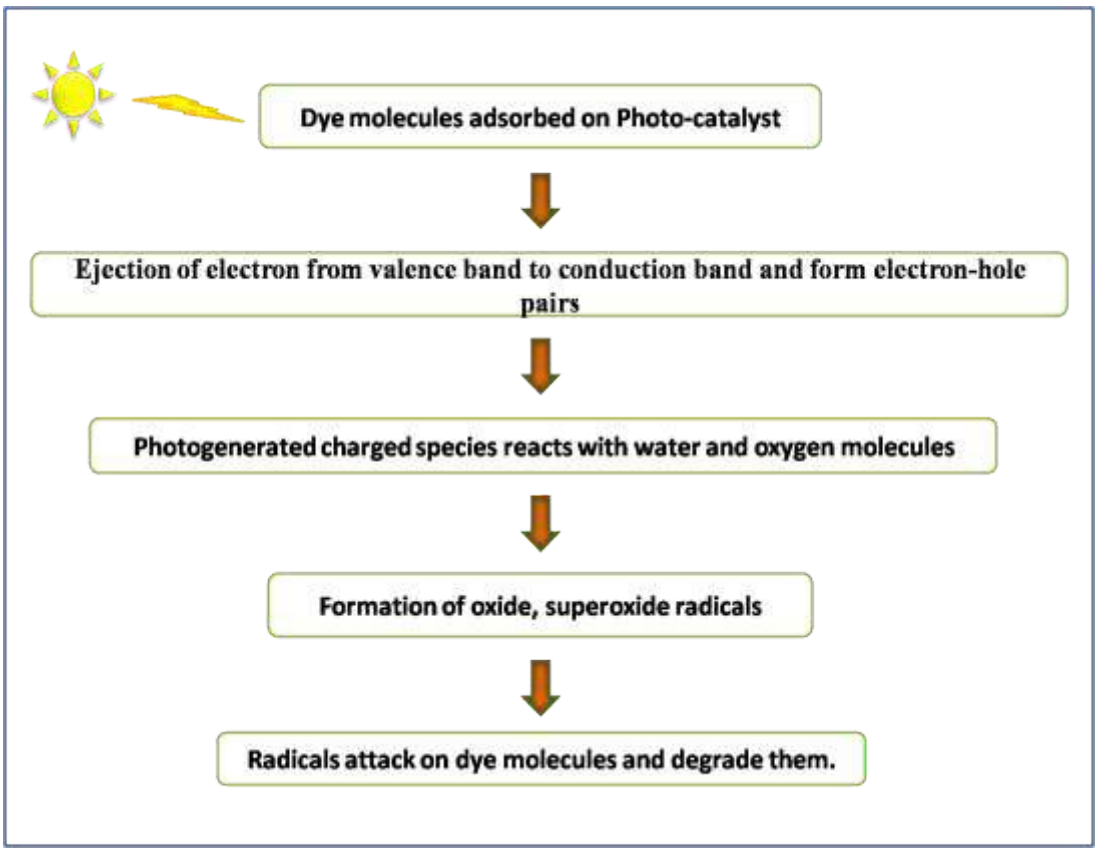

Figure 2.3. Flowchart showing the mechanism of photocatalysis

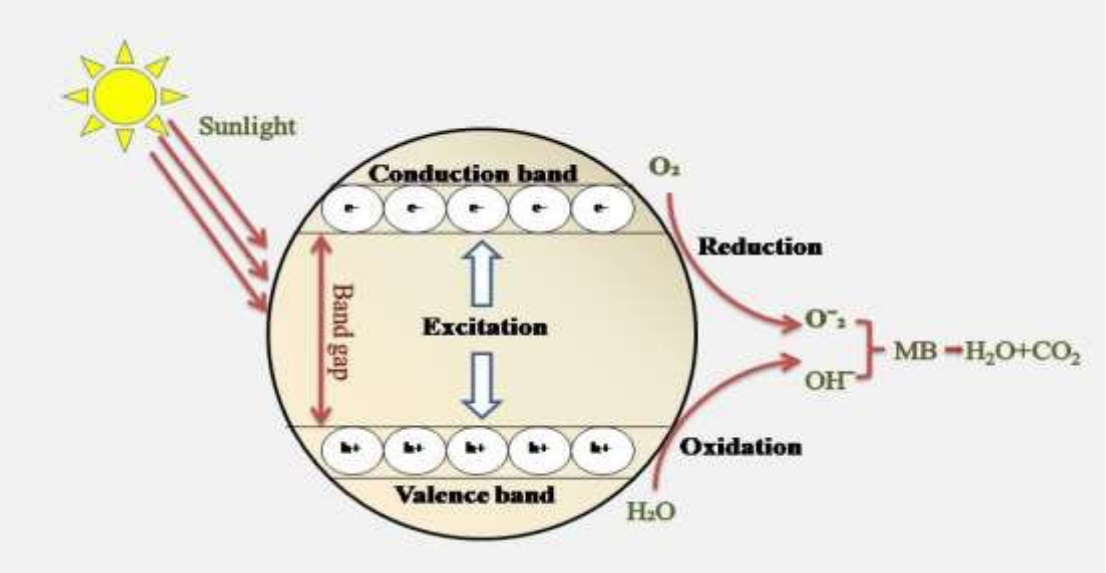

Figure 2.4. Effective reactive species involved in the photodegradation

2.8.2. MoS_2 nano-structures mediated photocatalysis of methylene blue

MoS_2 nano-structures and their heterojunctions are well known for their photocatalytic activity. Various researchers have studied the photodegradation of MB using MoS_2 nano-structures. A table (2.4) is included, highlighting various research that list MoS_2 nanocomposites functioning as photocatalysts for the degradation of different dyes.

Table 2.4. Different MoS_2 nano-heterostructure acted as photocatalyst to degrade MB

Nano-composite	**Dosage**	**Dye Conc.**	**Time**	**Removal (%)**	**References**
MoS_2/ZnO nanorods	0.15 g/L	-	20 mins	90	Ritika et al., 2018
Bi_2O_3/MoS_2 heterojunction	50 mg/ 50mL	10mg/L	100 mins	100	Ma et al., 2019
Layered MoS_2	0.05g	-	120 mins	80-97	Kisała et al., 2023
MoS_2/TiO_2	5mg/50ml	10 mg/L	5 h	100	Khan et al., 2018

MoS_2-FeZnO	0.15g	20mg/L	140 mins	95.2	Ghalajkhani, et al., 2018
Flower like MoS_2/TiO_2	25mg/200 mL	10mg/L	120 mins	99.5	Mutyala et al., 2020
MoS_2-GO	10mg/50 mL	10 ppm	60 mins	99	Ding et al., 2015
Mn@ MoS_2	-	-	55 mins	97	Sasi et al., 2023
Mn-doped Bi_2WO_6-GO/ MoS_2	50 mg/100ml	10 ppm	60 mins	99	Tahir et al., 2022
MoS_2	1 mg	10^{-5}	180 mins	43.5	Al Qaydi et al., 2024
MoS_2 nanobox graphitic-C_3N_4@TiO_2	30 mg/50 mL	10 ppm	60 mins	97.5	Karpuraranjith et al., 2022
MoS_2 nanostructure	-		70 mins	96	Sankaranarayanan et al., 2024
MoS_2/ TiO_2	-		120 mins	98.5	Chen et al., 2024
MoS_2/ carbon	10mg	-	90 mins	98	Adaikalapandi et al., 2024

2.9. MoS_2 as electrochemical sensor

MoS_2 has been considered as a better electrochemical sensor for real samples. For instance, a 3-D electrochemical sensor is constructed by physical deposition of MoS_2 nanosheets on the glass carbon electron for the detection of sulfamerazine in pork and

chicken samples showing limit of detection of 1.1×10^{-7} molL^{-1} with 86.0% to 102.0%, recovery (Sun et al., 2019). Similarly, the presence of cytotoxic and genotoxic agent trichloroacetamide (TCAM) can also be detected in the drinking water by hetero MoS_2 nanosheet (AgNPR@ MoS_2).The sensor provides the sensing ranges from 0.5−10 μM and 10−80 μM with LOD of 0.17 mM (Fang et al., 2021). Eventhough, glass carbon electrode mounted with MoS_2 nanoflakes and titanium oxide nanoparticles provides detectability of the antineoplastic agent in human blood plasma and urine. The electrochemical sensor has been shown limit of detection and limit of quantification values 9.8 and 32.94 nM respectively with five independent times reuseability (Mehmandoust et al., 2021).

A bimetallic sulfide of MoS_2 covered Samarium sulfide (α-Sm_2S_3/ MoS_2) based electrochemical sensor is constructed to determine the antineoplastic drug 5-Fluorouracil (5-FU) in the serum and urine with linear range of 0.1–1166 μM, and the low detection limit (0.015 μM at S/N = 3) (Mariyappan et al., 2020). Sha et al., 2019 have prepared a single step hydrothermal micro-flower shaped MoS_2 nanosheets imprinted on aluminium foil used as electrochemical sensor for the non-enzymatic detection of uric acid from the human urine showing better sensitivity 98.3 ± 1 nA μM^{-1} with LOD of 1.169 μM responding in less than 3 seconds. It is a bioanalytical lab on chip sensor with better sensitivity, selectivity, reuseability and affordability (Sha et al., 2019). A novel hybrid of MoS_2 nanosheets loaded with bimetallic nanoparticles (PtNi) was casted on glass carbon electrode to determine the simultaneous presence of uric acid and dopamine in the human urine. The electrochemical sensor has shown the same LOD for both samples as 0.1 μM (S/N = 3) and linear range for dopamine and uric acid is 0.5–150 μM and 0.5–600 μM respectively (Ma et al., 2019).

However, a molecularly imprinted polymer/ Au nanoparticles-MoS_2-graphene/GCE sensor was synthesized hydrothermally for the electrochemical detection of rutin (flavonoid) in the medicinal tablets, ginkgo biloba and buckwheat tea with LOD of 4 nmolL^{-1} and L.R. 0.01–45.0 μmolL^{-1}(Wang et al., 2021). Similarly, the ascorbic acid has been detected from the vitamin C tablet with the GCE fabricated with MoS_2 nanosheets and gold nanoparticles. The limit of detection and linear range of

sensitivity were $2.1x10^{-6}$ mol/L (S/N = 3) and $7.1\times10^{-4} \sim 2.77\times10^{-3}$ mol/L respectively (Huang et al., 2021). Moreover, self assembled electrochemical sensor comprising MoS_2 nanosheets imprinted on pomelo peel carbon have been designed for taxifolin detection. The sensor presented better selectivity with limit of detection to be 2.3×10^{-8} $molL^{-1}$ (S/N = 3) (Zhang et al., 2021).

For biochemical studies, MoS_2 have shown remarkable sensing properties. Hydrothermally synthesized MoS_2 nanosheets assembled on pencil graphite provides quantification of guanine and adenine concentration in calf-thymus DNA with linear range of 15–120 μM and 15–120 μM respectively (Vishnu et al., 2019). A biosensor made up of overoxidized polypyrrole/multi-walled carbon nanotube and molybdenum disulfide modified glassy carbon electrode (PPyox/ MWCNTs-MoS_2/GCE) is designed due to its electro-catalytical properties for determination of guanine and adenine simultaneously with L.R. of 5–30 μM and 30–120 μM and LOD (S/N = 3) of 1.6 μM and 1.7 μM for guanine and adenine (Geng et al., 2019).

For the sensing of environmental pollutants, MoS_2 has been a promising sensor. A nitrite sensor is fabricated with gold nanoparticles modified molybdenum disulfide and reduced graphene oxide providing synergistic effect of MoS_2 NS and GO NS as well as better catalytic property of gold nanoparticle. The sensor exhibited low detection limit (0.038 μM (S/N = 3) within 3 seconds of response time with L.R. of 0.2 μM-2600 μM (Yang et al., 2022).

Chapter 3:

Hypothesis and Research Objectives

3.1. Hypothesis

There are several methodologies developed until now for efficient wastewater treatment that include adsorption, biological treatment, and coagulation. However due to several limitations, there has been a need to develop an efficient methodology with less time consuming, more economical, more efficiency that requires less energy,etc.However photocatalysis have emerged to overshadow the reprecussions obtained from these techniques.Along with,the green nanotechnology have ease the process by limitizing the drawbacks obtained from the nanoparticles obtained from the other routes.The potential application of dichalcogenides in treating wastewater is also preferred due to their extraordinary properties.The exfoliation of molybdenum disulphide to nanosheets using ultrasonication and microwave using biosurfactants enhances its surface to volume ratio ,crucial for the photocatalytic performance of photocatalyst.The surface modification of the obtained nano-structures with carbon based quantum dots emphasize on their improved surface, thermal, mechanical and optical properties.The synergistic effect of the improved surface functionalization can be a promising product for photocatalytic and electrocatalytic applications.

In the proposed study, various biosurfactants will be explored for the liquid phase exfoliation of MoS_2 for wastewater treatment. The obtained nano-structures will be functionalized with quantum dots to generate MoS_2 nano-heterostructures and their potential application as photocatalyst and electrochemical sensor will be tested against azo dyes and antibiotic.

3.2. Research gap

There are myriads of research papers on the dye degradation but still the need for reliable/efficient, cost-effective, and eco-friendly treatment prevails. In addition, antibiotic presence in wastewater leads to antibiotic resistant. However, detection of antibiotics using nanomaterials prepared through chemical approach leads to pollution. The proposed work would be a greener alternative to the conventional dye treatment and antibiotic detection methods.

New greener material would be designed or unlocked for dye degradation future policies to solve the industrial as well as environmental problem. Green synthesis of

nano-structures will be more promising than the nano-structures obtained from other routes.

The synergistic effect of superstructure of MoS_2 will have significant contribution to effluent treatment.

3.3. Research Objectives

The research gap was addressed by following objectives:

- Biosurfactant mediated synthesis of MoS_2 nano-structures and its characterization.
- To prepare the MoS_2 nano-heterostructures with carbonaceous quantum dots through greener route and its characterization.
- Photocatalytic degradation of azo dyes using MoS_2 nano-heterostructures.
- Electrochemical sensing of antibiotic drug using MoS_2 nano-heterostructures.

Chapter 4:

Material & methods

4.1. Biosurfactant mediated synthesis of MoS_2 nano-structures and its characterization.

4.1.1. Selection of biosurfactant

After reviewing the literature, three biosurfactants, Gum Arabic, sodium alginate, and stem extract of T*inospora cordifolia* were selected.

4.1.2. Preparation of aqueous solution of Biosurfactant

The preparation of aqueous solution of biosurfactant was done by following some modifications in the methodologies followed by researchers (Xuan et al.,2017; Kesarla et al., 2014)

4.1.2.1. Preparation of aqueous solution of gum arabic

Gum arabic solution was prepared by adding 2 g of gum arabic to 250-mL beaker and 100 mL double distilled water (DDW) was added slowly. The mixture was subjected to stirring with a glass rod for 2–3 min. A homogeneous mixture was formed by heating the solution to 60°C for 30 minutes (Xuan et al., 2017).

4.1.2.2. Preparation of aqueous solution of sodium alginate

The aqueous solution of sodium alginate was prepared by mixing 1g of sodium alginate in 100ml of double distilled water. The solution was heated at 60-70°C for 15 minutes to make homogenous suspension of sodium alginate using heating mantle and stirred with the aid of glass rod. The aqueous solution of sodium alginate was kept for cooling (Xuan et al., 2017).

4.1.2.3. Preparation of aqueous solution of plant extract

1g of dried plant powder was added to 100mL of double distilled water followed by heating at 100°C until boil. After a complete boil, the solution was kept for cooling

and filtered using whatmann filter paper. The filtrate was collected and stored to be used as exfoliating agent (Kesarla et al., 2014).

4.2. **Synthesis of MoS_2 nano-structures**

100 mg of the bulk MoS_2 powder was added to the aqueous solution of biosurfactant (GA, SA, and PE) and placed in the bath sonicator for exfoliation. The sonication process lasted for 4 h at 70 W power output set at a 42 kHz frequency and the grayish color solution converted into dark green. The sample was ultra-sonicated using a bath sonicator of 2.5 L having temperature control. The sonicated solution is further exposed to microwave treatment at 900-Watt power for different time to get the desired product. Subsequently, the bulk material present in the suspension was removed by centrifugation at 3000 rpm for 15 min. The supernatant was centrifuged for 10 min at 6000 rpm to isolate the stable exfoliated MoS_2 nano-structures. Furthermore, the green-colored supernatant was collected. The obtained supernatant was placed in a hot air oven operated at 55 °C to get powdered MoS_2 NPs for characterization and applications (Kurapati et al., 2016; Coleman et al., 2011; Smith et al., 2011; de-Mello et al., 2010).

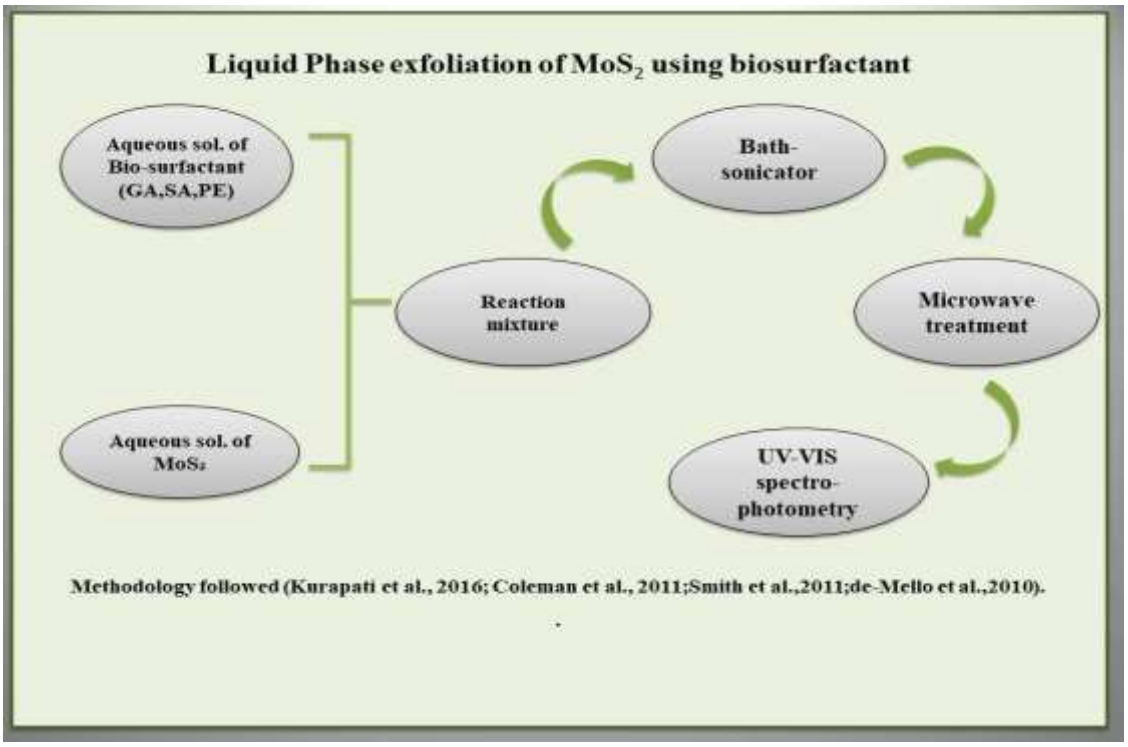

Figure 4.1. Overall methodology used for the LPE of MoS_2

Table 4.1. Different parameters used for the LPE of MoS_2

S.No	Bio-p.t	Biosurfactant surfactant (g/100mL)	MoS_2 conc. conc. (mg/100mL)	Sonication time(h)	Microwave treatment(mins)	H
1.	GA	2	100	4	20	7
2.	SA	1	50	4	20	4
3.	PE	1	100	4	20	7

4.3. Characterization of MoS_2 nano-structures

The investigation of optical characteristics of exfoliated MoS_2 NPs has been assessed using UV-vis spectroscopy. FTIR analysis was performed to indetify the biosurfactant coating of nanostructures. From the HR-TEM analysis, the morphology and internal

structure of the synthesized nanomaterial was obtained, as well as the average diameter and its crystal structure was obtained from XRD technique (Rani et al., 2020).

4.4. Synthesis of MoS_2 nano-heterostructures with carbonaceous quantum dots through greener route and its characterization.

1 g of MoS_2 nano-structures and 1 g of citric acid were mixed in pestle mortar to make a fine powder. The mixture was transferred to a glass beaker followed by heating at 300°C for 20 min. The liquid material was poured into pestle mortar and allowed to dry. The dried product was ground to a fine powder and washed with double distilled water to remove the unbounded GQDs from MoS_2. The filtrate was discarded and the washed fine powder was allowed to dry at 40-50 °C using a hot air oven.

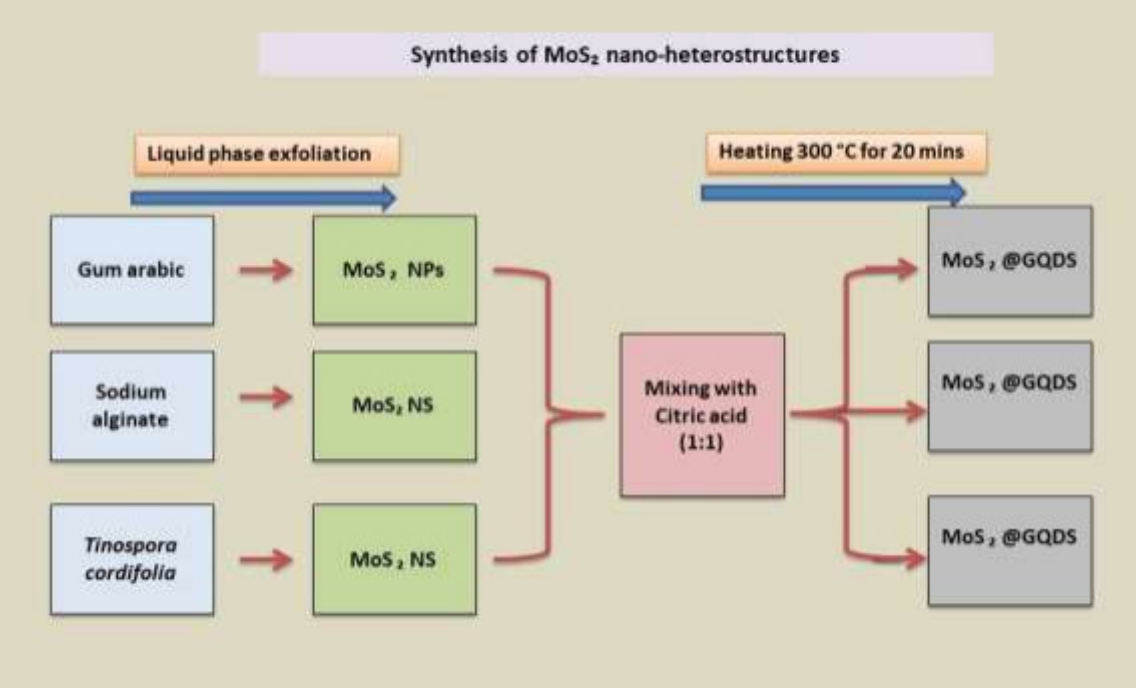

Figure 4.2. Overall methodology used for the synthesis of MoS_2 nano-heterostructures

4.5. Photocatalytic activity of MoS_2 nano-heterostructures

4.5.1. Photocatalytic activity of MoS_2 nano-heterostructures against methylene blue

The efficacy of MoS_2 nanostructure and MoS_2 nano-heterostructures was assessed by analyzing the rate of MB dye degradation under direct sunlight as reported in the literature (Sadhanala et al. 2018).. In this experimentation, 100 ppm (50 mL) aqueous solution of MB was treated with powdered MoS_2 nano-structures and nano-heterostructures at optimal pH. The reaction mixture was exposed to dark for 0.5 h to attain adsorption and desorption equilibrium and sunlight conditions for different intervals of time. After regular interval of time, 2 mL of the solution was collected and centrifuged at 4000 rpm for 20 min to remove the photocatalyst residues. The amount of dye was measured by recording UV–vis absorption at λ = 665 nm using UV–vis spectrophotometer, which has earlier also been reported to be the characteristic peak of MB (Fernández-Pérezand Marbán, 2020). In order to optimize the photocatalytic performance, various factors were standardized, concentration of photocatalyst, exposure time (irradiation), and pH. For elucidating the photocatalytic efficiency, different sets of samples were taken with varying concentration of photocatalyst (1–250 mg), irradiation time (0–8 h), and pH 3–11 range, respectively. To estimate the percentage (%) of degradation, the following equation is used.

Degradation (%) = $\frac{A_o - At}{A_o} * 100$ ……Equation (1)

where the symbols A_0 and A represent the absorbance before and after time "t" irradiation respectively.

Furthermore, the degradation kinetic was studied by normalized absorption C/C_0 plotted with respect to time

$\ln C/C_0 = -kt$……Equation (2)

where C is concentration at time t and C_0 is concentration at time $t = 0$.

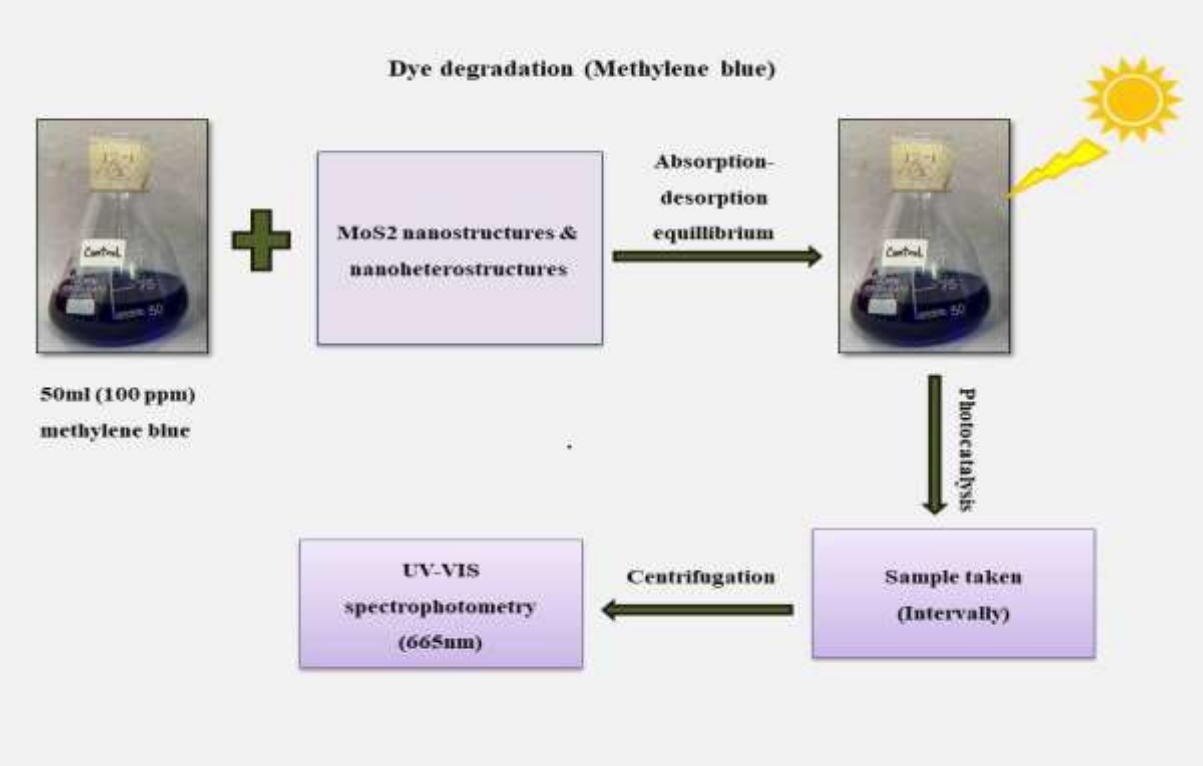

Figure 4.3. Overall methodology used for the photocatalytic activity of MoS_2 nano-heterostructures.

Table 4.2. Optimized conditions for MoS_2 nano-structures and nano-heterostructures for photocatalytic activity against MB.

S.No.	Photocatalyst	Irradiation time	Dose	pH	Sample taken
1.	GA- MoS_2 NPs	8 h	250 mg	7	1 h
2.	GA- MoS_2@GQDs	90 mins	250 mg	4	30 mins
3.	SA-MoS_2 NS	4 h	250 mg	9	1 h
4.	SA-MoS_2 @GQDs	30 mins	100 mg	9	10 mins
5.	PE-MoS_2 NS	1 h	50mg	9	15 mins
6.	PE-MoS_2 @GQDs	30 mins	20 mg	9	10 mins

4.5.2. Photocatalytic activity of MoS_2 nano-heterostructures against commercial blue

The photocatalytic activity of prepared nanostructure and nano-heterostructure was studied over the commercial blue (CB) dye (Atul direct blue 2 B (1.5%) under direct sunlight. To proceed with photodegradation analysis, optimized dose of MoS_2 nano-structures and nano-heterostructures was added to the 50 mL of 100 ppm CB solution and magnetically stirred for 30 min to achieve adsorption-desorption equilibrium followed by exposure to direct sunlight. Intervally, at a fixed time interval 2 mL of the reaction mixture was taken out and the collected sample was centrifuged at 4000 rpm for 20 min and supernatant was taken for evaluation of results. The concentration of dye was examined by UV-Vis spectrophotometer at maximum absorption (λ_{max} = 600 nm) of CB.

4.5.3. Photocatalytic activity of MoS_2 nano-heterostructures textile industrial sample

The green-synthesized MoS_2 nano-structures and nano-heterostructures were tested for their photocatalytic activity against the real textile waste sample containing MB at optimized conditions. To start with, optimized dose of powdered MoS_2 nanostructures and nano-heterostructures was added to 50-mL textile effluent at neutral pH and kept on a magnetic stirrer for 30 min to attain complete adsorption–desorption equilibrium. The reaction mixture samples were kept in the direct sunlight and intervally, 2 mL was centrifuged at 4000 rpm for 20 min followed by monitoring the absorption intensity measurement of real textile effluent at 550–555 nm (Fouda et al. 2021; Kaur et al., 2023).

4.6. Methodology for reusability of nanomaterial for photocatalyst

The reusability of MoS_2 nano-structures and nano-heterostructures for the photocatalytic degradation of MB under direct sunlight was successfully investigated. The nanomaterials were collected after centrifuging the reaction mixture after 1 cycle of photocatalytic degradation of MB. The centrifuged NPs were washed with ethanol to remove the MB residues attached to its surface and then dried at 60°C in hot air oven. The photocatalytic reusability of photocatalyst was evaluated by following same

protocol followed in first cycle. The dried photocatalyst were added to 50 mL of 100

ppm aqueous solution of MB and magnetically stirred in dark to obtain adsorption–desorption equilibrium. After 30 min, the reaction mixture was exposed to direct sunlight and sample was taken periodically to perform UV–vis analysis. Mainly, 5 cycles were run including initial cycle with 4 reuses (Saad Algarni et al. 2022).

4.7. Free radical trapping experiment

Free radical trapping experiment was performed to examine the contribution of hydroxyl and superoxide ions in the photocatalytic process. The complete test was done in three sets with triplicates. The experiment was conducted in the same manner as photocatalytic degradation of MB for set I, set II, and set III irrespective of addition of free radical scavengers (1 mM) in set II and set III. Two hundred fifty milligrams of photocatalyst was added to 50 mL (100 ppm) of MB for all three sets. Set I was taken as control and 1.0 mL of chloroform and DMSO was added in set II and set III. The reaction mixture was placed in direct sunlight and periodically sample was taken out for spectrophotometric analysis (Xu et al. 2018).

4.8. Electrochemical sensing of Ciprofloxacin using MoS_2 nano-heterostructures

The electroanalytical tests were conducted using a Metrohm Autolab electrochemical workstation (Model PGSTAT204N) equipped with a three-electrode setup. The setup included an Ag/AgCl reference electrode, a Pt wire auxiliary electrode, and a GCE working electrode. In addition, all experimental work utilised a citrate-buffer solution (CBS) with a pH of 7.4 as the electrolyte.

4.8.1. Fabrication of electrodes

This study utilised a drop-casting technique to create a glassy carbon working electrode (GCE). To generate the drop-casting solution, we mixed 5 mL of ethanol with 5 mg of biosurfactant mediated MoS_2@GQDs in a 1:1 proportion. Next, the solution was subjected to sonication for a duration of 30 minutes to acheive dispersion. Prior to alteration, we utilised alumina power slurries to clean and polish the unmodified GCE with a diameter of 3 mm, resulting in a surface that resembled a mirror. Subsequently, we subjected it to sonication in 100% ethanol followed by sonication in deionised water. Next, 5 µL of the 1 mg/mL MoS_2@GQDs suspension was carefully deposited onto the purified bare GCE surface and allowed it to desicate under a mercury bulb for a duration exceeding 10 minutes. After the drying process,

the GCE electrode, which had been either modified, now prepared for usage (Kumar et al., 2024).

4.9. Free radical scavenging activity of MoS_2 nano-structures and nanoheterostructures

The antioxidant activity was done using 2, 2-diphenyl-1-picrylhydrazyl (DPPH) method (Ahmad et al. 2022b; McDonald et al. 2001). The results were recorded as percentage of radical scavenging activity using 1 mg/mL ascorbic acid as standard and the antioxidant potentials of MoS_2 nanostructures and nano-heterostructures were observed. Methanolic ascorbic acid solution, 200–1000 μg/mL, and MoS_2 nanostructures and nano-heterostructures were mixed with 1 mL freshly prepared 0.3 mM methanolic DPPH separately. The solution was vortexed and thereafter incubated in the dark for 30 min at room temperature. Subsequently, the samples were analyzed at 517 nm using UV–vis spectrophotometer. DPPH was used as a control, and methanol was used as blank. The free radical scavenging activity was calculated as the percentage of inhibition using following equation (McDonald et al. 2001).

$$\% \text{ Activity} = \frac{OD\ of\ control - OD\ of\ sample}{OD\ of\ control} * 100$$

Here, OD represents the optical density.

4.10. Antimicrobial test

4.10.1. Test organisms

Bacterial strains, namely, *Escherichia coli* MTCC 295 and *Staphylococcus aureus* MTCC 7443, were used for antibacterial study.

4.10.2. Antimicrobial test

The glycerol stocks of *E. coli* MTCC 295 and *S. aureus* MTCC were cultured on Luria broth and were maintained at 37 °C for 24 h. Furthermore, 0.5 McFarland standard was used to adjust each strain to 10^8 cells/mL (Bhalodia and Shukla 2011). The antimicrobial effect of MoS_2 nano-structures and nano-heterostructures was determined by agar well diffusion method. Sterile spreader was used to spread the reference *E. coli* and *S. aureus* strains on the Muller Hinton agar media plates. Subsequently, six wells were made into the agar plates, with the help of 1000 μL tip. The five wells were separately poured with 100 μL of the synthesized MoS_2 nano-

structures, MoS_2 nano-heterostructures, citric acid, bulk MoS_2, positive, and negative controls. The streptomycin and sterile DDW were used as positive and negative control, respectively. The plates were incubated at 37 °C for 24 h. After incubation, the zone of inhibition was measured in millimeters (mm).

4.11. Safety testing of MoS_2 nanostructures and nano-heterostructures treated dye on human microbiota

Lactobacillus delbrueckii strain MTCC 10307 was used for safety testing. As a probiotic, it improves gastrointestinal health, strengthens immunity, and promotes a natural equilibrium of advantageous bacteria, so enhancing general well-being and supporting a better world. The effect of MB dye and MoS_2 nanostructures–treated dye on the growth of *L. delbrueckii* MTCC 10307 (a lactic acid bacterium) was studied using agar plate method. *L. delbrueckii* stock was revived in MRS (De Man, Rogosa, and Sharpe) broth and subsequently incubated at 37 °C for 24 h. In addition, nutritional agar plates were made, which contained dye samples that had not been treated, as well as dye samples that had been treated with **MoS_2** nanostructures and nano-heterostructures. *L. delbrueckii* culture culture was streaked on the plates with the help of an inoculating loop, and the plates were kept at 37 degrees Celsius for twenty-four hours in the incubator (Masi et al. 2021).The proliferation of the bacteria that are being studied on the MRS plate is evidence that the nanomaterials treated dye is favorable for the bacteria.On the other hand, the inhibition of bacterial growth demonstrates its harmful effect on the growth of bacteria.

Chapter 5:

Result & Discussion

5.1. Biosurfactant mediated synthesis of MoS_2 nano-structures and its characterization

5.1.1. Gum Arabic mediated synthesis of MoS_2 nano-structures

A simple, two-step, green process, and clean production of gum arabic–aided exfoliation and stabilization was implemented for the synthesis of MoS_2 NPs. Ultra-sonication and microwave-mediated exfoliation of MoS_2 was carried out in an aqueous solution of gum arabic. Sonication is one of the synthesis methodologies that can rapidly create MoS_2 NPs (Thangudu et al. 2020). Further, the synthesis is affected by various factors as discussed in the following sections.

5.1.1.1. Biosurfactant concentration

Six different concentrations of gum arabic solutions, 0.5, 1, 1.5, 2.0, 2.5, and 3.0 g/100 mL were examined for the optimization of bio-surfactant for the exfoliation of 100 mg of the MoS_2 powder (Fig. 5.1.(a)). To determine the optimum concentration, UV–vis analysis was performed to observe the absorbance intensity of exfoliated MoS_2. It was observed that 2g/100 mL of gum arabic have shown maximum peak compared to the rest of the concentration. Hence, 2 g/100 mL was the optimum gum arabic concentration for bulk MoS_2 exfoliation.

5.1.1.2. MoS_2 concentration

Furthermore, the experiments evaluating 1 mg/100 mL to 125 mg/100 mL bulk MoS_2 concentration at optimal 2 g/100 mL bio-surfactant concentration revealed that 100 mg/100 mL was the optimal MoS_2 concentration. After 4 h of sonication, the color of the solution changes and results into yellow to dark green color solutions using 1–125 mg/100 mL, respectively (Fig. 5.2.(b). The absorption spectrum showed a remarkable increase in peak with increase in concentration of MoS_2 till 100 mg; afterwards, the absorption intensity quenches probably due to the incapability of optimum concentration of bio-surfactant to exfoliate the higher concentration of MoS_2. These results revealed that 2.0 gm/100 mL of gum arabic solution and 100 mg/100 mL of MoS_2 concentration were considered optimum for the exfoliation process as the very low and high concentrations were not good for exfoliation process (Pu et al. 2012; Xuan et al. 2017).

5.1.1.3. Sonication time

To further investigate the optimal conditions studies, the sonication time was explored, as it is an important factor to achieve high exfoliation ratio. Fig.5.1.(c) shows there was an increase in the absorption intensity due to exfoliation of bulk MoS_2 to MoS_2 NPs with an increase in sonication time from 1 to 4 h. Furthermore, the color of solution changes to dark green revealing successful exfoliation. This is in agrrement with earlier studies (Rani et al., 2020). With increase in sonication time from 1 to 4 h, it was observed that there was increase in intensity revealing that there was increase in exfoliation along with decrease in number of layers of MoS_2 as compared to bulk counterpart (Kathiravan et al. 2019). The process of exfoliation in ultra-sonication showed significant increase in peak intensity with sonication time. However, using bio-surfactant-mediated exfoliation the same extent of exfoliation can be achieved in minimum time. Therefore, 4 h was taken as optimum sonication time for the exfoliation.

5.1.1.4. Microwave time

A step further to examine the effect of microwave, the sonicated samples was irradiated with the microwave. A single-mode microwave synthesis system was used for the experimentation. The sonicated MoS_2 was then exposed to microwave irradiation to explore its effect. The important part is to optimize the irradiation time. Therefore, effect of different irradiation times, 20, 25, 30, and 35 min with constant power, was also investigated as shown in Fig. 5.1.(d) (Wu et al. 2018). Samples irradiated for different time interval were centrifuged and the supernatant samples were subjected to UV–vis analysis. Spectral analysis revealed that 20 min of microwave irradiation is sufficient for the synthesis of fine MoS_2 NPs as blue shift stated after 20 min of microwave treatment.

5.1.1.5. pH

Additionally, the synthesis of MoS_2 NPs was affected by reaction mixture pH at optimized conditions of the synthesis. The pH range was taken from 2 to 11 in reaction mixture and it has been concluded that the basic conditions promoted the synthesis by providing the hydroxide ions that enhance the exfoliation of the MoS_2 layers up to pH 9. Thereafter, at higher basic pH, lower peak intensity was observed

that indicated poor stability of NPs synthesized (Fig 5.1.(e)). pH 7 was chosen for the synthesis as it makes the process green and clean as neutral pH has less or no adverse effect on the environment. To further check the significance of sequence of technique used for synthesis, the order of sonication and microwave treatment was reversed. The microwave irradiation treatment to the bulk MoS_2 was followed by sonication. It was found that reversing the process did not provide optimum results as clear from low peak intensity in MoS_2 NPs characteristic region (Fig 5.2.(a)). To examine the effect of sonication on bio-surfactant in terms of structural change, gum arabic was sonicated up to 7 h. The effect of sonication on gum arabic was negligible as no blue or red shift in the term of structure revealing its effectiveness to exfoliate in any sonication treatment (Fig 5.2.(b)). Furthermore, there was no effect on the UV–vis absorption of gum arabic in varying pH that indicated gum arabic can be used for the MoS_2 exfoliation at any pH conditions (Fig 5.2.(c)). The bare exfoliation experiments were conducted at optimal conditions in absence of gum arabic to find out the importance of gum arabic in synthesis of MoS_2 NPs. MoS_2 aqueous solution was subjected to sonication followed by microwave treatment using optimized conditions. The bare experiment did not result into exfoliation and synthesis of MoS_2 NPs as clear from absence of absorption peak in the MoS_2 NPs absorption region (Fig. 5.2.(d)). Hence, gum arabic was required as bio-surfactant for the synthesis of MoS_2 NPs at optimal physiochemical parameters used in this study.

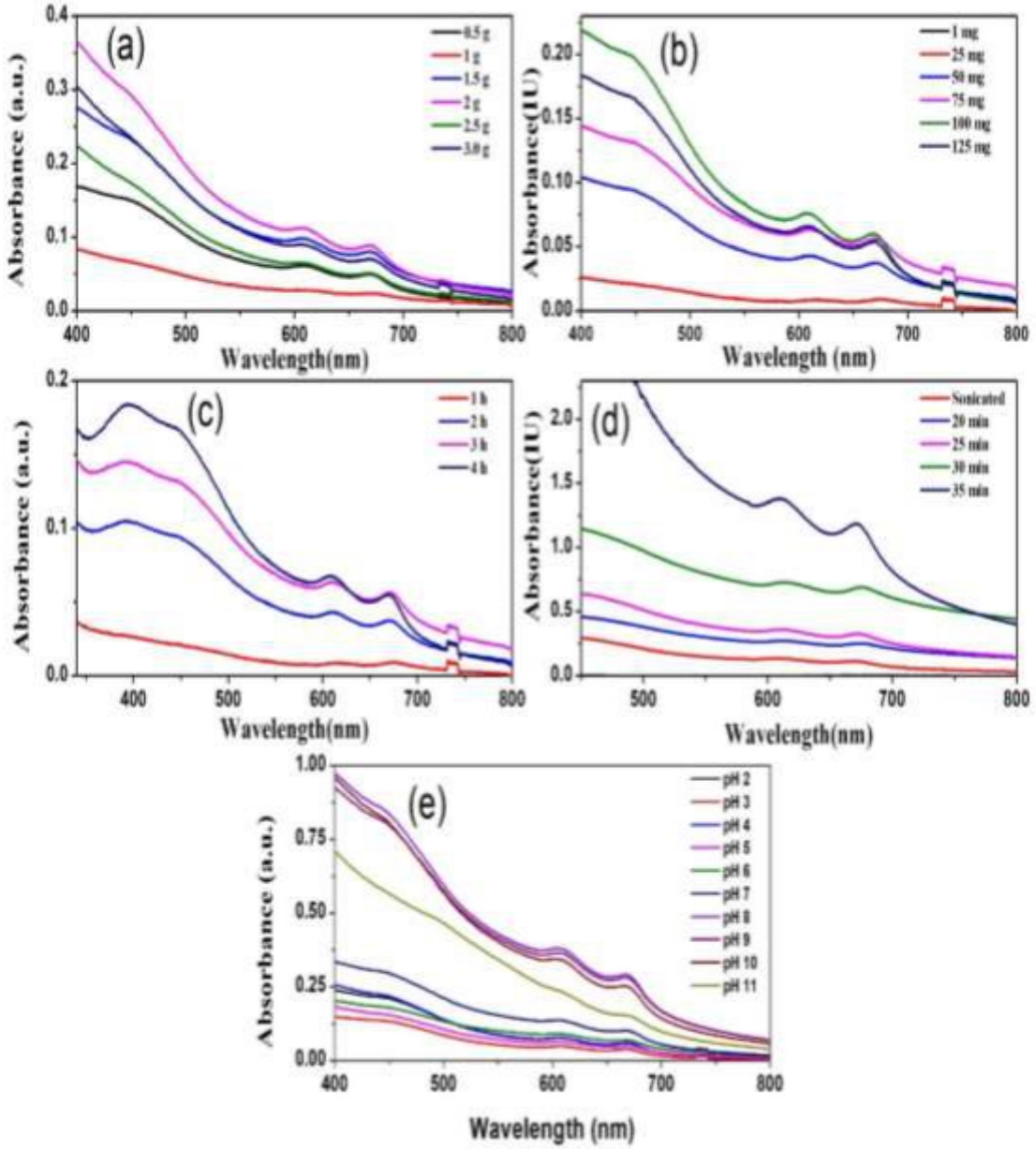

Figure 5.1. Different criteria affecting the synthesis of MoS_2 NPs using gum Arabic as exfoliating agent at different physiochemical parameters. (a) Gum Arabic, (b) Bulk MoS_2, (c) Sonication time. Increase in sonication time up to 4 h led to increase in peak intensity, (d) Microwave time (e) Effect of pH on the synthesis of MoS_2 NPs using gum Arabic as exfoliating agent. Two grams gum Arabic, 100 mg bulk MoS_2, 4h sonication, and 20 min sonication time and neutral pH 7 were selected as optimal conditions for MoS_2 NPs synthesis.

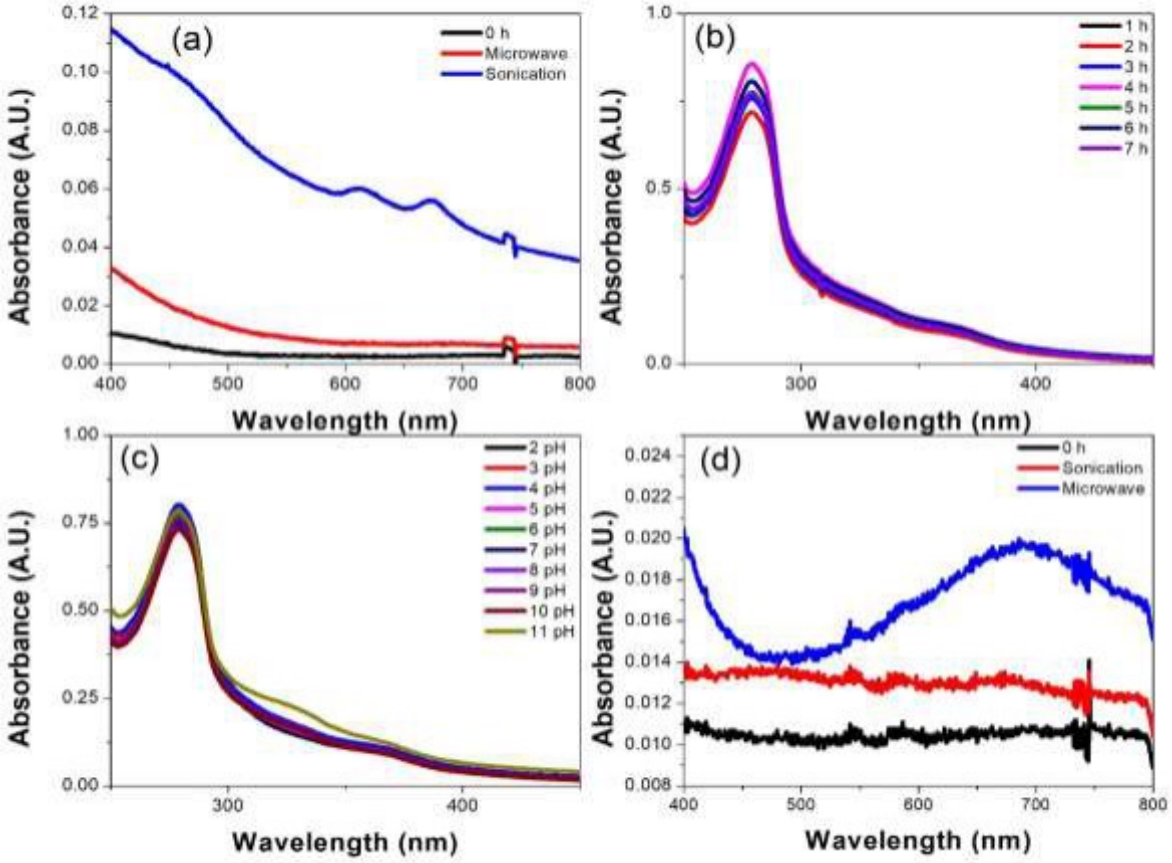

Figure 5.2. Control experiments to check the suitability and stability of gum arabic of reaction components and techniques for the synthesis of MoS_2 NPs. (a) Reverse technique where microwave was followed by sonication in the presence of gum arabic was used to confirm role of sequence of microwave and sonication steps. Low peak intensity designates low exfoliation potential if microwave and sonication are done in reverse order. (b) Effect of sonication on gum arabic at different time interval. This was a experiment to check if sonication of gum arabic can have false peaks in the UV-vis absorption region of MoS_2 NPs. (c) Effect of pH on the UV-vis absorption of gum Arabic. No change in absorption wavelength indicates exfoliation can be carried out at any pH, (d) Bare exfoliation experiment in the absence of gum Arabic. Bulk MoS_2 was subjected to sonication followed by microwave treatment. Low peak intensity and lack of MoS_2 NPs characteristic peak show no significant exfoliation in the absence of gum arabic.

5.1.2. Characterization of GA-MoS_2 NPs

5.1.2.1. UV–vis spectroscopic studies

After optimization of the fabrication conditions, the most important step was characterizing the sample. Out of the various available techniques, UV–vis spectrophotometer is one of the easily available techniques. Fig 5.3.(a) depicts the absorption spectrum of fabricated MoS_2 nanostructure with the absorption maximum at 395, 440, 605, and 668 nm, respectively. This is in agrement with earlier reports (Xuan et al. 2017). The appearance of broad absorption peaks centered at 395 and 440 nm arise due to the exciton transitions within Brillouin zone, P and Q points with high density of states (Ghayeb Zamharir et al. 2018), while the peaks centered at 605 and 668 nm arise due to the exciton transition in Brillouin zone in K points of MoS_2 (Ghayeb Zamharir et al.2018).

5.1.2.2. FTIR analysis of GA-MoS_2 NPs

Fig 5.3(b) depicts the FT-IR spectrum of both gum arabic (black line) and synthesized MoS_2 NPs (red line). It was used to confirm the presence of gum arabic through the identification of its functional groups on NPs surface. In the case of gum arabic, the presence of strong peaks at 3400 cm^{-1} appeared due to O–H stretching in inter- and intra-molecular hydrogen bonds (Lengyel et al. 2017). Peak at 2860 cm^{-1} was due to the occurrence of C-H stretching vibration (Seth and Sharma 2018). Peak centered at 1628 cm^{-1} originates due to the presence of COO^- functional group that indicated the presence of carboxylic group pertaining to uronic acid moitiety of gum acacia (Bashir and Haripriya 2016). On comparison with the FT-IR spectrum of MoS_2 NPs, there is 10 cm shift in the carboxylic peak which indicated the interaction of carboxylic units of gum arabic with the MoS_2 surface (Velayati et al. 2021). These results revealed the binding of gum arabic on the MoS_2 surface to synthesize the stable MoS_2 NPs.

5.1.2.3. Diffraction studies of GA-MoS_2 NPs

X-ray diffraction technique was used to study the crystallinity and crystallite particle size of the fabricated NPs (Fig. 5.3(c)). The appearance of broadness in the diffraction pattern revealed the amorphous nature of the sample that arises due to the occurrence of gum arabic on MoS_2 NPs surface as indicated by the FT-IR analysis. In addition, a

broad peak centered at 14.2° originated due to (002) plane and the broadness is due to the extremely fine size of the nano-structures (Li et al. 2017; Yang et al. 2019). The MoS_2 crystallite size was calculated by using the Debye Scherer formula (Sangar et al. 2019):

$$D = \frac{K\lambda}{\beta \cos\theta}$$

D was the mean size, K was a shape factor (approximately 0.9), λ is the X-ray wavelength (λ = 1.5418 Å), and β designates the broadening of line at half the maximum intensity. The crystallite size using Debye Scherer formula comes out to be 2.5 nm.

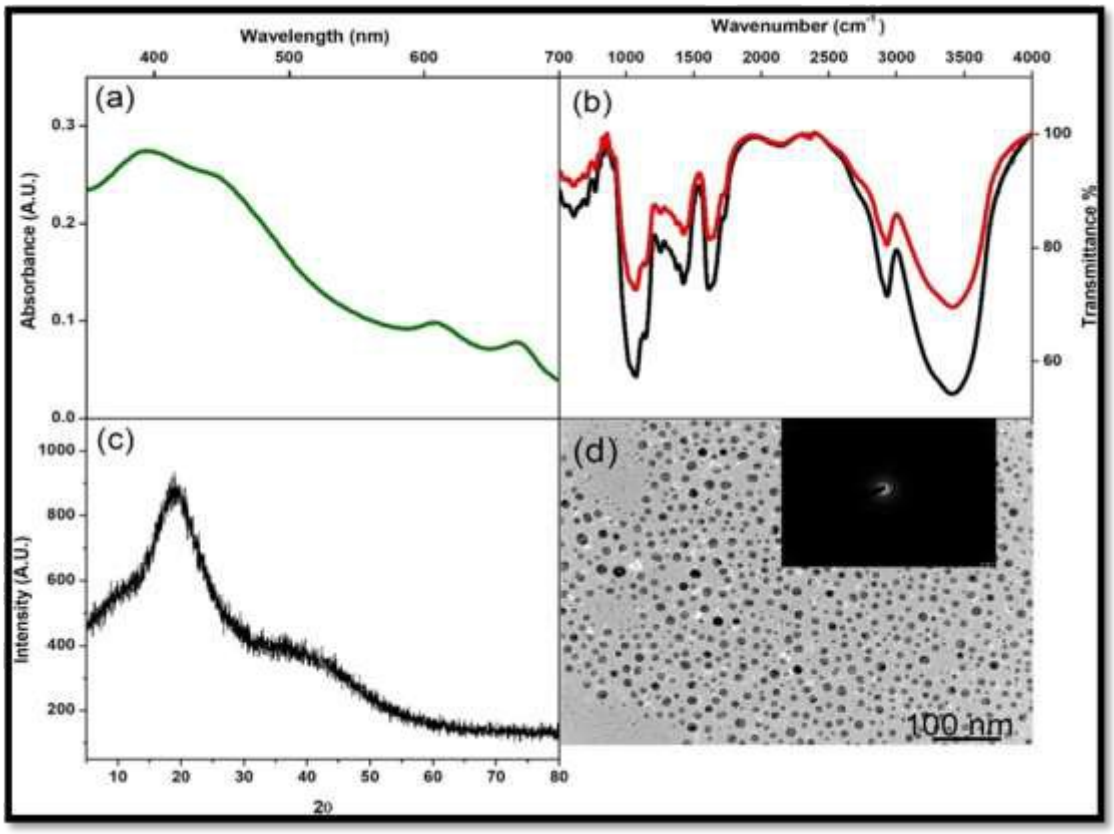

Figure 5.3. Characterization of as GA synthesized MoS_2 NPs. (a) UV–vis spectrum of MoS_2 NPs. (b) FT-IR spectrum of NPs to examine the functional group present (black-gum arabic; red MoS_2 NPs). (c) X-ray diffraction pattern of GA-MoS_2 NPs. (d) HR-TEM image of the NPs (inset SAED pattern).

5.1.2.4. Morphological studies

The morphological characterization of the synthesized MoS_2 NPs was conducted using HR-TEM (Fig. 5.3(d)). The MoS_2 NPs exhibited spherical morphology with very little polydispersity and the size is in quantum regime with quantum confinement. The high uniformity and mono-dispersity of MoS_2 NPs indicated their better dispersion in aqueous medium, as clear from dark green color of the solution (Chen et al. 2016). The NPs exhibited spherical morphology with average dimensions of 10–12 nm and are consistent with the crystallite size by Eq. 2. These results indicated the formation of MoS_2 NPs. Furthermore, selected area electron diffraction (SAED) pattern also indicated moderate crystallinity of the synthesized NPs resembling XRD results (Li et al. 2019b).

5.1.2. Sodium alginate mediated synthesis of MoS_2 nanostructures

5.1.2.1. Synthesis of SA-MoS_2 nanostructures

The synthesis of MoS_2 NS comprised an easy, two-step, ecologically sound method that produced sodium alginate mediated exfoliation by following liquid-phase exfoliation. In this technique, ultra-sonication, and microwave have played contributively in the exfoliation of bulk MoS_2 to MoS_2 NS. Ultra-sonication can be considered as most popular and promising technique cleaving nanosheets from bulk material using biosurfactant by weakening the intermolecular forces between the layers (Y. Liu & Li, 2020; Wu et al., 2018).

5.1.2.1.1. Biosurfactant concentration

The standardization of different parameters started with the optimization of the biosurfactant concentration. Different concentrations of sodium alginate, 1g, 2g and 3g were taken to exfoliate bulk MoS_2. The absorbance spectra obtained from UV-vis spectrophotometric analysis of test samples, supported the selection of concentration of biosurfactant. From various concentrations, 1.0g of sodium alginate exfoliated pristine MoS_2 maximally as it exhibited highest peak in the characterstic region of absorption spectrum (Fig 5.4.(a)).

5.1.2.1.2. Precursor concentration

Next, the amount of substrate selected for the liquid phase exfoliation was found to be 50mg/100mL from a range of 1mg/100mL, 25mg/mL, 50mg/100mL, 75mg/100mL, 100mg/100mL, and 125mg/100mL. It has been investigated that 50mg/mL was the most suitable choice to be exfoliated in proper proportion with the biosurfactant concentration due to its highest peak shown in the graph. The high SPR reflects the better synthesis of the nanomaterial (Fig 5.4.(b)).

5.1.2.1.3. Sonication time

Sonication plays a crucial role in the conversion of bulk material into the nanosheet form by decreasing the interlayer interactions. Here, 4 hours of liquid phase exfoliation were best fit for the synthesis of nanosheets by exhibiting a greenish grey homogenous mixture from immiscible pale-yellow solution. An increase in the trendline showing the absorption spectrum has been observed with increase in the sonication duration, representing the intensification of exfoliation process Fig 5.4.(c).

5.1.2.1.4. Microwave time

Microwave approach was used to fasten the exfoliation process initiated by the liquid phase exfoliation process. The combined effect of sonication and microwave facilitated the process of exfoliation to form thin layer nanosheets. Synthesis of MoS_2 NS using microwave process has earlier been documented. The extent of thinning of exfoliated MoS_2 NS obtained from the sonication depend on the exposure time of microwave treatment. Hence, microwave (5-20mins) exposure was provided to reaction mixture for different intervals to acquire MoS_2 NS. A period of 20 mins was selected as optimal microwave exposure time for the appropriate exfoliation. Fig 5.4.(d)).

5.1.2.1.5. pH

pH is an important factor affecting the complete synthesis procedure vividly. To determine the effect of pH on MoS_2 NS fabrication, the reaction mixture was carried out at 2- 11 pH. It was observed that pH 4 is most suitable for the exfoliation process revealing the favourability of acidic conditions in the exfoliation process (Fig 5.4.(e)).Apart from the optimization of these specific factors, the exfoliation of bulk MoS_2 was also conducted by keeping the finalized conditions similar in the absence

of sodium alginate. The obtained spectral graph did not show any specific peaks corresponding to MoS_2 NS. Consequently, to synthesize MoS_2 NS at the ideal physiochemical parameters used in this investigation, sodium alginate was needed as a bio-surfactant**.**

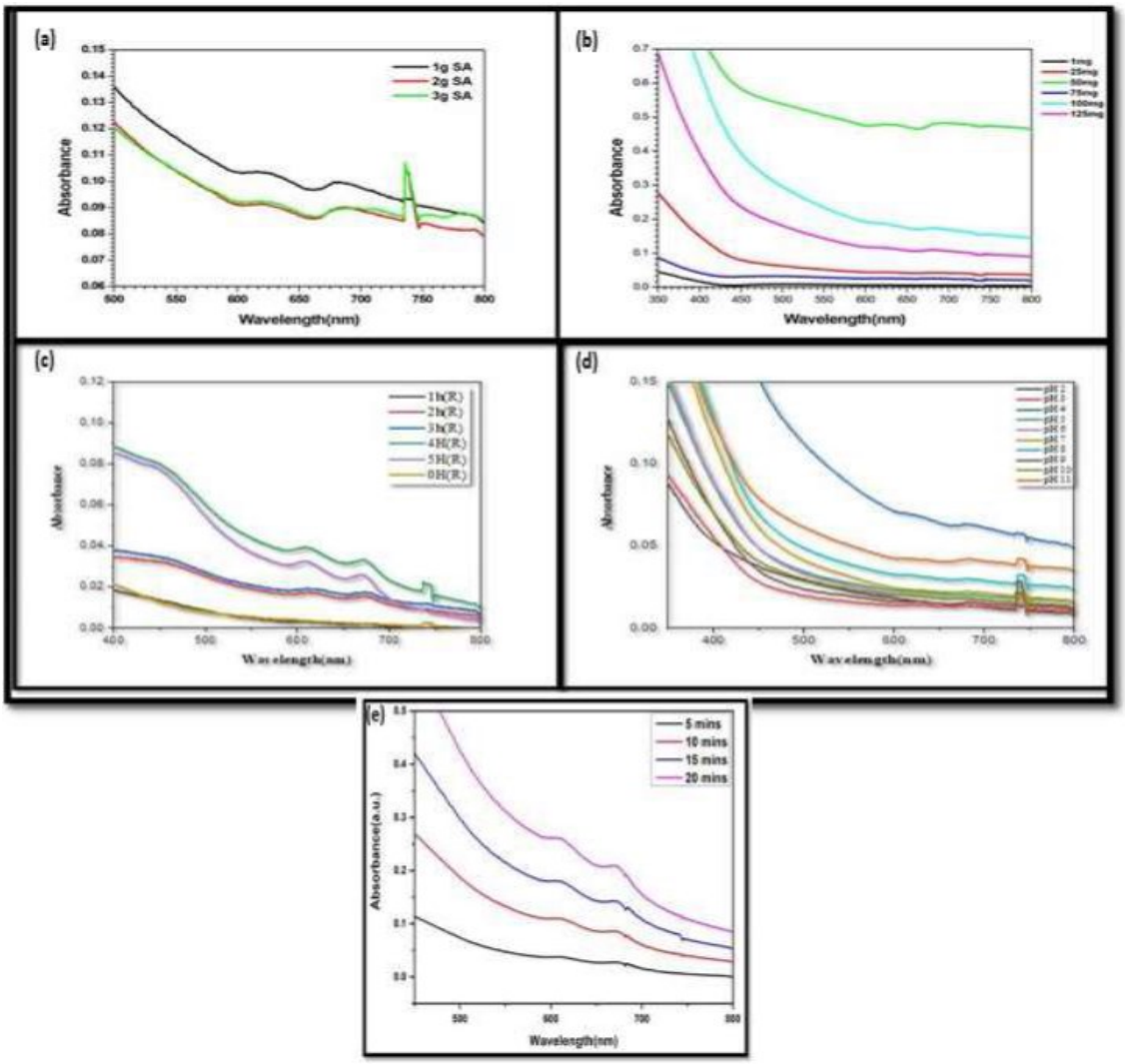

Figure 5.4. Different criteria affecting the synthesis of MoS_2 NS using sodium alginate as exfoliating agent at different physiochemical parameters. (a) Sodium alginate (b) Bulk MoS_2, (c) Sonication time. Increase in sonication time up to 4 h led to increase in peak intensity (d) Effect of pH on the synthesis of MoS_2 NS using sodium alginate as exfoliating agent.

5.1.2.2. Characterization of SA-MoS_2 nanostructures

5.1.2.2.1. UV–vis spectroscopic studies of SA-MoS_2 nanostructures

In case of MoS_2 NS, two characteristic absorption peaks were detected at 614 and 665 nm. These peaks are linked to the energy split from the enormous lateral dimensions of the valence band spin–orbital coupling in MoS_2 (Chaudhary et al., 2018; Mak et al., 2010). The bands at 665 and 614 nm originate from direct excitonic transitions occurring at the K point of the Brillouin zone (Fig 5.6(a)).

5.1.2.2.2. Functional group analysis of SA-MoS_2 nanostructures

The broadening of peaks on 3382.5 and 1031.73 cm^{-1} denoted the hydroxyl and C-O stretching vibrations due to presence of hydroxyl group. The stretching vibrations of hydroxyl groups (OH) and Mo–O bonds produce absorption bands at 1181 and 1695 cm^{-1}(Chaudhary et al., 2018). In the Fig 5.6.(b), the characteristic peaks observed at 601 and 930 cm^{-1} are related to the Mo–S and S–S elements. The peaks shown at 1412 and 1617 cm^{-1} were assigned to the Mo–O functional group (Ganesha et al., 2022; Huang et al., 2014).

5.1.2.2.3. Diffraction studies of SA-MoS_2 nanostructures

The X-ray diffractogram depicts some values of 2θ=29.19°,32.88°, 33.70°,49°, and 59.04° shows the presence of significant MoS_2 (Rani et al., 2020; Wei et al., 2021). The presence of sodium alginate is not clearly visible which indicated its utilization as a stabilizing agent (Xuan et al., 2017). The other two peaks located at 33.70° and 59.04° are corresponding to peak of MoS_2 (Y. D. Liu et al., 2013; X. Zhang et al., 2014). The absence of (002) at 14° reflections and broadness of peaks indicated that the obtained products are single layer or few layer graphene like MoS_2 (Hwang et al., 2011; Veeramalai et al., 2016; Wang & Li, 2007).

5.1.2.2.4. Morphological studies of SA-MoS_2 nanostructures

The morphological characterstics of the SA-MoS_2 NS were deduced from the HRTEM analysis. According to the images received, it has been observed that the MoS_2 NS were formed during the exfoliation process. MoS_2-NS possessed a sheet like morphology having 100 nm edges.

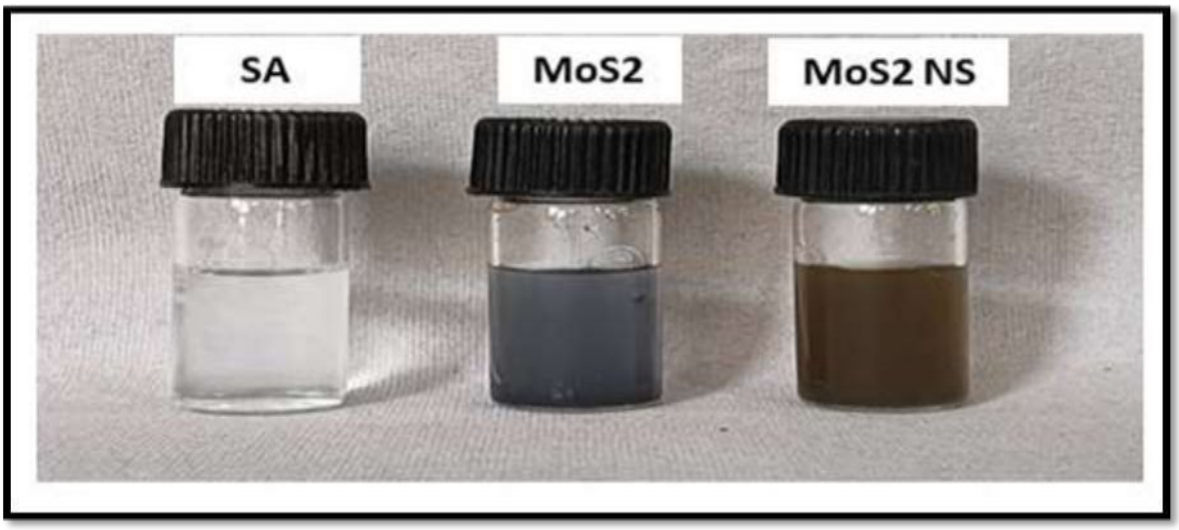

Figure 5.5. Visible observation of green color reflecting synthesis of MoS_2 NS showing successful exfoliation using sodium alginate.

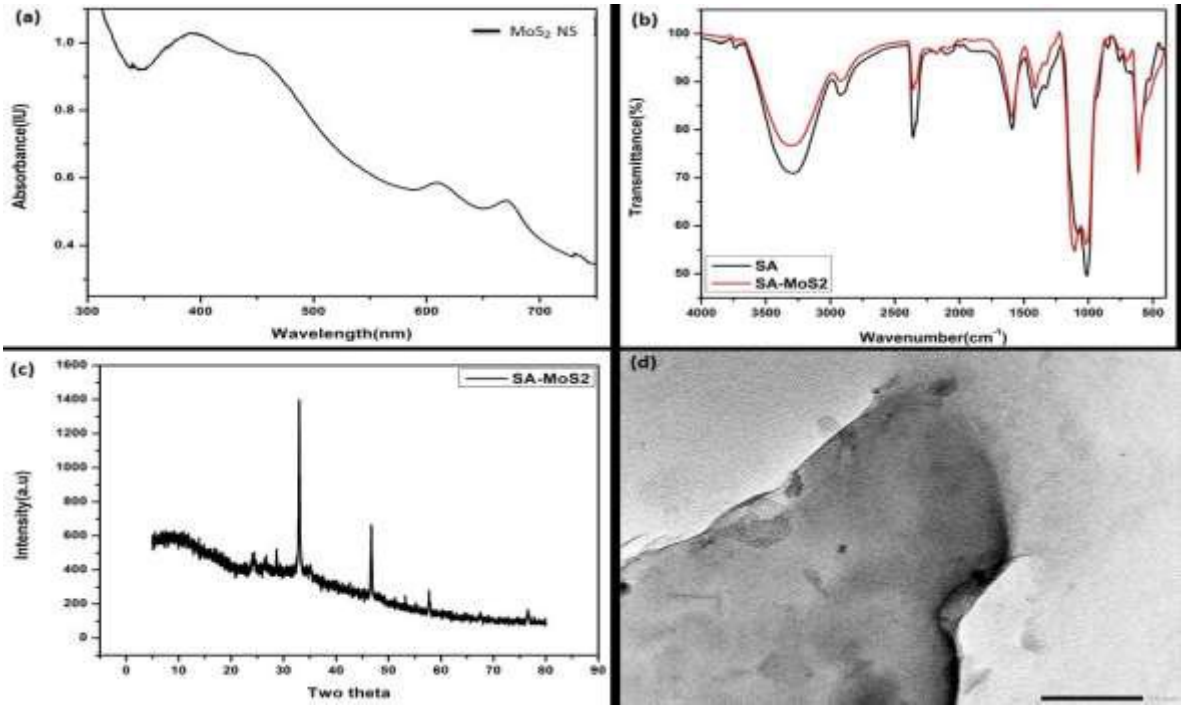

Figure 5.6. Characterization of as synthesized SA-MoS_2 NS. (a) UV–vis spectrum of MoS_2 NS. (b) FT-IR spectrum of NS to examine the functional group present (black-sodium alginate; red MoS_2 NS). (c) X-ray diffraction pattern of MoS_2 NS. (d) HR-TEM image of the NS.

5.1.3. *Tinospora cordifolia* stem extract (TcSE) mediated synthesis of MoS_2 nanostructures

5.1.3.1.1. Effect of TcSE and MoS_2 on the synthesis of TcSE-MoS_2 nanostructure

An aqueous TcSE was obtained by mixing 1g of plant powder in 100mL of double distilled water. The obtained plant extract was used as exfoliator and stabilizing agent for the liquid phase exfoliation of the MoS_2. The trials assessing the concentration of bulk MoS_2 ranging from 1-100 mg/100 mL revealed that 100 mg/100 mL TcSE was the optimum bio-surfactant concentration to produce MoS_2 nanostructure.

5.1.3.1.2. Sonication time

To explore deeper into the optimisation studies, the duration of sonication was examined, as it plays a crucial role in achieving a high exfoliation ratio. The figure illustrates that the absorption strength increased as the sonication period increased from 1 to 4 hours, indicating the exfoliation of bulk MoS_2 into MoS_2 NS. Moreover, the solution undergoes a transformation, turning it into a dark green color, which indicated that the exfoliation was successfully achieved. This agrees with earlier studies (Rani et al., 2020). As the sonication time increased from 1 to 4 hours, it was observed that the intensity also increased, indicating an increase in the exfoliation of MoS_2 and a decrease in the number of layers compared to the bulk counterpart. This phenomenon has previously been documented (Kathiravan et al., 2019). Ultra-sonication greatly enhanced the exfoliation process, resulting in a noticeable increase in peak as the sonication period increases. However, by utilising bio-surfactant-mediated exfoliation, the same level of exfoliation can be obtained in a shorter amount of time. Thus, a sonication time of 4 hours was determined to be the optimal duration for exfoliation.

5.1.3.1.3. Microwave time

To investigate impact of microwave on the exfoliation of bulk MoS_2, microwave irradiation was subsequently applied to the sonicated MoS_2. Making the most of the irradiation period is crucial. As shown in Fig 5.7.(c), the impact of various irradiation times 5, 10, 15, and 20 min with constant power was also examined. Samples with varying irradiation times were incubated, centrifuged, and the supernatant was

analysed using UV-vis spectroscopy. It was found that 20 min exposure of microwave was optimal for the synthesis of MoS_2 NS.

5.1.3.1.4. pH

It was observed that pH 7 is appropriate for maximum MoS_2 NS production. The prominent spectral peaks at 612 and 665 nm in the pH studies indicated that basic conditions were promoting the exfoliation process (Fig 5.7.(d)).

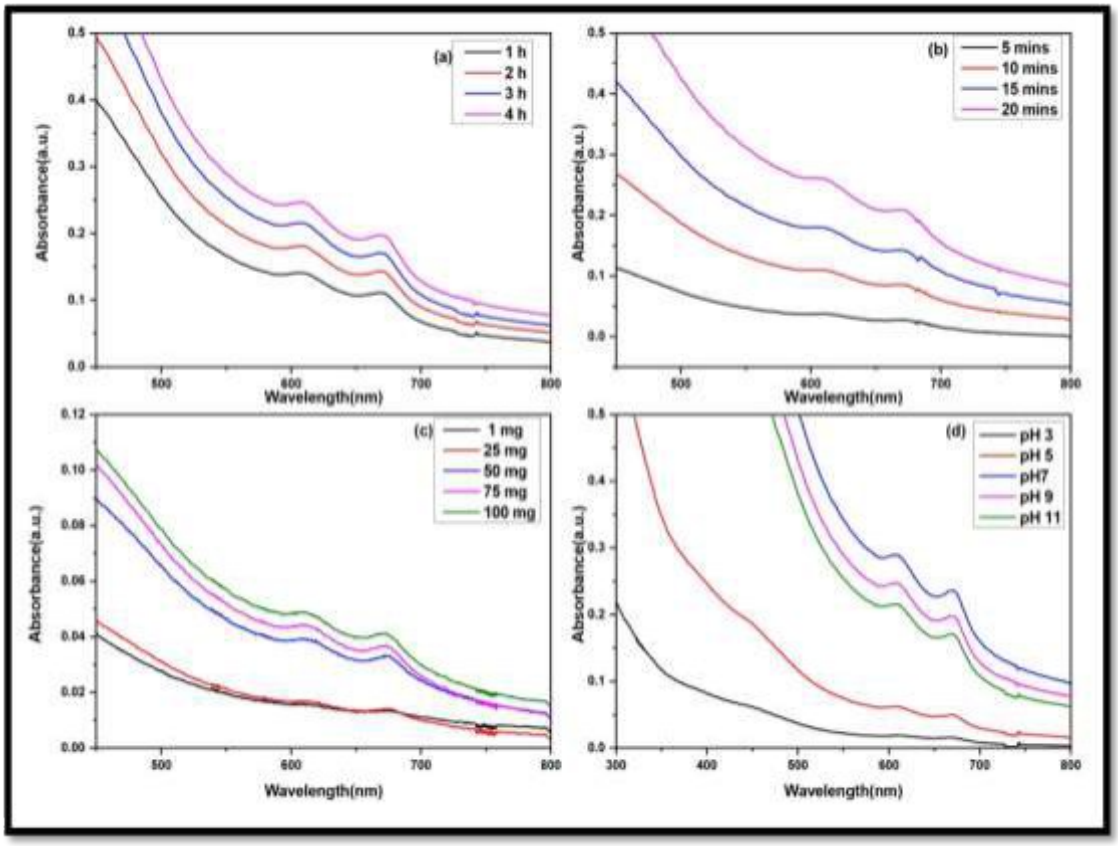

Figure.5.7. Optimization of parameters for the TcSE mediated MoS_2 nanostructure's synthesis: (a) Sonication time (b) Microwave time (c) Precursor concentration (d) pH.

5.1.3.2.Characterization of TcSE-MoS_2 nanostructure

5.1.3.2.1. UV–vis spectroscopic studies of TcSE-MoS_2 nanostructure

The structural analysis of the MoS_2 nanostructures was conducted by examining the optical absorption spectra by UV-vis spectroscopy as shown in the Fig 5.8.(a). The peaks observed at around 612 nm and 665 nm can be attributed to the inter-band excitonic transition occurring at the K point of the Brillouin zone. The spacing

between these peaks is caused by the spin orbit splitting of the transitions at the K point. The spectral intensity of exfoliated MoS_2 NS obtained through the combined process of bath sonication and microwave was proven to be successful for liquid phase exfoliation.

5.1.3.2.2. Functional group analysis of TcSE-MoS_2 nanostructure

A peak at around 3000-3600 cm^{-1} arises from the vibratory stretching of N-H and O-H bonds, resulting in a hump in the spectrum (Roy et al., 2019). The above phenomenon is associated with the flexing and elongating oscillations of the hydroxyl group of water molecules that have been adsorbed. The peak at 1187.14 cm^{-1} is attributed to the stretching vibration of S–O in MoS_2 NS (Mohammed et al., 2022). The absorption band ranging from 480-690 cm^{-1} can be attributed to the Mo-S vibration (Das et al., 2019). Furthermore, the spectrum shown in fig 5.8.(b) also exhibited distinct peaks in the range of 1000-1070 cm^{-1}, which can be attributed to the stretching vibrations of the C-O bond (Feng et al.,2016; Subitha et al., 2018).

5.1.3.2.3. Diffraction studies

The XRD spectrum has prominent peaks at 24.49° and 33.31°, which correspond to distinct crystallographic planes (Fig 5.8.(c). The lack of a distinct peak at 14° indicated the existence of individual strata or single layers. The non-availability of (002) reflections and the broadness of the peaks suggest that the produced products

Figure.5.8. Picture showing culture vials containing TcSE, MoS_2 and MoS_2 NS. Green color in last vial reflects successful exfoliation of MoS_2 NS showing using TcSE.

5.1.3.2.4. Morphological studies

are composed of either a single layer or a few layers of graphene-like MoS_2 (Hwang et al., 2011; Veeramalai et al., 2016; Wang & Li, 2007).Fig 5.8.(d) displays the boundary of a MoS_2 NS consisting of three layers with high resolution. The HR-TEM image demonstrated that the lattice structure of the MoS_2 NS remained intact throughout the exfoliation process. The electron diffraction pattern indicated that the MoS_2 nanosheets possesses a high degree of crystallinity (Liu et al., 2015).

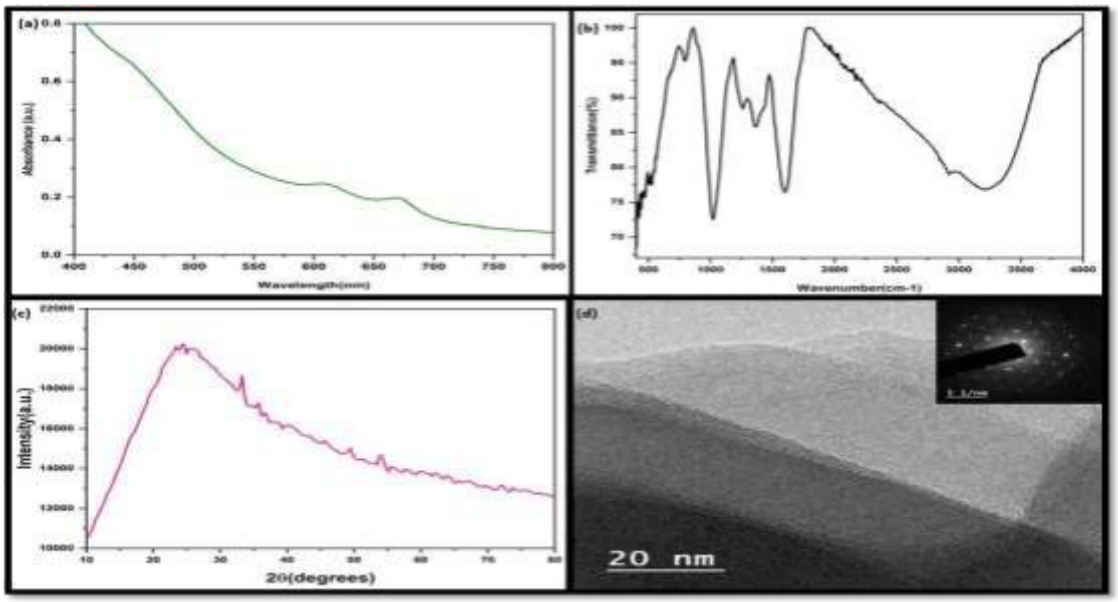

Figure.5.9. Characterization of as TcSE synthesized MoS_2 NS. (a) UV–vis spectrum of MoS_2 NS. (b) FT-IR spectrum of NS to examine the functional group present (c) X-ray diffraction pattern of MoS_2 NS. (d) HR-TEM image of the NS (inset SAED pattern).

5.2. Preparing MoS_2 nano-heterostructures containing carbonaceous quantum dots through greener route and their characterization

5.2.1. GA-MoS_2@GQDs

5.2.1.1. UV-Vis spectroscopic analysis of GA-MoS_2@GQDs

The UV-Vis spectra obtained for the GA-MoS_2@GQDs, showed a strong peak at 270 nm indicating the presence of GQDs along with MoS_2. The observed spectrum

confirmed the formation of the MoS_2@GQDs nanocomposite (Fig 5.10.(a)). Therefore, the optical absorption of the obtained composite ranged from 200 to 800 nm. Graphene have earlier been reported to shown π-π* transition of aromatic C–C bonds in the absorption band at 270 nm and tailing of the peak represented the presence of thick and thin layered sheets in the nanocomposite (Ali et al., 2020; Johra et al., 2014; Kandhasamy et al., 2022; Li et al., 2014)).

5.2.1.2. XRD analysis of GA-MoS_2@GQDs

In the XRD graph of nanocomposite (Fig 5.10.(b)), the peak at 14^0 originates from stacking layers confirming the layered structure of MoS_2. As per the literature, a clear peak at 26.3° was observed in the MoS_2@GQDs diffractogram, which may be the diffraction peak of graphene, indicating an existence of graphene in the composites (Zhong et al.,2019). Moreover, the broadness of peak implied the presence of less number of stacked, disordered layers with smaller crystallite size (Sahu and Mitra, 2015). From the broadness of the peaks, the amorphous nature of the synthesized nanocomposite can be estimated which is reflected by the SAED pattern. The SAED pattern of product have shown the faded concentric rings representing the non-crystallinity of the nanocomposite (Fig 5.10.(insat) (Li et al., 2021).

5.2.1.3. Morphological analysis of GA-MoS_2@GQDs

The morphological and internal architectural characteristics of MoS_2@GQDs were investigated using HR-TEM. The HR-TEM images (Fig 5.10. (c) has shown the fine structure of hybrid nanomaterials. From the figures, free style, and non-uniform trapping of MoS_2 nanostructures by fine dots (GQDs) was observed. The encapsulation of MoS_2 NPs by GQDs appeared in spherical round dots shape. In this nanocomposite, the MoS_2 NPs provided a high surface area for the loading of GQDs (Fig 5.10.(c)) (Yoon et al., 2017;Bongu et al., 2023).

5.2.1.4. FTIR analysis of GA-MoS_2@GQDs

The multiple peaks observed at 400–500 cm^{-1} indicated MoS_2 peak accounting for the bridging Mo–S bond in the form of Mo–S vibration perpendicular to the basal plane (Burman et al., 2016). The presence of a peak at 620 cm^{-1} is indicative of the Mo–S stretching vibration. The presence of sulphate groups can be attributed to the many peaks observed at 700–1150 cm^{-1}. Additionally, two distinct adsorption peaks at

3440 and 1610 cm^{-1} can be assigned to the stretching of O–H bonds and the bending of water molecules, respectively. This validates the existence of sulphate and water molecules as intercalants in the LPE process (Ali et al., 2020). In Fig 5.10.(d), for the graphene spectrum, the intense peak located at 1610 cm^{-1} can be attributed to the aromatic C=C stretching..

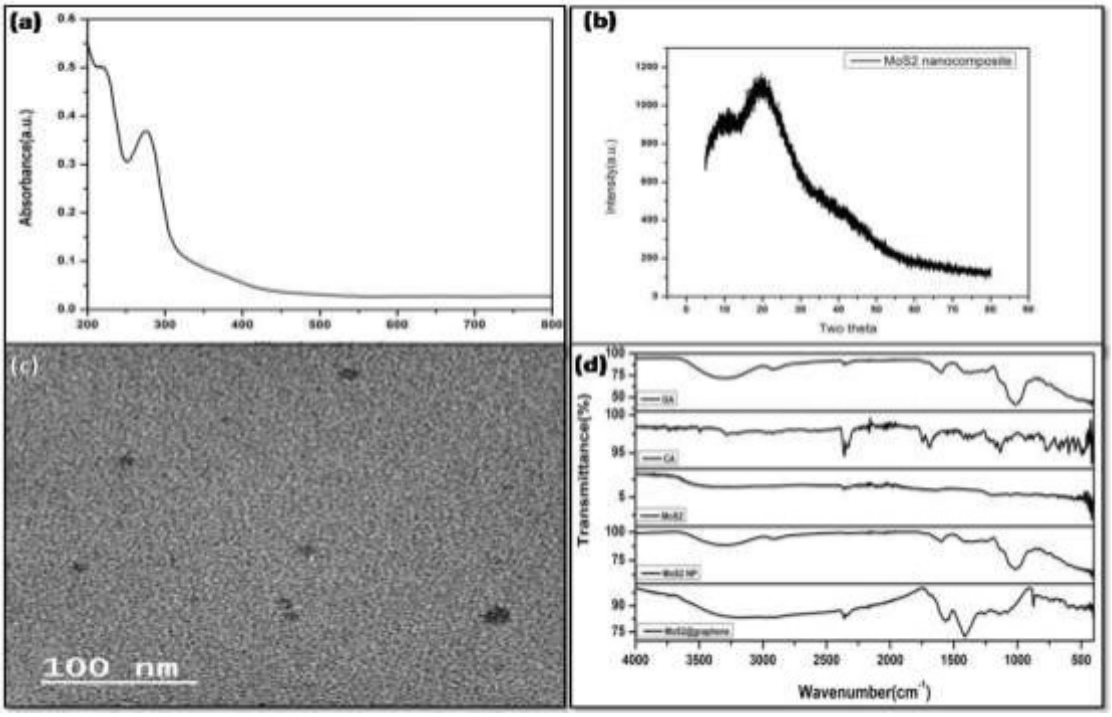

Figure 5.10. Characterization of synthesized MoS_2@GQDs. (a) UV–vis spectrum of MoS_2@GQDs (b) X-ray diffraction pattern of MoS_2@GQDs. (c) HR-TEM image of the MoS_2@GQDs (d) (b) FT-IR spectrum of NPs to examine the functional group present in the gum arabic (GA); citric acid (CA), MoS_2, MoS_2 NPs, and MoS_2@GQDs.

In contrast, the absence of a C=O peak around 1715 cm^{-1} indicated the insignificant amount of oxidation of graphene. However, there is not obvious peak around 1700–1900 cm^{-1} in the MoS_2 @GQDs hybrids spectrum, indicating that the disappearance of C=O and COOH groups (Fig 5.10.(d) (Wang et al., 2018; Zou et al., 2019). Furthermore, a peak of MoS_2@GQDs at 1000-1100 cm^{-1} is attributed to the C–N bond found in the GQDs (Hu et al., 2013).

5.2.2. SA-MoS_2@GQDs

5.2.2.1. UV-Vis spectrophotometric analysis of SA-MoS_2@GQDs

A prominent peak indicating the existence of the GQDs in the nanocomposite has been seen within the wavelength region, 200-300 nm. The presence of a distinct peak at 205 nm and a smaller peak at 237 nm indicated the production of a composite material consisting of MoS_2 and GQDs. This is attributed to the conjugation between the two components. Additionally, the blue shift observed can be attributed to the reduced size of the quantum dots in the Fig 5.11(a) (Ali et al., 2020; Johra et al., 2014; Kandhasamy et al., 2022; Li et al., 2015).

5.2.2.2. Diffraction studies of SA-MoS_2@GQDs

The XRD spectrum of MoS_2 nanosheets have a highly pronounced peak at 14.43°, which corresponds to the 002 crystal planes of pure MoS_2 nanosheets. Furthermore, there were clear peaks observed at angles of 33.44°, 39.55°, 49.74°, and 58.29°, which correspond to the diffraction planes of (100), (103), (006), and (105) accordingly. These peaks indicate the production of a well-organized layered structure, and the results are consistent with the XRD data previously published for MoS_2 (Silambarasan et al., 2021; Bhardwaj et al., 2020). Additionally, a diffraction peak was detected at around 22.5° in the MoS_2@GQDs samples, indicating the presence of the (002) plane of graphene. This verifies the existence graphene and its successful reduction in the composite material (Liu et al., 2020). The peaks at approximately $2\theta = 25.43°$, 29.50°, 31.6°, 32.63°, and 60.33° were well matched with diffractogram analysis of GQDs obtained from the citric acid (Ifrah et al., 2022). The XRD investigation confirmed the successful formation of GQDs on the surface of MoS_2 nanosheet, which agrees with the observed TEM properties (Fig 5.11(b)).

5.2.2.3. Morphological studies of SA-MoS_2@GQDs

An investigation using HR-TEM was conducted to examine the atomic arrangement of the MoS_2@GQDs nanocomposite in its original state. The HR-TEM image of the MoS_2@GQDs composite clearly shows the microstructure of layers of MoS_2 that is densely loaded with identifiable GQDs (Guo et al., 2017). The figure clearly illustrated the presence of single to few layers of MoS_2 sheets, as well as tiny crystals of GQDs. A significant quantity of QDs was observed to have developed on the edge

sites of the MoS_2 nanosheets, as evident in Fig 5.11(c). This phenomenon can be ascribed to the presence of defects in the edge area, which create additional active sites for the formation of GQDs. GQDs have the potential to occupy the empty spaces on the surface of MoS_2 potentially reducing the impact of defects in MoS_2 (Xin et al., 2019; Yoon et al., 2017; Bongu et al., 2023).

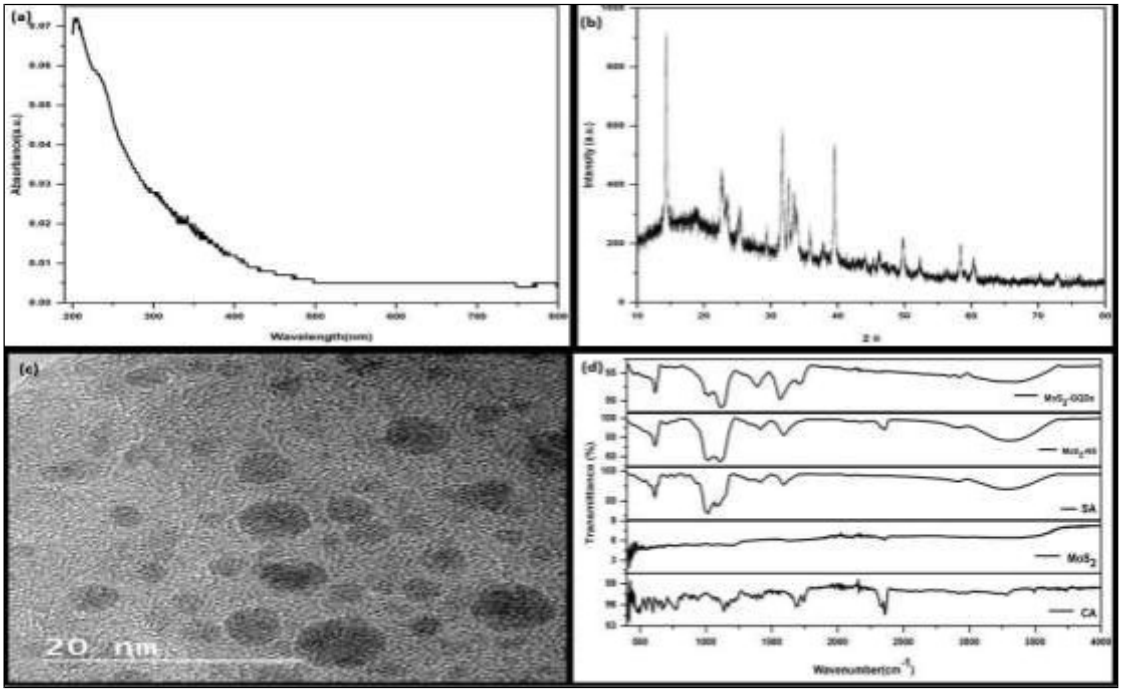

Figure 5.11. Characterization of synthesized MoS_2@GQDs. (a) UV–vis spectrum of MoS_2 @GQDs (b) X-ray diffraction pattern of MoS_2@GQDs. (c) HR-TEM image of the MoS_2 @GQDs (d) (d) FT-IR spectrum of NPs to examine the functional group present citric acid (CA), MoS_2, sodium alginate (SA); MoS_2 NS, and MoS_2 @GQDs.

5.2.2.4. Functional group analysis of SA-MoS_2@GQDs

The presence of several peaks in the 400-500 cm^{-1} range confirmed the presence of the MoS_2 peak. These peaks are caused by the Mo-S bond, specifically the vibration of the Mo-S bond at right angle to the basal plane. A peak present at 613.65 cm^{-1} exhibited the Mo-S vibrations. The presence of a peak at 3341 cm^{-1} indicated involvement of hydroxyl groups in the exfoliation process (Wang et al., 2017). The

reduction of citric acid to GQDs is indicated by the decrease in the peak intensity of the oxygen-rich functional groups in citric acid (Vinoth et al., 2016). Additional peaks were seen at 1473.59, 1704.24, 1808.48, and 1111.03 cm^{-1}, which were attributed to the –C=C, –C=O, and –C–O functional groups of GQDs, respectively as shown in the Fig 5.11(d) (Bhardwaj et al., 2020). A significant peak at the 1569.59 cm^{-1}) reveals the occurrence of GQDs in the nanocomposite (Sun et al., 2013).

5.2.3. TcSE-MoS_2@GQDs

5.2.3.1. UV-Vis spectrophotometric analysis of *TcSE*-MoS_2@GQDs

From the literature review, it has been evident that the UV-Vis spectra demonstrated a π-π* absorption band at a wavelength of 270 nm, indicating the synthesis of MoS_2-GQDs. In this study, the absorption spectra showing peaks at 205 and 245nm were ascribed to the successful synthesis of nanocomposite (Ali et al., 2020; Johra et al., 2014; Kandhasamy et al., 2022; Li et al., 2015).

5.2.3.2. Diffraction studies of TcSE-MoS_2@GQDs

In the XRD spectra of MoS_2@GQDs, there is a peak that is extremely prominent at 14.30°. This peak corresponds to the 002 crystal planes of pure MoS_2 nanosheets. In addition, distinct peaks can be seen at angles of 33.54°, 39.74°, 49.68°, and 58.53° that, correspond to the diffraction planes of (100), (103), (006), and (105) respectively. The presence of these peaks is indicative of the formation of a layered structure that is well-organized, and the findings agree with the XRD data of previous literature (Silambarasan et al., 2021; Bhardwaj et al., 2020). The peaks seen at around $2\theta = 32.76°$, 35.86, 44.25 as well as 60.70°, closely corresponded to the XRD analysis of GQDs derived from citric acid (Ifrah et al., 2022).

5.2.3.3. Morphological analysis of TcSE-MoS_2@GQDs

The HR-TEM images have conclusively demonstrated the embellishment of MoS_2 nanosheets with graphene quantum dots. The extensive surface area and edges of MoS_2 nanosheets offer an ideal platform for GQDs to occupy the empty spaces and form linkages with the base. At 20nm scale, it has been clearly observed that GQDs are finely sprinkled on the MoS_2 nanosheets. GQDs have taken a proper fit place in the voids present on the MoS_2 nanosheets due to edge effects (Xin et al., 2019; Yoon et al., 2017; Bongu et al., 2023).

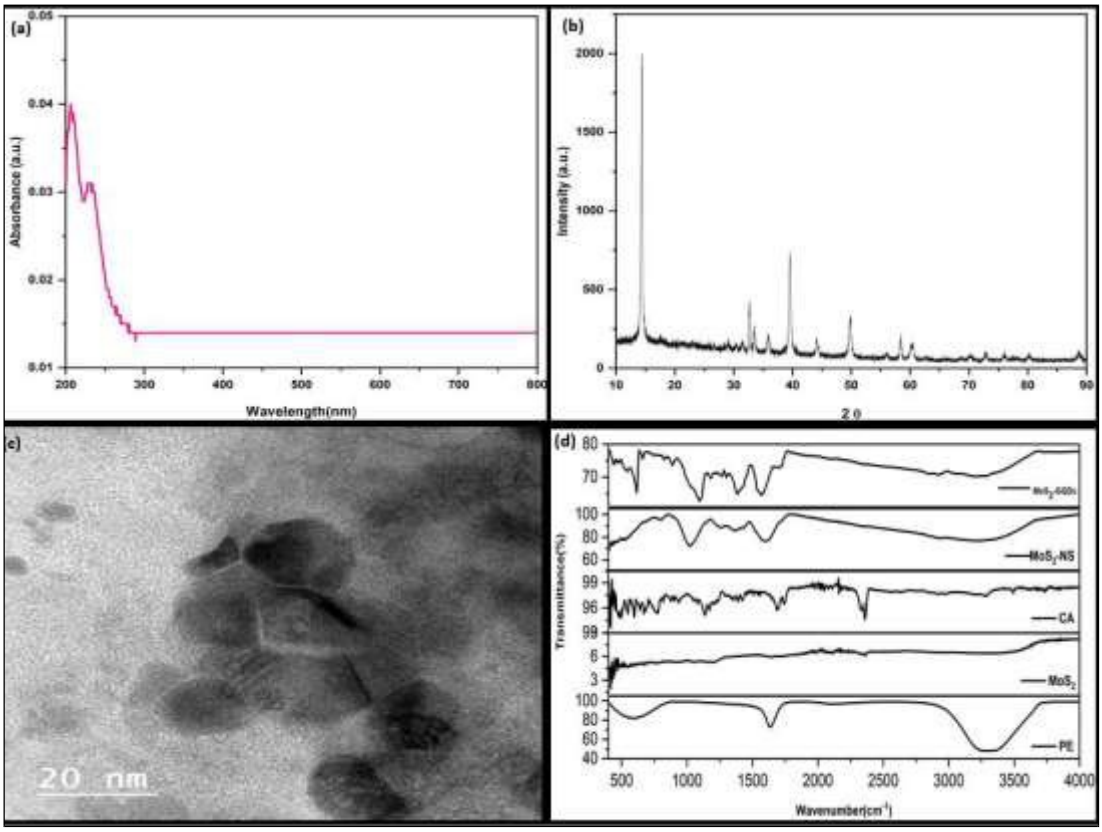

Figure 5.12. Characterization of synthesized MoS_2@GQDs (a) UV–vis spectrum of MoS_2@GQDs (b) X-ray diffraction pattern of MoS_2@GQDs. (c) HR-TEM image of the MoS_2 @GQDs (d) (b) FT-IR spectrum of NPs to examine the functional group present plant extract (PE); MoS_2, citric acid (CA), MoS_2 NS, and MoS_2 @GQDs.

5.2.3.4. FTIR analysis of TcSE-MoS_2@GQDs

The prominent peak observed at 1568.63 cm^{-1} in the MoS_2@GQDs spectrum is attributed to the stretching vibration of C=C bond, indicating that the GQDs are predominantly constituted of C=C bonds and present in the nanocomposite (Sun et al., 2013). The significant peaks at 615.17 and 1387.40 cm^{-1} are related to the C–S and Mo–S bonds, which confirm the presence of MoS_2. The absence of distinct peaks corresponding to oxygenated groups, such as O–H, C=O, and C–O groups, in the MoS_2@GQDs nanocomposites confirmed the successful reduction of GO (Yang et al., 2022). The decrease in the crowdy and maximum intensity in the 400-500cm^{-1}

region of MoS_2-GQDs, when compared to bulk MoS_2, indicated the successful exfoliation of the material. The reduction of peak intensity at 1642 cm^{-1} in the nanocomposite shows the utilization of the phytochemical constituents of plant extract in the exfoliation process.

5.3. Photocatalytic degradation of azo dye using MoS_2 nano-heterostructures

5.3.1. Photocatalytic degradation of MB using GA-MoS_2 nano-structures

The catalytic activity of MoS_2 NPs depends on different factors. To achieve maximum efficiency, it is essential to explore the ideal reaction conditions, comprising sunlight exposure, photocatalyst concentration, and pH; absorption intensity was monitored by changing these parameters as represented in Fig. 5.13.(a-c). It was observed that these parameters play a crucial role in photodegradation.

5.3.1.1. Effect of irradiation time

To check the efficiency of MoS_2 NPs to photo-degrade MB, 250 mg of GA-MoS_2 NPs was mixed with 50 mL of 100 ppm dye solution. The reaction mixture was kept in direct sunlight and the different reaction factors were optimized for better results. There was a decrease in the absorbance with increase in incubation time from 0 to 8 h indicating the degradation of MB (Fig. 5.13(a). To further estimate the percentage (%) of degradation, Eq. 1 was used. Fig 5.13(a) represented the degradation rate in percent with time.

With an increase in the exposure time, the percentage dye degradation was found to increase. Around 98% of the MB degradation was achieved after 8 h of irradiation. It was concluded that the equilibrium for degradation process was attained in 8 h with removal of 98% of MB. Thus, the reference time for the further optimization was taken as 8 h. To best of our knowledge, it is first report revealing maximum degradation rate with pristine MoS_2 that means MoS_2 NPs without any heterostructures as well as doping.

5.3.1.2. Effect of catalyst dose

Fig. 5.13(b) represents the absorption spectrum of dye with 1–250 mg of MoS_2 NPs after 8 h of irradiation time. The absorbance intensity was found to decrease with an increase in the amount of the MoS_2 NPs used (Fig. 5.13(b)) and 250 mg photocatalyst dose has shown linear degradation pattern. Therefore, 250 mg of MoS_2 NPs was

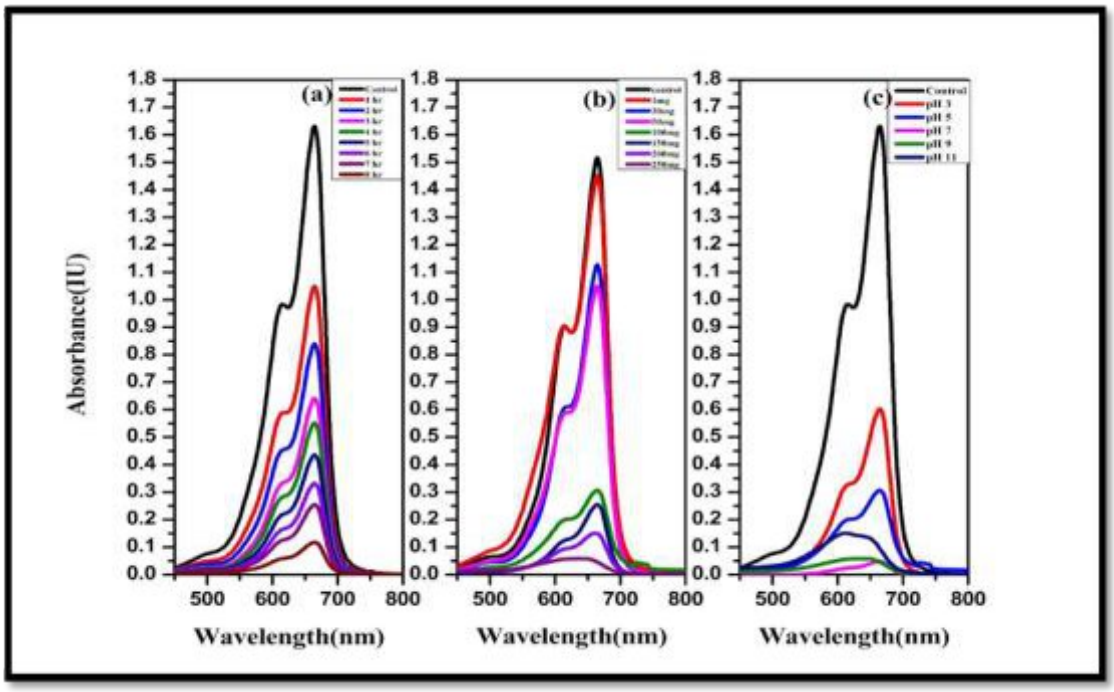

Figure.5.13. UV-vis spectrum of reaction mixture showing effect of various factors on the photocatalytic degradation of MB using gum arabic synthesised MoS_2 NPs (a) Irradiation time (b) photocatalyst concentration (c) pH.

considered optimal photocatalyst for degradation of 50 mL of 100 ppm MB when irradiated for 8 h. The reason of not opting for the concentration above 250 mg of photocatalyst is the interference of photocatalyst to the absorbance spectrum of MB.

5.3.1.3. Effect of pH

pH is a useful parameter to modify the catalytic activity of material. The catalytic degradation efficiency of synthesized MoS_2 NPs affects its surface charge and electron transferability. Different sets of experiment were performed at 3, 5, 7, 9, and 11 pH to reveal its influence on photodegradation of MB (Fig 5.13(c). These studies revealed that the pH 9 led to 100% removal of dye within 8 h of photo exposure showing the basic environment improves for the degradation of MB whereas the acidic medium at pH = 3 showed maximum 50% degradation after 8 h of exposure. The neutral solution with pH 7 showed 98% degradation within 8 h which was considered optimal pH as neutral pH is appropriate for the biological organisms and as per environmental health perspective. MB is a cationic dye, whereas the MoS_2 NPs

are negatively charged at higher pH due to which the electrostatic interaction between the photocatalyst and dye molecules increases, resulting into their better adsorption on the photocatalyst surface. For MoS_2 NPs, there was more production of ROS at alkaline pH than acidic one which enhances the rate of photodegradation (Alarifi et al., 2021; Monga et al. 2020).

5.3.1.4. Degradation studies at optimum parameter

Reaction mixtures containing 50 mL of 100 ppm MB solution was treated with 250 mg of MoS_2 NPs at pH 7 were kept in direct sunlight for 8 h and UV–vis absorption spectra were recorded at an interval of 60 min (Fig. 5.14(a)). There was continuous decrease in the absorption intensity with an increase in incubation time. Maximum degradation was observed in the first 1 h and there was continuous increase in the percent degradation thereafter and 98% of the dye was degraded after 8 h of sunlight irradiation (Fig. 5.14(b)). Furthermore, to examine the rate constant, Eq. 2 was used and ln C/C_0 was plotted against time and it was found out to be 0.00707 min^{-1}.

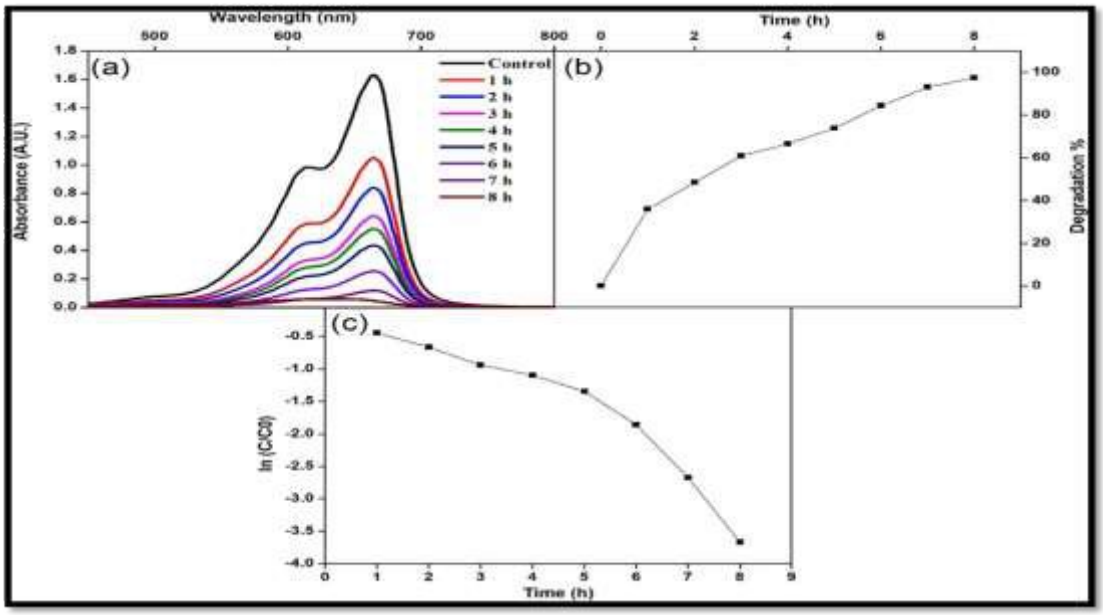

Figure 5.14. Degradation studies of MB at optimized degradation condition; (a) UV–vis spectrum of dye degradation at different time interval, (b) percentage MB degradation with different time intervals, and (c) ln C/C_0 vs time.

5.3.1.5. Photocatalytic degradation of commercial blue using GA-MoS_2 nano-structures

The findings revealed that 98.12±0.15% of CB have been degraded in 45 minutes of irradiation at the optimal conditions standardized for MB degradation. The percentage degradation w.r.t. time revealed the photo dependent reduction of dye molecules in the Fig 5.15(b). The rate kinetics were deduced from the graph presenting $\ln(C/C_0)$.

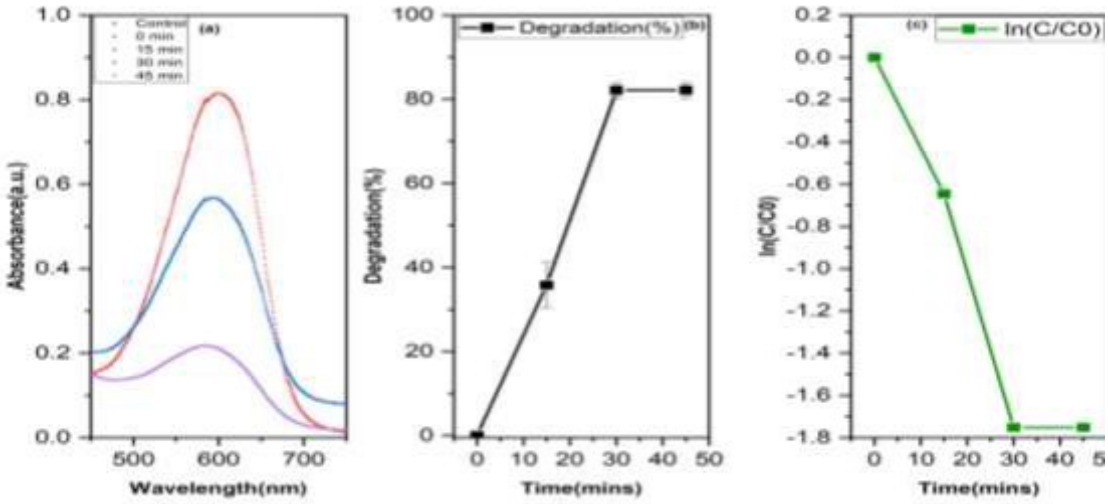

Figure 5.15. Degradation of CB at optimized degradation condition using MoS_2 NPs; (a) UV–vis spectrum of dye degradation at different time interval, (b) percentage CB degradation with time interval, and (c) ln C/C_0 vs time.

5.3.1.6. Degradation efficiency for real textile effluent

To further examine the practical applicability of the present system, the real textile effluent samples were examined for degradation studies using the present photocatalyst with the standardized conditions (Fig. 5.16). UV–vis response of the textile dye with time and significant quenching was observed as the time passes indicate the successful treatment of textile dye effluent Fig. 5.16(a). There was significant degradation as the 98.89% of dye degradation within 150 min (Fig.5.16 (b and c)). The complete color change of effluent was pictorially represented and the pictures reveal that the color is vanished and left with light yellow–colored transparent solution after completion of reaction (Fig.5.16 (d and e)).

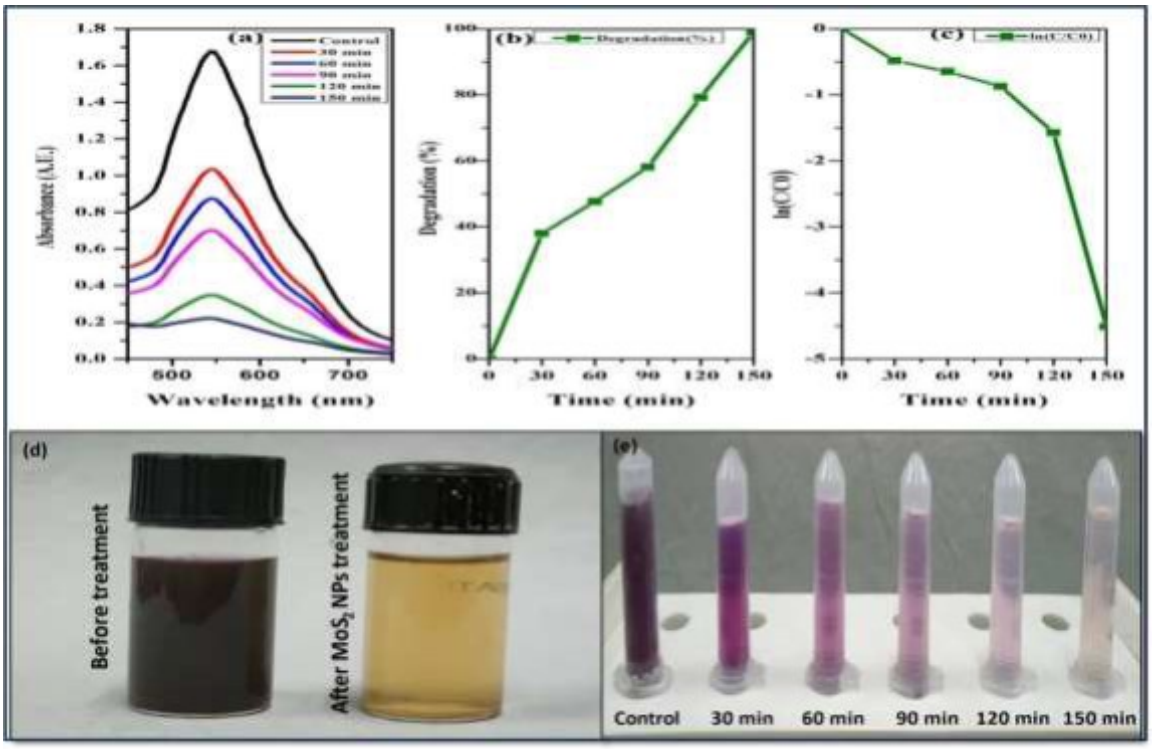

Figure 5.16. Photocatalytic degradation of textile industry wastewater sample containing MB using GA-MoS_2 NPs. (a) UV–vis spectrum of dye degradation. (b) Degradation percentage. (c) ln (C/C_0) plot of degradation. (d) Discoloration of textile water sample containing MB. (e) Pictorial representation of the wastewater treated by MoS_2 NPs at different incubation time

5.3.1.7. Reusability of GA-MoS_2 NPs as photocatalyst against MB

Reusability of NPs depends on various factors like stability, chemical composition, and nature of NPs. It has been found that the potential photocatalytic activity of MoS_2 NPs decreased in each subsequent reuse by 20%, 48%, and 60% in three reuse cycles. On the fourth reuse, negligible photodegradation was observed due to loss of NPs. To discuss the decrease in photodegradation percentage of potent photocatalyst, there are several responsible factors: Firstly, the mass of photocatalyst decreased with washing and drying process. Hence, the concentration of photocatalyst was reduced to significantly lower amount as compared to initial concentration. Furthermore, the

surface activity of photocatalyst may be reduced due to blockage of active sites (Saad Algarni et al., 2022).

5.3.1.8. Free radical trap experiment using GA-MoS_2 NPs

The free radical trapping experiment represented the scavenger studies in which the free radicals generated from the photocatalyst were scavenged by purposefully added scavengers and their effect on percentage degradation of MB was evaluated. In this

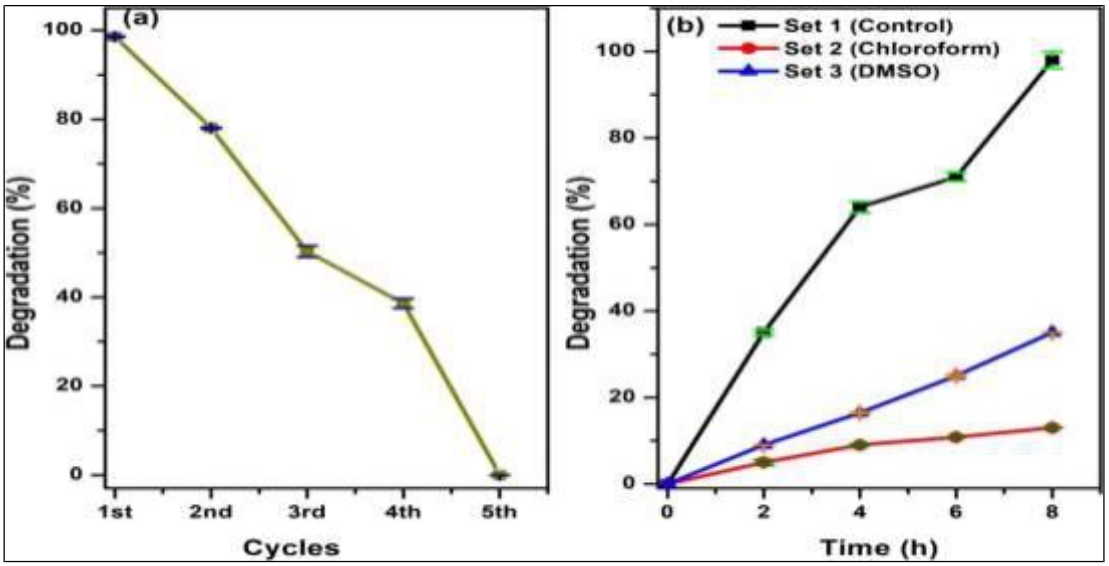

Figure 5.17(a) The percentage MB degradation of MoS_2 NPs with multiple cycles showing reusability. (b) Photocatalytic degradation of MB in the presence of scavengers.

study, it was found that the set 1 (control) without any scavenger showed 98% of dye degradation. On the contrary, set 2 and set 3 exhibited very less photodegradation. Chloroform and DMSO are scavengers of superoxide and hydroxyl ions, respectively. The results remarkably showed inhibition of MB degradation in presence of DMSO, indicating the superoxide is main contributive reactive species. Hydroxyl ions also influenced the photodegradation of MB but the effect of hydroxyl ion is secondary in comparison to superoxide (Fig.5.17 (b)).

5.3.2. Photocatalytic degradation of MB using GA-MoS_2 nano-heterostructures (MoS_2 @GQDs)

5.3.2.1. Effect of irradiation time

The photocatalytic capability of sample was studied under the direct solar irradiation. The exposure of sunlight to the reaction mixture significantly affected the percentage degradation of dye. According to the results, increase in irradiation time enhanced the degradation effectiveness of photocatalyst. To study the influence of irradiation time, the same samples were exposed to different time intervals and the obtained results were comparatively analyzed. Fig. 5.18(a) Enhanced irradiation exposure provides more contact time for chromophores interaction with the photocatalyst surface and decomposition of the chromophore, which emits the characteristic colour of the MB. This is one of the causes for reduction in the wavelength of the absorbance at 665 nm with irradiation time. A standardized irradiation time of 90 min was considered optimal to obtain 98.85±0.99% degradation of MB.

5.3.2.2. Effect of catalyst dose

An optimal dose of photocatalyst would improve the photocatalytic degradation in a better way. As we increase the concentration of photocatalyst, the degradation rate also increases due to presence of more active sites present on the nanophotocatalyst. To study the effect of catalyst dose on the degradation efficiency, the concentration of photocatalyst varied from 50 mg to 250 mg at the same concentration of MB. From Fig. 5.18(b), the kinetic studies were elucidated that an increase in the rate of MB degradation with an increase in concentration of the nanophotocatalyst, and then plateaued after achieving equilibrium. At 250mg/50mL of MB solution, the degradation efficiency was enhanced from 84% to 98.94% with an increase in dose from 50 to 250 mg by providing 90 mins of direct sunlight exposure, respectively. The functionalization of MoS_2@GQDs provided the additional active site for the formation of electron-hole pair for photocatalysis.

5.3.2.3. Effect of pH

pH plays a vital role in the photocatalytic process by affecting the active surface charge of nanocomposite. Using 1M hydrochloric acid (HCl) and 1M sodium hydroxide (NaOH), the pH of MB solution was calibrated. The effect of the solution

pH on the rate of photocatalytic degradation was investigated by varying pH 3, 5, 7, 9 and 11 at constant 100ppm dye concentration and 250mg/50 mL photocatalyst amount for MB. It is evident from the graph Fig 5.18(c) that the acidic conditions are more favorable to enhance the degradation efficiency of photocatalyst.

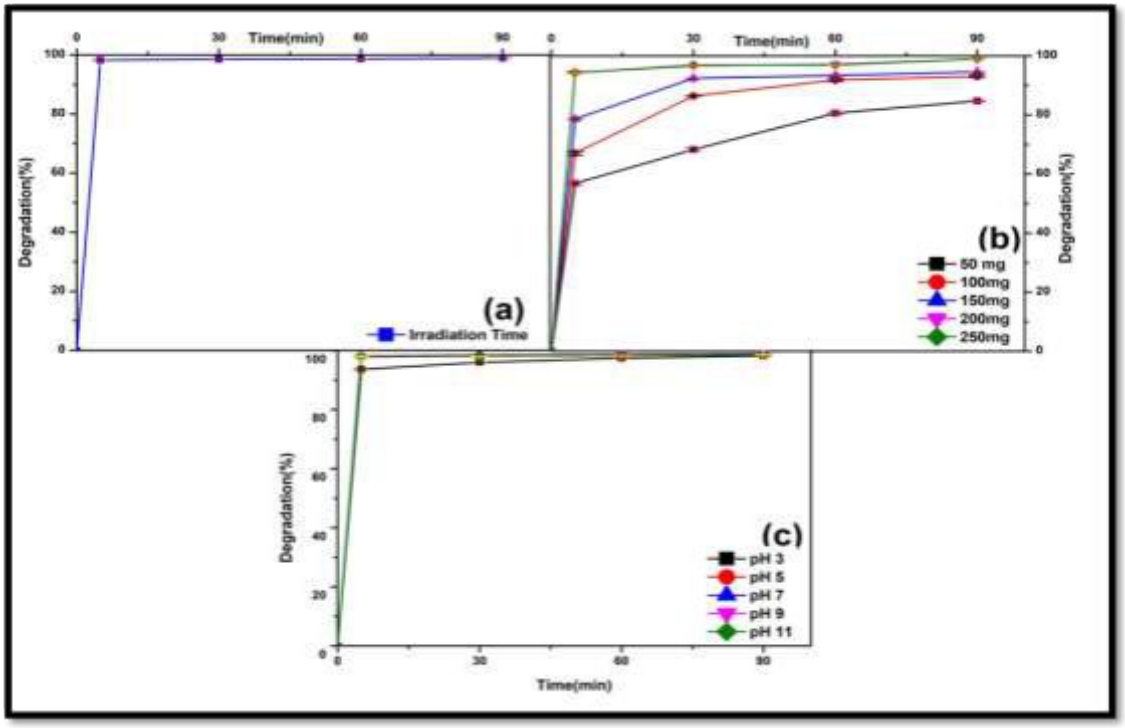

Figure.5.18. UV-vis spectrum of reaction mixture showing effect of various factors on the photocatalytic degradation of MB using MoS_2@GQDs. (a) Irradiation time (b) Photocatalyst concentration (c) pH.

5.3.2.4. Optimum parameter degradation efficiency

By considering the optimized parameters, a final experimentation has been set up in which the 250 mg of nanocomposite was added to the 50 mL of 100 ppm dye solution of MB kept at pH 7. The reaction mixture was magnetically stirred for 30 mins for attaining the adsorption-desorption equilibrium and exposed to the direct sunlight for 90 min. After every 30 min, the samples were taken out from reaction mixture for UV-vis spectral analysis as shown in Fig 5.19(a). With respect to time, there was a decrease in the absorbance intensity representing the increase in percentage

degradation of dye. Finally, using optimized parameters, 98.85±0.99% of MB was degraded in 90 min and the % degradation of dye is shown in Fig 5.19(b). To examine the rate constant, ln C/C_0 is plotted against time and calculated rate constant were -0.03167 min^{-1} for MB as shown in Fig 5.19(c).

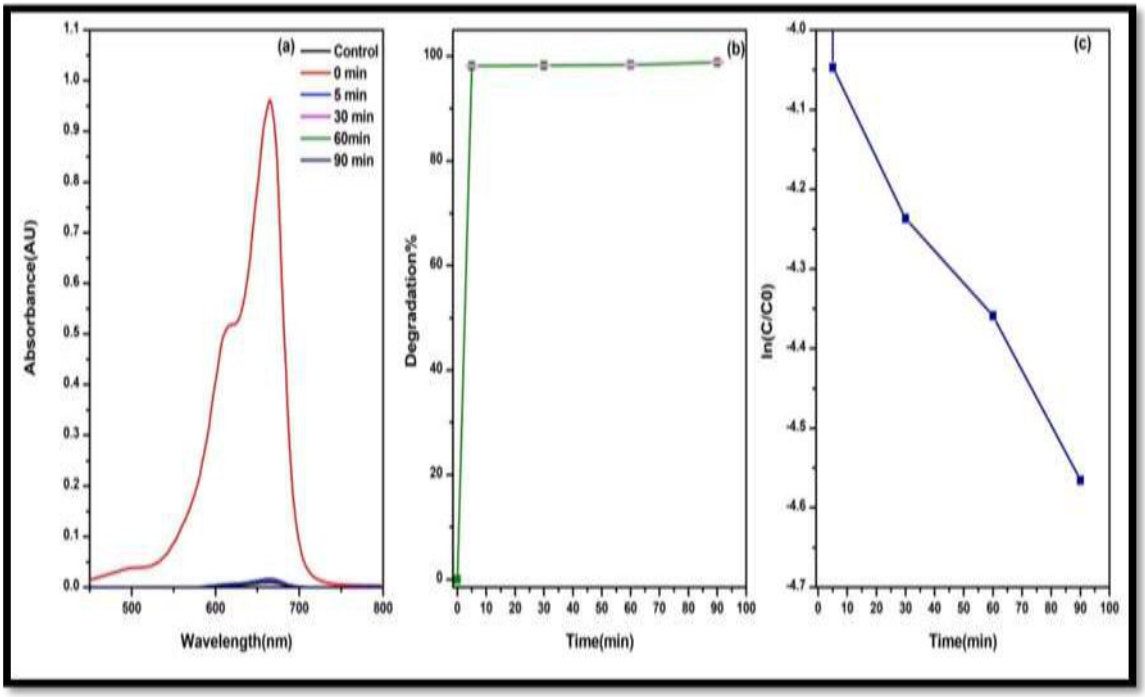

Figure 5.19. Photodegradation studies of MB on optimized parameters. (a) UV-spectrum of MB dye (b) Degradation (%) of MB dye (c) ln (C/C_0) plot of MB.

5.3.2.5. Photocatalytic degradation of commercial blue using GA-MoS_2 nano-heterostructures (MoS_2 @GQDs)

To evaluate the other applicability of the synthesized nanocomposite, photocatalysis based experimentation was performed on commercial dye i.e. Atul direct blue 2 B (1.5%) using the present photocatalyst with the standardized conditions as shown in Fig. From the UV-vis spectral analysis, it has been found that 86.66+0.08% of Atul direct blue 2 B (1.5%) dye degradation occurred in 20 min after which equilibrium plateau was obtained as shown in Fig 5.20(a). A plot depicting the % degradation w.r.t. time is shown in figure along with examining the rate constant by plotting ln

C/C_0. Fig.5.20(c) have shown the rate constant plots and values found to be -0.09887 min^{-1} for the respective dye.

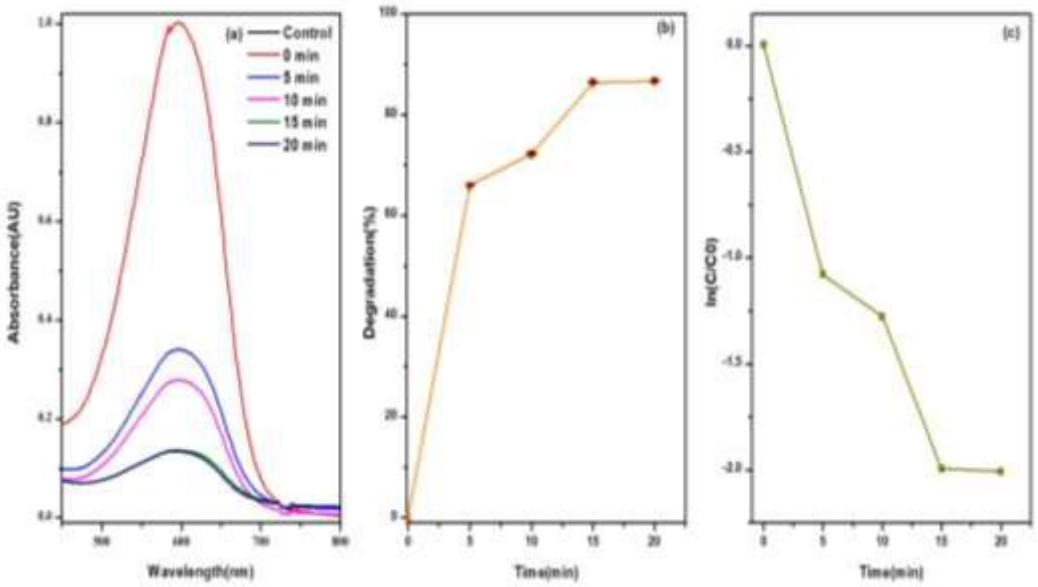

Figure.5.20. Photocatalytic degradation of commercial blue (CB) at optimal conditions (a) UV-spectrum of CB (b) Degradation (%) of CB (c) ln (C/C_0) plot of CB.

5.3.2.6. Degradation efficiency for real textile effluent

Using standardized conditions for the azo dye (lab) and commercial dyes, the real textile effluent was also treated with dose of 250 mg/ 50 mL at pH of 7 and irradiation time of 90 min. In the effluent sample 93.092+0.008% of degradation of dye was obtained as shown in fig 5.21(a). The percentage degradation and ln C/C_0 has been plotted against the time which accounted for the rate constant to be 0.02898 min^{-1} fig 5.21 (b) and (c). The sample taken out from the reaction mixture under observation has shown the complete degradation of color/dye content present in the sample w.r.t. time. At the end, pale yellow transparent solution has been recovered confirming the efficiency of nanomaterial as photocatalyst for the remediation of wastewater.

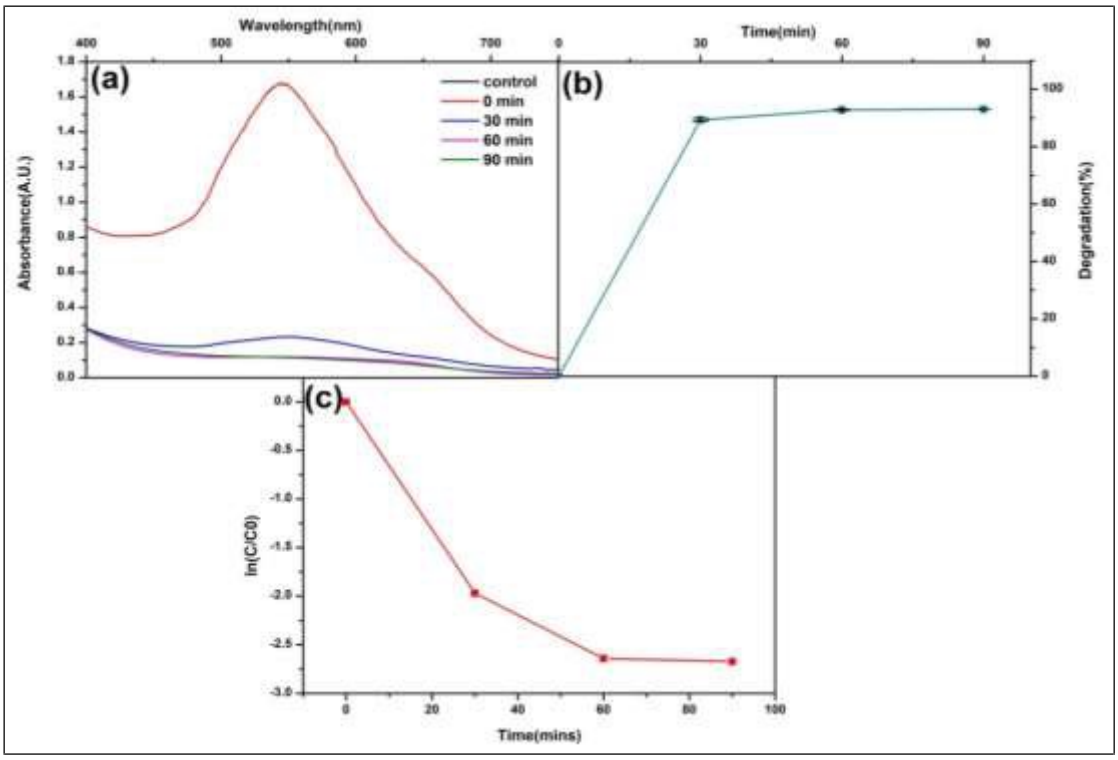

Figure.5.21. Photocatalytic degradation of textile industry wastewater sample. (a) UV–Vis. spectrum of dye degradation. (b) Degradation percentage. (c) ln (C/C_0) plot of degradation.

5.3.2.7. Reusability of GA-MoS_2 nano-heterostructures (MoS_2@GQDs against MB

Fig 5.22(a) display the recyclability study of nanocomposite for MB degradation under optimized conditions to check its reusability potential. The findings suggested that nanocomposite could be used three times successively to obtain half of photodegradation. The percentage of MB photodegradation found was 98.85± 0.09, 90.23 ±0.125, 84.35± 0.264, 74.85± 0.287, and 67.38± 0.311% in successive cycles from first to fifth cycle (Fig 5.22a).

5.3.2.8. Free radical trap experiment using GA-MoS_2 nano-heterostructures (MoS_2 @GQDs

It was found that for control, the photocatalytic degradation of MB presented the complete degradation by 98.85±0.99%. On the contrary, the reaction mixture

containing the chloroform had shown 48.67±0.24% for MB. Similarly, 50.08±0.026% and 45.11±0.52% degradation had occurred in set 3. From this data, it is evident that when chloroform (quencher of superoxide radical) and DMSO (quencher of hydroxyl radicals) were introduced in the solution, the degradation (%) of MB slowed down by half, implying that the photogenerated superoxide's and hydroxyl play significant role in the photocatalytic process with more or less equal contribution. Fig 5.22(b).

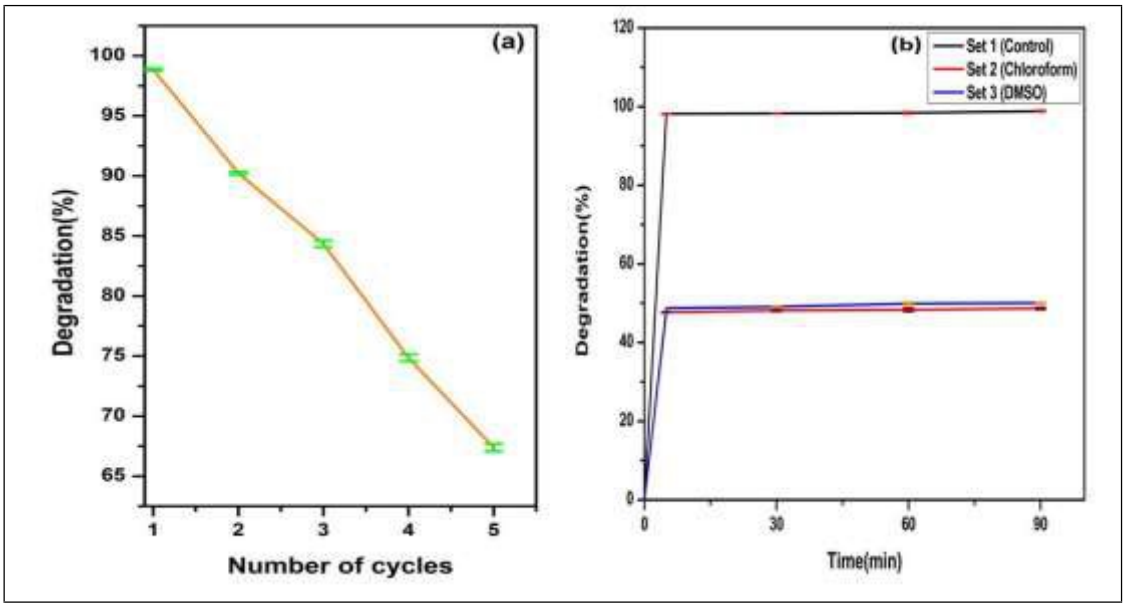

Figure 5.22. (a) The degradation percentage of MoS_2@GQDs with multiple cycles showing reusability. (b) Photocatalytic degradation of MB in the presence of scavengers.

5.3.3. Photocatalytic degradation of MB using SA-MoS_2 NS

5.3.3.1. Irradiation time

From a range of different contact time between the photocatalyst and dye molecules, 4 hours of sunlight exposure was optimal for the better degradation of MB. It has been observed that the percent degradation was about 56.68±2.1, 75.40±1.43, 94.75±0.59, and 98.81±0.12 for the MoS_2 NS photocatalyst exposed to 1 h, 2h, 3 h, and 4 h irradiation time, respectively (Fig 5.23(a)). The absorption spectra showed a regular decrease in the presence of photocatalysts with increasing irradiation time.

An irradiation time is defined as the interaction period of nanocatalyst with dye molecules to produce free radicals responsible for the photocatalysis. Generally, the percentage of dye degradation is closely correlated with the length of the irradiation period (I. Khan et al., 2022). Although more free radicals get generated over time, the degradation percentage increased until it reaches a plateau, being a prime reason behind photoreduction of dye. These findings show that the band gap and photocatalytic activity are both enhanced with increasing irradiation duration. As a result of the narrowing band gap, the photocatalytic process should be enhanced (Khan et al., 2022 ; Li et al., 2019).

5.3.3.2. Photocatalyst dose

The effect of the amount of MoS_2 NS on the photocatalytic degradation of MB dye is shown in Fig 5.23(b). A sharp decrease in the trendline has been observed while increasing the photocatalyst dose. Providing 4 hours of contact time, a complete photoreduction of 57.51±1.74%, 69.95±1.61%, 82.33±0.18%, 91.71±0.54%, and 98.81±0.122% has been obtained using 50 mg, 100 mg, 150mg, 200 mg, and 250 mg, respectively. Thus, 250mg was chosen to be optimal for the degradation of dye in visible light due to potential of degrading chromic component at higher extent.

Higher amount of photocatalyst refers to the presence of more nano-structures containing large number of active sites present on their surface. An increase in the active sites will lead to the adsorption of more dye molecules on their surface, undergoing more redox reactions to release more free radicals species (Negash et al., 2023; Vasiljevic et al., 2020). The photodegradation process is accelerated by the large quantity of free radicals generated.

5.3.3.3. pH

The effect of pH on the photocatalytic mechanism was investigated by adjusting the pH of the initial reaction solution at acidic, neutral, and basic values. From the analysis it is clear that pH 9 (basic conditions) produced highest 98.95±0.97% degradation in 4h sunlight exposure. Being cationic dye, the dye molecules have property to split into ions with a negative charge in the basic conditions.

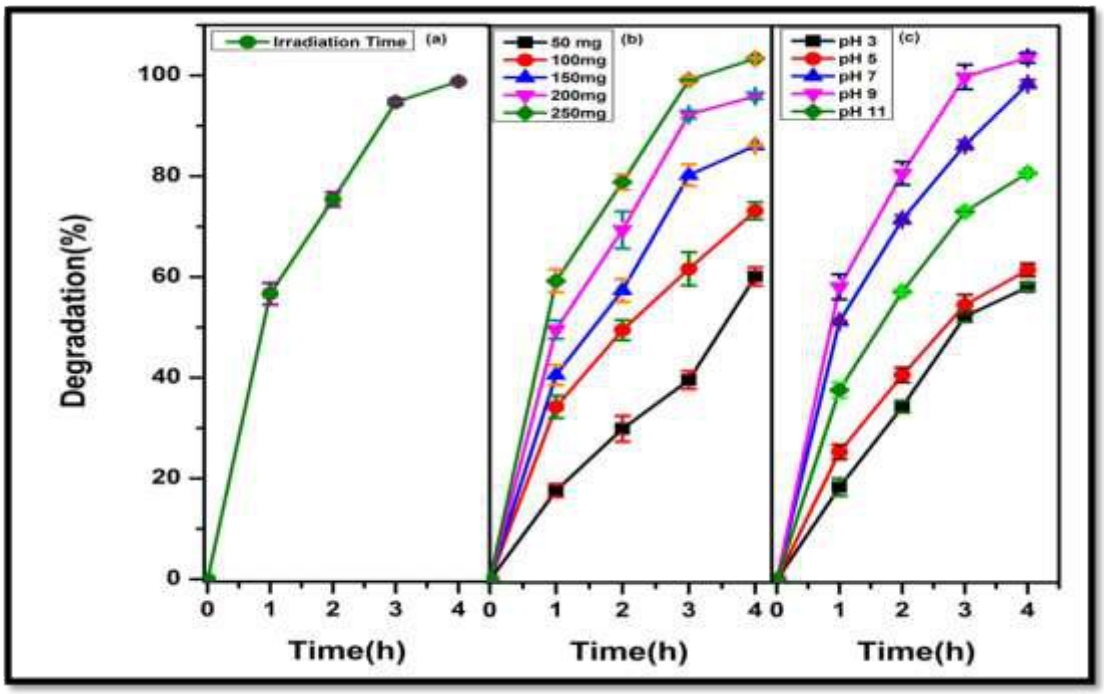

Figure 5.23. UV-vis spectrum of reaction mixture showing effect of various factors on the photocatalytic degradation of MB using SA synthesised MoS_2 NS (a) Irradiation time (b) Photocatalyst concentration (c) pH.

The strong electrostatic interaction between the positively (+vely) charged cationic dye MB and the substantially negatively (-vely) charged MoS_2 NS enables the dye to be adsorbed onto the surface of the MoS_2 NS. This electrostatic interaction also helps to improve the adsorptive property, which in turn improves the degradation efficiency (Qasim et al., 2020; Ritika et al., 2018).

5.3.3.4. Optimum parameter degradation efficiency

The catalytic activity of the MoS_2 NS was evaluated *via* the photodegradation of MB dye as monitored with a UV-vis spectrophotometer. A time-varying measurement has been conducted to determine the MB dye's most strong peak's absorbance decrease at 665 nm. On applying the optimized conditions to the final photodegradation test, 98.81±4.12% of methylene blue has been degraded in 4 hours at pH 9.0. The rate constant calculated from the data was calculated to be -0.070 min^{-1}.

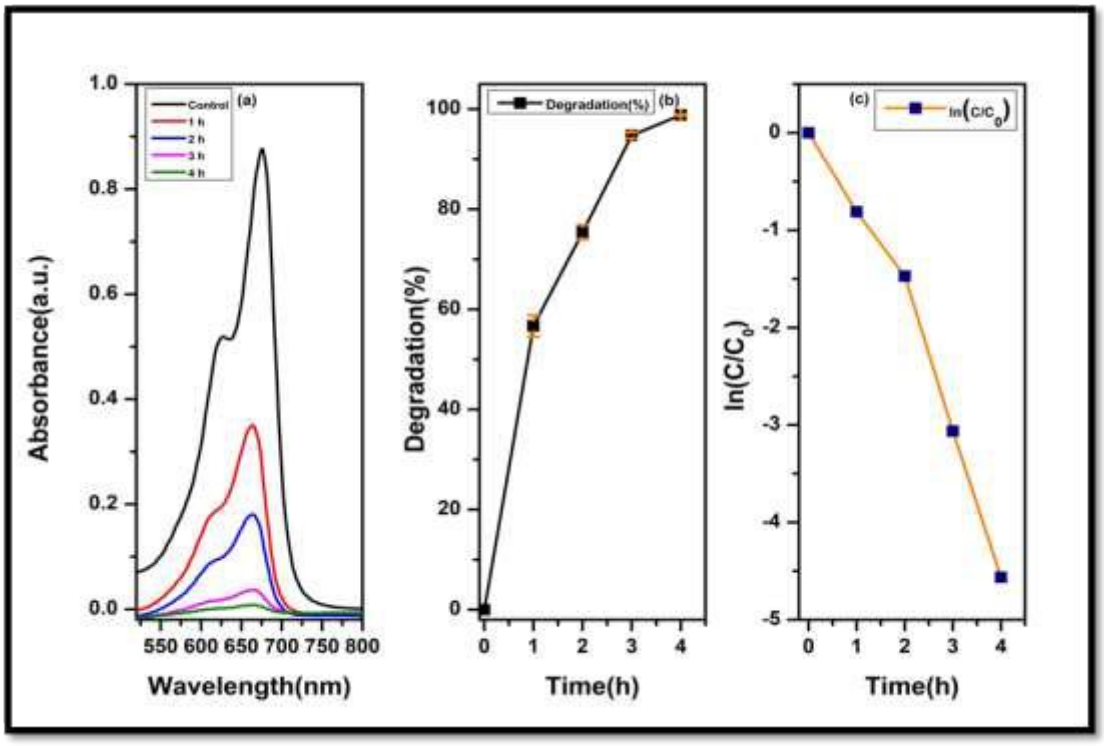

Figure 5.24. Photodegradation studies of MB on optimized parameters (a) UV-spectra of MB dye (b) Degradation (%) of MB dye (c) ln (C/C_0) plot of MB.

5.3.3.5. Photocatalytic degradation of commercial blue using SA-MoS_2 NS

The test sample containing 50mL of 100ppm CB solution added with 250mg of MoS_2 NS, adjusted with pH 9.0 was exposed to sunlight for irradiation. After analysis of results, it was found that 94.79±0.77 % of commercial blue was degraded in half an hour. The absorption spectra were recorded at an interval of 15 minutes to check the photocatalytic performance of the MoS_2 NS at λ_{max} = 600 nm. A decrease in absorption intensity representing the commercial blue showed the reduction in concentration of dye in the test sample. From kinetic studies of Fig. 5.25(c), the rate constant calculated was found to be -0.168 min^{-1}.

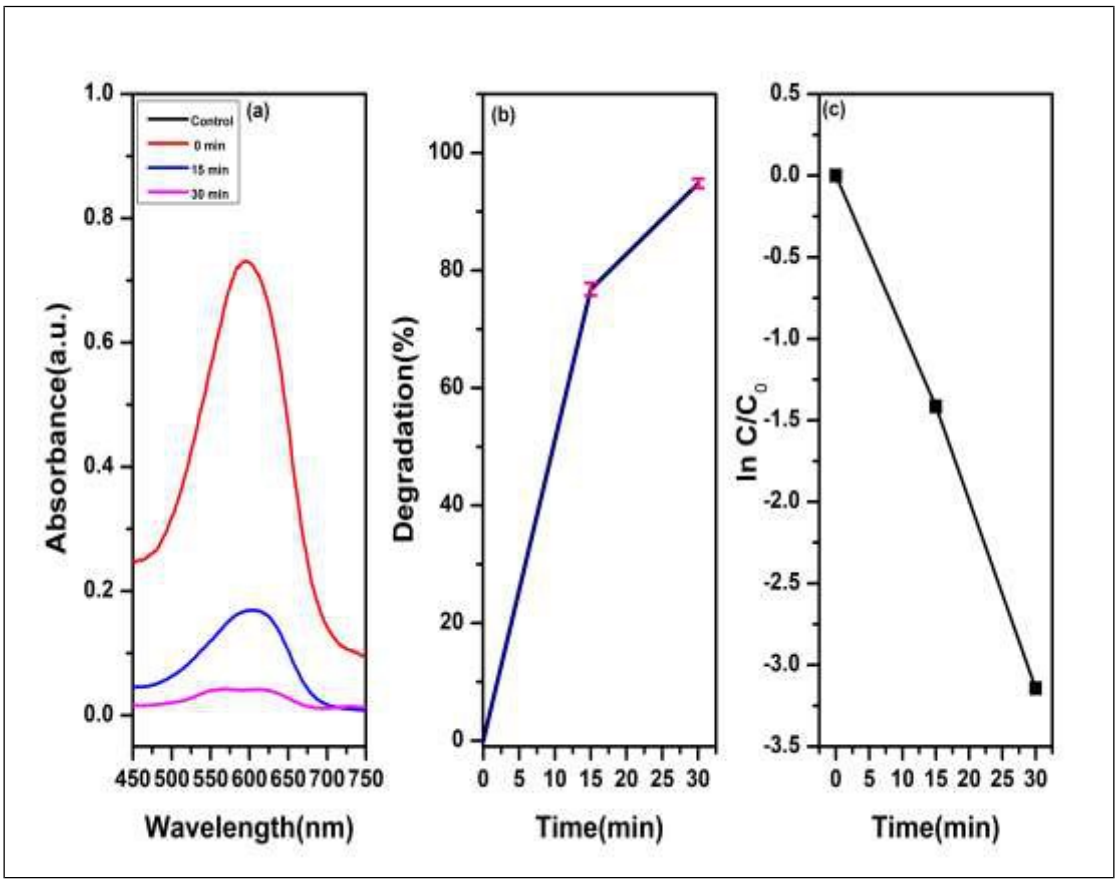

Figure 5.25. Photocatalytic degradation of commercial blue (CB) at optimal conditions (a) UV-spectrum of CB (b) Degradation (%) of CB (c) ln (C/C_0) plot of CB.

5.3.3.6. Degradation efficiency for real textile effluent

The applicability of the synthesized MoS_2 NS was evaluated against the real industrial effluent collected from the dye house. The three times diluted dye sample was treated with 250mg of nanocatalyst and conditioned at pH 9.0 for 1h sunlight treatment. From the findings observed at λ_{max}=545-500nm, it has been inquired that 94.09±0.50% dye present in the effluent has been photodegraded by synthesized material. These outcomes demonstrate the system's effectiveness in practical settings and its promise for quick and effective degradation of textile effluents. From kinetic studies of Fig. 5.26 (c), the rate constant was found to be -0.089 min^{-1}.

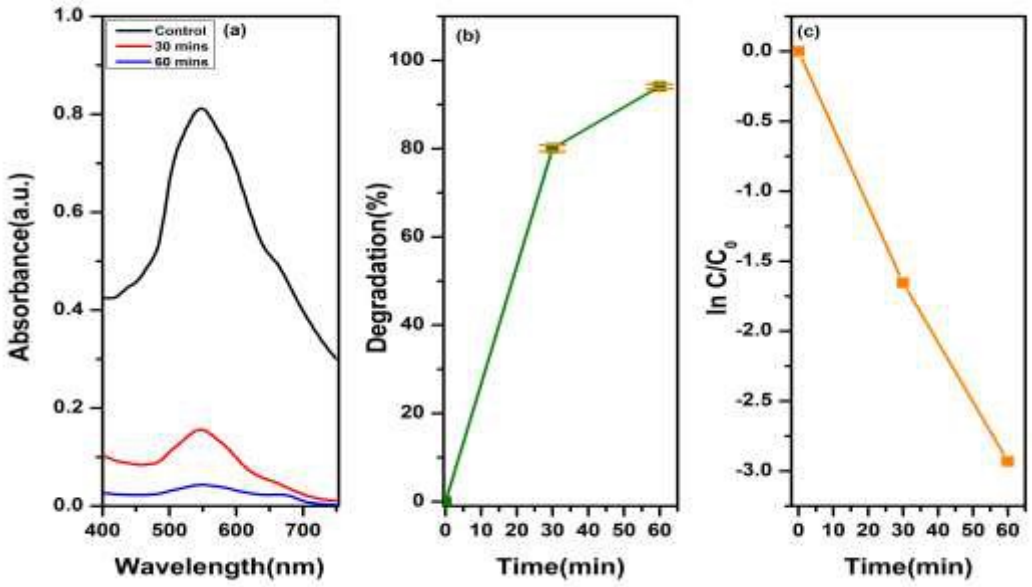

Figure 5.26. Photocatalytic degradation of textile industry wastewater sample (a) UV–Vis. spectrum of dye degradation. (b) Degradation percentage. (c) ln (C/C_0) plot of degradation.

5.3.3.7. Reusability of SA-MoS_2 nano-structures against MB

The figure illustrates a study on the recyclability of a nanocomposite for the degradation of MB under identical experimental settings, aiming to assess its potential for reuse. The results indicated that the nanocomposite could be employed in only 2 cycles to achieve a 30% reduction in photodegradation. The observed rates of MB photodegradation were 98.81±4.12, 30.18± 1.5%, and 0% in the first, second, and third cycles, respectively (Fig 5.27(a)).

5.3.3.8. Free radical trap activity using SA-MoS_2 nano-structures

The study revealed that the photocatalytic degradation of MB achieved 98.81±4.12% degradation rate under controlled conditions. In contrast, the reaction mixture that contained chloroform (superoxide quencher), exhibited a measurement of 42% photoreduction for MB. In set 3 containing DMSO (hydroxyl quencher), there was 50% degradation of MB. From the fndings, it was concluded that superoxides play a vital role in the photodegradation as compare to hydroxyl reactive species (Fig 5.27(b)).

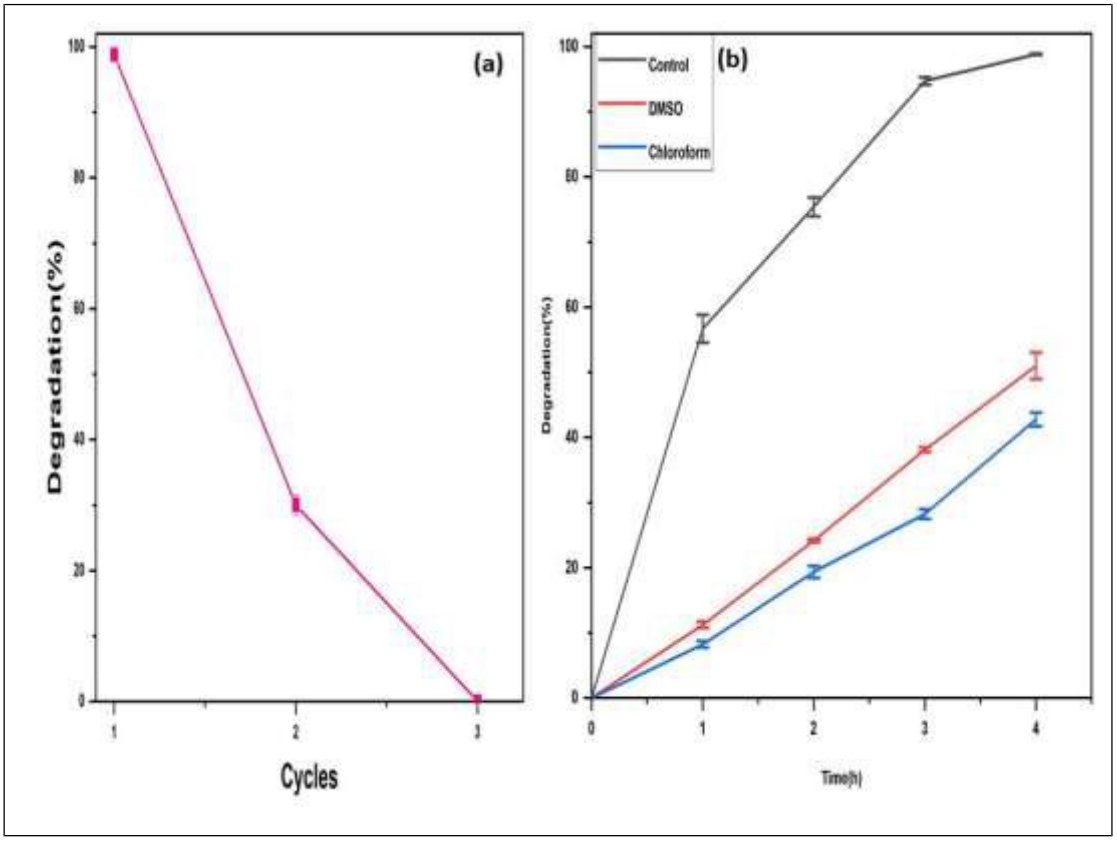

Figure 5.27. (a) The degradation percentage of MoS_2 NS with multiple cycles showing reusability. (b) Photocatalytic degradation of MB in the presence of scavengers.

5.3.4. Photocatalytic degradation of MB using SA-MoS_2 @GQDs

5.3.4.1. Effect of irradiation time

The photocatalytic degradation experiment was conducted over a range of contact time from 0-30 min using 100mg/50mL SA-MoS_2@GQDs for MB dye. With increase in irradiation time, the more contact time provided better photodegradation as the absorbance intensity of MB was found to decrease. The maximum degradation was achieved at 30 mins with 96.54±1.24% dye removal. Equilibrium was attained after half an hour of irradiation, indicating the saturated efficacy of photocatalyst to remove the dye. Increase in degradation rate can be explained in terms of availability of active sites on the catalyst surface and sunlight penetration into the suspension because of increased screening effect and scattering of light (Fig 5.28(a)). Basically, longer

irradiation time provides facilitated more contact time to saturate the photocatalyst active sites to adsorbs the dye molecules as well as provide optimum number of photon essential for the degradation of dye molecules (Pu et al., 2012; Qi et al., 2015).

5.3.4.2. Effect of photocatalyst concentration

The effect of photocatalyst SA-MoS_2@GQDs concentration on the photocatalytic degradation of azo dyes (MB) was investigated. The photocatalytic degradation

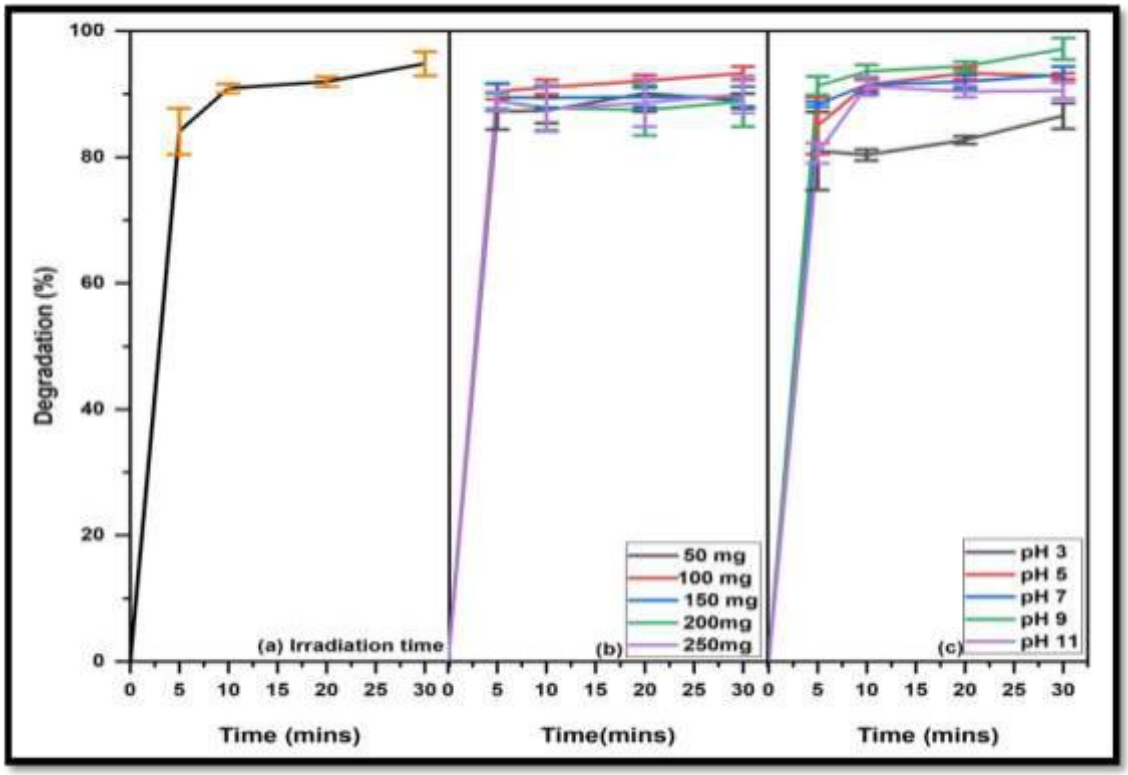

Figure 5.28. UV-Vis spectrum of reaction mixture showing effect of various factors on the photocatalytic degradation of MB using SA-MoS_2@GQDs. (a) Irradiation time (b) photocatalyst concentration (c) pH.

experiments were carried out at different concentrations of photocatalyst 50, 100, 150, 200, and 250mg using constant 100 ppm MB concentration. It has been evaluated that with an increase in the photocatalyst concentration, the rate of degradation decreased after some concentration as shown in Fig 5.28(b).It has been reported in various research papers that with an increase in the concentration of photocatalyst, the rate of

dye degradation decreases. The subsequent decrease in photodegradation can be easily explained by the continued rise in catalyst dosage.

Once the optimal level is surpassed, the suspended SA-MoS_2@GQDs in the reaction mixture combine, due to which the quantity of sunlight reaches the catalyst's active sites has decreased. As a result, the reaction rate drops (Aisien et al., 2013).

5.3.4.3. Effect of pH

pH is a key parameter in photocatalytic reactions. The effect of pH on photocatalytic degradation of dye solution in the range of 3–11 was investigated while keeping other parameters constant. The pH of the reaction mixture was adjusted by adding 1M NaOH and 1M HCl. Fig 5.28(c) compares the results of photocatalytic degradation of dye as a function of reaction pH. A change in the surface charge of a photocatalyst can be generated by changing the pH of the reaction mixture as shown in Fig 5.28(c).

Increasing the pH of the reaction mixture, also enhanced the dye removal. At highly basic pH, multiple interlayer anions present in nanocomposite facilitated the adsorption of MB on its surface which enhanced the transfer of generated carrier charges to photocatalyst surface. Additionally, more basic environment was found to decrease the photodegradation efficiency of nanocomposite. Hence, pH 9 was optimal for photodegradation.

5.3.4.4. Optimum parameter degradation efficiency

Concluding the final outcomes, 100mg of photocatalyst, 100 ppm of dye concentration, 30 mins of irradiation, and pH 9 were the optimal conditions for better photodegradation. After optimization, a triplicate of final experimentation was done. For experimentation, 50 mL of 100 ppm dye solution (MB) was treated with 100mg of photocatalyst at pH 9 for 30mins. Fig 5.29 (a) depicts the absorbance studies of MB dye at different time intervals. With an increase in time frame the absorbance quenches quite efficiently and by using eq. (1) the change in degradation rate was plotted with time as shown in fig 5.29 (b). The average degradation efficiency under optimum conditions was achieved at 97.16±1.70%. From kinetic studies as shown in Fig. 5.29(c), the rate constant was calculated that was found to be -0.077 min^{-1}.

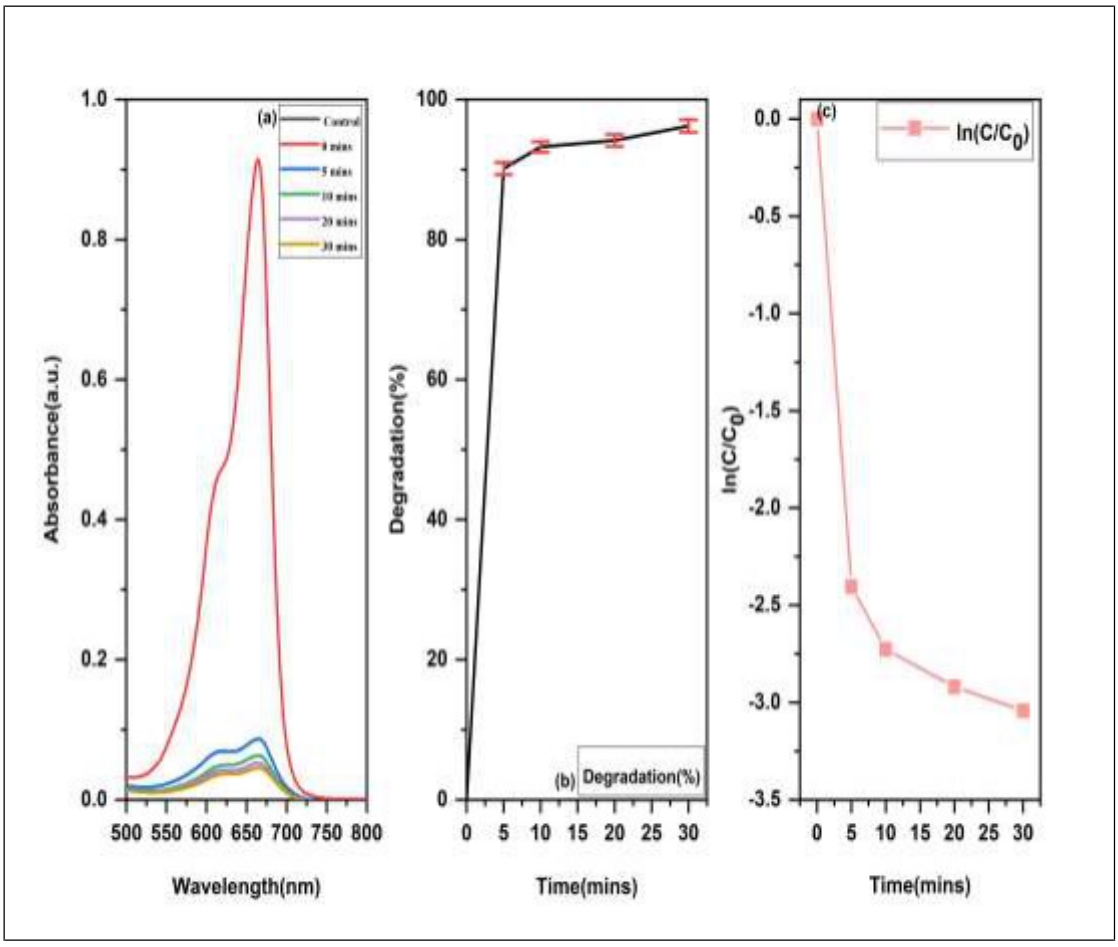

Figure 5.29. Photodegradation studies of MB on optimized parameters. (a) UV-vis spectrum of MB dye (b) Degradation (%) of MB dye (c)ln (C/C_0) plot of MB.

4.3.4.5. Photocatalytic degradation of commercial blue using SA-MoS_2 nano-heterostructures (MoS_2 @GQDs)

The photodegradation of commercial blue dye was conducted using 100mg of MoS_2@GQDs at 9.0 pH using 100 ppm of CB. The findings revealed a decrease in dye concentration that reached 93.83±1.15% within 15-minutes (Fig 5.30(a)). No additional degradation was seen after 15 minutes of incubation that indicated the nanocomposite has reached its maximal potential.

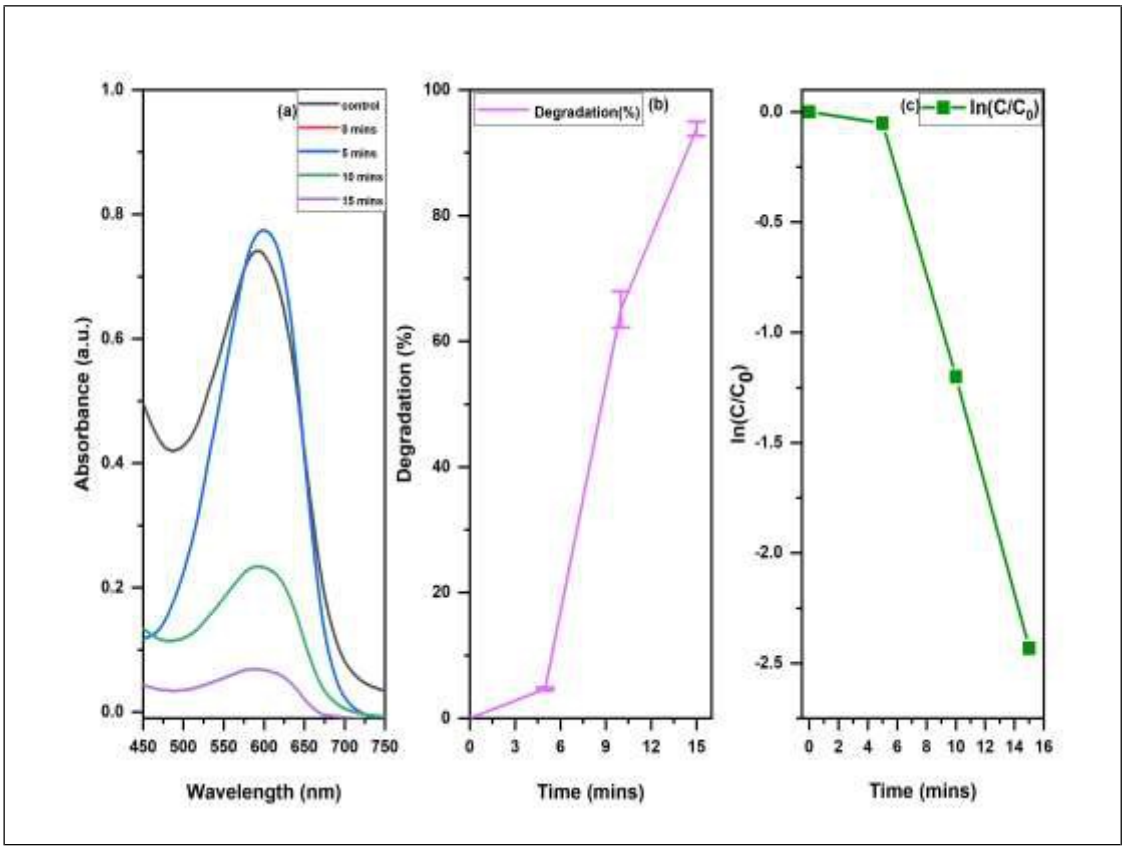

Figure.5.30. Photocatalytic degradation of commercial blue (CB) at optimal conditions (a) UV-spectrum of CB (b) Degradation (%) of CB (c) ln (C/C_0) plot of CB.

5.3.4.6. Degradation efficiency for real textile effluent

The textile effluent was treated with a dose of 100 mg/50 mL at a pH of 9 and an irradiation time of 30 minutes, using the same optimized parameters for the commercial dyes and MB. Fig 5.31(a) displays the spectral curve, which indicated that the dye present in the effluent sample has degraded by 95.20±0.98%. Plotting the percentage deterioration and ln C/C_0 versus time allowed for the rate constant calculated as -0.088 min^{-1} (Fig 5.31(b) and (c)). The sample removed from the reaction mixture for observation has demonstrated full deterioration of the sample's colour and dye concentration over time. In the end, a translucent, pale-yellow solution was recovered, demonstrating the effectiveness of MoS_2@GQDs as the best photocatalyst for wastewater treatment bioremediation.

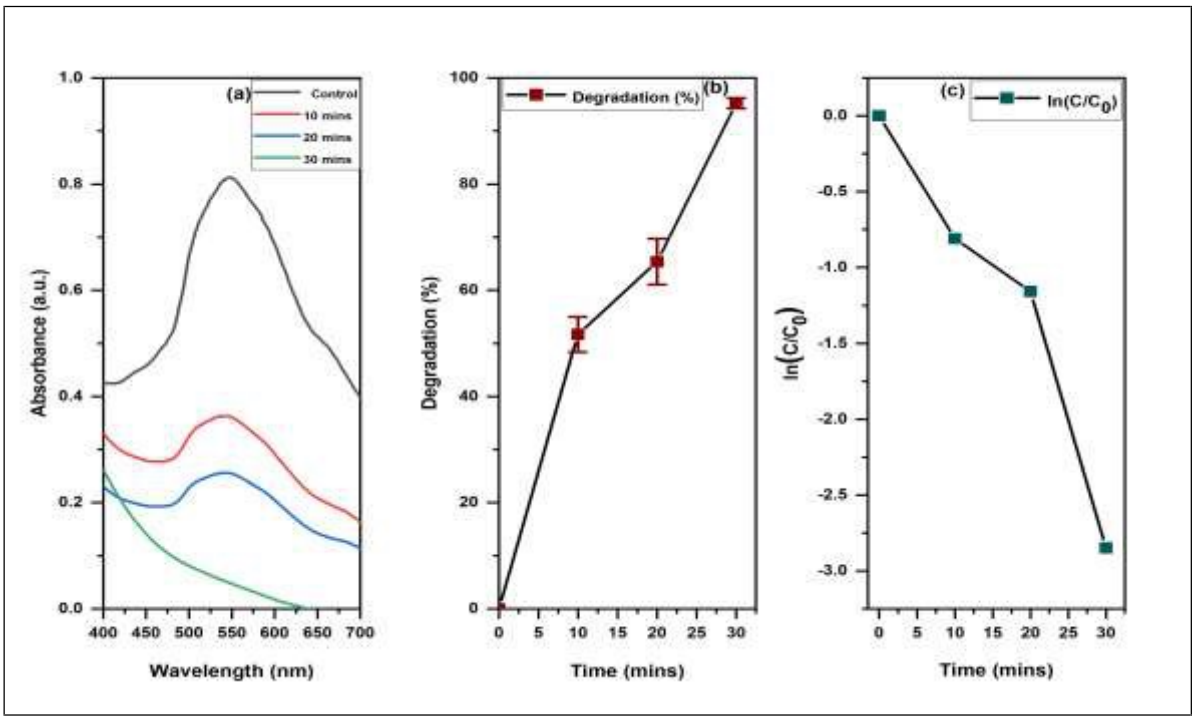

Figure 5.31. Photocatalytic degradation of textile industry wastewater sample. (a) UV–Vis. spectrum of dye degradation (b) Degradation percentage (c) ln (C/C_0) plot of degradation.

5.3.4.7. Reusability of SA-MoS_2 nano-heterostructures (MoS_2 @GQDs against MB

The reusability potential of the SA-MoS_2@GQDs was tested in an experiment involving MB degradation under optimal condition. After three consecutive uses, nanocomposite could achieve 24.10% photodegradation, as per the findings. As depicted in Fig 5.32(a), the percentage of MB photodegradation decreased from the 1st to 4th cycle, going as follows: 96.22±0.9, 52.32±0.74, 24.10±0.65, and 8.35±0.9%, respectively. After fourth cycle, there was no photocatalytic activity left in the nanocomposite.

5.3.4.8. Free radical trap experiment using SA-MoS_2 nano-heterostructures (MoS_2 @GQDs)

The total degradation of 96.22±0.9% was observed for control from the photocatalytic degradation of MB. Conversely, the reaction combination with the chloroform had indicated 49.54±0.52% for MB. In the test sample containing DMSO, similarly,

51.24±0.74% degradation had happened. From this data, it was clear that the degradation of MB slowed down by half when chloroform (quencher of superoxide radical) and DMSO (quencher of hydroxyl radicals) were added in the solution, suggesting that the photogenerated superoxide's and hydroxyl play major role in the photocatalytic process with Fig.5.32(b).

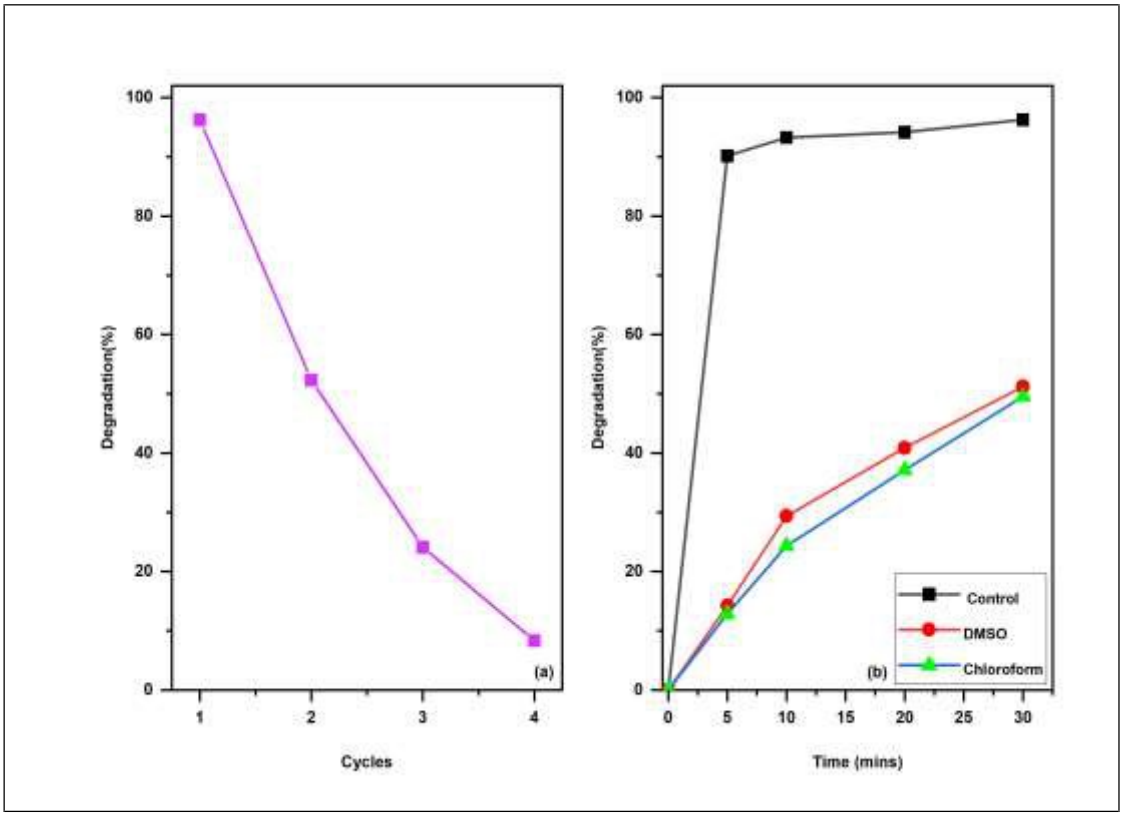

Figure 5.32. (a) The degradation percentage of MoS_2@GQDs with multiple cycles showing reusability. (b) Photocatalytic degradation of MB in the presence of scavengers.

5.3.5. Photocatalytic degradation of MB using TcSE mediated MoS_2 NS

5.3.5.1.Effect of iIrradiation time

In order to assess the effectiveness of TcSE-MoS_2 NS in photocatalysis of MB, 100 mg of MoS_2 NS were combined with 50 mL of a 100-ppm dye solution. The reaction mixture was exposed to direct sunlight while optimising several parameters to enhance the outcomes. The absorbance decreased as the incubation time increased

from 0-60 mins, demonstrating the breakdown of MB (Fig 5.33(a). To further calculate the percentage of degradation, Equation 1 was utilised. Fig 5.33(a) depicts the proportion of degradation rate over time. A direct relationship between the irradiation time and photodegradation of MB was observed due to more contact time and better reaction exposure.

5.3.5.2. Effect of catalyst dose

An investigation was conducted to examine the impact of photocatalyst concentration on the process of photocatalytic degradation of MB dyes. The photocatalytic degradation studies were conducted utilising variable concentrations of photocatalyst, ranging from 10, 20, 30, 40, and 50mg, while maintaining a constant dye concentration of 100 ppm. The rate of deterioration enhanced with elevating the photocatalyst dose due to presence of more active sites to be available for oxidation-reduction process. From the fig. 5.33(b), a linear relationship can be seen between photocatalyst concentration and degradation (%). Hence, 50 mg was best fit for further experimentation.

5.3.5.3. Effect of pH

pH has an important function in photocatalytic processes. An investigation was executed to examine the change in the degradation (%) of dye solution when the pH of reaction mixture was varied from 3–11, with all other parameters held constant. The pH of the reaction mixture was modified by the addition of 1M NaOH and 1M HCl. Fig. 5.33(a-c) illustrated the relationship between the pH of the reaction and the outcomes of photocatalytic degradation of dye. Modifying the pH of the reaction mixture, as seen in Fig 5.33(c), can induce a modification in the surface attributes of a photocatalyst.

Elevating the pH of the reaction mixture resulted in a heightened efficacy in dye removal. At a significantly alkaline pH, the presence of many anions across layers in the nanocomposite promotes the adsorption of MB onto its surface, hence increasing the transfer of produced carrier charges to the surface of the photocatalyst. In addition, highly basic environment has reduced the effectiveness of photodegradation in the nanocomposite. Therefore, pH 9 was determined to be the most favourable condition for photodegradation.

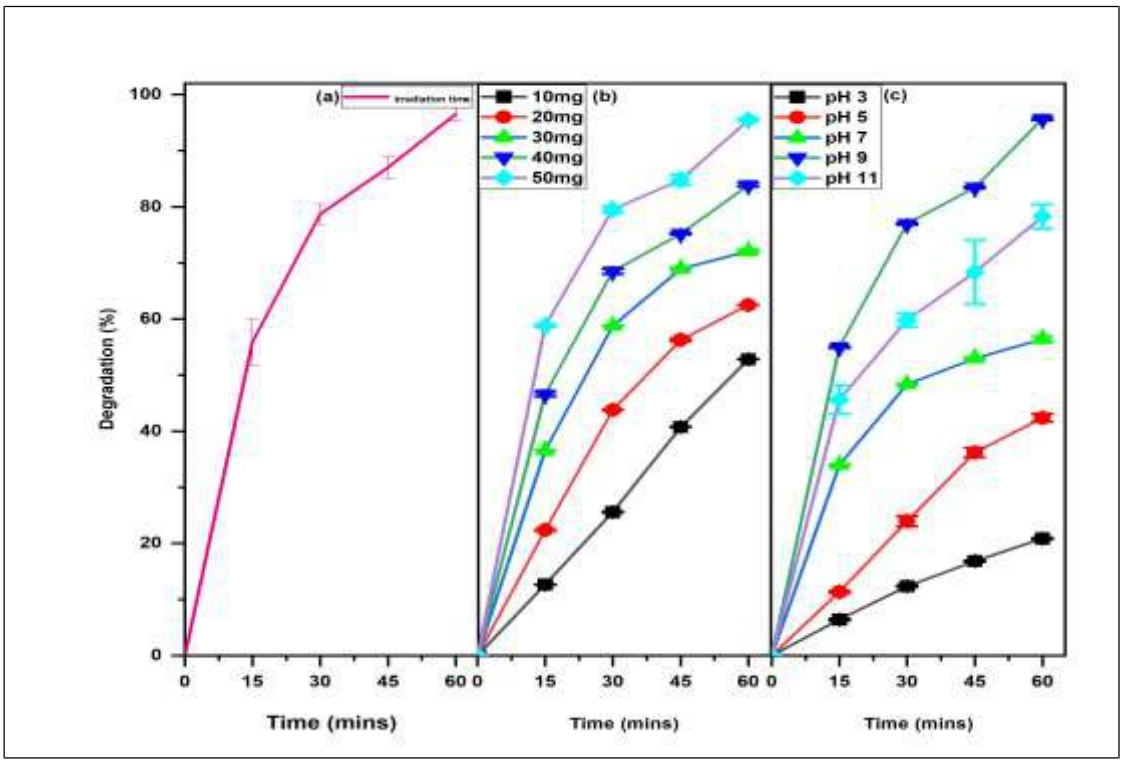

Figure 5.33. UV-vis spectrum of reaction mixture showing effect of various factors on the photocatalytic degradation of MB using TcSE-MoS_2 NS. (a) Irradiation time (b) Photocatalyst concentration (c) pH.

5.3.5.4. Optimum parameters degradation efficiency

The ideal parameters for achieving better photodegradation were determined to be 50mg of photocatalyst, 100ppm azo dye concentration, an irradiation time of 60 minutes, and a pH of 9. Following optimisation, the final experiments were conducted in triplicate. To conduct an experiment, a 50 mL solution containing 100 ppm of dye (MB) was exposed to 100 mg of photocatalyst at a pH level of 9 for a duration of 60 minutes. Fig 5.34(a) illustrated the analysis of absorbance of MB dye at various time periods. As the time frame increases, the absorbance was found to decrease significantly. By using equation (1), the variation in degradation rate was plotted against time, as depicted in fig 5.34(b). The degrading efficiency reached an average of 96.56±1.24% under optimal conditions.

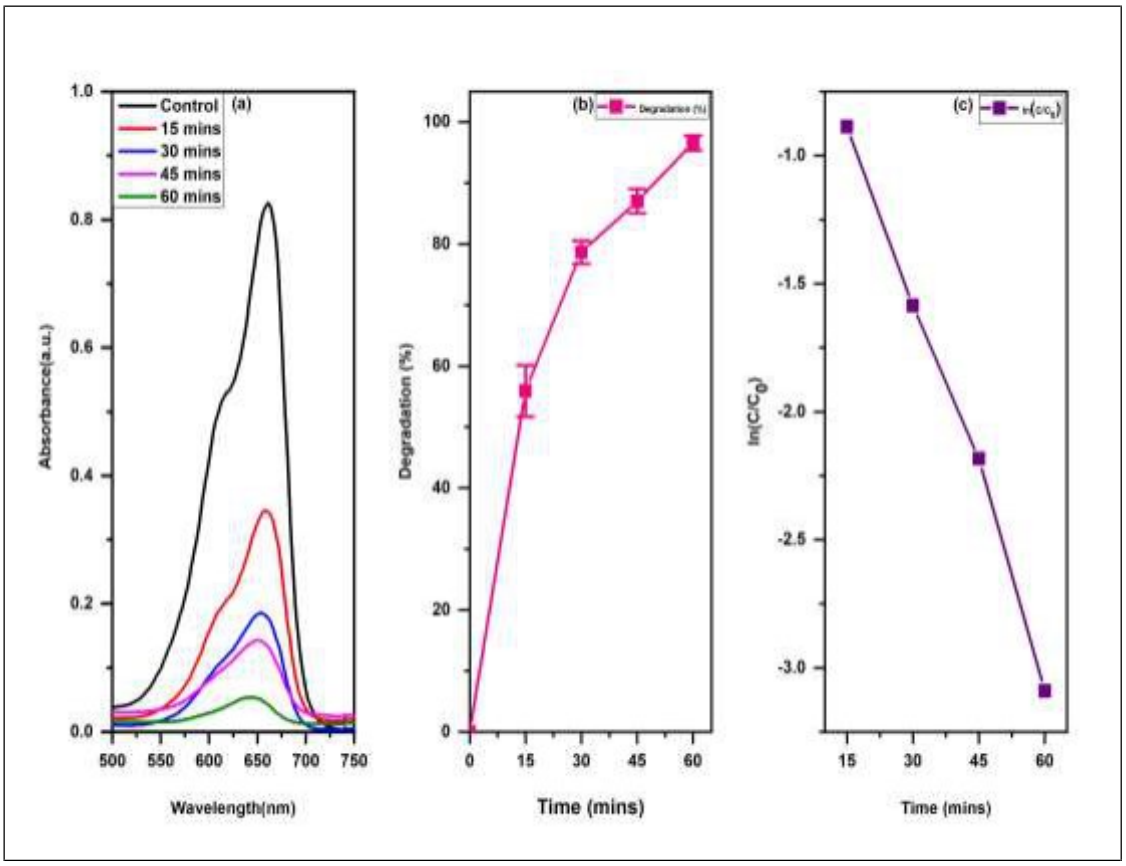

Figure 5.34. Photodegradation studies of MB on optimized parameters using TcSE-MoS_2 NS. (a) UV-spectrum of MB (b) Degradation (%) of MB dye (c) ln (C/C_0) plot of MB.

5.3.5.5. Photocatalytic degradation of commercial blue using TcSE mediated MoS_2 NS

A concentration of 100 ppm of CB was used in the photodegradation of commercial blue dye. The reaction was carried out using 50 milligrams of MoS_2 NS at pH 9. The dye concentration diminished by 82.17±1.8% over a period of 30 minutes. The computed rate constant from the rate kinetics was -0.058 min^{-1}.

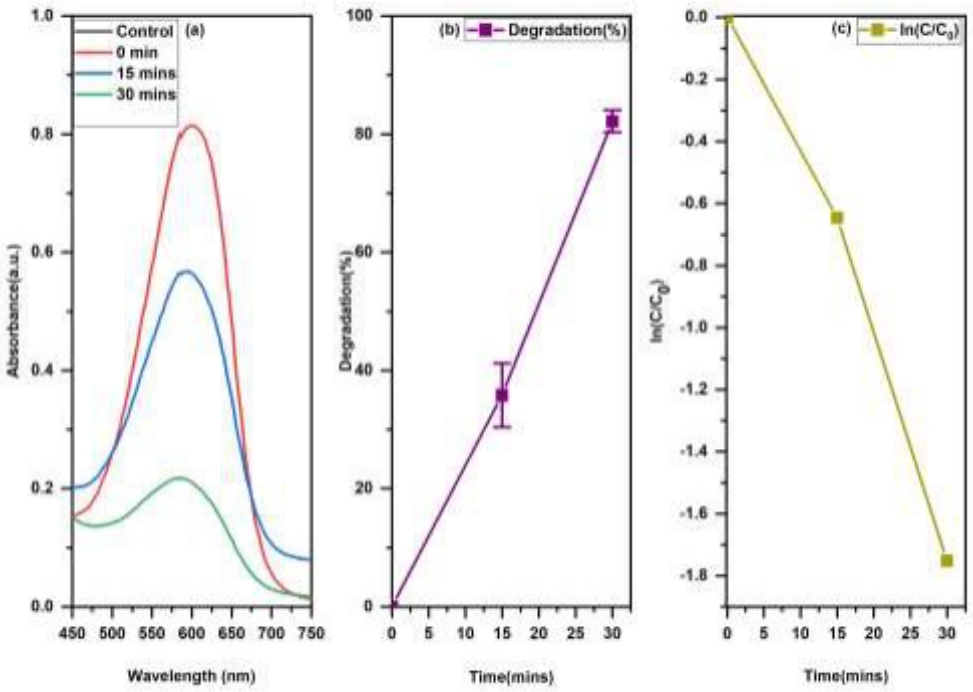

Figure 5.35. Photocatalytic degradation of commercial blue (CB) using TcSE-MoS_2 NS at optimal conditions. (a) UV-spectrum of CB (b) Degradation (%) of CB (c) ln (C/C_0) plot of CB.

5.3.5.6. Degradation efficiency for real textile effluent

Using the same optimal conditions for the commercial dyes and MB azo dye, the textile effluent was treated with 50 mg/50 mL TcSE-MoS_2 NS at pH 9 for 30 minutes. This experiment was done in triplicate. According to the spectral curve, which is depicted in Fig 5.36(a), the dye that was present in the effluent sample has degraded by 91.65+1.47%. After plotting the percentage of deterioration and the ln C/C_0 against time, it was possible to estimate that the rate constant was -0.085min^{-1} (fig 5.36 (b) and (c)).

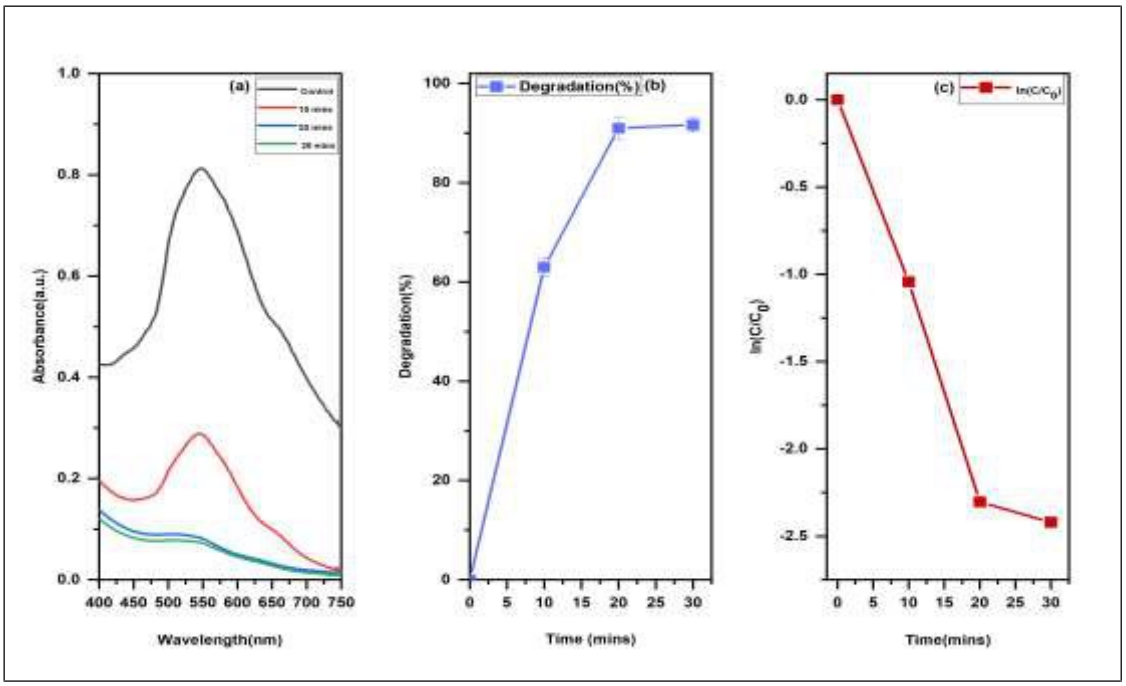

Figure.5.36. Photocatalytic degradation of textile industry wastewater sample using TcSE-MoS_2 NS. (a) UV–Vis. spectrum of dye degradation. (b) Degradation percentage. (c) ln (C/C_0) plot of degradation.

5.3.5.7. Reusability of TcSE-MoS_2 nano-heterostructures (MoS_2 @GQDs) against MB

From the Fig 5.37(a) representing reusability efficiency of the nanostructure, it was found that on successive reuse cycle, the photodegradation percentage was drops by 43% in the second cycle and 83% in 3rd cycle, respectively. Upto 4th cycle, the photocatlyst did not exhibited any photodegradation characteristics.

5.3.5.8. Free radical trap experiment using TcSE-MoS_2 nano-heterostructures (MoS_2 @GQDs

Using 50 mg of photocatalysts, an active species trapping experiment was conducted to study the mechanism of MB photodegradation. It is evident from the Fig 5.37(b) that the addition of scavengers significantly affected the photodegradation potential of nanocomposite revealing the active participation of free radicals in photodegradation. The degradation of MB was reduced to 25% and 77%, respectively, with the addition

of DMSO and chloroform. It has been found that superoxide have significant role in photodegradation of MB.

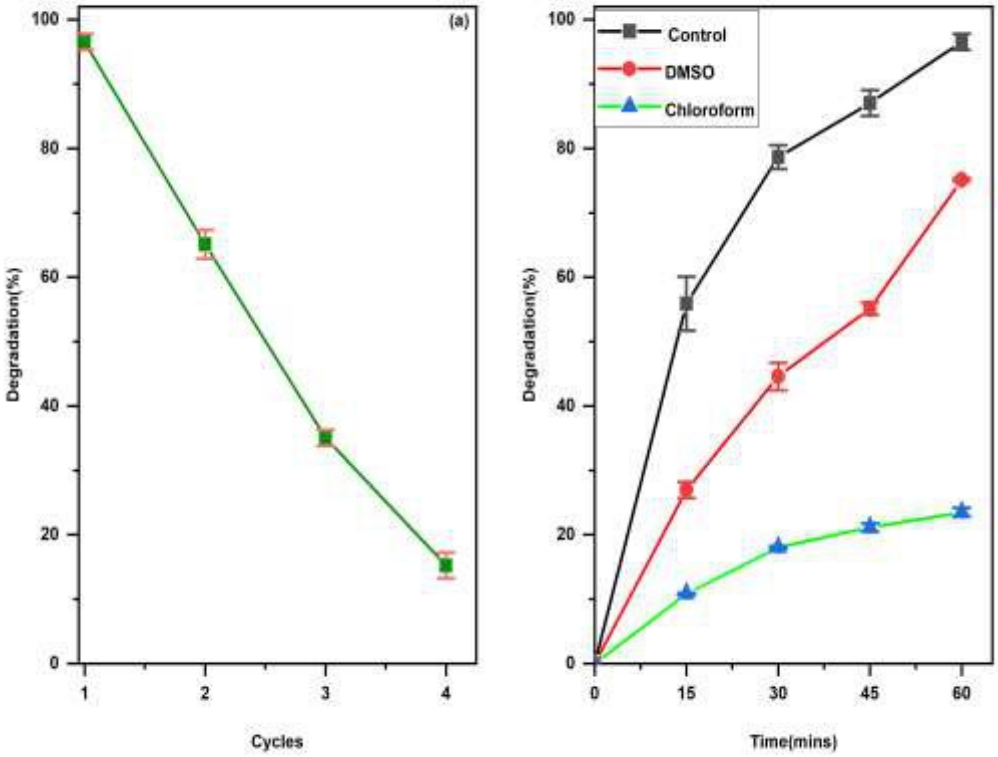

Figure 5.37.(a) The degradation percentage of MoS_2 NS with multiple cycles showing reusability (b) Photocatalytic degradation of MB in the presence of scavengers.

5.3.6. Photocatalytic degradation of MB using TcSE mediated MoS_2@GQDs

5.3.6.1. Effect of irradiation time

To optimize the optimum sunlight exposure for the photodegradation of the MB, the reaction mixture containing 50 mL of 100ppm MB dye and 20 mg of photocatalyst was exposed to direct sunlight for different interval of time. From the results and observations, it has been concluded that increasing the exposure time led to enhanced photodegradation. Hence, the highest photoreduction of MB was obtained after half an hour irradiation time

.

5.3.6.2. Effect of photocatalyst dose

A range of 10-50 mg of photocatalyst was added to 50 mL of MB (100ppm) for 30 minutes of contact time. The findings revealed that increasing the photocatalyst concentration enhanced the dye degradation efficiency upto a level. However, increase in the photocatalyst dose beyond 20 mg drops the photocatalytic efficiency of the material. A decline in the percent degradation of MB suggested the selection of photocatlyst dose as 20 mg(fig.38(b).

5.3.6.3. Effect of pH

Photocatalytic reactions majorly rely on pH. With all other factors held constant, we studied how a pH range of 3–11 affected the photocatalytic degradation of a dye solution. A solution of 1M NaOH and 1M HCl was added to the reaction mixture to change its pH. The photocatalytic degradation of dye findings as a function of reaction pH are shown in Fig 5.38(c). As demonstrated in Fig 5.38(c), altering the pH of the reaction mixture can cause a photocatalyst's surface charge to vary. From the figures, it was found that basic conditions fastened and improved the efficiency of photocatalyst to degrade MB. Hence pH 9 was considered best fit for final experimentation.

5.3.6.4. Degradation studies at optimum parameter

After optimizing the settings, a final experiment was conducted. In this experiment, 20 mg of nanocomposite was added to a 50 mL solution of 100 ppm MB dye at pH 9. The reaction mixture was agitated using a magnetic stirrer for 30 mins to achieve adsorption-desorption equilibrium, and then it was exposed to direct sunshine for 30 minutes. The samples were extracted from the reaction mixture for UV-Vis spectral analysis every 10 minutes (Fig 5.39a). Regarding the passage of time, there is a decline in the intensity of absorbance, which indicates a rise in the percentage of dye degradation. After optimizing the conditions, 94.85±4.8% of MB was destroyed during a 30-minute timeframe. The degradation percentage of the dye is illustrated in fig 5.39(b). The rate constant was determined by plotting the natural logarithm of the concentration ratio (ln C/C_0) against time. The computed rate constant for MB was found to be -0.03167 min^{-1}, as shown in Fig 5.39(c).

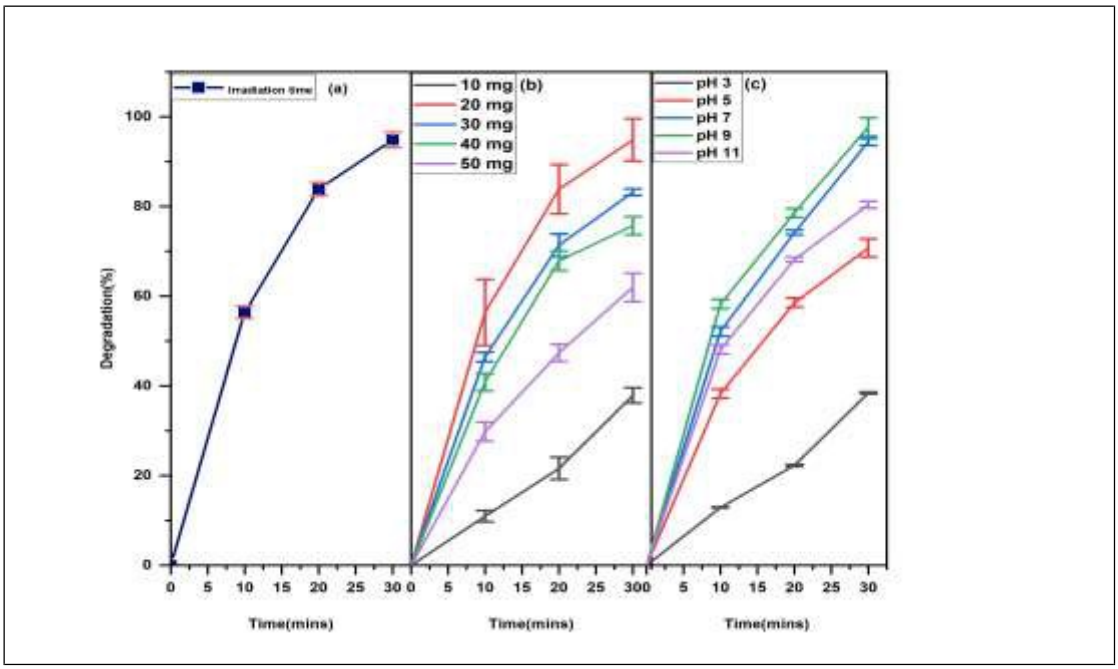

Figure 5.38. UV-vis spectrum of reaction mixture showing effect of various factors on the photocatalytic degradation of MB using TcSE-MoS_2@GQDs. (a) Irradiation time (b) photocatalyst concentration (c) pH.

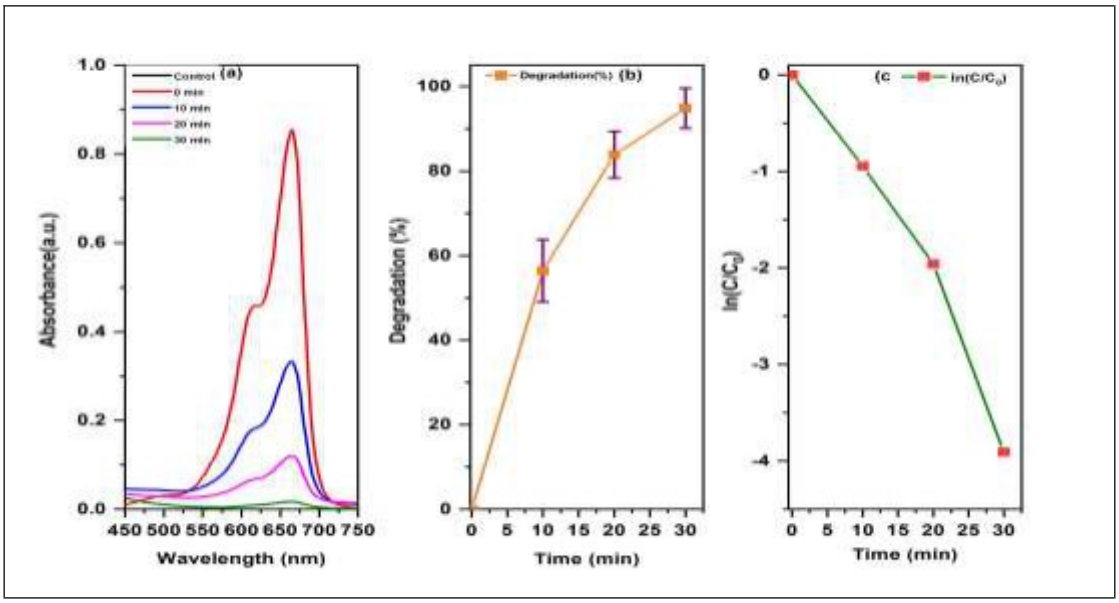

Figure 5.39. Photodegradation studies of MB on optimized parameters using TcSE-MoS_2@GQDs. (a) UV-vis spectrum of MB dye (b) Degradation (%) of MB dye (c)ln (C/C_0) plot of MB.

5.3.6.5. Photocatalytic degradation of commercial blue using TcSE-MoS_2 nano-heterostructures (MoS_2 @GQDs)

TcSE-MoS_2@GQDs were found to degrade CB with 94.8± 3.8 % efficiency at standardized conditions for the MB (dose=50mg, pH=9 and for 30 minutes). The spectral analysis of the figure exhibited a decrease in the peak intensity signifying the reduction in the dye concentration with time. Further, the graph 5.40 showing percentage degradation w.r.t. time and ln(C/C_0) graph have resulted to show the reaction kinetics.

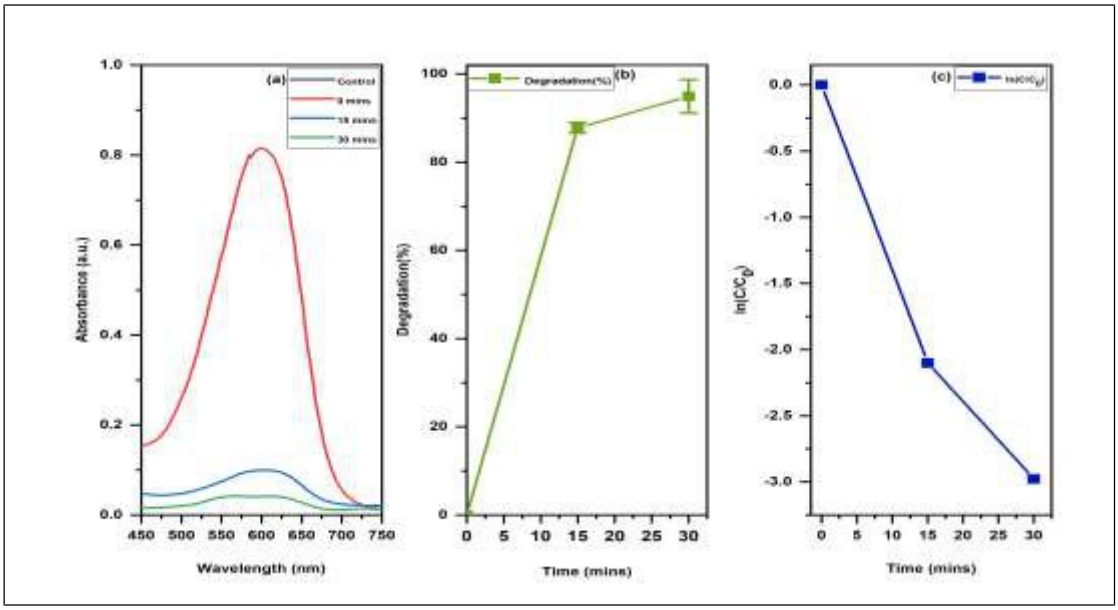

Figure 5.40. Photodegradation studies of commercial blue on optimized parameters using TcSE-MoS_2@GQDs. (a) UV-spectrum of CB dye (b) Degradation (%) of CB dye (c) ln (C/C_0) plot of CB.

5.3.6.6. Degradation efficiency for real textile effluent

The experiment conducted for the photocatalytic activity of TcSE MoS_2@GQDs against the industrial sample was done in triplicates at the optimal conditions standardized for the MB and CB. From the findings and fig (5.41), it has been found that 87.92±3.6% of industrial dye effluent was photodegraded in a span of 20 minutes. From kinetic studies of Fig. 5.41 (c), the rate constant calculated to be -0.70 min^{-1}. The pseudo-first-order kinetics describe the reaction kinetics involved in the

photocatalytic degradation of MB using nanomaterial as increase in the photodegradation was directly proportion to the photocatalyst dose.

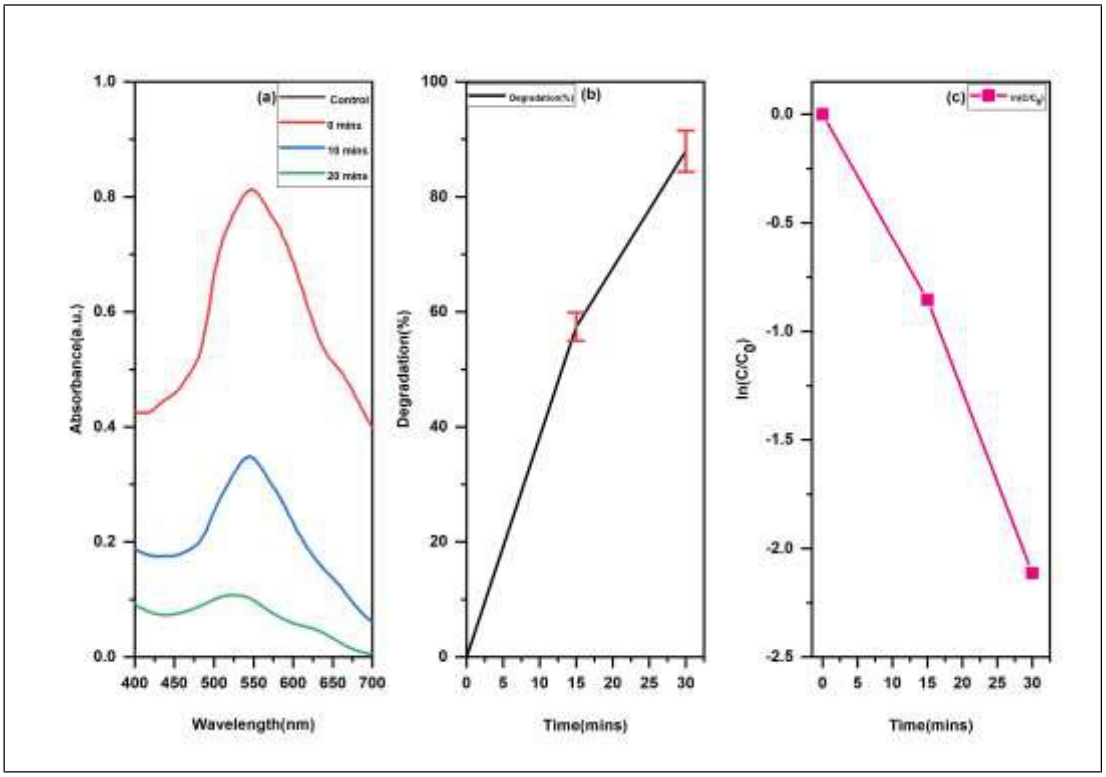

Figure 5.41. Photocatalytic degradation of textile industry wastewater sample using TcSE-MoS_2@GQDs. (a) UV–Vis spectrum of dye degradation. (b) Degradation percentage. (c) ln (C/C_0) plot of degradation.

5.3.6.7. Reusability of TcSE-MoS_2 nano-heterostructures (MoS_2 @GQDs) against MB

Reusability of TcSE-MoS_2@GQDs as catalyst depends on several components like chemical composition, stability, and morphology of nanocomposite. The potential photocatalytic activity of MoS_2@GQDs dropped on reuse by 43.58%, 40%, and 100% in three consecutive cycles (Fig 5.42(a)). It was due to loss of nanocomposite and non-avalibility of active sites on the nanocomposite which caused very minimal photodegradation on the consecutive reuse. Several potential causes can help to explain the declining photodegradation percentage of a strong photocatalyst: First, the

mass of the photocatalyst dropped through the washing and drying cycles. As a result, the photocatalyst concentration dropped to far less than its starting level. Second, obstruction of active sites could lower the surface activity of the photocatalyst (Saad Algarni et al. 2022).

5.3.6.8. Free radical trap experiment using TcSE-MoS_2 nano-heterostructures (MoS_2 @GQDs

The photodegradation mechanism of MB was investigated in an active species trapping experiment. This experiment utilized photocatalysts consisting of 50 mg of photocatalyst. The addition of DMSO has minimal impact on the deterioration of MB (Fig 5.42(b)). Nevertheless, the inclusion of chloroform and DMSO resulted in a reduction in MB degradation to 61% and 35%, respectively. Therefore, it can be inferred that superoxide and hydroxyl were the primary active species. However, the hydroxyl species plays a major contributive role in photodegradation.

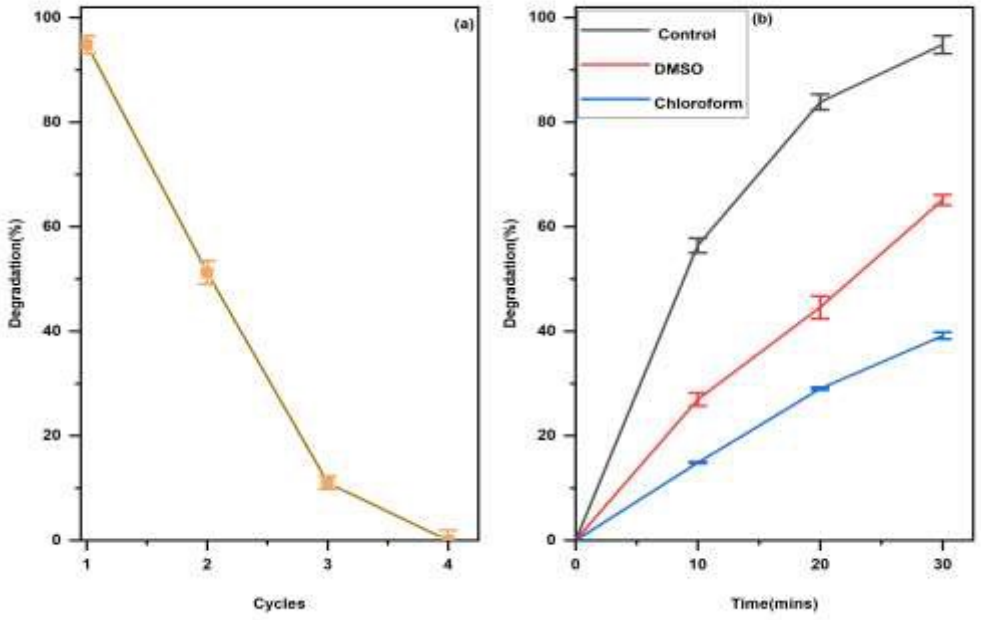

Figure 5.42.(a) The degradation percentage of MoS_2@GQDs with multiple cycles showing reusability. (b) Photocatalytic degradation of MB in the presence of scavengers.

Table 5.1. Summary of the photodegradation % of MoS_2 nanostructures and nano-heterostructures against MB, CB, Industrial sample (IS).

Dye.	**GA-MoS_2 NP**	**GA-MoS_2 @GQDs**	**SA- MoS_2 NS**	**GA- MoS_2 @GQDs**	**TcSE-MoS_2 NS**	**TcSE-MoS_2 @GQDs**
MB	98% (8h)	98.85± 0.99% (90 mins)	98.81± 4.12% (4h)	97.16± 1.70% (30 mins)	96.56± 1.24% (1 h)	94.85± 4.8% (30 mins)
CB	98.12± 0.15% (45mins)	86.66± 0.08% (15 mins)	94.79± 0.77% (30 mins)	93.83± 1.15% (15 mins)	82.17± 1.8 (30 mins)	94.8± 3.8% (30 mins)
IS	98.89% (150mins)	93.092± 0.008% (90 mins)	94.09± 0.50% (1h)	95.20± 0.98% (30 mins)	91.65± 1.47% (30 mins)	87.92± 3.6% (20 mins)

5.4. Electrochemical sensing of antibiotic drugs using MoS_2 nano-heterostructures

5.4.1. Electrochemical sensing of ciprofloxacin using GA-MoS_2 nano-heterostructure

The voltammetric characteristics of ciprofloxacin were examined at the bare gum arabic and modified GA2 electrode using cyclic voltammetry (CV) and DPV techniques. The experiments were conducted at a scan rate of 100 mVs^{-1} within the potential range of -0.4 to 0.8 V. Due to absence of inadequate electron transfer kinetics at the bare (GA) and the lack of the target analyte in the control solution, no

signal was reflected using blank solution. The peak exhibiting a positive electric current is known as the anodic peak (Ipa) or oxidation peak, whilst the peaks displaying a negative electric current are referred to as the cathodic peak currents (Ipc) or reduction peak (Kumar et al., 2024).

Fig 5.43. displays the cyclic voltammograms (CVs) of a bare and modified GA2 in a 0.1 M CBS (Citrate-Buffered Saline) solution at pH 4.0. The solution also contains 50 μM (micromolar) of CPRO. The oxidation of CPRO is irreversible. The oxidation peak potentials are 0.477 V at the bare and 0.328 V at the modified GA2. Furthermore, at bare GCE, CPRO peaks were moderately broad and weak, reflecting a slower electron transfer mechanism. For functionalized GA2, the peaks with precise forms and increased peak currents were found. The enhanced current responses of the modified electrode were attributed to enhanced conductivity and the nanoscale effective surface area.

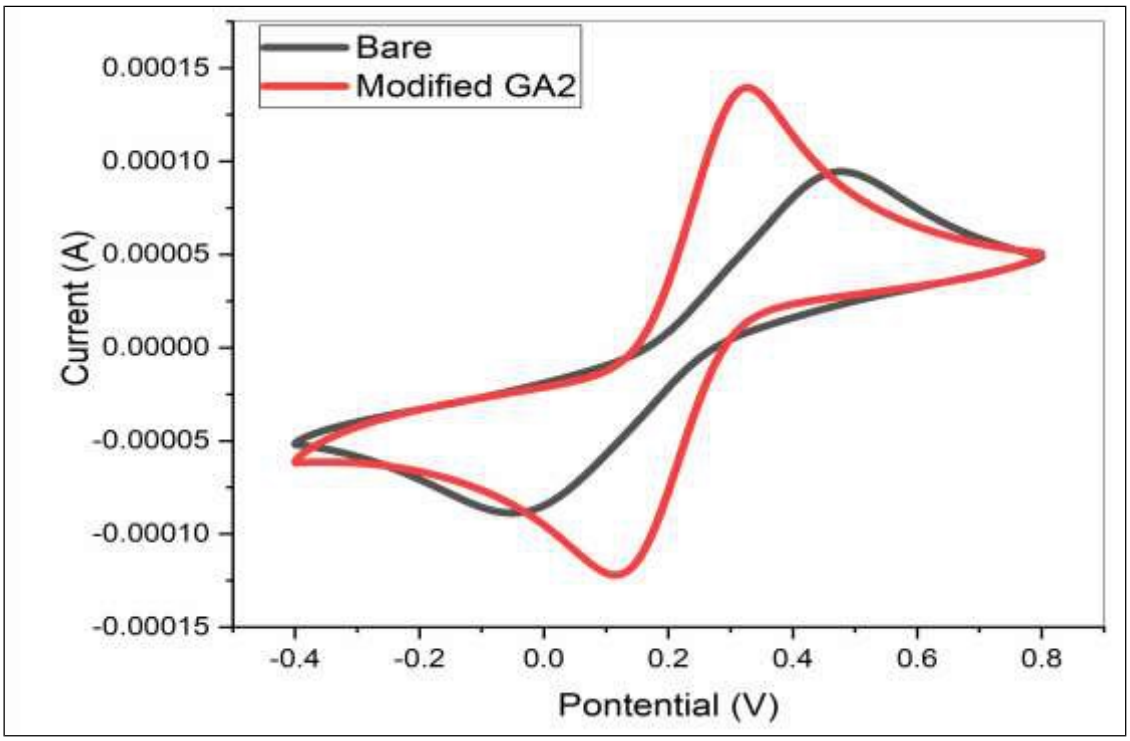

Figure 5.43. Electrochemical response of modified GA2 and bare electrode in Fe^{+2}/Fe^{+3}.

The change in the oxidation and reduction potential of catalyst shows its sensitivity towards the sensing of CPRO. Hence, a significant rise in the peak current was responsible for the oxidation of CPRO, indicating an enhancement in responsive surface area actively involved and reliable electrochemical activity of the modified GA2. The graph shows the activity of GA2 modified electrode was higher as compare to bare electrode.

5.4.1.1. Optimization of prime factors for electrochemical sensing of ciprofloxacin

5.4.1.1.1. pH

An investigation was conducted on the electrochemical behaviour of a solution containing fifty micromolar (50 μM) of ciprofloxacin in 0.1 M of CBS. The investigation utilised a technique called square wave voltammetry (SWV) and was carried out within a pH range of 2.0–7.0. The scan rate used for the investigation was 100mVs^{-1}. The peak potential and current responses of CPRO exhibited a significant variation when the pH of buffer was elevated from highly basic to neutral (2.0 to 7.0), as shown in Fig.5.44, indicating that the oxidation of CPRO is influenced by the pH of the supporting buffer.

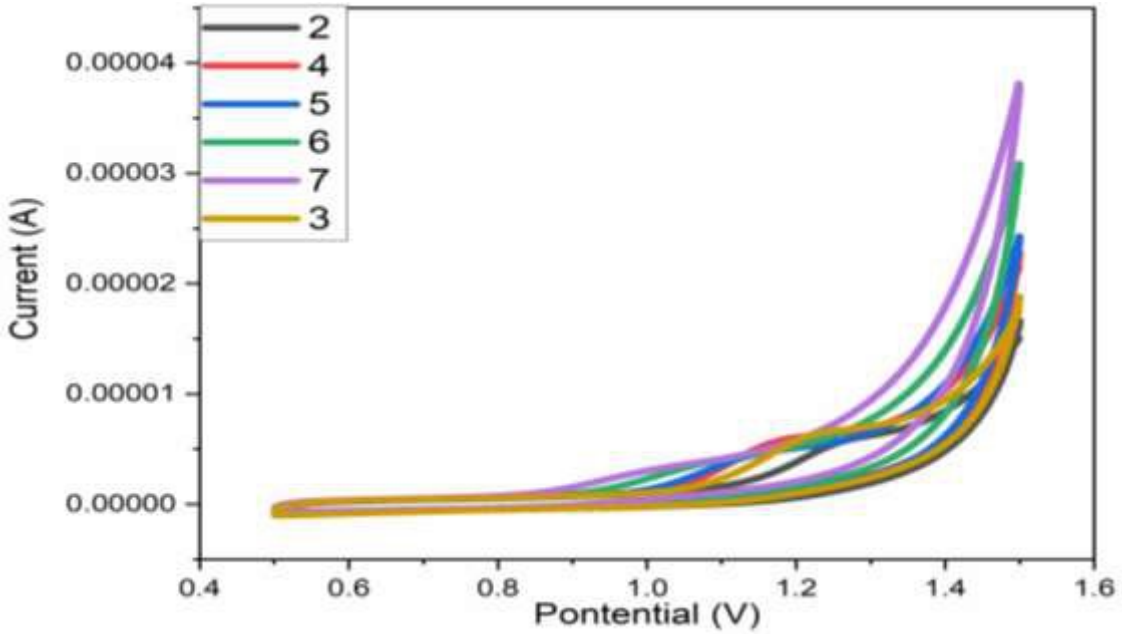

Figure 5.44. Electrochemical Response of ciprofloxacin using modified electrode GA2 at different pH.

An increase in the pH of the solution was observed to enhance the electrochemical response of the nanomaterials. However, a subsequent rise in the pH resulted into a decrease in the oxidation peak current. Consequently, a pH of 4.0 was selected as the most favourable value for following studies.

This graph shows that the electrochemical response of modified electrode for the oxidation of ciprofloxacin is maximum at pH 4.

Chemical reaction

The carboxylic group exhibited more acidic properties in comparison to the hydroxyl group. Hence the proton from the carboxylic acid will transfer to the OH (hydroxyl) group when the piperazinyl ring undergoes oxidation. The deprotonation process is the cause of the hypsochromic shift in the π to π* electronic transformation of the attached carboxylic acid (COOH) (Ipte et al.,2019). Fig. 5.45 demonstrated the mechanism behind the deprotonation of ciprofloxacin.

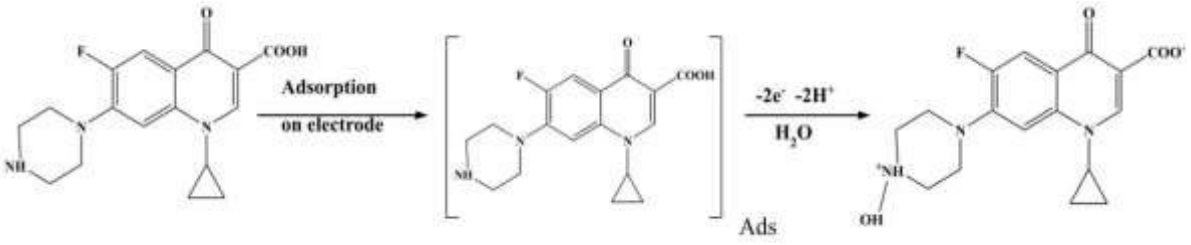

Figure 5.45. Mechanism of deprotonation of Ciprofloxacin.

5.4.1.1.2. Scan rate

The influence of scan rate on the maximum current (A) and maximum potential (V) of ciprofloxacinin a 0.1 M CBS solution with a pH of 4.0 was examined using cyclic voltammetry at scan rates varying from 0.4 to 1.6 V. An incremental rise in the maximum current was noticed as the scan speeds increase from 10 to 140 Vs^{-1}, as demonstrated in Fig. 5.46. Furthermore, there was a change in the highest possible potential to a higher positive level, which confirmed that the process of ciprofloxacin oxidation on the functionalized GA2 surface cannot be reversed.

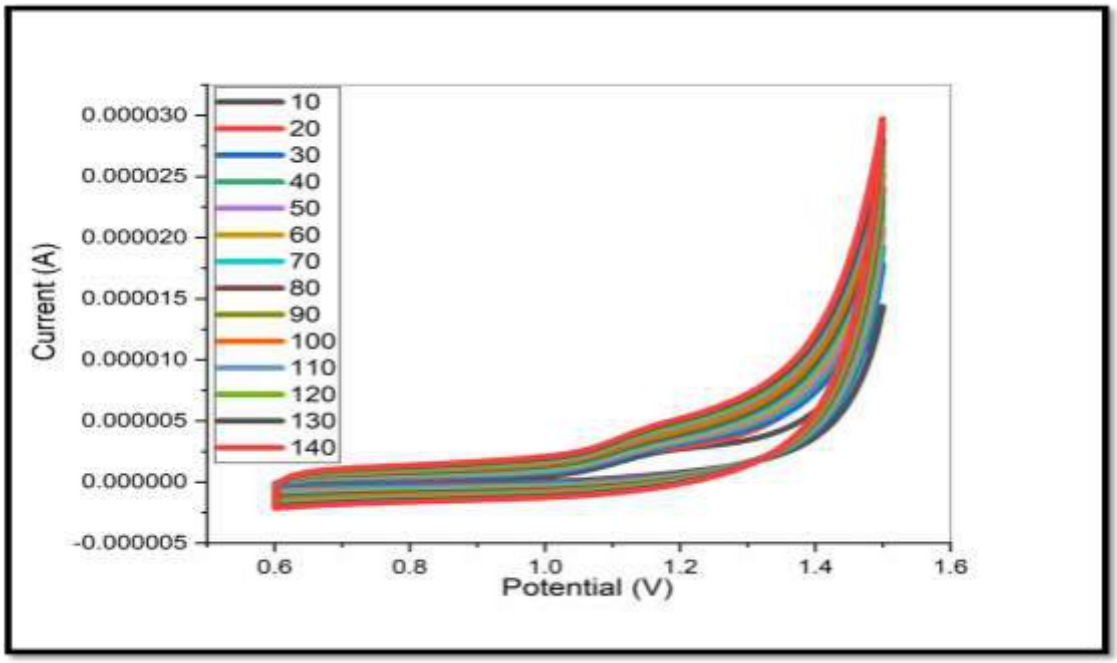

Figure 5.46. Scan rate of ciprofloxacin in presence of modified GA2 at different scan rate.

The linear relationship between the square root of scan rate and the peak potential is depicted in Fig. 5.47.

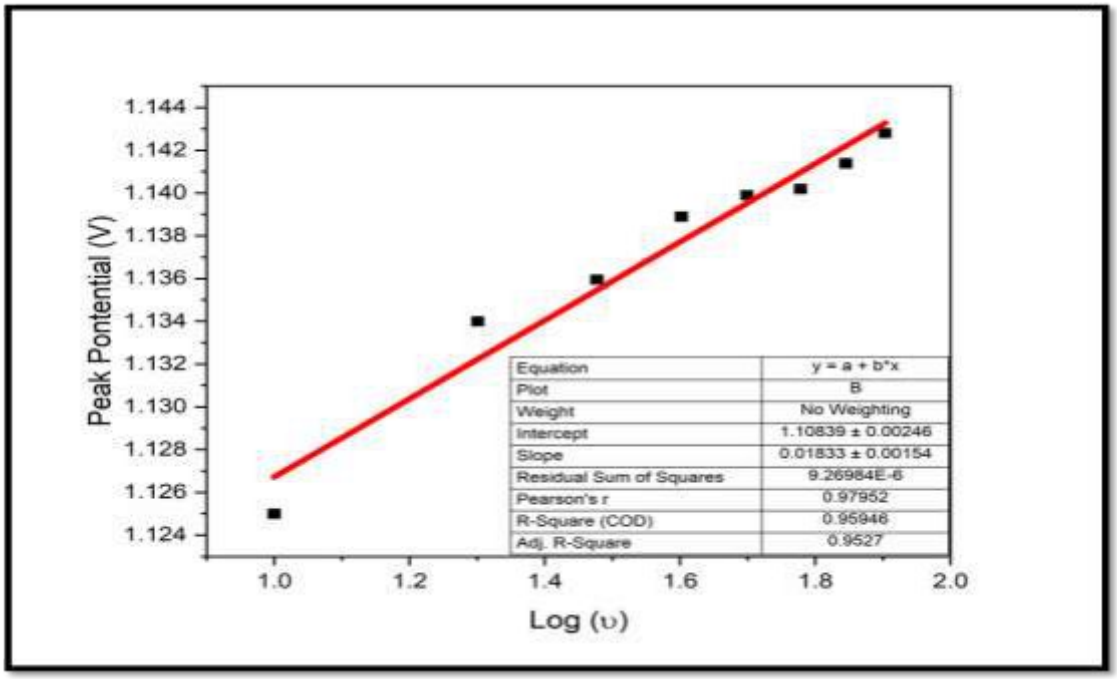

Figure 5.47. Represents the log of scan rate vs peak potential (GA2).

The regression equation for Ip (μA) is a straight line with slope 0.01833 with 0.96 coefficient of determination (R^2). Hence, linearity in this graph showed that the oxidation of ciprofloxacin was totally irreversible.

Fig. 5.48 displays the linearity among the peak current and $υ^{1/2}$ (root square of scan velocity). The regression equation for Ip (A) was 0.01833 $υ^{1/2}$–1.108, with a 0.98 coefficient of determination (R^2). It was essentially characterised as electrode, controlled by diffusion and irreversible in response. It was responsible for the voltammetric oxidation of ciprofloxacin at the responsive surface of improved GA2. Linearity in this graph revealed that the oxidation process was diffusion controlled.

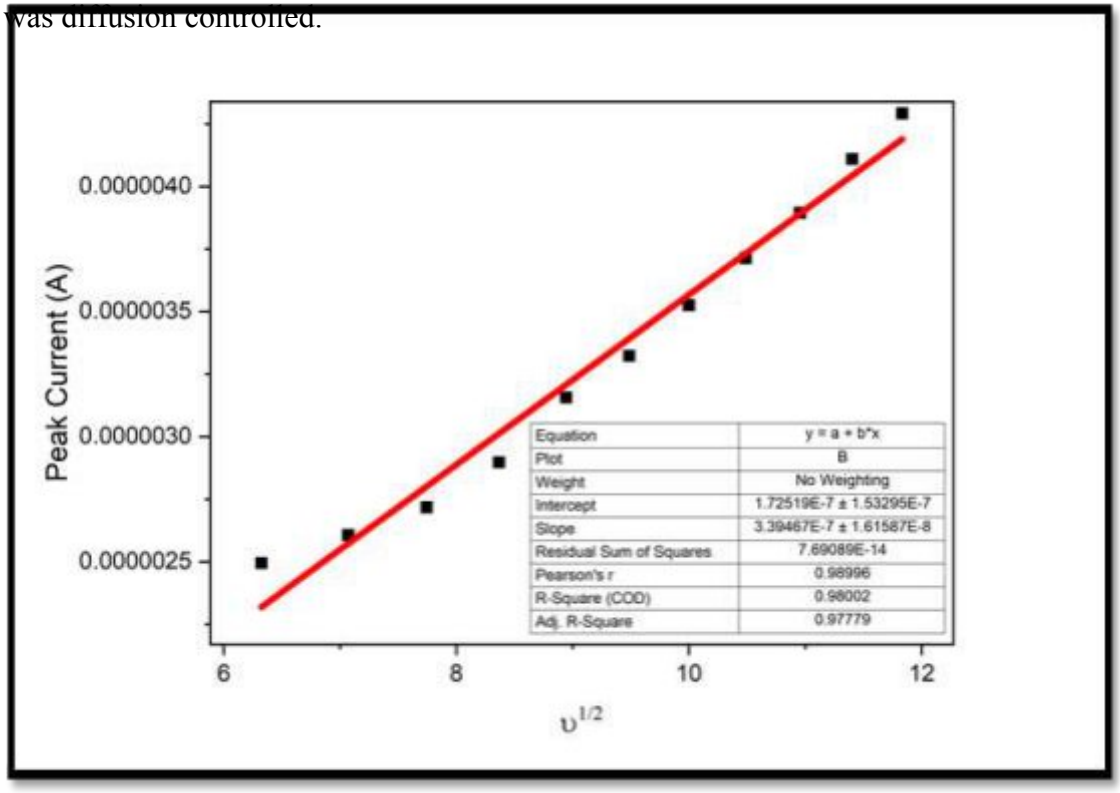

Figure 5.48. Plot of square root of scan rate with peak current (GA2).

5.4.1.1.3. Analytical performance

The analytical performance of sensor, modified GA2, was assessed using DPV at their standardized conditions. Fig 5.49 exhibited the voltammograms of nanocomposite with potential ranging from +0.5 V to +1.3 V, while varying the amounts of ciprofloxacin. The current of nanocomposite increased with increasing CIP

concentration from 3µM to 14µM. The linearity obtained from modified GA2 depicted in the (fig 5.49), ranged from 3µM to 14µM with a 0.979 determination coefficient (r^2) (Gissawong et al., 2021).

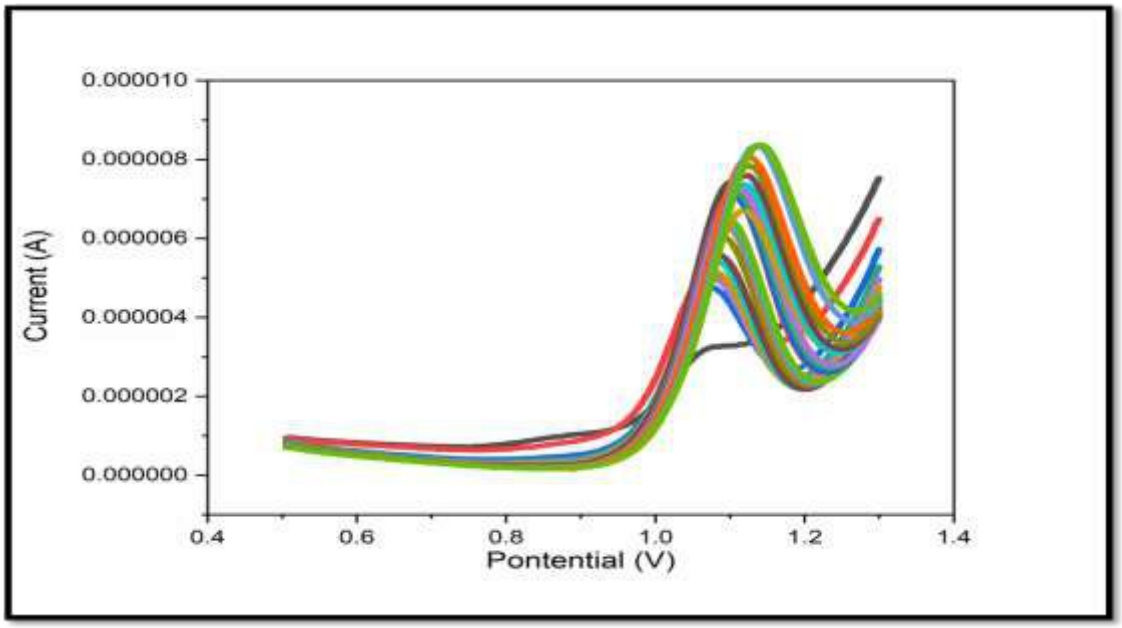

Figure 5.49. Differential pulse voltammograms of different concentration of ciprofloxacin (GA2).

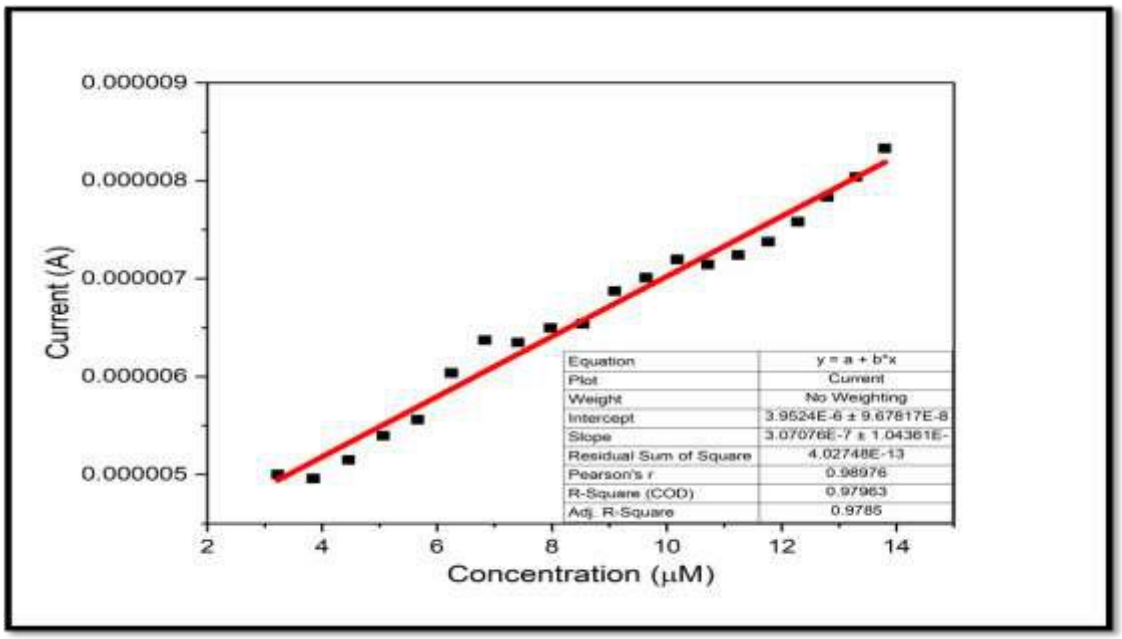

Figure 5.50. Calibration curve of Ciprofloxacin Sensitivity = Slope of calibration curve/Area of electrode (Sensitvity = 8.99 µA/µM $cm^{2)}$.

5.4.2. Electrochemical Sensing of Ciprofloxacin using SA-MoS_2 nano-heterostructure

The voltammetric characteristics of ciprofloxacin were examined using most used techniques i.e. differential pulse voltammetry (DPV) and cyclic voltammetry (CV), both on the unmodified sodium alginate and improved SA2 electrode. The studies 112were carried out using a scanning rate of 100mVs^{-1} throughout a potential range ranging from -0.4V to 0.8 V. The oxidation peak potentials shown by the bare and modified SA were 0.338 V and 0.311 V, respectively. Additionally, the reduction potential shown for the bare and modified SA2 were 0.108V and 0.133V, respectively. It was found that there is an insignificant change in the modified electrode and the bare electrode (fig 5.51).

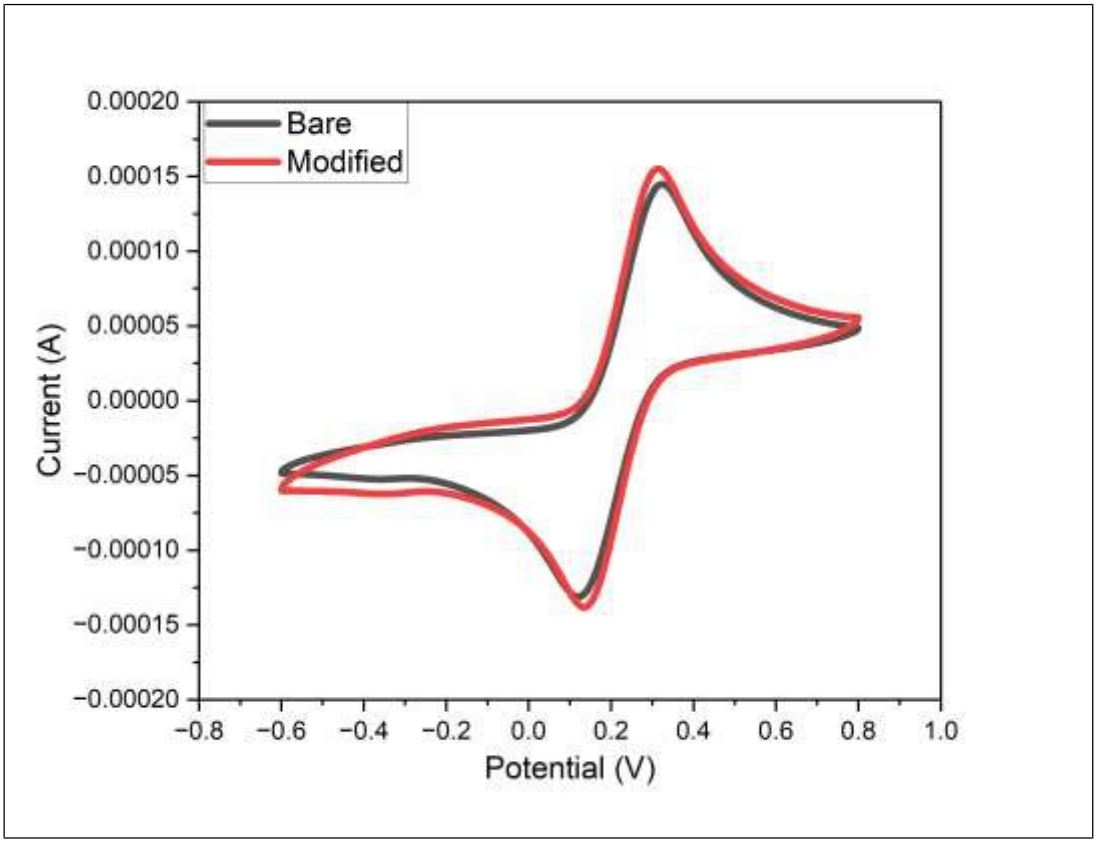

Figure 5.51. Electrochemical response of modified SA2 and bare electrode in Fe^{+2}/Fe^{+3}.

5.4.2.1. Optimization of prime factors for electrochemical sensing of Ciprofloxacin

5.4.2.1.1. pH

An electrochemical performance examination was conducted on a solution containing fifty micromolar (50µM) of antibiotic, ciprofloxacin dissolved in 0.1 M of CBS. Using a method known as square wave voltammetry (SWV), the study was conducted within the pH range of 2-7. In this study, a scan rate of 100mVs^{-1} was employed. The oxidation of CPRO is affected by the pH level of the supporting electrolyte solution, as demonstrated in Fig 5.52, where the maximum potential and current responses of CPRO showed substantial differences as the pH of the buffer was enhanced from 2.0 to 7.0.

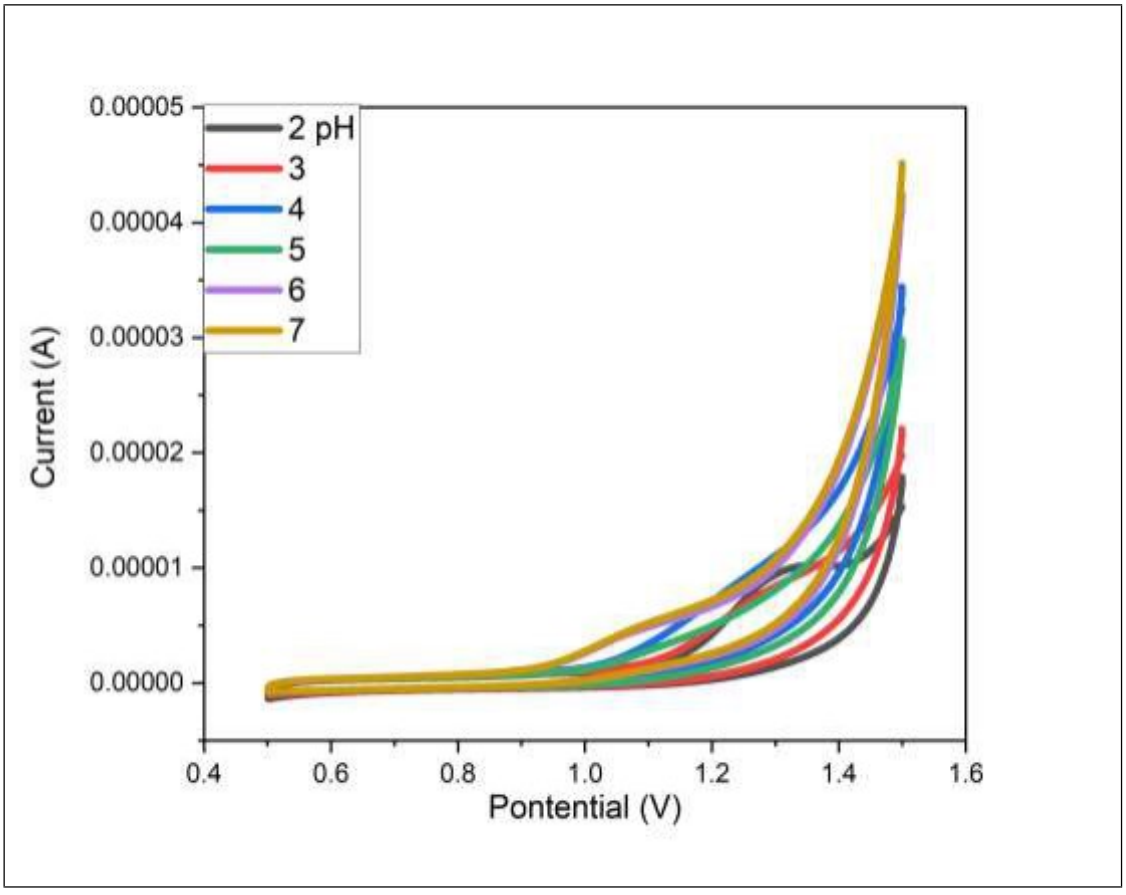

Figure 5.52. Electrochemical response of ciprofloxacin using modified electrode SA2 at different pH (SA2).

From the pH scan study, it was observed that pH 7 is optimal for the electrochemical sensing of CPRO. A significant increase was observed at pH 7 as compared to other pH. Therefore, pH 7.0 was selected for subsequent investigations.

The graph illustrates that the improved electrode exhibited the highest electrochemical response for the oxidation process of ciprofloxacin at a pH level of 7.

5.4.2.1.2. Scan rate

Employing cyclic voltammetry with scan speeds varying from 0.5 to 1.5 V, the impact of scan rate on the maximum current (A) as well as potential (V) of CPRO in a 0.1 M CBS solution with a pH of 7.0 was investigated. Fig 5.53 shows that when the scan rates increase from 10 to 150 Vs^{-1}, the peak current increases progressively. Further evidence dictated that the CPRO surface oxidation at modified SA2 was irreversible and the change in peak potential to a positive value.

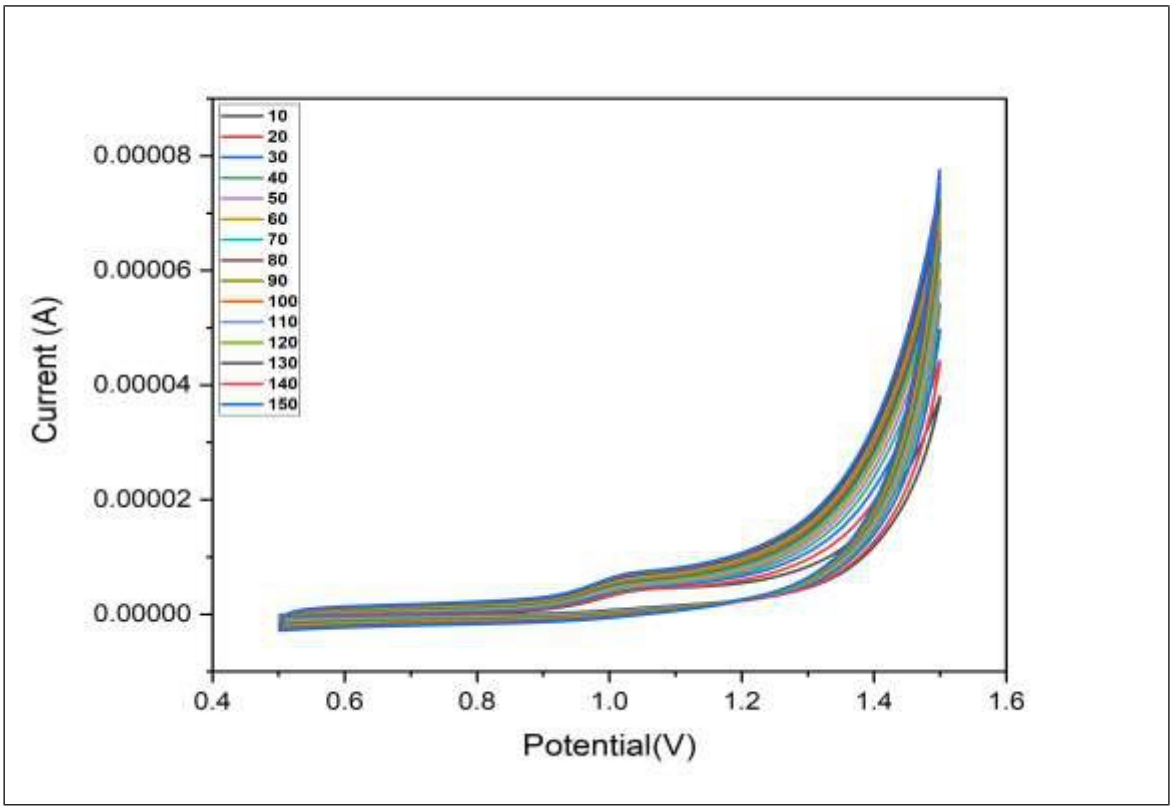

Figure 5.53. Scan rate of ciprofloxacin in presence of modified at different scan rate.

Fig 5.54 represents the linear relationship between the peak potential and the scan rate. 5.46v1/2 $(mVs^{-1})^{1/2}$–10.25 was the regression equation for Ip (μA), and its coefficient of determination (R^2) was 0.99. Thus, linearity in this graph indicated that ciprofloxacin oxidation was completely irreversible.

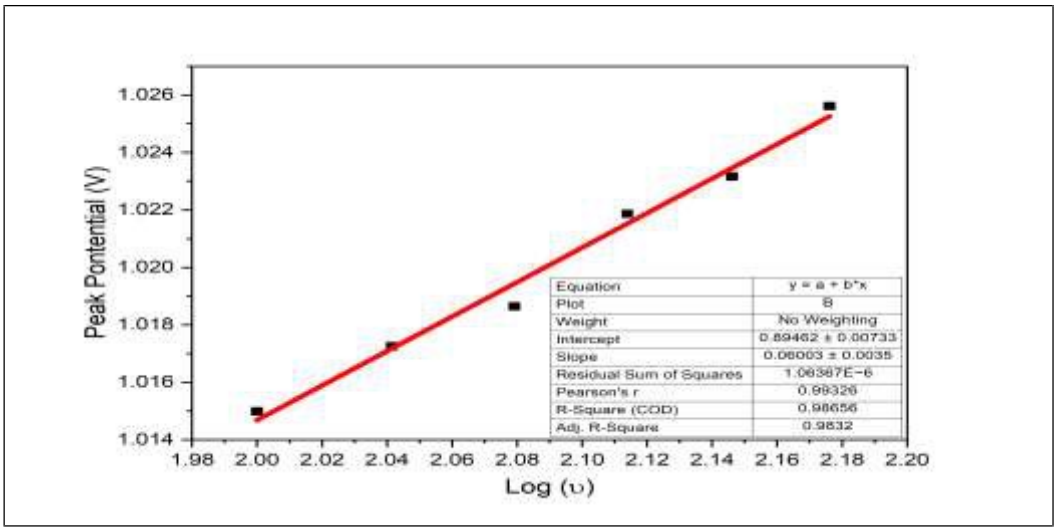

Figure 5.54. Represents the log of scan rate vs peak potential (SA2).

Fig 5.55 shows that peak current was directly proportional to the square root of the scan rate. Ip (A) can be represented by the regression equation 5.46v1/2 $(mVs^{-1})^{1/2}$-10.25, and the coefficient of determination (R^2) was 0.99.

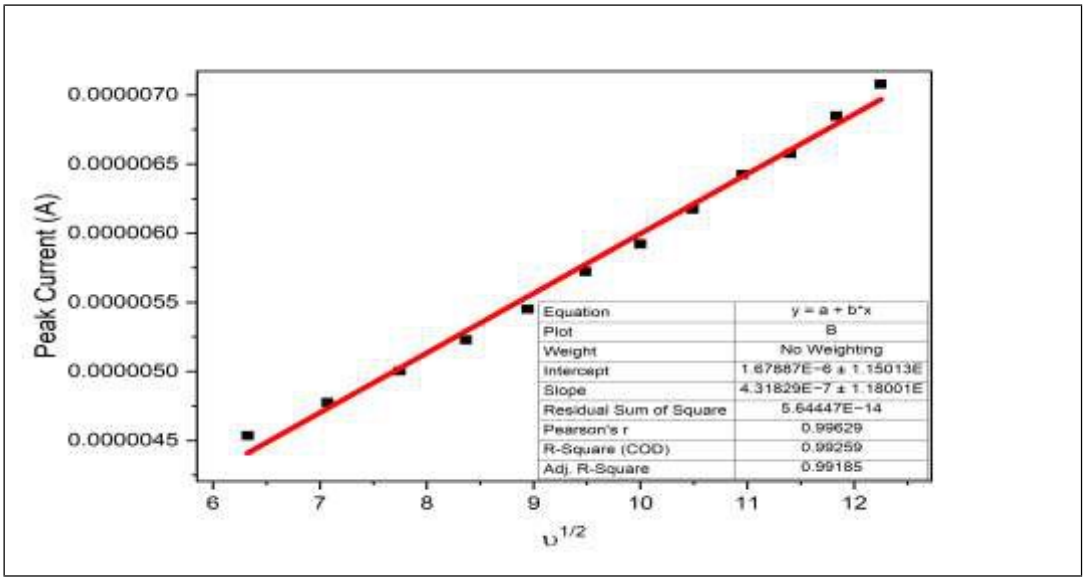

Figure 5.55. Plot of square root of scan rate with peak current (SA2).

An irreversible diffusion driven electrode technique was employed to accomplish the voltammetric oxidation of ciprofloxacin on the surface of modified GA2. The fact that these graphs were found to be linear indicating that the oxidation process was controlled by diffusion.

5.4.2.1.3. Analytical performance

Under optimized conditions, DPV was used to evaluate the analytical performance of the modified SA2 sensor. Fig (5.56) displays the voltammograms of the nanocomposite, illustrating the relationship between ciprofloxacin content and potential within a span of +0.5 V to +1.3 V. Considering an elevation in ciprofloxacin concentration from 3µM to 14µM, the current through the nanocomposite also rose. The results of the modified SA2's linearity, as shown in fig 5.57, varied between 7.5µM and 13µM, and the determination coefficient (R^2) was 0.9789 (Gissawong et al., 2021). The calibration curve showing the positive relationship between the concentration of ciprofloxacin and current in the Figure 5.57, demonstrated the elevation in current with increase in the antibiotic concentration.

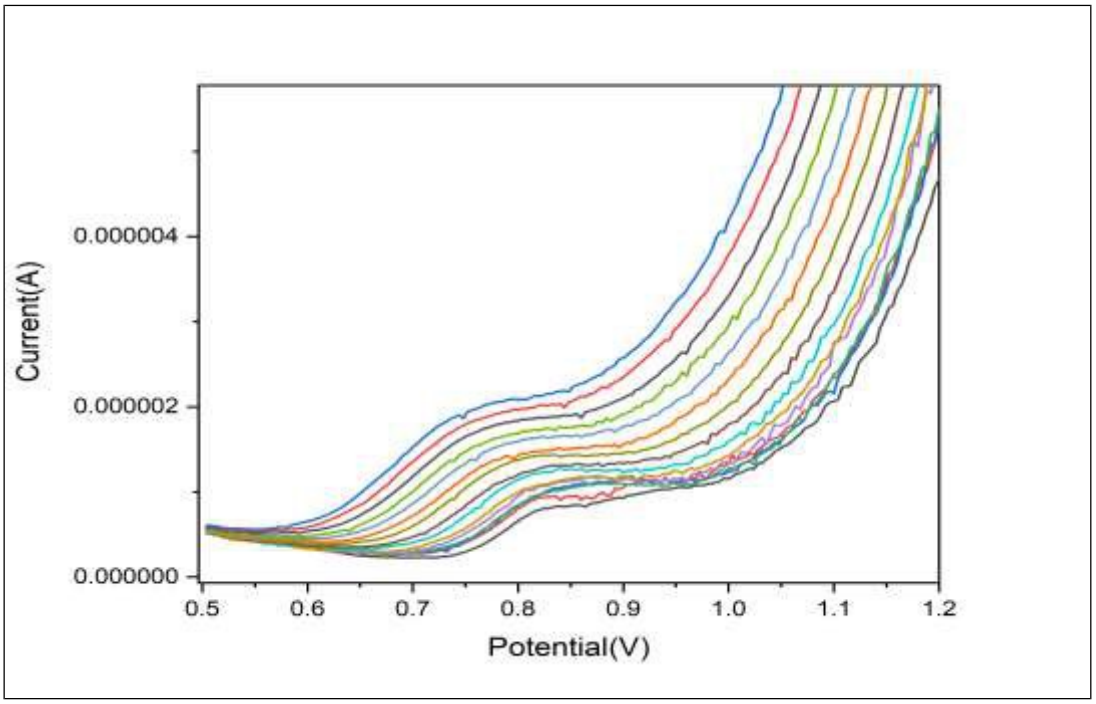

Figure 5.56. Differential pulse voltammograms of different concentrations of ciprofloxacin (SA2).

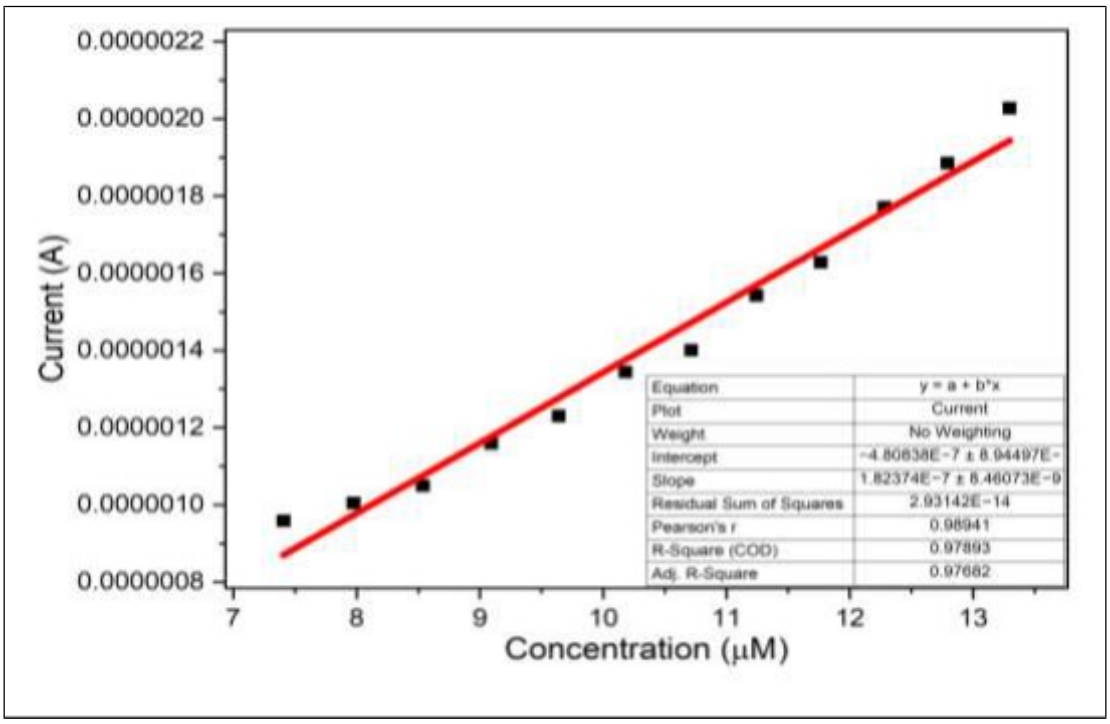

Figure. 5.57. Calibration curve of Ciprofloxacin for SA2 nanocomposite.

5.5. DPPH free radical scavenging activity

The antioxidant activity testing revealed that the MoS_2 nanostructures and nanoheterostructures have free radical scavenging property (Fig.5.58). There was an increase in the percent free radical scavenging activity with an increase in the nanocomposite concentration. The free radical scavenging activity of MoS_2 nanostructures and nano-heterostructures was comparable with standard antioxidant, ascorbic acid. The maximum free radical scavenging activity shown by ascorbic acid was 81.6 ± 0.6%. On the contrary, the MoS_2 nanostructures and MoS_2@GQDs obtained from the gum arabic have shown 82.93±0.43% and 84.93±0.55% free radical scavenging at the highest concentration (1000µg/mL), respectively (Fig 5.58(a)). The MoS_2 nanosheets obtained from the sodium alginate have shown maximum 88.46±3.42% at highest concentration whereas the nano-heterostructures obtained from SA have shown 100% scavenging at 600µg/mL concentration (Fig 5.58(b)). Additionally, at 1000µg/ml concentration of nanocomposite, the TcSE-MoS_2

nanosheets and its nano-heterostructure have exhibited 93.53±1.18% and 100% antioxidative efficiency.

According to literature review, the fascinating property of MoS_2 as anti-oxidant agent has been found depending on the different redox mechanistic involved in reactions (Kang et al., 2023). The role of MoS_2 NPs as anti-oxidant and photocatalytic agent have also been reported by the researcher (Fakhri and Nejad, 2016). Along with, graphene is known for its anti-oxidative characteristics due to hydroxyl and superoxide radical scavenging activity (Qiu et al., 2014). The synergistic effect of nanocomposite containing both graphene and MoS_2 nanosheets makes it potent

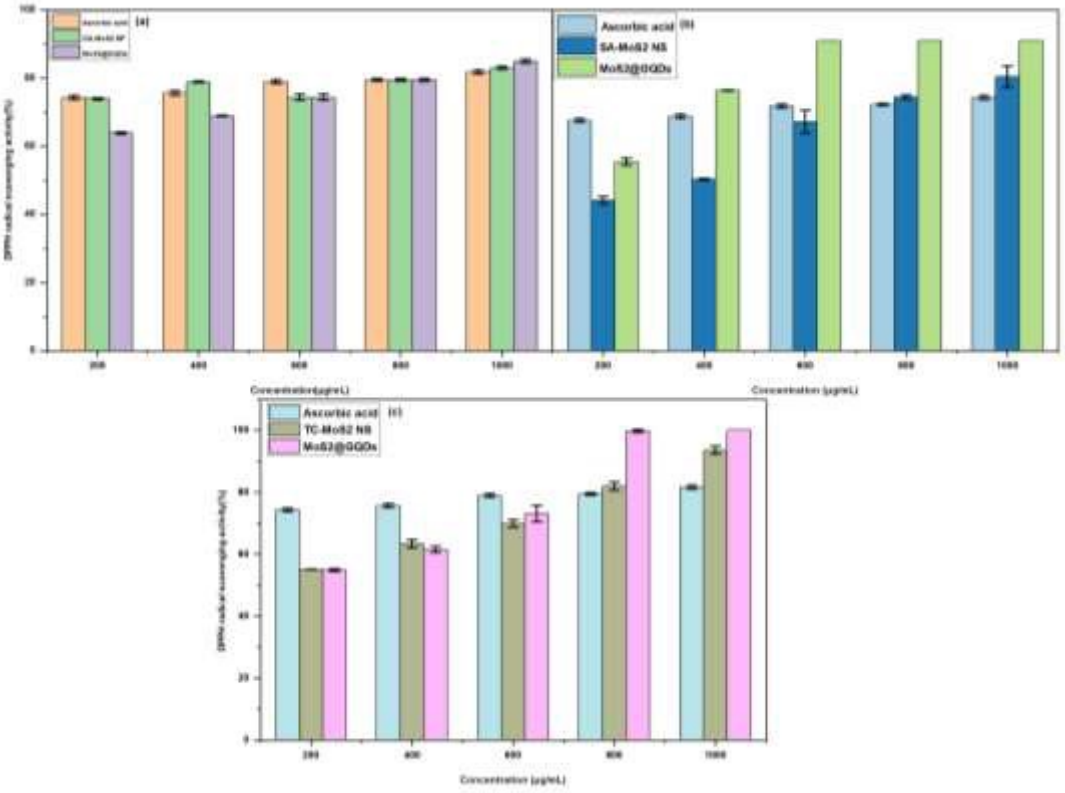

Figure.5.58. Percent free radical scavenging activity (%) of MoS_2 nanostructures and nano-heterostructures was studied using DPPH assay. Ascorbic acid was used as positive control and was used to compare the antioxidant activity of MoS_2 nanostructures and nano-heterostructures. The percent DPPH scavenging activity of MoS_2 nano-structures and nano-heterostructures at 1 mg/mL dose was comparable to ascorbic acid.

antioxidant agent. Similarly, cellulose/MoS_2@GO nanocomposite have shown 50% and 51% of free radical scavenging activity against $DPPH^{\bullet}$ and $ABTS^{\bullet+}$ (Pervaiz et al., 2023) .

5.6. Antimicrobial activity

Well diffusion agar assay revealed the formation of clear zone around the well-containing 1 mg/mL MoS_2 nano-structures and MoS_2 nano-heterostructures. The diameter of the clear zone suggests the material possessed antibacterial activity which can inhibit the bacterial growth. *E. coli* was more susceptible to the nanocomposite than *S. aureus* strain. The zone of inhibition in the case of *E. coli* MTCC 495 and *S. aureus* MTCC 7443 are presented in following table 5.2.

Table 5.2. Presenting zone of inhibition shown by MoS_2 nano-structure and nanoheterostructures.

Test sample	**Anti-biotic**	**Gum Arabic**		**Sodium alginate**		***Tinospora cordifolia***	
		GA-MoS_2 NPs	GA-MoS_2 @GQDs	SA-MoS_2 NS	SA-MoS_2 @GQDs	*TcSE*-MoS_2 NS	*TcSE*-MoS_2 @GQDs
E. coli	24.2±4.29	14±2.5	20±1.3	17.3±2.1	25±0.8	35±1.9	42±2.9
S. aureus	26.6±2.56	21±1.8	24.5±1.7	24.3±1.1	27.4±1.4	24.9±1.1	27.4±1.8

5.7. Safety studies

Microorganisms found in the human body, specifically bacteria found in the gut, are essential for human health, development, and immune functioning. Lactobacillus is probiotic lactic acid bacteria commonly found in the human gut. The agar plates with untreated MB dye solution showed a few colonies (Fig. 5.59(a) whereas the agar plates containing MoS_2 nanostructures–treated dye solution had better growth (Fig. 5.59(b,c,d) (Somashekaraiah et al. 2019). MB has earlier been reported to induce toxic to lactobacillus strains. Similarly, untreated CB and untreated IS did not exhibit any kind of bacterial growth on the plate showing its toxicity to microorganims. On

the contrary, the plates containing treated CB and IS have shown growth of microflora on the plates for CB (Fig. 5.59(f-g) and IS (Fig. 5.60(i-j).

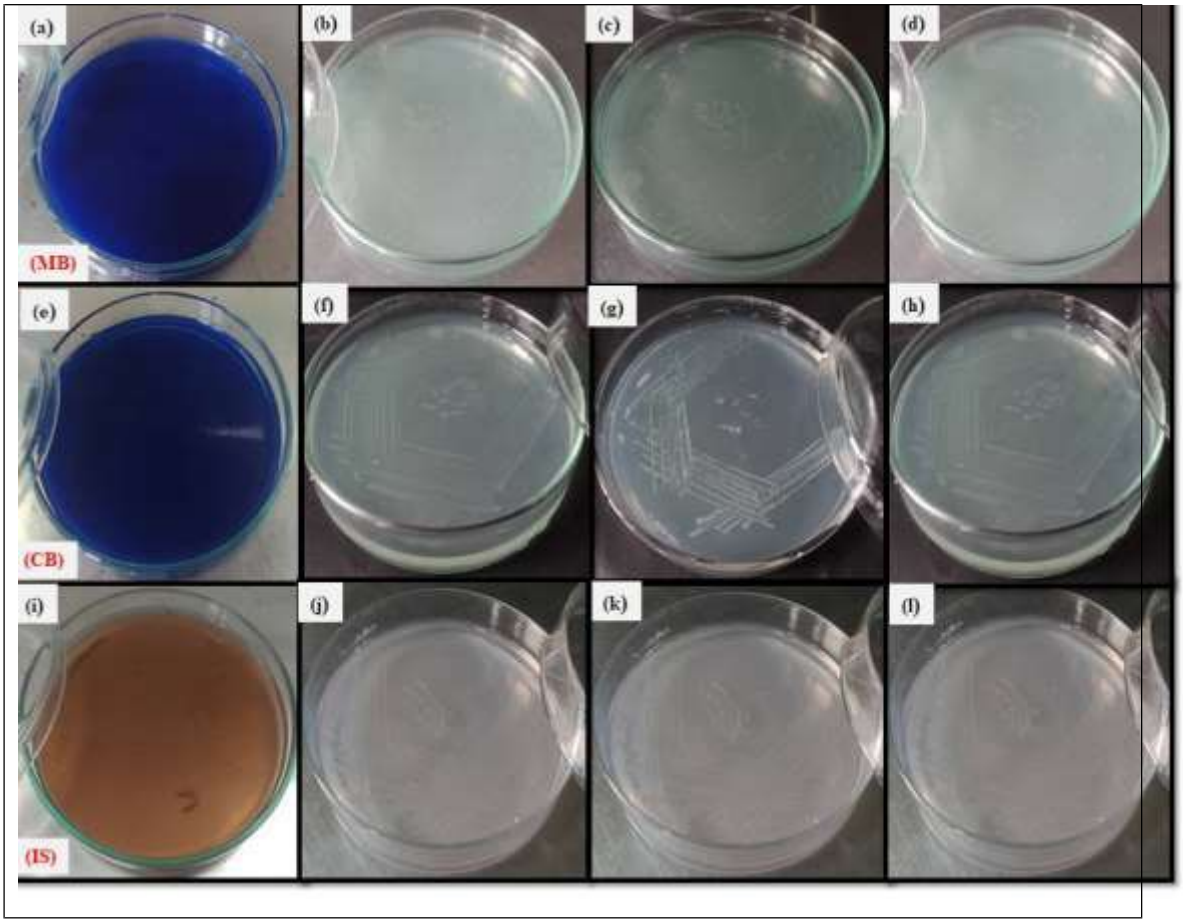

Figure 5.59. (a) Untreated MB (b,c,d) MoS_2 nano-heterostructures-treated MB (MoS_2@GQDS synthesized from GA, SA, and TcSE) and (e) untreated CB (f,g,h) MoS_2 nano-heterostructures-treated CB (MoS_2@GQDS synthesized from GA, SA, and TcSE) (i) Untreated IS (j,k,l) MoS_2 nano-heterostructures-treated CB (MoS_2@GQDS synthesized from GA, SA, and TcSE). There was no growth of *L. delbrueckii* over untreated MB, CB, and IS indicating its toxic nature while MoS_2 nano-heterostructures–treated MB, CB, and IS has shown growth of *L. delbrueckii* proving safe nature of treated MB.

Chapter 6:

Summary and future scope

Liquid phase exfoliation using sonicator and microwave treatment synergistically convert the pristine MoS_2 into different MoS_2 nanostructures namely, nanoparticle and nanosheets with the aid of biosurfactants, gum arabic, sodium alginate, and stem extract of *Tinospora cordifolia.* The decoration of the obtained MoS_2 nanostructures with the carbon quantum dots obtained from the citric acid by providing high temperature led to the synthesis of MoS_2 nano-heterostructures. The obtained MoS_2 nanostructures and nano-heterostructures were characterized using UV-Vis spectroscopy, XRD, FT-IR, and HR-TEM. The nano-heterostructures have the collective extraordinary properties of nanosheets and quantum dots, which significantly enhanced the photocatalytic and electrochemical performance of the nanocomposite. The various parameters, photocatalyst dose, irradiation time, and pH have impacted the efficiency of nanocomposite as photocatalyst. The synthesized nanocomposite have showing significant photodegradation of methylene blue, commercial blue as well as textile industry water by showing 80-99% of photocatalytic activity. Along with, the electrochemical studies have embarked the potential application of these nano-heterostructures as good electroactive component for sensing purpose. Additionally, the antioxidative and antimicrobial effectivity of nano-heterostructures have shown their usefulness for biological applications. The safety studies have nullified the toxic effect of treated samples with nanocomposites. Hence, the usage of these nanocomposites can be promising for the environment as well as biological applications.

Future scope

- Various physical and chemical methods have earlier been reported for the exfoliation of the MoS_2. The greener route of exfoliation of bulk materials are still at a nascent stage which can be improved by taking cost-effectiveness and low energy use into the consideration.
- In the future, optimization of the sensing conditions will help in the improvement and performance of the nano-heterostructure, and in combination with other EIS techniques will find new ways for future research. Thus,

nanoheterostructures will be more promising for the sensing of other antibiotics and other pollutants from the wastewater and environment.

- The application of these nano-heterostructures for the biological applications including agriculture, drug delivery, nanosensing, tissue engineering, in vitro and in vivo applications can be tested for the better unveiling of the unexplored characteristics of the nanocomposites.
- The commercialization of the nano-based sensor can be achieved after a dedicative investement of time and dedication.
- Further, the nanotoxicity studies of the nanomaterial at *in vitro* and *in vivo* level will reveal their potential for various human applications.

From this research work, it has been concluded that MoS_2 nanostructures and nano-heterostructures are potent photocatalyst and electrochemical agents. The different combinations of the nano-heterostructures can be syntheiszed for better results. The reusability can be significantly improved by incorporating combination of carbon-based nanoparticles for the future application.

Chapter 7:

References

1. Adaikalapandi, S., Thangadurai, T. D., Sivakumar, S., & Manjubaashini, N. (2024). Decoration of 2 H-MoS2 on the surfaces of activated carbon derived from bamboo stem biomass waste: A regenerative novel architecture for effective degradation of methylene blue under natural light. *Colloids and Surfaces A: Physicochemical and Engineering Aspects*, *684*, 133039.
2. Aksorngul, I., Buawat, N., Ngernsutivorakul, T., Botta, R., & Yotprayoonsak, P. (2024). Facile and efficient preparation of hemicellulose-assisted MoS2 nanosheets via green liquid-phase exfoliation method. *Surfaces and Interfaces*, *45*, 103835.
3. Akeredolu, B. J., Ahemen, I., Amah, A. N., Onojah, A. D., Shakya, J., Gayathri, H. N., & Ghosh, A. (2024). Improved liquid phase exfoliation technique for the fabrication of MoS2/graphene heterostructure-based photodetector. *Heliyon*, *10*(3).
4. Ahmad Zaini, M. A., & Sudi, R. M. (2018). Valorization of human hair as methylene blue dye adsorbents. *Green processing and synthesis*, *7*(4), 344-352.
5. Ahmad, A., Tariq, S., Zaman, J. U., Perales, A. I. M., Mubashir, M., & Luque, R. (2022). Recent trends and challenges with the synthesis of membranes: Industrial opportunities towards environmental remediation. *Chemosphere*, *306*, 135634.
6. Ahmad, M. M., Kotb, H. M., Mushtaq, S., Waheed-Ur-Rehman, M., Maghanga, C. M., & Alam, M. W. (2022). Green synthesis of Mn+ Cu bimetallic nanoparticles using Vinca rosea extract and their antioxidant, antibacterial, and catalytic activities. *Crystals*, *12*(1), 72.
7. Ahmad, S., Khan, S. B., Asiri, A. M., Marwani, H. M., & Kamal, T. (2020). Polypeptide and copper oxide nanocomposite hydrogel for toxicity elimination of wastewater. *Journal of Sol-Gel Science and Technology*, *96*, 382-394.
8. Aisien, F. A., Amenaghawon, N. A., & Ekpenisi, E. F. (2013). Photocatalytic decolourisation of industrial wastewater from a soft drink compan. *UNIZIK Journal of Engineering and Applied Sciences*, *9*(1), 11-16.

9. Ajmal, A., Majeed, I., Malik, R. N., Idriss, H., & Nadeem, M. A. (2014). Principles and mechanisms of photocatalytic dye degradation on TiO 2 based photocatalysts: a comparative overview. *Rsc Advances*, *4*(70), 37003-37026.

10. Akhtar, A. B. T., Naseem, S., Yasar, A., & Naseem, Z. (2021). Persistent organic pollutants (POPs): sources, types, impacts, and their remediation. *Environmental Pollution and Remediation*, 213-246.

11. Akhtar, N., Syakir Ishak, M. I., Bhawani, S. A., & Umar, K. (2021). Various natural and anthropogenic factors responsible for water quality degradation: A review. *Water*, *13*(19), 2660.

12. Al Qaydi, M., Rajput, N. S., Lejeune, M., Bouchalkha, A., El Marssi, M., Cordette, S., ... & Jouiad, M. (2024). Intermixing of MoS2 and WS2 photocatalysts toward methylene blue photodegradation. *Beilstein Journal of Nanotechnology*, *15*(1), 817-829.

13. Alarifi, I. M., Al-Ghamdi, Y. O., Darwesh, R., Ansari, M. O., & Uddin, M. K. (2021). Properties and application of MoS2 nanopowder: characterization, Congo red dye adsorption, and optimization. *journal of materials research and technology*, *13*, 1169-1180.

14. Ali, G. A., Thalji, M. R., Soh, W. C., Algarni, H., & Chong, K. F. (2020). One-step electrochemical synthesis of MoS 2/graphene composite for supercapacitor application. *Journal of Solid State Electrochemistry*, *24*, 25-34.

15. Allen, S. J., Gan, Q., Matthews, R., & Johnson, P. A. (2005). Mass transfer processes in the adsorption of basic dyes by peanut hulls. *Industrial & engineering chemistry research*, *44*(6), 1942-1949.

16. Ambrosi, A., Sofer, Z., & Pumera, M. (2015). Lithium intercalation compound dramatically influences the electrochemical properties of exfoliated MoS2. *Small*, *11*(5), 605-612.

17. Anushree, C., & Philip, J. (2019). Efficient removal of methylene blue dye using cellulose capped Fe3O4 nanofluids prepared using oxidation-precipitation method. *Colloids and Surfaces A: Physicochemical and Engineering Aspects*, *567*, 193-204.

18. Arde, S. M., Patil, A. D., Mane, A. H., Salokhe, P. R., & Salunkhe, R. S. (2020). Synthesis of quinoxaline, benzimidazole and pyrazole derivatives under the catalytic influence of biosurfactant-stabilized iron nanoparticles in water. *Research on Chemical Intermediates*, *46*, 5069-5086.

19. Ashar, A., Shoaib, M., Bhutta, Z. A., Munir, H., Muzammil, I., & Ali, M. (2022). A Combination of Physicochemical and biological methods for azo dye degradation. In *Microbial Remediation of Azo Dyes with Prokaryotes* (pp. 279-298). CRC Press.

20. Athira, K., Gurrala, L., & Kumar, D. V. R. (2021). Biosurfactant-mediated biosynthesis of CuO nanoparticles and their antimicrobial activity. *Applied Nanoscience*, *11*(4), 1447-1457.
21. Ayodhya, D., & Veerabhadram, G. (2018). A review on recent advances in photodegradation of dyes using doped and heterojunction based semiconductor metal sulfide nanostructures for environmental protection. *Materials today energy*, *9*, 83-113.
22. Bafana, A., Devi, S. S., & Chakrabarti, T. (2011). Azo dyes: past, present and the future. *Environmental Reviews*, *19*(NA), 350-371.
23. Bakur, A., Niu, Y., Kuang, H., & Chen, Q. (2019). Synthesis of gold nanoparticles derived from mannosylerythritol lipid and evaluation of their bioactivities. *Amb Express*, *9*, 1-9.
24. Barciela, P., Perez-Vazquez, A., & Prieto, M. A. (2023). Azo dyes in the food industry: Features, classification, toxicity, alternatives, and regulation. *Food and Chemical Toxicology*, *178*, 113935.
25. Bashir, M., & Haripriya, S. (2016). Assessment of physical and structural characteristics of almond gum. *International Journal of Biological Macromolecules*, *93*, 476-482.
26. Bayee, P., Amani, H., Najafpour, G. D., & Kariminezhad, H. (2020). Experimental investigations on behaviour of rhamnolipid biosurfactant as a green stabilizer for the biological synthesis of gold nanoparticles. *International Journal of Engineering*, *33*(6), 1054-1060.

27. Bhalodia, N. R., & Shukla, V. J. (2011). Antibacterial and antifungal activities from leaf extracts of Cassia fistula l.: An ethnomedicinal plant. *Journal of advanced pharmaceutical technology & research*, *2*(2), 104-109.
28. Bhardwaj, H., Marquette, C. A., Dutta, P., Rajesh, & Sumana, G. (2020). Integrated graphene quantum dot decorated functionalized nanosheet biosensor for mycotoxin detection. *Analytical and Bioanalytical Chemistry*, *412*, 7029-7041.
29. Bilai, M., Khan, M. R., & Sayyed, R. Z. (2022). Biosurfactant mediated synthesis and stabilization of nanoparticles. In *Microbial Surfactants* (pp. 158-168). CRC Press.
30. Bongu, C. S., Krishnan, M. R., Soliman, A., Arsalan, M., & Alsharaeh, E. H. (2023). Flexible and freestanding MoS2/graphene composite for high-performance supercapacitors. *ACS omega*, *8*(40), 36789-36800.
31. Borthakur, P., Boruah, P. K., Hussain, N., Silla, Y., & Das, M. R. (2017). Specific ion effect on the surface properties of Ag/reduced graphene oxide nanocomposite and its influence on photocatalytic efficiency towards azo dye degradation. *Applied Surface Science*, *423*, 752-761.
32. Burman, D., Ghosh, R., Santra, S., & Guha, P. K. (2016). Highly proton conducting MoS 2/graphene oxide nanocomposite based chemoresistive humidity sensor. *Rsc Advances*, *6*(62), 57424-57433.
33. Cai, D., Xiao, S., Nan, H., Gu, X., & Ostrikov, K. (2018). Robust Fabrication of Quantum Dots on Few-Layer MoS2 by Soft Hydrogen Plasma and Post-Annealing. *Particle & Particle Systems Characterization*, *35*(6), 1800060.
34. Chai, B., Xu, M., Wang, C., Yan, J., & Ren, Z. (2018). One-step hydrothermal preparation of MoS2 loaded on CdMoO4/CdS hybrids for efficient photocatalytic hydrogen evolution. *Catalysis Communications*, *110*, 10-13.
35. Chaudhary, N., Khanuja, M., & Islam, S. S. (2018). Hydrothermal synthesis of MoS2 nanosheets for multiple wavelength optical sensing applications. *Sensors and Actuators A: Physical*, *277*, 190-198.

36. Chen Y-X, Wu C-W, Kuo T-Y, Chang Y-L, Jen M-H, Chen I-WP (2016) Large-scale production of large-size atomically thin semiconducting molybdenum dichalcogenide sheets in water and its application for supercapacitor. Sci Rep 6:26660

37. Chen, L., Ou, S. F., Nguyen, T. B., Chuang, Y., Chen, C. W., & Dong, C. D. (2024). In-situ hydrothermal synthesis of MoS2/TiO2 nanocomposites for enhanced and stable photocatalytic performance: Methylene blue degradation pathway and mechanism. *Journal of the Taiwan Institute of Chemical Engineers*, 105436.

38. Chequer, F. D., de Oliveira, G. A. R., Ferraz, E. A., Cardoso, J. C., Zanoni, M. B., & de Oliveira, D. P. (2013). Textile dyes: dyeing process and environmental impact. *Eco-friendly textile dyeing and finishing*, *6*(6), 151-176.

39. Choudhari, J. K., Verma, M. K., Choubey, J., Singh, A. J. S., & Sahariah, B. P. (2022). Bioremediation of Azo Dyes. In *Microbial Remediation of Azo Dyes with Prokaryotes* (pp. 171-182). CRC Press.

40. Choudhury, A., Lahkar, J., Saikia, B. K., Singh, A. K. A., Chikkaputtaiah, C., & Boruah, H. P. D. (2021). Strategies to address coal mine-created environmental issues and their feasibility study on northeastern coalfields of Assam, India: a review. *Environment, Development and Sustainability*, *23*(7), 9667-9709.

41. Chung, K. T. (2016). Azo dyes and human health: A review. *Journal of Environmental Science and Health, Part C*, *34*(4), 233-261

42. Coleman, J. N., Lotya, M., O'Neill, A., Bergin, S. D., King, P. J., Khan, U., ... & Nicolosi, V. (2011). Two-dimensional nanosheets produced by liquid exfoliation of layered materials. *Science*, *331*(6017), 568-571.

43. Crini, G., Lichtfouse, E., Wilson, L. D., & Morin-Crini, N. (2018). Adsorption-oriented processes using conventional and non-conventional adsorbents for wastewater treatment. *Green adsorbents for pollutant removal: fundamentals and design*, 23-71.

44. Cui, W., Xu, S., Yan, B., Guo, Z., Xu, Q., Sumpter, B. G., ... & Wang, Y. (2017). Triphasic 2D Materials by Vertically Stacking Laterally Heterostructured 2H-/1T′-MoS2 on Graphene for Enhanced Photoresponse. *Advanced Electronic Materials*, *3*(7), 1700024.
45. Cui, Y., Wang, T., Liu, J., Hu, L., Nie, Q., Tan, Z., & Yu, H. (2021). Enhanced solar photocatalytic degradation of nitric oxide using graphene quantum dots/bismuth tungstate composite catalysts. *Chemical Engineering Journal*, *420*, 129595.
46. Daniloska, V., Keddie, J. L., Asua, J. M., & Tomovska, R. (2014). MoS2 nanoplatelet fillers for enhancement of the properties of waterborne pressure-sensitive adhesives. *ACS Applied Materials & Interfaces*, *6*(24), 22640-22648.
47. Das, S., Tama, A. M., Dutta, S., Ali, M. S., & Basith, M. A. (2019). Facile high-yield synthesis of MoS2 nanosheets with enhanced photocatalytic performance using ultrasound driven exfoliation technique. *Materials Research Express*, *6*(12), 125079.
48. de Lima, R. O. A., Bazo, A. P., Salvadori, D. M. F., Rech, C. M., de Palma Oliveira, D., & de Aragão Umbuzeiro, G. (2007). Mutagenic and carcinogenic potential of a textile azo dye processing plant effluent that impacts a drinking water source. *Mutation Research/Genetic Toxicology and Environmental Mutagenesis*, *626*(1-2), 53-60.
49. de-Mello, G. B., Smith, L., Rowley-Neale, S. J., Gruber, J., Hutton, S. J., & Banks, C. E. (2017). Surfactant-exfoliated 2D molybdenum disulphide (2D-MoS 2): the role of surfactant upon the hydrogen evolution reaction. *RSC advances*, *7*(58), 36208-36213.
50. Deng, R., Yi, H., Fan, F., Fu, L., Zeng, Y., Wang, Y., ... & Su, Y. (2016). Facile exfoliation of MoS 2 nanosheets by protein as a photothermal-triggered drug delivery system for synergistic tumor therapy. *RSC advances*, *6*(80), 77083-77092.
51. Devi, A. P., Padhi, D. K., Mishra, P. M., & Behera, A. K. (2021). Bio-Surfactant assisted room temperature synthesis of cubic Ag/RGO

nanocomposite for enhanced photoreduction of Cr (VI) and antibacterial activity. *Journal of Environmental Chemical Engineering*, *9*(2), 104778.

52. Ding, Y., Zhou, Y., Nie, W., & Chen, P. (2015). MoS2 –GO nanocomposites synthesized via a hydrothermal hydrogel method for solar light photocatalytic degradation of methylene blue. *Applied Surface Science*, *357*, 1606-1612.
53. Domingues, E., Fernandes, E., Gomes, J., Castro-Silva, S., & Martins, R. C. (2021). Olive oil extraction industry wastewater treatment by coagulation and Fenton's process. *Journal of Water Process Engineering*, *39*, 101818.
54. Dong, H., Chen, D., Wang, K., & Zhang, R. (2016). High-yield preparation and electrochemical properties of few-layer MoS 2 nanosheets by exfoliating natural molybdenite powders directly via a coupled ultrasonication-milling process. *Nanoscale research letters*, *11*, 1-14.
55. Duraisamy, S., Ganguly, A., Sharma, P. K., Benson, J., Davis, J., & Papakonstantinou, P. (2021). One-step hydrothermal synthesis of phase-engineered MoS2 /MoO3 electrocatalysts for hydrogen evolution reaction. *ACS Applied Nano Materials*, *4*(3), 2642-2656.
56. El Mragui, A., Zegaoui, O., & da Silva, J. C. E. (2021). Elucidation of the photocatalytic degradation mechanism of an azo dye under visible light in the presence of cobalt doped TiO2 nanomaterials. *Chemosphere*, *266*, 128931.
57. Eltaboni, F., Bader, N., El-Kailany, R., Elsharif, N., & Ahmida, A. (2022). Dyes: a comprehensive review. *J. Chem. Rev*, *4*(4), 313-330.
58. Esmaeili-Zare, M., Salavati-Niasari, M., & Sobhani, A. (2012). Simple sonochemical synthesis and characterization of HgSe nanoparticles. *Ultrasonics sonochemistry*, *19*(5), 1079-1086.
59. Fakhri, A., & Nejad, P. A. (2016). Antimicrobial, antioxidant and cytotoxic effect of Molybdenum trioxide nanoparticles and application of this for degradation of ketamine under different light illumination. *Journal of Photochemistry and Photobiology B: Biology*, *159*, 211-217.
60. Fan, X., Xu, P., Zhou, D., Sun, Y., Li, Y. C., Nguyen, M. A. T., ... & Mallouk, T. E. (2015). Fast and efficient preparation of exfoliated 2H MoS_2 nanosheets

by sonication-assisted lithium intercalation and infrared laser-induced 1T to 2H phase reversion. *Nano letters*, *15*(9), 5956-5960.

61. Fang, X., Zeng, Z., Li, Q., Liu, Y., Chu, W., Maiyalagan, T., & Mao, S. (2021). Ultrasensitive detection of disinfection byproduct trichloroacetamide in drinking water with Ag nanoprism@ MoS2 heterostructure-based electrochemical sensor. *Sensors and Actuators B: Chemical*, *332*, 129526.

62. Feng, J., Cerniglia, C. E., & Chen, H. (2012). Toxicological significance of azo dye metabolism by human intestinal microbiota. *Frontiers in bioscience (Elite edition)*, *4*, 568

63. Feng, J., Cerniglia, C. E., & Chen, H. (2012). Toxicological significance of azo dye metabolism by human intestinal microbiota. *Frontiers in bioscience (Elite edition)*, *4*, 568.

64. Feng, X., Wen, P., Cheng, Y., Liu, L., Tai, Q., Hu, Y., & Liew, K. M. (2016). Defect-free MoS_2 nanosheets: Advanced nanofillers for polymer nanocomposites. *Composites Part A: Applied Science and Manufacturing*, *81*, 61-68.

65. Fernandez-Perez, A., & Marban, G. (2020). Visible light spectroscopic analysis of methylene blue in water; what comes after dimer?. *ACS omega*, *5*(46), 29801-29815.

66. Fioravanti, F., Martínez, S., Delgado, S., García, G., Rodriguez, J. L., Tejera, E. P., & Lacconi, G. I. (2023). Effect of MoS2 in doped-reduced graphene oxide composites. Enhanced electrocatalysis for HER. *Electrochimica Acta*, *441*, 141781.

67. Floriano, J. M., Rosa, E. D., do Amaral, Q. D. F., Zuravski, L., Chaves, P. E. E., Machado, M. M., & de Oliveira, L. F. S. (2018). Is tartrazine really safe? In silico and ex vivo toxicological studies in human leukocytes: a question of dose. *Toxicology Research*, *7*(6), 1128-1134.

68. Fouda, A., Hassan, S. E. D., Saied, E., & Hamza, M. F. (2021). Photocatalytic degradation of real textile and tannery effluent using biosynthesized magnesium oxide nanoparticles (MgO-NPs), heavy metal adsorption,

phytotoxicity, and antimicrobial activity. *Journal of Environmental Chemical Engineering*, *9*(4), 105346.

69. Ga'al, H., Yang, G., Fouad, H., Guo, M., & Mo, J. (2021). Mannosylerythritol lipids mediated biosynthesis of silver nanoparticles: an eco-friendly and operative approach against chikungunya vector Aedes albopictus. *Journal of Cluster Science*, *32*, 17-25.
70. Ganesha, H., Veeresh, S., Nagaraju, Y. S., Vandana, M., Basappa, M., Vijeth, H., & Devendrappa, H. (2022). 2-Dimensional layered molybdenum disulfide nanosheets and CTAB-assisted molybdenum disulfide nanoflower for high performance supercapacitor application. *Nanoscale Advances*, *4*(2), 521–531.
71. Gao, M., Wang, Z., Yang, C., Ning, J., Zhou, Z., & Li, G. (2019). Novel magnetic graphene oxide decorated with persimmon tannins for efficient adsorption of malachite green from aqueous solutions. *Colloids and Surfaces A: Physicochemical and Engineering Aspects*, *566*, 48-57.
72. Garg, M., Chatterjee, M., Sharma, A. L., & Singh, S. (2020). Label-free approach for electrochemical ferritin sensing using biosurfactant stabilized tungsten disulfide quantum dots. *Biosensors and Bioelectronics*, *151*, 111979.
73. Geng, X., Bao, J., Huang, T., Wang, X., Hou, C., Hou, J., ... & Huo, D. (2019). Electrochemical sensor for the simultaneous detection of guanine and adenine based on a PPyox/MWNTs-MoS2 modified electrode. *Journal of The Electrochemical Society*, *166*(6), B498.
74. Ghalajkhani, A., Haghighi, M., & Shabani, M. (2018). Efficient photocatalytic degradation of methylene blue in aqueous solution over flowerlike nanostructured MoS2 -FeZnO staggered heterojunction under simulated solar-light irradiation. *Journal of Photochemistry and Photobiology A: Chemistry*, *359*, 145-156.
75. Ghasemipour, P., Fattahi, M., Rasekh, B., & Yazdian, F. (2020). Developing the ternary ZnO doped MoS2 nanostructures grafted on CNT and reduced graphene oxide (RGO) for photocatalytic degradation of aniline. *Scientific reports*, *10*(1), 4414.

76. Ghayeb Zamharir, S., Karimzadeh, R., & Aboutalebi, S. H. (2018). Laser-assisted tunable optical nonlinearity in liquid-phase exfoliated MoS 2 dispersion. *Applied Physics A*, *124*, 1-8.
77. Gissawong, N., Srijaranai, S., Boonchiangma, S., Uppachai, P., Seehamart, K., Jantrasee, S., ... & Mukdasai, S. (2021). An electrochemical sensor for voltammetric detection of ciprofloxacin using a glassy carbon electrode modified with activated carbon, gold nanoparticles and supramolecular solvent. *Microchimica Acta*, *188*(6), 208.
78. Gómez-Graña, S., Perez-Ameneiro, M., Vecino, X., Pastoriza-Santos, I., Perez-Juste, J., Cruz, J. M., & Moldes, A. B. (2017). Biogenic synthesis of metal nanoparticles using a biosurfactant extracted from corn and their antimicrobial properties. *Nanomaterials*, *7*(6), 139.
79. Gottlieb, A., Shaw, C., Smith, A., Wheatley, A., & Forsythe, S. (2003). The toxicity of textile reactive azo dyes after hydrolysis and decolourisation. *Journal of Biotechnology*, *101*(1), 49-56.
80. Guan, G., Liu, S., Cheng, Y., Zhang, Y. W., & Han, M. Y. (2018). BSA-caged metal clusters to exfoliate MoS 2 nanosheets towards their hybridized functionalization. *Nanoscale*, *10*(23), 10911-10917.
81. Guan, G., Zhang, S., Liu, S., Cai, Y., Low, M., Teng, C. P., ... & Han, M. Y. (2015). Protein induces layer-by-layer exfoliation of transition metal dichalcogenides. *Journal of the American Chemical Society*, *137*(19), 6152-6155.
82. Guan, Z., Wang, C., Li, W., Luo, S., Yao, Y., Yu, S., ... & Wong, C. P. (2018). A facile and clean process for exfoliating MoS2 nanosheets assisted by a surface active agent in aqueous solution. *Nanotechnology*, *29*(42), 425702.
83. Guo, B., Yu, K., Li, H., Qi, R., Zhang, Y., Song, H., ... & Chen, M. (2017). Coral-shaped MoS2 decorated with graphene quantum dots performing as a highly active electrocatalyst for hydrogen evolution reaction. *ACS applied materials & interfaces*, *9*(4), 3653-3660.

84. Guo, J., Liu, C., Sun, Y., Sun, J., Zhang, W., Si, T., ... & Zhang, X. (2018). N-doped MoS2 nanosheets with exposed edges realizing robust electrochemical hydrogen evolution. *Journal of Solid State Chemistry*, *263*, 84-87.
85. Gürses, A., Açıkyıldız, M., Güneş, K., Gürses, M. S., Gürses, A., Açıkyıldız, M., ... & Gürses, M. S. (2016). Classification of dye and pigments. *Dyes and pigments*, 31-45.
86. Han, Q., Cai, S., Yang, L., Wang, X., Qi, C., Yang, R., & Wang, C. (2017). Molybdenum disulfide nanoparticles as multifunctional inhibitors against Alzheimer's disease. *ACS Applied Materials & Interfaces*, *9*(25), 21116-21123.
87. Hashemi, S. H., & Kaykhaii, M. (2022). Azo dyes: sources, occurrence, toxicity, sampling, analysis, and their removal methods. In *Emerging freshwater pollutants* (pp. 267-287). Elsevier.
88. He, Z., & Que, W. (2016). Molybdenum disulfide nanomaterials: Structures, properties, synthesis and recent progress on hydrogen evolution reaction. *Applied Materials Today*, *3*, 23-56.
89. Hu, C., Liu, Y., Yang, Y., Cui, J., Huang, Z., Wang, Y., ... & Rong, J. (2013). One-step preparation of nitrogen-doped graphene quantum dots from oxidized debris of graphene oxide. *Journal of Materials Chemistry B*, *1*(1), 39-42.
90. Hu, C., Liu, Y., Yang, Y., Cui, J., Huang, Z., Wang, Y., ... & Rong, J. (2013). One-step preparation of nitrogen-doped graphene quantum dots from oxidized debris of graphene oxide. *Journal of Materials Chemistry B*, *1*(1), 39-42.
91. Huang, K.-J., Zhang, J.-Z., Shi, G.-W., & Liu, Y.-M. (2014). Hydrothermal synthesis of molybdenum disulfide nanosheets as supercapacitors electrode material. *Electrochimica Acta*, *132*, 397–403.
92. Huang, L., Bao, J., Quan, W., Li, X., Zhao, T., Ning, Y., ... & Tian, H. (2023). Design and synthesis of Z-scheme LaFeO3/MoS2/graphene heterojunction with enhanced photocatalytic performance. *Journal of Alloys and Compounds*, *934*, 167948.
93. Huang, M., Tian, H., Zhou, P., Ma, S., Chen, J., Zhang, N., & Zhang, K. (2021). Electrochemical sensor for detection of ascorbic acid based on MoS2 -

AuNPs modified glassy carbon electrode. *International Journal of Electrochemical Science*, *16*(1), 151014.

94. Hwang, H., Kim, H., & Cho, J. (2011). MoS2 nanoplates consisting of disordered graphene-like layers for high rate lithium battery anode materials. *Nano letters*, *11*(11), 4826-4830.
95. Ifrah, Z., Shah Rukh, A., Muhammad Nauman, S., Maryam, S., & Rahat, U. (2022). Fluorescence quenching of graphene quantum dots by chloride ions: A potential optical biosensor for cystic fibrosis. *Frontiers in Materials*, *9*, 857432.
96. Ikram, M., Hassan, J., Imran, M., Haider, J., Ul-Hamid, A., Shahzadi, I., ... & Ali, S. (2020). 2D chemically exfoliated hexagonal boron nitride (hBN) nanosheets doped with Ni: synthesis, properties and catalytic application for the treatment of industrial wastewater. *Applied Nanoscience*, *10*, 3525-3528.
97. Ikram, M., Raza, A., Shahzad, K., Haider, A., Haider, J., Durrani, A. K., ... & Ikram, M. (2021). Advanced Carbon Materials: Base of 21st Century Scientific Innovations in Chemical, Polymer, Sensing & Energy Engineering. *21st Century Advanced Carbon Materials for Engineering Applications: A Comprehensive Handbook*, 15.
98. Ipte, P. R., Sahoo, S., & Satpati, A. K. (2019). Spectro-electrochemistry of ciprofloxacin and probing its interaction with bovine serum albumin. *Bioelectrochemistry*, *130*, 107330.
99. Iwuozor, K. O., Ighalo, J. O., Emenike, E. C., Ogunfowora, L. A., & Igwegbe, C. A. (2021). Adsorption of methyl orange: A review on adsorbent performance. *Current Research in Green and Sustainable Chemistry*, *4*, 100179.
100. Jaleel UC, J. R., Devi KR, S., Pinheiro, D., & Mohan, M. K. (2022). Structural, morphological and optical properties of MoS2-based materials for photocatalytic degradation of organic dye. *Photochem*, *2*(3), 628-650.

101. Jawaid, A., Nepal, D., Park, K., Jespersen, M., Qualley, A., Mirau, P., ... & Vaia, R. A. (2016). Mechanism for liquid phase exfoliation of MoS2 . *Chemistry of Materials*, *28*(1), 337-348.

102. Jeon, W., Cho, Y., Jo, S., Ahn, J. H., & Jeong, S. J. (2017). Wafer-Scale Synthesis of Reliable High-Mobility Molybdenum Disulfide Thin Films via Inhibitor-Utilizing Atomic Layer Deposition. *Advanced Materials*, *29*(47), 1703031.

103. Jiang, J. W. (2015). Graphene versus MoS2 : A short review. *Frontiers of Physics*, *10*(3), 287-302.

104. Johra, F. T., Lee, J. W., & Jung, W. G. (2014). Facile and safe graphene preparation on solution based platform. *Journal of Industrial and Engineering Chemistry*, *20*(5), 2883-2887.

105. Kandhasamy, D. M., Muthu Mareeswaran, P., Chellappan, S., Namasivayam, D., Aldahish, A., & Chidambaram, K. (2021). Synthesis and photoluminescence properties of MoS2/graphene heterostructure by liquid-phase exfoliation. *ACS omega*, *7*(1), 629-637.

106. Kang, M., Chai, K., Lee, S., Oh, J. H., Bae, J. S., & Payne, G. F. (2023). Revealing Redox Behavior of Molybdenum Disulfide and Its Application as Rechargeable Antioxidant Reservoir. *ACS Applied Materials & Interfaces*, *15*(35), 41362-41372.

107. Kao, L. H., Chuang, K. S., Catherine, H. N., Huang, J. H., Hsu, H. J., Shen, Y. C., & Hu, C. (2023). MoS2-coupled coniferous ZnO for photocatalytic degradation of dyes. *Journal of the Taiwan Institute of Chemical Engineers*, *142*, 104638.

108. Karamat, S., Hassan, M. U., Pan, J. S., Tabassam, L., & Oral, A. (2020). Chemical vapor deposition of molybdenum disulphide on platinum foil. *Materials Chemistry and Physics*, *249*, 123017.

109. Karpuraranjith, M., Chen, Y., Rajaboopathi, S., Ramadoss, M., Srinivas, K., Yang, D., & Wang, B. (2022). Three-dimensional porous MoS2 nanobox embedded g-C3N4@ TiO2 architecture for highly efficient

photocatalytic degradation of organic pollutant. *Journal of Colloid and Interface Science*, *605*, 613-623.

110. Kathiravan, D., Huang, B. R., Saravanan, A., Prasannan, A., & Hong, P. D. (2019). Highly enhanced hydrogen sensing properties of sericin-induced exfoliated MoS2 nanosheets at room temperature. *Sensors and Actuators B: Chemical*, *279*, 138-147.

111. Kaur, M., Gautam, A., Guleria, P., Singh, K., & Kumar, V. (2022). Green synthesis of metal nanoparticles and their environmental applications. *Current Opinion in Environmental Science & Health*, *29*, 100390.

112. Kaur, M., Kumar, V., Awasthi, A., & Singh, K. (2023). Gum arabic–assisted green synthesis of biocompatible MoS2 nanoparticles for methylene blue photodegradation. *Environmental Science and Pollution Research*, *30*(52), 112847-112862.

113. Kesarla, M. K., Mandal, B. K., & Bandapalli, P. R. (2014). Gold nanoparticles by Terminalia bellirica aqueous extract–a rapid green method. *Journal of Experimental Nanoscience*, *9*(8), 825-830.

114. Khalid, A., & Mahmood, S. (2014). The biodegradation of azo dyes by actinobacteria. In *Microbial Degradation of Synthetic Dyes in Wastewaters* (pp. 297-314). Cham: Springer International Publishing.

115. Khalid, A., Zubair, M., & Ihsanullah. (2018). A comparative study on the adsorption of Eriochrome Black T dye from aqueous solution on graphene and acid-modified graphene. *Arabian Journal for Science and Engineering*, *43*, 2167-2179.

116. Khan, I., Saeed, K., Zekker, I., Zhang, B., Hendi, A. H., Ahmad, A., ... & Khan, I. (2022). Review on methylene blue: Its properties, uses, toxicity and photodegradation. *Water*, *14*(2), 242.

117. Khan, R., Riaz, A., Javed, S., Jan, R., Akram, M. A., & Mujahid, M. (2018). Synthesis and characterization of MoS2 /TiO2 nanocomposites for

enhanced photocatalytic degradation of methylene blue under sunlight irradiation. *Key Engineering Materials*, *778*, 137-143.

118. Khan, S., Guan, Q., Liu, Q., Qin, Z., Rasheed, B., Liang, X., & Yang, X. (2022). Synthesis, modifications and applications of MILs Metal-organic frameworks for environmental remediation: The cutting-edge review. *Science of the Total Environment*, *810*, 152279.

119. Khan, S., Noor, A., Khan, I., Muhammad, M., Sadiq, M., & Muhammad, N. (2022). Photocatalytic Degradation of Organic Dyes Contaminated Aqueous Solution Using Binary CdTiO2 and Ternary NiCdTiO2 Nanocomposites. *Catalysts*, *13*(1), 44.

120. Khayyat, L. I., Essawy, A. E., Sorour, J. M., & Soffar, A. (2018). Sunset Yellow and Allura Red modulate Bcl2 and COX2 expression levels and confer oxidative stress-mediated renal and hepatic toxicity in male rats. *PeerJ*, *6*, e5689.

121. Kiran, G. S., Selvin, J., Manilal, A., & Sujith, S. (2011). Biosurfactants as green stabilizers for the biological synthesis of nanoparticles. *Critical reviews in biotechnology*, *31*(4), 354-364.

122. Kirk-Othmer Encyclopedia of Chemical Technology (1981). 3rd ed., Volumes 1-26. New York, NY: *John Wiley and Sons*, 1978-1984., p. V13: 370.

123. Kisała, J., Wojnarowska-Nowak, R., & Bobitski, Y. (2023). Layered MoS2 : effective and environment-friendly nanomaterial for photocatalytic degradation of methylene blue. *Scientific Reports*, *13*(1), 14148.

124. Kosswattaarachchi, A. M., & Cook, T. R. (2018). Repurposing the industrial dye methylene blue as an active component for redox flow batteries. *ChemElectroChem*, *5*(22), 3437-3442.

125. Krishnamurthi, V. R., Niyonshuti, I. I., Chen, J., & Wang, Y. (2021). A new analysis method for evaluating bacterial growth with microplate readers. *PLoS One*, *16*(1), e0245205.

126. Kulik, K., Lenart-Boroń, A., & Wyrzykowska, K. (2023). Impact of antibiotic pollution on the bacterial population within surface water with special focus on mountain rivers. *Water*, *15*(5), 975.

127. Kumar, A., & Pandey, G. (2017). A review on the factors affecting the photocatalytic degradation of hazardous materials. *Mater. Sci. Eng. Int. J*, *1*(3), 1-10.

128. Kumar, S., Sharma, R., Singh, D., Awasthi, A., Kumar, V., & Singh, K. (2024). Tungsten sulphide decorated carbon nanotube based electroanalytical sensing of neurotransmitter dopamine. *Electrochimica Acta*, *475*, 143584.

129. Kurapati, R., Backes, C., Ménard-Moyon, C., Coleman, J. N., & Bianco, A. (2016). White graphene undergoes peroxidase degradation. *Angewandte Chemie*, *128*(18), 5596-5601

130. Lang, Y., Xu, S., & Zhang, C. (2023). Hydrothermal Synthesis of Molybdenum Disulfide Quantum Dots for Highly Sensitive Detection of Iron Ions in Protein Succinate Oral Solution. *Micromachines*, *14*(7), 1368.

131. Lawagon, C. P., & Amon, R. E. C. (2020). Magnetic rice husk ash'cleanser'as efficient methylene blue adsorbent. *Environmental Engineering Research*, *25*(5), 685-692.

132. Lee, Y. Y., Moon, J. H., Choi, Y. S., Park, G. O., Jin, M., Jin, L. Y., ... & Kim, J. M. (2017). Visible-light driven photocatalytic degradation of organic dyes over ordered mesoporous Cd x Zn1–x S materials. *The Journal of Physical Chemistry C*, *121*(9), 5137-5144.

133. Lengyel, J., Ončák, M., Herburger, A., van der Linde, C., & Beyer, M. K. (2017). Infrared spectroscopy of $O^{\cdot}-$ and $OH-$ in water clusters: evidence for fast interconversion between $O^{\cdot}-$ and $OH^{\cdot}$ $OH-$. *Physical Chemistry Chemical Physics*, *19*(37), 25346-25351.

134. Li, B., Jiang, L., Li, X., Ran, P., Zuo, P., Wang, A., ... & Lu, Y. (2017). Preparation of monolayer MoS2 quantum dots using temporally shaped femtosecond laser ablation of bulk MoS2 targets in water. *Scientific reports*, *7*(1), 11182.

135. Li, B., Wang, T., Wang, X., Wu, X., Wang, C., Miao, F., ... & Cao, Y. (2019). Engineered recombinant proteins for aqueous ultrasonic exfoliation and dispersion of biofunctionalized 2D materials. *Chemistry–A European Journal*, *25*(34), 7991-7997.

136. Li, B., Wang, T., Wang, X., Wu, X., Wang, C., Miao, F., ... & Cao, Y. (2019). Engineered recombinant proteins for aqueous ultrasonic exfoliation and dispersion of biofunctionalized 2D materials. *Chemistry–A European Journal*, *25*(34), 7991-7997.

137. Li, F., Li, J., Cao, Z., Lin, X., Li, X., Fang, Y., ... & Li, R. (2015). MoS 2 quantum dot decorated RGO: a designed electrocatalyst with high active site density for the hydrogen evolution reaction. *Journal of Materials Chemistry A*, *3*(43), 21772-21778.

138. Li, H., Wu, J., Yin, Z., & Zhang, H. (2014). Preparation and applications of mechanically exfoliated single-layer and multilayer MoS2 and WSe2 nanosheets. *Accounts of chemical research*, *47*(4), 1067-1075.

139. Li, H., Wu, J., Yin, Z., & Zhang, H. (2014). Preparation and applications of mechanically exfoliated single-layer and multilayer MoS2 and WSe2 nanosheets. *Accounts of chemical research*, *47*(4), 1067-1075

140. Li, H., Xiong, Y., Wang, Y., Ma, W., Fang, J., Li, X., ... & Fang, P. (2022). High piezocatalytic capability in CuS/MoS2 nanocomposites using mechanical energy for degrading pollutants. *Journal of Colloid and Interface Science*, *609*, 657-666.

141. Li, J., Liu, X., Pan, L., Qin, W., Chen, T., & Sun, Z. (2014). MoS 2–reduced graphene oxide composites synthesized via a microwave-assisted method for visible-light photocatalytic degradation of methylene blue. *Rsc Advances*, *4*(19), 9647-9651.

142. Li, M., Addad, A., Zhang, Y., Barras, A., Roussel, P., Amin, M. A., ... & Boukherroub, R. (2021). Flower-like Nitrogen-co-doped MoS2@ RGO composites with excellent stability for supercapacitors. *ChemElectroChem*, *8*(15), 2903-2911.

143. Li, Y., Wang, X., Liu, M., Luo, H., Deng, L., Huang, L., ... & Xu, Y. (2019). Molybdenum disulfide quantum dots prepared by bipolar-electrode electrochemical scissoring. *Nanomaterials*, *9*(6), 906.

144. Li, Z., Meng, X., & Zhang, Z. (2018). Recent development on MoS2-based photocatalysis: A review. *Journal of Photochemistry and Photobiology C: Photochemistry Reviews*, *35*, 39-55.

145. Liu, J., Hu, Z., Zhang, Y., Li, H. Y., Gao, N., Tian, Z., ... & Liu, H. (2020). MoS 2 nanosheets sensitized with quantum dots for room-temperature gas sensors. *Nano-Micro Letters*, *12*, 1-13.

146. Liu, J., Zeng, Z., Cao, X., Lu, G., Wang, L. H., Fan, Q. L., ... & Zhang, H. (2012). Preparation of MoS2 -polyvinylpyrrolidone nanocomposites for flexible nonvolatile rewritable memory devices with reduced graphene oxide electrodes. *Small*, *8*(22), 3517-3522.

147. Liu, L., Liu, Z., Huang, P., Wu, Z., & Jiang, S. (2016). Protein-induced ultrathin molybdenum disulfide (MoS 2) flakes for a water-based lubricating system. *RSC advances*, *6*(114), 113315-113321.

148. Liu, W., Zhao, C., Zhou, R., Zhou, D., Liu, Z., & Lu, X. (2015). Lignin-assisted exfoliation of molybdenum disulfide in aqueous media and its application in lithium ion batteries. *Nanoscale*, *7*(21), 9919-9926.

149. Liu, Y. D., Ren, L., Qi, X., Yang, L. W., Hao, G. L., Li, J., ... & Zhong, J. X. (2013). Preparation, characterization and photoelectrochemical property of ultrathin MoS2 nanosheets via hydrothermal intercalation and exfoliation route. *Journal of alloys and compounds*, *571*, 37-42.

150. Liu, Y., & Li, R. (2020). Study on ultrasound-assisted liquid-phase exfoliation for preparing graphene-like molybdenum disulfide nanosheets. *Ultrasonics sonochemistry*, *63*, 104923.

151. Lu, G., Nagbanshi, M., Goldau, N., Mendes Jorge, M., Meissner, P., Jahn, A., ... & Mueller, O. (2018). Efficacy and safety of methylene blue in the treatment of malaria: a systematic review. *BMC medicine*, *16*, 1-16.

152. Luo, R., Xu, W. W., Zhang, Y., Wang, Z., Wang, X., Gao, Y., ... & Chen, M. (2020). Van der Waals interfacial reconstruction in monolayer

transition-metal dichalcogenides and gold heterojunctions. *Nature communications*, *11*(1), 1011.

153. Luo, S., Dong, S., Lu, C., Yu, C., Ou, Y., Luo, L., ... & Sun, J. (2018). Rational and green synthesis of novel two-dimensional WS2/MoS2 heterojunction via direct exfoliation in ethanol-water targeting advanced visible-light-responsive photocatalytic performance. *Journal of colloid and interface science*, *513*, 389-399.

154. Luxa, J., Jankovský, O., Sedmidubský, D., Medlín, R., Maryško, M., Pumera, M., & Sofer, Z. (2016). Origin of exotic ferromagnetic behavior in exfoliated layered transition metal dichalcogenides MoS 2 and WS 2. *Nanoscale*, *8*(4), 1960-1967.

155. Ma, L., Zhang, Q., Wu, C., Zhang, Y., & Zeng, L. (2019). PtNi bimetallic nanoparticles loaded MoS2 nanosheets: Preparation and electrochemical sensing application for the detection of dopamine and uric acid. *Analytica chimica acta*, *1055*, 17-25.

156. Ma, Z., Hu, L., Li, X., Deng, L., Fan, G., & He, Y. (2019). A novel nano-sized MoS2 decorated Bi2O3 heterojunction with enhanced photocatalytic performance for methylene blue and tetracycline degradation. *Ceramics International*, *45*(13), 15824-15833.

157. Madhusudhana, N., Yogendra, K., & Mahadevan, K. M. (2012). A comparative study on Photocatalytic degradation of Violet GL2B azo dye using CaO and TiO2 nanoparticles. *Int. J. Eng. Res. Appl*, *2*(5), 1300-1307.

158. Mahmoodi, N., Faraji, M., & Ziarati, P. (2016). Simultaneous determination of sunset yellow and carmoisine in orange flavored soft drink samples by high-performance liquid chromatography. *IOSR Journal of Applied Chemistry*, *9*(8), 79-83.

159. Majeed, A., Ibrahim, A. H., Al-Rawi, S. S., Iqbal, M. A., Kashif, M., Yousif, M., ... & Hussain, S. A. (2024). Green Organo-Photooxidative Method for the Degradation of Methylene Blue Dye. *ACS omega*, *9*(10), 12069-12083.

160. Mak, K. F., Lee, C., Hone, J., Shan, J., & Heinz, T. F. (2010). Atomically Thin MoS 2: A New Direct-Gap Semiconductor. *Physical Review Letters*, *105*(13), 136805.

161. Malakar, C., Patowary, K., Deka, S., & Kalita, M. C. (2021). Synthesis, characterization, and evaluation of antibacterial efficacy of rhamnolipid-coated zinc oxide nanoparticles against Staphylococcus aureus. *World Journal of Microbiology and Biotechnology*, *37*, 1-14.

162. Mandal, T., Maity, S., Dasgupta, D., & Datta, S. (2010). Advanced oxidation process and biotreatment: Their roles in combined industrial wastewater treatment. *Desalination*, *250*(1), 87-94.

163. Mani, S., & Bharagava, R. N. (2016). Exposure to crystal violet, its toxic, genotoxic and carcinogenic effects on environment and its degradation and detoxification for environmental safety. *Reviews of Environmental Contamination and Toxicology Volume 237*, 71-104.

164. Manzoor, J., & Sharma, M. (2020). Impact of textile dyes on human health and environment. In *Impact of textile dyes on public health and the environment* (pp. 162-169). IGI Global.

165. Mariyappan, V., Keerthi, M., Chen, S. M., & Boopathy, G. (2020). Facile synthesis of α-Sm2S3/MoS2 bimetallic sulfide as a high-performance electrochemical sensor for the detection of antineoplastic drug 5-fluorouracil in a biological samples. *Journal of The Electrochemical Society*, *167*(11), 117506.

166. Masi, C., Gemechu, G., & Tafesse, M. (2021). Isolation, screening, characterization, and identification of alkaline protease-producing bacteria from leather industry effluent. *Annals of Microbiology*, *71*, 1-11.

167. Mason, T. J. (2002). Uses of power ultrasound in chemistry and processing. *Applied sonochemistry*.

168. Mathew, S., Antony, A., & Kathyayini, H. (2020). Degradation of azo dye under visible light irradiation over nanographene oxide–zinc oxide nanocomposite as catalyst. *Applied Nanoscience*, *10*(1), 253-262.

169. Matte, H. R., Gomathi, A., Manna, A. K., Late, D. J., Datta, R., Pati, S. K., & Rao, C. N. R. (2010). MoS 2 and WS 2 analogues of graphene. *Angewandte Chemie International Edition*, *24*(49), 4059-4062.

170. McDonald, S., Prenzler, P. D., Antolovich, M., & Robards, K. (2001). Phenolic content and antioxidant activity of olive extracts. *Food chemistry*, *73*(1), 73-84.

171. Mehmandoust, M., Çakar, S., Özacar, M., Salmanpour, S., & Erk, N. (2021). Electrochemical sensor for facile and highly selective determination of antineoplastic agent in real samples using glassy carbon electrode modified by 2D-MoS 2 NFs/TiO 2 NPs. *Topics in Catalysis*, 1-13.

172. Melnikova-Kominkova, Z., Jurkova, K., Vales, V., Drogowska-Horná, K., Frank, O., & Kalbac, M. (2019). Strong and efficient doping of monolayer MoS 2 by a graphene electrode. *Physical Chemistry Chemical Physics*, *21*(46), 25700-25706.

173. Mohammed, M. S. A. I. A., Shitu, A., & Ibrahim, A. (2014). Removal of methylene blue using low cost adsorbent: a review. *Research Journal of Chemical Sciences ISSN*, *2231*, 606X.

174. Mohammed, R., Ali, M. E. M., Abdel-Moniem, S. M., & Ibrahim, H. S. (2022). Reusable and highly stable MoS2 nanosheets for photocatalytic, sonocatalytic and thermocatalytic degradation of organic dyes: Comparative study. *Nano-Structures & Nano-Objects*, *31*, 100900.

175. Monga, D., Ilager, D., Shetti, N. P., Basu, S., & Aminabhavi, T. M. (2020). 2D/2d heterojunction of MoS2/g-C3N4 nanoflowers for enhanced visible-light-driven photocatalytic and electrochemical degradation of organic pollutants. *Journal of environmental management*, *274*, 111208.

176. Mukherjee, S., Maiti, R., Midya, A., Das, S., & Ray, S. K. (2015). Tunable direct bandgap optical transitions in MoS2 nanocrystals for photonic devices. *Acs Photonics*, *2*(6), 760-768.

177. Mulu, M., RamaDevi, D., Belachew, N., & Basavaiah, K. (2021). Hydrothermal green synthesis of MoS 2 nanosheets for pollution abatement and antifungal applications. *RSC advances*, *11*(40), 24536-24542.

178. Munoz, R., López-Elvira, E., Munuera, C., Frisenda, R., Sánchez-Sánchez, C., Martín-Gago, J. Á., & García-Hernández, M. (2022). Direct growth of graphene-MoS2 heterostructure: Tailored interface for advanced devices. *Applied Surface Science*, *581*, 151858.

179. Mutyala, S., Mohamed Jaffer Sadiq, M., Gurulakshmi, M., Suresh, C., Krishna Bhat, D., Shanthi, K., & Mathiyarasu, J. (2020). Disintegration of flower-like MoS2 to limply allied layers on spherical nanoporous TiO2: Enhanced visible-light photocatalytic degradation of methylene blue. *Journal of Nanoscience and Nanotechnology*, *20*(2), 1118-1129.

180. National Center for Biotechnology Information (2024). PubChem Compound Summary for CID 6099, Methylene Blue. Retrieved July 23, 2024 from https://pubchem.ncbi.nlm.nih.gov/compound/Methylene-Blue

181. Negash, A., Mohammed, S., Weldekirstos, H. D., Ambaye, A. D., & Gashu, M. (2023). Enhanced photocatalytic degradation of methylene blue dye using eco-friendly synthesized rGO@ZnO nanocomposites. *Scientific Reports*, *13*(1), 22234.

182. Neto, A. H., & Novoselov, K. J. M. E. (2011). Two-dimensional crystals: beyond graphene. *Materials Express*, *1*(1), 10-17.

183. Nguyen, E. P., Carey, B. J., Daeneke, T., Ou, J. Z., Latham, K., Zhuiykov, S., & Kalantar-Zadeh, K. (2015). Investigation of two-solvent grinding-assisted liquid phase exfoliation of layered MoS2 . *Chemistry of Materials*, *27*(1), 53-59.

184. Nguyen, P. Y., Carvalho, G., Reis, M. A., & Oehmen, A. (2021). A review of the biotransformations of priority pharmaceuticals in biological wastewater treatment processes. *Water Research*, *188*, 116446.

185. Niu, L., Coleman, J. N., Zhang, H., Shin, H., Chhowalla, M., & Zheng, Z. (2016). Production of two-dimensional nanomaterials via liquid-based direct exfoliation. *Small*, *12*(3), 272-293.

186. Novoselov, K. S., Jiang, D., Schedin, F., Booth, T. J., Khotkevich, V. V., Morozov, S. V., & Geim, A. K. (2005). Two-dimensional atomic

crystals. *Proceedings of the National Academy of Sciences*, *102*(30), 10451-10453.

187. Obotey Ezugbe, E., & Rathilal, S. (2020). Membrane technologies in wastewater treatment: a review. *Membranes*, *10*(5), 89.

188. Ogunyemi, S. O., Zhang, M., Abdallah, Y., Ahmed, T., Qiu, W., Ali, M. A., ... & Li, B. (2020). The bio-synthesis of three metal oxide nanoparticles (ZnO, MnO2, and MgO) and their antibacterial activity against the bacterial leaf blight pathogen. *Frontiers in Microbiology*, *11*, 588326.

189. Oladoye, P. O., Ajiboye, T. O., Omotola, E. O., & Oyewola, O. J. (2022). Methylene blue dye: Toxicity and potential elimination technology from wastewater. *Results in Engineering*, *16*, 100678.

190. Parida, V. K., Srivastava, S. K., Gupta, A. K., & Rawat, A. (2023). A review on nanomaterial-based heterogeneous photocatalysts for removal of contaminants from water. *Materials Express*, *13*(1), 1-38.

191. Patel, P., Gupta, P., Sujata, K. M., & Solanki, R. G. (2024). Photocatalytic degradation of methylene blue dye using copper selenide nanoparticles prepared by co-precipitation method. *Journal of Cluster Science*, *35*(1), 191-199.

192. Pena-Alvarez, M., del Corro, E., Morales-Garcia, A., Kavan, L., Kalbac, M., & Frank, O. (2015). Single layer molybdenum disulfide under direct out-of-plane compression: low-stress band-gap engineering. *Nano letters*, *15*(5), 3139-3146.

193. Peng, H., Wang, D., & Fu, S. (2020). Tannic acid-assisted green exfoliation and functionalization of MoS2 nanosheets: Significantly improve the mechanical and flame-retardant properties of polyacrylonitrile composite fibers. *Chemical Engineering Journal*, *384*, 123288.

194. Pervaiz, M., Ur Rehman, M., Ali, F., Younas, U., Sillanpaa, M., Kausar, R., ... & Mazid, M. A. (2023). [Retracted] Biomolecule Protective and Photocatalytic Potential of Cellulose Supported MoS2/GO Nanocomposite. *Bioinorganic Chemistry and Applications*, *2023*(1), 3634726.

195. Płaza, G. A., Chojniak, J., & Banat, I. M. (2014). Biosurfactant mediated biosynthesis of selected metallic nanoparticles. *International Journal of Molecular Sciences*, *15*(8), 13720-13737.

196. Pomicpic, J., Dancel, G. C., Cabalar, P. J., & Madrid, J. (2020). Methylene blue removal by poly (acrylic acid)-grafted pineapple leaf fiber/polyester nonwoven fabric adsorbent and its comparison with removal by gamma or electron beam irradiation. *Radiation Physics and Chemistry*, *172*, 108737.

197. Pozzati, M., Boll, F., Crisci, M., Domenici, S., Smarsly, B., Gatti, T., & Wang, M. (2024). Systematic Investigation on the Surfactant-Assisted Liquid-Phase Exfoliation of MoS2 and WS2 in Water for Sustainable 2D Material Inks. *physica status solidi (RRL)–Rapid Research Letters*, 2400039.

198. Pu, N. W., Wang, C. A., Liu, Y. M., Sung, Y., Wang, D. S., & Ger, M. D. (2012). Dispersion of graphene in aqueous solutions with different types of surfactants and the production of graphene films by spray or drop coating. *Journal of the Taiwan Institute of Chemical Engineers*, *43*(1), 140-146.

199. Qasim, S., Zafar, A., Saif, M. S., Ali, Z., Nazar, M., Waqas, M., ... & Hasan, M. (2020). Green synthesis of iron oxide nanorods using Withania coagulans extract improved photocatalytic degradation and antimicrobial activity. *Journal of Photochemistry and Photobiology B: Biology*, *204*, 111784.

200. Qi, Y., Wang, N., Xu, Q., Li, H., Zhou, P., Lu, X., & Zhao, G. (2015). A green route to fabricate MoS 2 nanosheets in water–ethanol–CO 2. *Chemical Communications*, *51*(31), 6726-6729.

201. Qiu, Y., Wang, Z., Owens, A. C., Kulaots, I., Chen, Y., Kane, A. B., & Hurt, R. H. (2014). Antioxidant chemistry of graphene-based materials and its role in oxidation protection technology. *Nanoscale*, *6*(20), 11744-11755.

202. Qu, D., Gu, Y., Feng, L., & Han, J. (2017). High content analysis technology for evaluating the joint toxicity of sunset yellow and sodium sulfite in vitro. *Food chemistry*, *233*, 135-143.

203. Rahaman, M., Ahmed, M. H., Sadman, S. M., & Islam, M. R. (2023). Defect mediated visible light induced photocatalytic activity of Co3O4 nanoparticle decorated MoS2 nanoflower: A combined experimental and theoretical study. *Heliyon*, *9*(3).

204. Rajan, A. P., & Anandan, S. (2017). Investigation of carcinogenic and mutagenic property of food colour using catfish Clarias Batrachus by using alkaline single-cell gel electrophoresis (comet) assay and micronucleus assay. *Int. J. Med. Res. Pharmacol. Sci*, *4*(7), 29-34.

205. Rajan, M. S., John, A., & Thomas, J. (2023). Perylene nanoparticle-sensitized MoS 2: an efficient solar photocatalyst for the degradation of pollutants. *New Journal of Chemistry*, *47*(3), 1349-1359.

206. Rane, A. N., Baikar, V. V., Ravi Kumar, V., & Deopurkar, R. L. (2017). Agro-industrial wastes for production of biosurfactant by Bacillus subtilis ANR 88 and its application in synthesis of silver and gold nanoparticles. *Frontiers in Microbiology*, *8*, 492.

207. Rane, A. N., Geetha, S. J., & Joshi, S. J. (2021). Biosurfactants: production and role in synthesis of nanoparticles for environmental applications. *Biosurfactants for a sustainable future: production and applications in the environment and biomedicine*, 183-206.

208. Rani, A., Patel, A. S., Chakraborti, A., Singh, K., & Sharma, P. (2021). Enhanced photocatalytic activity of plasmonic Au nanoparticles incorporated MoS2 nanosheets for degradation of organic dyes. *Journal of Materials Science: Materials in Electronics*, *32*(5), 6168-6184.

209. Rani, A., Singh, K., Patel, A. S., Chakraborti, A., Kumar, S., Ghosh, K., & Sharma, P. (2020). Visible light driven photocatalysis of organic dyes using SnO2 decorated MoS2 nanocomposites. *Chemical Physics Letters*, *738*, 136874.

210. Rashid, R., Shafiq, I., Akhter, P., Iqbal, M. J., & Hussain, M. (2021). A state-of-the-art review on wastewater treatment techniques: the effectiveness of adsorption method. *Environmental Science and Pollution Research*, *28*, 9050-9066.

211. Rathi, B. S., & Kumar, P. S. (2022). Sustainable approach on the biodegradation of azo dyes: a short review. *Current Opinion in Green and Sustainable Chemistry*, *33*, 100578.

212. Raza, A., Qumar, U., Haider, A., Naz, S., Haider, J., Ul-Hamid, A., ... & Kanoun, M. B. (2021). Liquid-phase exfoliated MoS 2 nanosheets doped with p-type transition metals: a comparative analysis of photocatalytic and antimicrobial potential combined with density functional theory. *Dalton Transactions*, *50*(19), 6598-6619

213. Ritika, Kaur, M., Umar, A., Mehta, S. K., Singh, S., Kansal, S. K., ... & Alothman, O. Y. (2018). Rapid solar-light driven superior photocatalytic degradation of methylene blue using MoS2 -ZnO heterostructure nanorods photocatalyst. *Materials*, *11*(11), 2254.

214. Ritika, Kaur, M., Umar, A., Mehta, S. K., Singh, S., Kansal, S. K., ... & Alothman, O. Y. (2018). Rapid solar-light driven superior photocatalytic degradation of methylene blue using MoS2-ZnO heterostructure nanorods photocatalyst. *Materials*, *11*(11), 2254.

215. Roy, S., Mondal, A., Yadav, V., Sarkar, A., Banerjee, R., Sanpui, P., & Jaiswal, A. (2019). Mechanistic insight into the antibacterial activity of chitosan exfoliated MoS2 nanosheets: membrane damage, metabolic inactivation, and oxidative stress. *ACS applied bio materials*, *2*(7), 2738-2755.

216. Saad Algarni, T., Abduh, N. A., Al Kahtani, A., & Aouissi, A. (2022). Photocatalytic degradation of some dyes under solar light irradiation using ZnO nanoparticles synthesized from Rosmarinus officinalis extract. *Green chemistry letters and reviews*, *15*(2), 460-473.

217. Sadhanala, H. K., Senapati, S., Harika, K. V., Nanda, K. K., & Gedanken, A. (2018). Green synthesis of MoS 2 nanoflowers for efficient

degradation of methylene blue and crystal violet dyes under natural sun light conditions. *New Journal of Chemistry*, *42*(17), 14318-14324.

218. Saha, B., Debnath, A., & Saha, B. (2022). Fabrication of PANI@ Fe–Mn–Zr hybrid material and assessments in sono-assisted adsorption of methyl red dye: uptake performance and response surface optimization. *Journal of the Indian Chemical Society*, *99*(9), 100635.

219. Sahu, T. S., & Mitra, S. (2015). Exfoliated MoS2 sheets and reduced graphene oxide-an excellent and fast anode for sodium-ion battery. *Scientific reports*, *5*(1), 12571.

220. Samy, O., Zeng, S., Birowosuto, M. D., & El Moutaouakil, A. (2021). A review on MoS2 properties, synthesis, sensing applications and challenges. *Crystals*, *11*(4), 355.

221. Sangar, S., Sharma, S., Vats, V. K., Mehta, S. K., & Singh, K. (2019). Biosynthesis of silver nanocrystals, their kinetic profile from nucleation to growth and optical sensing of mercuric ions. *Journal of Cleaner Production*, *228*, 294-302.

222. Sankaranarayanan, S., Subramanian, S., Hussain, S., & Mamidipudi, G. K. (2024). Hierarchical nanostructures of MoS2 for visible light photocatalytic degradation of methylene blue dye. *Physica B: Condensed Matter*, *692*, 416383.

223. Sarker, M. R., Chowdhury, M., & Deb, A. K. (2019). Reduction of color intensity from textile dye wastewater using microorganisms: a review. *Int. J. Curr. Microbiol. Appl. Sci*, *8*(02), 3407-3415.

224. Sasi, S., Beegum, B., Thomas, C., Joseph, L. M., Shinoj, V. K., & Reshmi, R. (2023). Active sites rich manganese doped MoS2 nanostructures with enhanced photodegradation of methylene blue dye. *Journal of Alloys and Compounds*, *951*, 169856.

225. Sehrawat, P., Rana, S., Mehta, S. K., & Kansal, S. K. (2022). Optimal synthesis of MoS2/Cu2O nanocomposite to enhance photocatalytic

performance towards indigo carmine dye degradation. *Applied Surface Science*, *604*, 154482.

226. Seravalli, L., & Bosi, M. (2021). A review on chemical vapour deposition of two-dimensional MoS2 flakes. *Materials*, *14*(24), 7590.

227. Seth, S., & Sharma, S. K. (2018, May). Development of transition metal dichalcogenide based quantum dots for light emitting diodes. In *AIP Conference Proceedings* (Vol. 1953, No. 1). AIP Publishing.

228. Sha, R., Vishnu, N., & Badhulika, S. (2019). MoS2 based ultra-low-cost, flexible, non-enzymatic and non-invasive electrochemical sensor for highly selective detection of Uric acid in human urine samples. *Sensors and Actuators B: Chemical*, *279*, 53-60.

229. Sharma, B., Menon, S., Mathur, S., Kumari, N., & Sharma, V. (2021). Decolorization of malachite green dye from aqueous solution using biosurfactant-stabilized iron oxide nanoparticles: process optimization and reaction kinetics. *International Journal of Environmental Science and Technology*, *18*, 1739-1752.

230. She, X., Wu, J., Zhong, J., Xu, H., Yang, Y., Vajtai, R., ... & Ajayan, P. M. (2016). Oxygenated monolayer carbon nitride for excellent photocatalytic hydrogen evolution and external quantum efficiency. *Nano Energy*, *27*, 138-146.

231. Shepida, M., Kuntyi, O., Sozanskyi, M., & Sukhatskiy, Y. (2021). Sonoelectrochemical synthesis of antibacterial active silver nanoparticles in rhamnolipid solution. *Advances in Materials Science and Engineering*, *2021*(1), 7754523.

232. Shikha, S., Chaudhuri, S. R., & Bhattacharyya, M. S. (2020). Facile one pot greener synthesis of sophorolipid capped gold nanoparticles and its antimicrobial activity having special efficacy against gram negative Vibrio cholerae. *Scientific reports*, *10*(1), 1463.

233. Shubha, J. P., Kavalli, K., Adil, S. F., Assal, M. E., Hatshan, M. R., & Dubasi, N. (2022). Facile green synthesis of semiconductive ZnO

nanoparticles for photocatalytic degradation of dyes from the textile industry: A kinetic approach. *Journal of king saud university-science*, *34*(5), 102047.

234. Siddiqui, S. I., Allehyani, E. S., Al-Harbi, S. A., Hasan, Z., Abomuti, M. A., Rajor, H. K., & Oh, S. (2023). Investigation of Congo red toxicity towards different living organisms: a review. *Processes*, *11*(3), 807.

235. Silambarasan, K., Harish, S., Hara, K., Archana, J., & Navaneethan, M. (2021). Ultrathin layered MoS2 and N-doped graphene quantum dots (N-GQDs) anchored reduced graphene oxide (rGO) nanocomposite-based counter electrode for dye-sensitized solar cells. *Carbon*, *181*, 107-117.

236. Singh, A. K., Mathew, K., Zhuang, H. L., & Hennig, R. G. (2015). Computational screening of 2D materials for photocatalysis. *The journal of physical chemistry letters*, *6*(6), 1087-1098.

237. Sivaraman, C., Vijayalakshmi, S., Leonard, E., Sagadevan, S., & Jambulingam, R. (2022). Current developments in the effective removal of environmental pollutants through photocatalytic degradation using nanomaterials. *Catalysts*, *12*(5), 544.

238. Sivaranjani, P. R., Janani, B., Thomas, A. M., Raju, L. L., & Khan, S. S. (2022). Recent development in MoS2-based nano-photocatalyst for the degradation of pharmaceutically active compounds. *Journal of Cleaner Production*, *352*, 131506.

239. Smith, R. J., King, P. J., Lotya, M., Wirtz, C., Khan, U., De, S., ... & Coleman, J. N. (2011). Large-scale exfoliation of inorganic layered compounds in aqueous surfactant solutions. *Advanced materials*, *23*(34), 3944-3948.

240. Smith, R. J., King, P. J., Lotya, M., Wirtz, C., Khan, U., De, S., ... & Coleman, J. N. (2011). Large-scale exfoliation of inorganic layered compounds in aqueous surfactant solutions. *Advanced materials*, *23*(34), 3944-3948.

241. Somashekaraiah, R., Shruthi, B., Deepthi, B. V., & Sreenivasa, M. Y. (2019). Probiotic properties of lactic acid bacteria isolated from neera: a

naturally fermenting coconut palm nectar. *Frontiers in microbiology*, *10*, 1382.

242. Stiborová, M., Martínek, V., Rýdlová, H., Hodek, P., & Frei, E. (2002). Sudan I is a potential carcinogen for humans: evidence for its metabolic activation and detoxication by human recombinant cytochrome P450 1A1 and liver microsomes. *Cancer Research*, *62*(20), 5678-5684.

243. Su, S., Han, X., Lu, Z., Liu, W., Zhu, D., Chao, J., ... & Wang, L. (2017). Facile synthesis of a MoS2 –Prussian blue nanocube nanohybrid-based electrochemical sensing platform for hydrogen peroxide and carcinoembryonic antigen detection. *ACS Applied Materials & Interfaces*, *9*(14), 12773-12781.

244. Subitha, M., & Bindhu, B. (2018). Overview on preparation of molybdenum disulfide nanoflakes. In *Proceedings of the international conference on advanced nanostructures*.

245. Sun, Y., Wang, S., Li, C., Luo, P., Tao, L., Wei, Y., & Shi, G. (2013). Large scale preparation of graphene quantum dots from graphite with tunable fluorescence properties. *Physical Chemistry Chemical Physics*, *15*(24), 9907-9913.

246. Sun, Y., Xu, L., Waterhouse, G. I., Wang, M., Qiao, X., & Xu, Z. (2019). Novel three-dimensional electrochemical sensor with dual signal amplification based on MoS2 nanosheets and high-conductive NH2-MWCNT@ COF for sulfamerazine determination. *Sensors and Actuators B: Chemical*, *281*, 107-114.

247. Sundar, S., & Ganesh, V. (2020). Bio-assisted preparation of efficiently architectured nanostructures of γ-Fe2O3 as a molecular recognition platform for simultaneous detection of biomarkers. *Scientific reports*, *10*(1), 15071

248. Szkoda, M., Zarach, Z., Nadolska, M., Trykowski, G., & Trzciński, K. (2022). SnO2 nanoparticles embedded onto MoS2 nanoflakes-An efficient catalyst for photodegradation of methylene blue and photoreduction of hexavalent chromium. *Electrochimica Acta*, *414*, 140173.

249. Tahir, N., Zahid, M., Bhatti, I. A., & Jamil, Y. (2022). Fabrication of visible light active Mn-doped Bi2WO6-GO/MoS2 heterostructure for enhanced photocatalytic degradation of methylene blue. *Environmental Science and Pollution Research*, *29*(5), 6552-6567.

250. Tahir, N., Zahid, M., Jillani, A., Yaseen, M., & Abbas, Q. (2023). Ternary silver tungstate-MoS2/graphene oxide heterostructure nanocomposite for enhanced photocatalysis under visible light and antibacterial activity. *Journal of Photochemistry and Photobiology A: Chemistry*, *436*, 114376.

251. Tan, Y., Yu, K., Yang, T., Zhang, Q., Cong, W., Yin, H., ... & Zhu, Z. (2014). The combinations of hollow MoS 2 micro@ nano-spheres: one-step synthesis, excellent photocatalytic and humidity sensing properties. *Journal of Materials Chemistry C*, *2*(27), 5422-5430.

252. Tavker, N., & Sharma, M. (2020). Designing of waste fruit peels extracted cellulose supported molybdenum sulfide nanostructures for photocatalytic degradation of RhB dye and industrial effluent. *Journal of environmental management*, *255*, 109906.

253. Thakur, V., Sharma, E., Guleria, A., Sangar, S., & Singh, K. (2020). Modification and management of lignocellulosic waste as an ecofriendly biosorbent for the application of heavy metal ions sorption. *Materials Today: Proceedings*, *32*, 608-619.

254. Thangudu, S., Lee, M. T., & Rtimi, S. (2020). Tandem synthesis of high yield MoS2 nanosheets and enzyme peroxidase mimicking properties. *Catalysts*, *10*(9), 1009.

255. Thomas, N., Mathew, S., Nair, K. M., O'Dowd, K., Forouzandeh, P., Goswami, A., ... & Pillai, S. C. (2021). 2D MoS2: structure, mechanisms, and photocatalytic applications. *Materials Today Sustainability*, *13*, 100073.

256. Tien, T. M., Chen, C. H., Huang, C. T., & Chen, E. L. (2022). Photocatalytic degradation of methyl orange dyes using green synthesized MoS2/Co3O4 nanohybrids. *Catalysts*, *12*(11), 1474.

257. Tuteja, S. K., Duffield, T., & Neethirajan, S. (2017). Liquid exfoliation of 2D MoS 2 nanosheets and their utilization as a label-free electrochemical immunoassay for subclinical ketosis. *Nanoscale*, *9*(30), 10886-10896.

258. Ullah, H., Khan, Z., Nasir, J. A., Balkan, T., Butler, I. S., Kaya, S., & Rehman, Z. U. (2021). Green synthesis of mesoporous MoS2 nanoflowers for efficient photocatalytic degradation of Congo red dye. *Journal of Coordination Chemistry*, *74*(14), 2302-2314.

259. Uysal, H., Genç, S., & Ayar, A. (2017). Toxic effects of chronic feeding with food azo dyes on Drosophila melanogaster Oregon R. *Scientia Iranica*, *24*(6), 3081-3086.

260. Varrla, E., Backes, C., Paton, K. R., Harvey, A., Gholamvand, Z., McCauley, J., & Coleman, J. N. (2015). Large-scale production of size-controlled MoS2 nanosheets by shear exfoliation. *Chemistry of Materials*, *27*(3), 1129-1139.

261. Vasi, S., Giofrè, S. V., Perathoner, S., Mallamace, D., Abate, S., & Wanderlingh, U. (2024). X-ray Characterizations of Exfoliated MoS2 Produced by Microwave-Assisted Liquid-Phase Exfoliation. *Materials*, *17*(16), 3887.

262. Vasiljevic, Z. Z., Dojcinovic, M. P., Vujancevic, J. D., Jankovic-Castvan, I., Ognjanovic, M., Tadic, N. B., ... & Nikolic, M. V. (2020). Photocatalytic degradation of methylene blue under natural sunlight using iron titanate nanoparticles prepared by a modified sol–gel method. *Royal Society open science*, *7*(9), 200708.

263. Vecino, X., Rodríguez-López, L., Rincón-Fontán, M., Cruz, J. M., & Moldes, A. B. (2021). Nanomaterials synthesized by biosurfactants. In *Comprehensive analytical chemistry* (Vol. 94, pp. 267-301). Elsevier

264. Veeramalai, C. P., Li, F., Liu, Y., Xu, Z., Guo, T., & Kim, T. W. (2016). Enhanced field emission properties of molybdenum disulphide few layer nanosheets synthesized by hydrothermal method. *Applied Surface Science*, *389*, 1017–1022.

265. Velayati, M., Hassani, H., Sabouri, Z., Mostafapour, A., & Darroudi, M. (2021). Biosynthesis of Se-Nanorods using Gum Arabic (GA) and

investigation of their photocatalytic and cytotoxicity effects. *Inorganic Chemistry Communications*, *128*, 108589.

266. Verble, J. L., & Wieting, T. J. (1970). Lattice mode degeneracy in Mo S 2 and other layer compounds. *Physical review letters*, *25*(6), 362.

267. Verma, R. K., Sankhla, M. S., Rathod, N. V., Sonone, S. S., Parihar, K., & Singh, G. K. (2021). Eradication of fatal textile industrial dyes by wastewater treatment. *Biointerface Res. Appl. Chem*, *12*, 567-587.

268. Vinoth, R., Patil, I. M., Pandikumar, A., Kakade, B. A., Huang, N. M., Dionysios, D. D., & Neppolian, B. (2016). Synergistically enhanced electrocatalytic performance of an N-doped graphene quantum dot-decorated 3D MoS2 –graphene nanohybrid for oxygen reduction reaction. *Acs Omega*, *1*(5), 971-980.

269. Vishnu, N., & Badhulika, S. (2019). Single step grown MoS2 on pencil graphite as an electrochemical sensor for guanine and adenine: A novel and low cost electrode for DNA studies. *Biosensors and Bioelectronics*, *124*, 122-128.

270. Vo, Q. V., Thao, L. T. T., Manh, T. D., Van Bay, M., Truong-Le, B. T., Hoa, N. T., & Mechler, A. (2024). Reaction of methylene blue with OH radicals in the aqueous environment: mechanism, kinetics, products and risk assessment. *RSC advances*, *14*(37), 27265-27273.

271. Wang, C., Jin, J., Sun, Y., Yao, J., Zhao, G., & Liu, Y. (2017). In-situ synthesis and ultrasound enhanced adsorption properties of MoS2 /graphene quantum dot nanocomposite. *Chemical Engineering Journal*, *327*, 774-782.

272. Wang, H., Duan, Y., Fei, G., Yan, T., Kang, Y. M., & Dionysiou, D. D. (2023). Design, synthesis and modification of 2D nanomaterials-based photocatalysts for pollutant degradation and photodegradation experiments from lab-scale to grand-scale. *Chemical Engineering Journal*, 147219.

273. Wang, H., Li, C., Fang, P., Zhang, Z., & Zhang, J. Z. (2018). Synthesis, properties, and optoelectronic applications of two-dimensional MoS 2 and MoS 2-based heterostructures. *Chemical Society Reviews*, *47*(16), 6101-6127.

274. Wang, Q., & Li, J. (2007). Facilitated Lithium Storage in MoS_2 Overlayers Supported on Coaxial Carbon Nanotubes. *The Journal of Physical Chemistry C*, *111*(4), 1675–1682.

275. Wang, Y., Pan, C., Chu, W., Vipin, A. K., & Sun, L. (2019). Environmental remediation applications of carbon nanotubes and graphene oxide: Adsorption and catalysis. *Nanomaterials*, *9*(3), 439.

276. Wang, Y., Zhang, B., Tang, Y., Zhao, F., & Zeng, B. (2021). Fabrication and application of a rutin electrochemical sensor based on rose-like AuNPs-MoS2 -GN composite and molecularly imprinted chitosan. *Microchemical Journal*, *168*, 106505.

277. Wang, Y., Zhen, M., Liu, H., & Wang, C. (2018). Interlayer-expanded MoS 2/graphene composites as anode materials for high-performance lithium-ion batteries. *Journal of Solid State Electrochemistry*, *22*, 3069-3076.

278. Wei, C., Hou, Z., Sun, H., & Wang, J.-G. (2021). Ultrafine MoS2 Nanosheets Vertically Patterned on Graphene for High-Efficient Li-Ion and Na-Ion Storage. *Frontiers in Chemistry*, *9*, 802788.

279. Wu, W., Xu, J., Tang, X., Xie, P., Liu, X., Xu, J., ... & Fan, T. (2018). Two-dimensional nanosheets by rapid and efficient microwave exfoliation of layered materials. *Chemistry of Materials*, *30*(17), 5932-5940.

280. Xia, D. D., Gong, F., Pei, X., Wang, W., Li, H., Zeng, W., ... & Papavassiliou, D. V. (2018). Molybdenum and tungsten disulfides-based nanocomposite films for energy storage and conversion: A review. *Chemical Engineering Journal*, *348*, 908-928.

281. Xin, X., Zhang, Y., Guan, X., Cao, J., Li, W., Long, X., & Tan, X. (2019). Enhanced performances of PbS quantum-dots-modified MoS2 composite for NO2 detection at room temperature. *ACS applied materials & interfaces*, *11*(9), 9438-9447.

282. Xu, H., Gao, B., Cao, H., Chen, X., Yu, L., Wu, K., ... & Fu, J. (2014). Nanoporous activated carbon derived from rice husk for high performance supercapacitor. *Journal of Nanomaterials*, *2014*(1), 714010.

283. Xu, X., Sun, Y., Fan, Z., Zhao, D., Xiong, S., Zhang, B., ... & Liu, G. (2018). Mechanisms for· O 2-and· OH production on flowerlike BiVO4 photocatalysis based on electron spin resonance. *Frontiers in chemistry*, *6*, 64.

284. Xuan, D., Zhou, Y., Nie, W., & Chen, P. (2017). Sodium alginate-assisted exfoliation of MoS2 and its reinforcement in polymer nanocomposites. *Carbohydrate polymers*, *155*, 40-48.

285. Yang, C., Dong, W., Cui, G., Zhao, Y., Shi, X., Xia, X., ... & Wang, W. (2017). Highly efficient photocatalytic degradation of methylene blue by P2ABSA-modified TiO 2 nanocomposite due to the photosensitization synergetic effect of TiO 2 and P2ABSA. *RSC advances*, *7*(38), 23699-23708.

286. Yang, C., Wang, Y., Wu, Z., Zhang, Z., Hu, N., & Peng, C. (2022). Three-dimensional MoS2 /reduced graphene oxide nanosheets/graphene quantum dots hybrids for high-performance room-temperature NO2 gas sensors. *Nanomaterials*, *12*(6), 901.

287. Yang, X., Chen, Z., Fang, J., Yang, Q., Zhao, W., Qian, X., ... & Chen, M. (2019). Freestanding 3D MoS2 nanosheets/graphene aerogel heterostructure as a recyclable photocatalyst for efficiently degrading antibiotic residues. *Materials Letters*, *252*, 5-7.

288. Yang, Y., Lei, Q., Li, J., Hong, C., Zhao, Z., Xu, H., & Hu, J. (2022). Synthesis and enhanced electrochemical properties of AuNPs@ MoS2/rGO hybrid structures for highly sensitive nitrite detection. *Microchemical Journal*, *172*, 106904.

289. Yoon, J., Shin, J. W., Lim, J., Mohammadniaei, M., Bapurao, G. B., Lee, T., & Choi, J. W. (2017). Electrochemical nitric oxide biosensor based on amine-modified MoS2 /graphene oxide/myoglobin hybrid. *Colloids and Surfaces B: Biointerfaces*, *159*, 729-736.

290. Yu, H., Zhu, H., Dargusch, M., & Huang, Y. (2018). A reliable and highly efficient exfoliation method for water-dispersible MoS2 nanosheet. *Journal of colloid and interface science*, *514*, 642-647.

291. Yu, J., Ma, D., Mei, L., Gao, Q., Yin, W., Zhang, X., ... & Zhao, Y. (2018). Peroxidase-like activity of MoS 2 nanoflakes with different

modifications and their application for H 2 O 2 and glucose detection. *Journal of Materials Chemistry B*, *6*(3), 487-498.

292. Yu, J., Ma, X., Yin, W., & Gu, Z. (2016). Synthesis of PVP-functionalized ultra-small MoS 2 nanoparticles with intrinsic peroxidase-like activity for H 2 O 2 and glucose detection. *RSC advances*, *6*(84), 81174-81183.

293. Yuan, Y., Guo, R. T., Hong, L. F., Ji, X. Y., Li, Z. S., Lin, Z. D., & Pan, W. G. (2021). Recent advances and perspectives of MoS2-based materials for photocatalytic dyes degradation: a review. *Colloids and Surfaces A: Physicochemical and Engineering Aspects*, *611*, 125836.

294. Yuwen, L., Yu, H., Yang, X., Zhou, J., Zhang, Q., Zhang, Y., ... & Wang, L. (2016). Rapid preparation of single-layer transition metal dichalcogenide nanosheets via ultrasonication enhanced lithium intercalation. *Chemical communications*, *52*(3), 529-532.

295. Zafar, S., Bukhari, D. A., & Rehman, A. (2022). Azo dyes degradation by microorganisms–An efficient and sustainable approach. *Saudi Journal of Biological Sciences*, *29*(12), 103437.

296. Zangeneh, H., Farhadian, M., & Zinatizadeh, A. A. (2020). A reusable visible driven N and C–N doped TiO2 magnetic nanocomposites for photodegradation of direct red 16 azo dye in water and wastewater. *Environmental Technology*, 1-16.

297. Zeng, Z., Yin, Z., Huang, X., Li, H., He, Q., Lu, G., ... & Zhang, H. (2011). Single-layer semiconducting nanosheets: high-yield preparation and device fabrication. *Angewandte Chemie International Edition*, *47*(50), 11093-11097.

298. Zhang, C., Hu, D. F., Xu, J. W., Ma, M. Q., Xing, H., Yao, K., ... & Xu, Z. K. (2018). Polyphenol-assisted exfoliation of transition metal dichalcogenides into nanosheets as photothermal nanocarriers for enhanced antibiofilm activity. *Acs Nano*, *12*(12), 12347-12356.

299. Zhang, J., Miao, S., Tu, Q., Shi, M., Zou, L., Liu, S., & Wang, G. (2018). Effect of butorphanol on opioid-induced cough: a meta-analysis of

randomized controlled trials. *Drug Design, Development and Therapy*, 3263-3268.

300. Zhang, X., Cao, Q., Guo, Z., Zhang, M., Zhou, M., Zhai, Z., & Xu, Y. (2021). Self-assembly of MoS2 nanosheet on functionalized pomelo peel derived carbon and its electrochemical sensor behavior toward taxifolin. *Inorganic Chemistry Communications*, *129*, 108631.

301. Zhang, X., Tang, H., Xue, M., & Li, C. (2014). Facile synthesis and characterization of ultrathin MoS2 nanosheets. *Materials Letters*, *130*, 83–86.

302. Zhang, X., Zhang, Q., Sun, Y., Zhang, P., Gao, X., Zhang, W., & Guo, J. (2016). MoS2-graphene hybrid nanosheets constructed 3D architectures with improved electrochemical performance for lithium-ion batteries and hydrogen evolution. *Electrochimica Acta*, *189*, 224-230.

303. Zhang, Y., Wang, Y., Di, M., Zhou, B., Xu, W., Wu, N., ... & Zhong, W. (2020). Synergy of dopants and defects in ultrathin 2D carbon nitride sheets to significantly boost the photocatalytic hydrogen evolution. *Chemical Engineering Journal*, *385*, 123938

304. Zhong, Y., Shi, T., Huang, Y., Cheng, S., Chen, C., Liao, G., & Tang, Z. (2019). Three-dimensional MoS 2/graphene aerogel as binder-free electrode for li-ion battery. *Nanoscale research letters*, *14*, 1-8.

305. Zhou, S., Du, Z., Li, X., Zhang, Y., He, Y., & Zhang, Y. (2019). Degradation of methylene blue by natural manganese oxides: kinetics and transformation products. *Royal Society open science*, *6*(7), 190351.

306. Zou, L., Qu, R., Gao, H., Guan, X., Qi, X., Liu, C., ... & Lei, X. (2019). MoS2/RGO hybrids prepared by a hydrothermal route as a highly efficient catalytic for sonocatalytic degradation of methylene blue. *Results in Physics*, *14*, 102458.

Appendix A

S. No.	Chemicals	Company
1.	Ascorbic acid	Loba Chemicals
2.	Chloroform	Loba Chemicals
3.	Citric acid	Loba Chemicals
4.	Ciprofloxacin	HiMedia
5.	Commercial blue (CB) dye	Atul dye
6.	Dimethyl sulfoxide (DMSO)	Loba Chemicals
7.	2, 2-diphenyl-1-picrylhydrazyl (DPPH),	HiMedia
8.	Gum arabic	Loba Chemicals
9.	Luria broth (LB),	HiMedia
10.	Methylene blue dye	Loba Chemicals
11.	MoS_2 (99% purity)	Loba Chemicals
12.	Mueller Hinton Agar (MHA)	HiMedia
13.	Nutrient agar (NA)	HiMedia
14.	Nutrient broth (NB)	HiMedia
15.	Sodium alginate	Loba Chemicals
16.	Textile industrial sample	Vardhaman yarns & threads mill, Hoshiarpur
17.	*Tinospora cordifolia* stem powder	Local market

Instruments

S. No.	Instruments	Company
1.	Autoclave	Relitech
2.	Bath ultrasonicator	Citizen CD-4820
3.	Centrifuge	REMI
4.	FT-IR	PerkinElmer 1750 FT-IR spectrophotometer
5.	Heating mantle	Labfit
6.	High-resolution TEM	JEOL,JEM 2100 plus
7.	Hot air oven	NSW-143
8.	Hot plate	NSW-India
9.	Incubator	Labfit
10.	Laminar air flow(LAF)	Rescholar
11.	Magnetic stirrer	REMI-2MLH
12.	Microwave	IFB Model-30SC3
13.	Mini centrifuge	Neuations Ifuge-M08 VT
14.	pH meter	Max electronics
15.	UV–vis spectrophotometer	LasanyModel no.LI-2800 Ex
16.	Vortex	Spinix
17.	Weighing balance	Uni Bloc
18.	X-ray diffractometer	Panalyticals XPert Pro Bruker D8 Advance

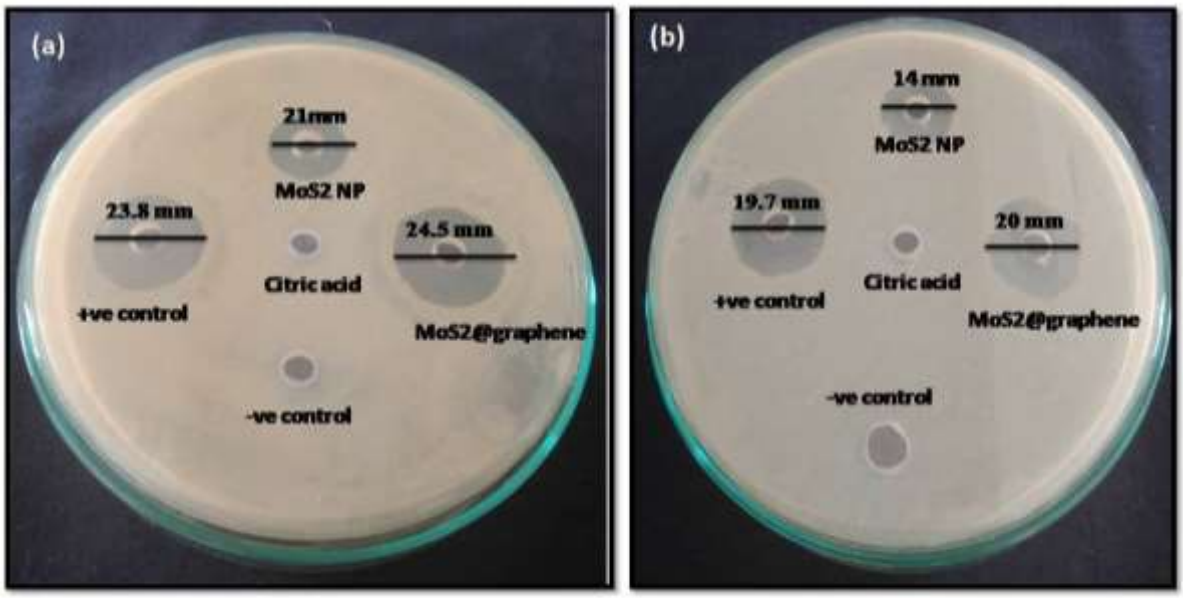

***S.aureus* MTCC 7443** ***E.coli* MTCC 495**

1. Antibacterial activity of Gum Arabic mediated MoS_2 NS and MoS_2@GQDs on Muller Hinton agar medium plate through well diffusion method against(a) *E. coli* and (b) *S. aureus*. Streptomycin antibiotic and sterile DDW were used as positive and negative controls, respectively. Zone of inhibition that designates antibacterial activity is measured in mm. The antibiotic was used as half of the concentration w.r.t. test sample.

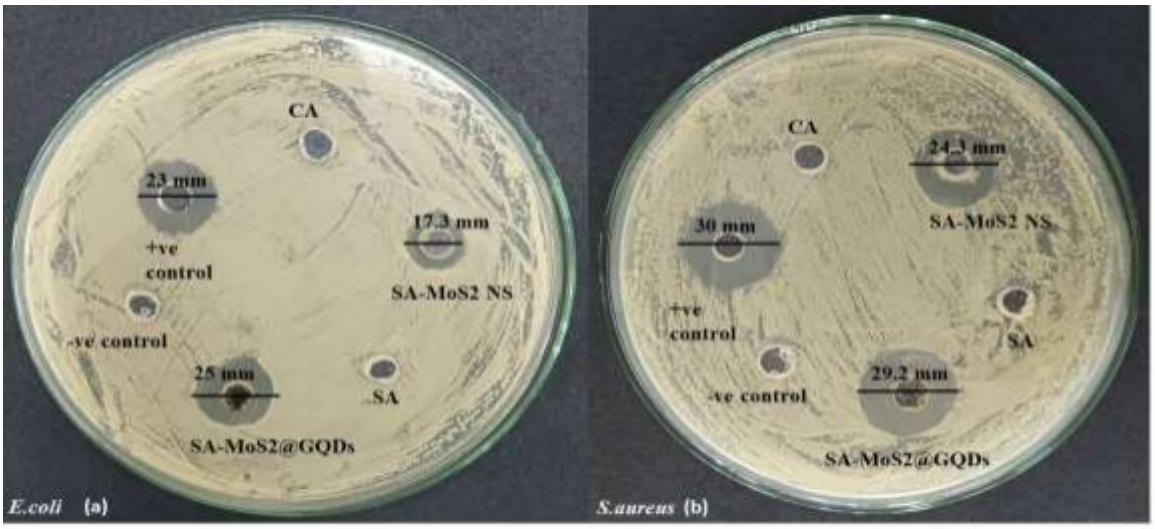

2.Antibacterial activity of MoS_2 nanosheet and MoS_2@GQDs obtained from sodium alginate on Muller Hinton agar medium plate through well diffusion method against(a) *E. coli* and (b) *S. aureus*. Streptomycin antibiotic and sterile DDW were used as positive and negative controls, respectively. Zone of inhibition that designates antibacterial activity is measured in mm.

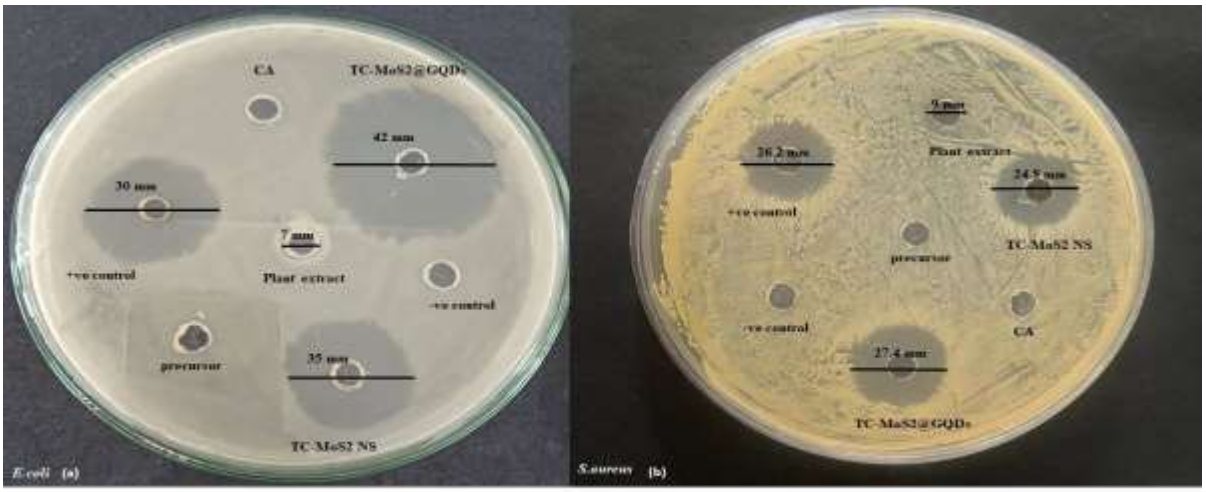

3. Antibacterial activity of MoS_2 nanosheet and MoS_2@GQDs obtained from *Tinospora cordifolia* on Muller Hinton agar medium plate through well diffusion method against(a) *E. coli* and (b) *S. aureus*. Streptomycin antibiotic and sterile DDW were used as positive and negative controls, respectively. Zone of inhibition that designates antibacterial activity is measured in mm.

Appendix B

List of publications

1. Kaur, M., Kumar, V., Awasthi, A., & Singh, K. (2023). Gum arabic–assisted green synthesis of biocompatible MoS_2 nanoparticles for methylene blue photodegradation. *Environmental Science and Pollution Research*, *30*(52), 112847-112862.

2. Kaur, M., Gautam, A., Guleria, P., Singh, K., & Kumar, V. (2022). Green synthesis of metal nanoparticles and their environmental applications. *Current Opinion in Environmental Science & Health*, *29*, 100390.

Environmental Science and Pollution Research (2023) 30:112847–112862
https://doi.org/10.1007/s11356-023-30116-4

RESEARCH ARTICLE

Gum arabic–assisted green synthesis of biocompatible MoS_2 nanoparticles for methylene blue photodegradation

Mandeep Kaur[1] · Vineet Kumar[1] · Abhishek Awasthi[2] · Kulvinder Singh[2]

Received: 13 April 2023 / Accepted: 24 September 2023 / Published online: 16 October 2023

Abstract

The current work reports the gum arabic–mediated greener synthesis of MoS_2 nanoparticles (NPs) and its utilization for the solar light–assisted degradation of methylene blue. Furthermore, the safety analyses were performed on human-beneficial gut bacterium, *L. delbrueckii*, and human blood cells to confirm the biocompatibility of NPs synthesized. Antioxidant and antimicrobial activities were done to explore their usefulness for biological applications. Sonication and microwave treatment were used to obtain spherical 10–12 nm MoS_2 NPs as characterized using high-resolution transmission electron microscopy. FT-IR characterization revealed the occurrence of gum arabic on the NPs surface. The MoS_2 NPs exhibited ~ 98% MB degradation within 8 h under direct sunlight exposure. Moreover, the reusability studies have also been evaluated and free radical trapping experiments indicated that superoxide ($\bullet O_2^-$) is the dominant active species of the reaction system. Furthermore, 98.89% MB degradation efficiency was observed within 150 min in the case of real textile industry MB effluent samples. Untreated MB inhibited the growth of *L. delbrueckii* on MRS agar plates, while growth was observed in the case of MoS_2 NPs–treated MB samples indicating safety of current MB degradation approach. MoS_2 NPs inhibited the growth of *E. coli* MTCC1698 and *S. aureus* MTCC 3160 with 26 mm and 21 mm zone of inhibition, respectively. Furthermore, MoS_2 NPs have shown antioxidant properties, resulting in 82.3 ± 0.43% of DPPH scavenging activity which was comparable to ascorbic acid (81.6 ± 0.6%), a standard antioxidant molecule. The NPs have not shown any hemolytic activity at 0.0625 and 0.125 mg/mL doses to human blood proving their biocompatible nature. Gum arabic–synthesized biocompatible MoS_2 NPs have good potential to treat MB released as waste from the textile industry and other biological applications.

Keywords Bio-surfactant · MoS_2 NPs · Methylene blue (MB) · Real textile effluent · Antimicrobial · Antioxidant · Hemolysis efficiency

Introduction

In the recent years, environmental issues become one of the major concerns throughout the world (Wang et al. 2019). Several researchers around the globe are working on various environmental problems (Ahmad et al. 2022a; Akhtar et al. 2021a; Choudhury et al. 2021; Khan et al. 2022). In this context, water pollution is the most important issue as around 80% of the waste from different sources is discharged in the water system (Akhtar et al. 2021b). Several groups have developed various sensing tools for the qualitative and quantitative assessment of different toxic chemical in the water system; however, monitoring the concentration of the toxic chemicals is not the end solution (Singh 2020; Umar et al. 2018). Instead, the complete removal of these chemicals by various means may lead to proper treatment of wastewater (Guleria et al. 2022; Thakur et al. 2020, 2021).

There are several methodologies developed until now for efficient wastewater treatment that include adsorption, biological treatment, and coagulation. However due to several limitations, there has been a need to develop an efficient methodology that is economical, energy-efficient, and require less time (Thakur et al. 2020). In

Responsible Editor: Sami Rtimi

✉ Vineet Kumar
vineetkumar22@gmail.com

[1] Department of Biotechnology, School of Bioengineering and Biosciences, Lovely Professional University, Phagwara, Punjab 144411, India

[2] Department of Biotechnology, School of Basic and Applied Sciences, Maharaja Agrasen University, Baddi, Himachal Pradesh 174103, India

[3] Department of Chemistry, DAV College, Sector 10, Chandigarh, UT 160011, India

Available online at www.sciencedirect.com

ScienceDirect

Current Opinion in Environmental Science & Health

Green synthesis of metal nanoparticles and their environmental applications

Mandeep Kaur[1,a], Ayushi Gautam[2,a], Praveen Guleria[2], Kulvinder Singh[3] and Vineet Kumar[1]

Abstract

Nanotechnology is a multi-disciplinary field with diverse applications. The use of nanoparticles (NPs) for environmental applications is a current trend. Among various types of NPs, metallic NPs are widely used for environmental applications. Greener synthesis of NPs is preferred over chemical and physical methods as it is an eco-friendly, cost-effective, and sustainable approach. In green synthesis, plant parts are mainly used as reducing and capping agents. Extract prepared from leaves, bark, fruits, and flowers has been used for the synthesis of metallic NPs of various sizes and shapes. Biosurfactant extracted from plant, microorganism and other biological resources have also been used for metallic NPs synthesis. The bio-fabricated metallic NPs are useful for the detection and removal of dyes, antibiotics, and metal ions.

Addresses

[1] Department of Biotechnology, Lovely Professional University, Phagwara, Punjab 144411, India

[2] Department of Biotechnology, Faculty of Life Sciences, DAV University, Jalandhar, Punjab 144012, India

[3] Department of Chemistry, DAV College, Sector 10, Chandigarh 160011, India

Corresponding authors: Kumar, Vineet (vineetkumar22@gmail.com); Singh, Kulvinder (kulvinderchem@gmail.com)

[a] Authors contributed equally.

Current Opinion in Environmental Science & Health 2022, 29:100390

This review comes from a themed issue on **Environmental Technologies 2022: Nanomaterials as materials for extraction, sensing, and detection of environmental contaminants**

Edited by **Muhammad Sajid**

For complete overview of the section, please refer to the article collection - Environmental Technologies 2022: Nanomaterials as materials for extraction, sensing, and detection of environmental contaminants

https://doi.org/10.1016/j.coesh.2022.100390

Keywords

Metallic NPs, Green synthesis, Dye removal, Antibiotic degradation, Nanosensor.

Introduction

Nanoscience has gained remarkable attention due to its diverse applications in multiple fields. The cornerstone of nanoscience is the cost-effective synthesis of nanoparticles (NPs) with unique physical, chemical, optical, electrochemical, and thermal properties [1,2]. The applications of NPs in the environment sector have good potential to overcome the challenges of environmental sustainability [3]. The presence of dye, antibiotics, and metal ions in large amounts poses serious health problems.

Among various types of NPs, metallic NPs are the most commonly used for the detection and removal of dye, antibiotics, and metal ions. Currently, preparing metallic NPs via the green route is the most promising approach as it uses materials with no or low toxicity. Green synthesis of metallic NPs follows the principles of green chemistry. Hence, the obtained NPs are biocompatible [4]. Besides, NPs are known for their contribution to dyes, and toxic chemicals removed from the waste [5]. Furthermore, NPs exhibited a tendency to detect and remove other wastewater contaminants as discussed elsewhere [6].

Green synthesis of metal nanoparticles

Green synthesis refers to the synthesis of NPs using environmentally friendly biological reducing and stabilizing agents present in the plants, microorganisms, or biosurfactants. Metal ions present in the reaction mixture are reduced to metal atoms by reducing agents. The metal atoms undergo clustering to get stabilized and form NPs. Clustering for a longer time after the reduction process leads to an increase in NPs size. The biosurfactants binding to the surface stop the clustering process to a different extent leading to the formation of NPs of various sizes [7,8]. Good biosurfactant activity leads to a decrease in the size of NPs while poor biosurfactant activity leads to an increase in the NPs size. The activity depends upon the amount or the nature of the reducing, and stabilization agent. A single molecule may act as a reducing as well as a stabilizing agent. Various physiochemical factors, incubation temperature, pH, metal ion concentration, reducing and stabilizing agent/biosurfactant concentration can be varied to obtain stable NPs (Figure 1).

Microorganisms-mediated metallic NPs synthesis

Microorganisms are cheap and renewable reducing agents acting as small factories for the synthesis of NPs following a safe, economical and green route, and

List of Conferences

1. 44th world conference on Applied Science, Engineering & Technology(44th WCASET-2023).This conference was held at malaysia on 25th and 26th November, 2023.

IFERP

CERTIFICATE
OF PRESENTATION

44th World Conference on Applied Science, Engineering & Technology (44th WCASET-2023)

25th & 26th November 2023 | Hybrid Conference

This is to Certify that Mandeep Kaur of Lovely Professional University,Phagwara,Punjab presented his/her worthy Paper titled Synthesis of MoS2 Nanoparticle using Sodium alginate and its potential photocatalytic activity against azo dye during the "44th World Conference on Applied Science, Engineering & Technology (44th WCASET-2023)" Organized by Institute For Educational Research and Publication (IFERP) Malaysia Society held on 25th & 26th November 2023 as a Virtual Conference.

2. International Conference on recent innovations in biotechnology (ICRIB_2023) was held at Chennai on 21st september to 23rd september.

SATHYABAMA
INSTITUTE OF SCIENCE AND TECHNOLOGY
(DEEMED TO BE UNIVERSITY)
Accredited with Grade "A++" by NAAC | 12B status by UGC | Approved by AICTE
Jeppiaar Nagar, Rajiv Gandhi Salai, Chennai - 600 119

INTERNATIONAL CONFERENCE ON RECENT INNOVATIONS IN BIOTECHNOLOGY (ICRIB-2023)

Certificate of Presentation

Supported By CSIR, New Delhi

This is to certify that Miss.MANDEEP KAUR of LOVELY PROFESSIONAL UNIVERSITY has presented a paper (Oral) entitled SYNTHESIS, CHARACTERIZATION AND APPLICATION OF GUM ARABIC SYNTHESIZED MoS2 NANOSTRUCTURES In the International Conference on Recent Innovations in Biotechnology (ICRIB-2023) organized by Sathyabama Institute of Science and Technology, Chennai during 21st-23rd September, 2023.

Dr. S. Johnson, CONVENER
Dr. A. Madan Kumar, CONVENER
Dr. A. Dayanandan, ORGANIZING SECRETARY
Dr. T. Sasipraba, VICE-CHANCELLOR

List of other publications

1. Kaur, M., Singh, K., & Kumar, V. (2024). Green Synthesis of Silver Nanoparticles Using *Penicillium camemberti* and its Biological Applications. *BioNanoScience*, 1-15.

2. Kaur, M., Singh, J., Chauhan, M., Kumar, V., & Singh, K. (2024). Green synthesis of TiO_2-Al_2O_3-$ZnFe_2O_4$ nanocomposite using the *Hibiscus rosa sinesis* and evaluation of its photocatalytic applications. *Open Ceramics*, *18*, 100571.

3. Kaur, M., Guleria, P., & Kumar, V. (2023). Nanomaterials for Diagnosis and Treatment of Lung Cancer: A Review of Recent Patents. *Recent Patents on Anti-Cancer Drug Discovery*, *18*(2), 114-124.

4. Kaur, M.,Wadhwa A., & Kumar, V. (2021). Pectin-Based Nanomaterials: Synthesis, Toxicity and Applications.Chem .AsianJ,20534